

LASER INTERFEROMETER GRAVITATIONAL WAVE OBSERVATORY
- LIGO -

=====

LIGO SCIENTIFIC COLLABORATION

Technical Note

LIGO-T1500060-v1

Updated: 2022-10

**aLIGO Output Mode Cleaner:
Optical Testing and Results**

Koji Arai, Jeffery Lewis, William Z. Korth

Distribution of this document:

LIGO Scientific Collaboration

California Institute of Technology
LIGO Project, MS 100-36
Pasadena, CA 91125
Phone (626) 395-2129
Fax (626) 304-9834
E-mail: info@ligo.caltech.edu

Massachusetts Institute of Technology
LIGO Project, Room NW22-295
Cambridge, MA 02139
Phone (617) 253-4824
Fax (617) 253-7014
E-mail: info@ligo.mit.edu

LIGO Hanford Observatory
Route 10, Mile Marker 2
Richland, WA 99352
Phone (509) 372-8106
Fax (509) 372-8137
E-mail: info@ligo.caltech.edu

LIGO Livingston Observatory
19100 LIGO Lane
Livingston, LA 70754
Phone (225) 686-3100
Fax (225) 686-7189
E-mail: info@ligo.caltech.edu

<http://www.ligo.org/>

Contents

1	Objective and scope	15
2	Test of individual optical components	15
2.1	Characterization of the curved mirrors	15
2.1.1	Curvature radii for the curved mirrors	15
2.1.2	Thickness of the curved mirrors	23
2.1.3	Characterization of the curvature center	23
2.2	Characterizations of the OMC prism mirrors	26
2.2.1	Wedge angle measurement	26
2.2.2	Prism perpendicularity test	30
2.2.3	Data sheet values for the mirror reflectivities and transmissivities	34
2.2.4	Measurement of the mirror transmissivities	35
2.2.5	Mirror scattering measurement at Caltech	40
2.2.6	Mirror scattering measurement at UC Fullerton	42
2.3	Characterization of the PZTs	42
2.3.1	PZT Wedge angle	42
2.3.2	PZT actuator DC response & length-to-angle coupling	43
2.3.3	Determination of the mirror arrangement for the PZT subassemblies	43
2.3.4	PZT endurance test 1: High repetition test	50
2.3.5	PZT endurance test 2: Reverse voltage test	51
2.4	Photodiode and photodetector test	54
2.4.1	DCPD diode test	54
2.4.2	DCPD diode response test	60
2.4.3	Dependence of the photodiode response on the incident angle	61
2.4.4	DCPD preamp test	62
2.4.5	High QE DCPD diode test	62
2.4.6	High QE DCPD reflectivity test	63
2.4.7	High QE DCPD dark current measurement	63
2.4.8	High QE DCPD responsivity measurement	64
2.4.9	Effect of air-baking on high QE DCPD	66

2.4.10	High QE DCPD dark noise measurement	68
2.4.11	High QE high power exposure test	73
2.4.12	High QE DCPD capacitance measurement	77
2.5	Miscellaneous measurements	77
2.5.1	Breadboard size measurement	79
2.5.2	UV epoxy thickness	79
2.5.3	Power meter calibration	79
3	Test of the integrated OMC breadboards	81
3.1	Experimental setup	82
3.2	Cavity geometry test	85
3.2.1	Cavity absolute length measurement with detuned locking	85
3.2.2	Cavity length and finesse measurement with RFAM injection	86
3.2.3	Transverse-mode spacing measurement	87
3.3	Power budget	87
3.4	PZT characterization	89
3.4.1	PZT response: DC scan	89
3.4.2	PZT response: AC scan	90
3.5	Photodiode alignment	90
3.5.1	DCPD/QPD shim height adjustment	90
3.5.2	QPD housing alignment	90
3.5.3	DCPD housing alignment / DCPD&QPD photos	91
3.6	Misc measurements	91
3.6.1	Weight	91
3.7	Backscatter measurement 1	92
3.8	Backscatter measurement 2	95
3.9	Vibrational property	99
3.9.1	Vibrational test of the OMC breadboard	99
3.9.2	FEM analysis of the resonant modes for the components	101
3.10	Test results for OMC(001)	110
3.10.1	Summary of the OMC(001) tests	110

3.10.2	Cavity absolute length measurement with detuned locking	110
3.10.3	Cavity length and finesse measurement with RFAM injection	110
3.10.4	Transverse-mode spacing measurement	112
3.10.5	Power budget for OMC(001)	116
3.10.6	PZT response DC/AC	116
3.10.7	DCPD/QPD shim height adjustment	117
3.10.8	QPD alignment	120
3.10.9	Alignment / beam spot photos	120
3.10.10	Balance Mass Distribution	120
3.11	Test results for OMC(002)	124
3.11.1	Summary of the OMC(002) tests	124
3.11.2	Cavity absolute length measurement with detuned locking	124
3.11.3	Cavity length and finesse measurement with RFAM injection	124
3.11.4	Transverse-mode spacing measurement	127
3.11.5	Power budget for OMC(002)	131
3.11.6	PZT response DC/AC	131
3.11.7	DCPD/QPD shim height adjustment	133
3.11.8	QPD alignment	133
3.11.9	Alignment / beam spot photos	135
3.11.10	Forensic study of the damaged OMC(002)	136
3.12	Test results for OMC(003)	140
3.12.1	Summary of the OMC(003) tests	140
3.12.2	Cavity absolute length measurement with detuned locking	140
3.12.3	Cavity length and finesse measurement with RFAM injection	140
3.12.4	Transverse-mode spacing measurement	141
3.12.5	Power budget for OMC(003)	143
3.12.6	PZT response DC/AC	143
3.12.7	DCPD/QPD shim height adjustment	147
3.12.8	QPD alignment	147
3.12.9	Alignment / beam spot photos	149
3.13	Test results for OMC(002R2)	150

3.13.1	Summary of the OMC(002R2) tests	150
3.13.2	Cavity absolute length measurement with detuned locking	150
3.13.3	Cavity length and finesse measurement with RFAM injection	150
3.13.4	Transverse-mode spacing measurement	152
3.13.5	Power budget for OMC(002R2)	156
3.13.6	PZT response DC/AC	156
3.13.7	DCPD/QPD shim height	156
3.13.8	QPD alignment	157
3.13.9	Alignment / beam spot photos	159
3.13.10	Balance Mass Distribution	161
3.14	Test results for OMC(004)	162
3.14.1	Summary of the OMC(004) tests	162
3.14.2	Cavity absolute length measurement with detuned locking	162
3.14.3	Cavity length and finesse measurement with RFAM injection	162
3.14.4	Transverse-mode spacing measurement	164
3.14.5	Power budget for OMC(004)	168
3.14.6	PZT response DC/AC	168
3.14.7	DCPD/QPD shim height adjustment	169
3.14.8	QPD alignment	169
3.14.9	Alignment / beam spot photos	171
Appendices		175
A Mirror List		175
B DCPD dimensions		177
C Cavity axis alignment		177
D DCPD/QPD/PZT/Preamplifier arrangement		179

List of Figures

1	Optical setup for the mirror curvature measurement.	17
2	Electrical setup for the mirror curvature measurement.	17
3	Measured TMS/FSR of the curved mirror C1	18
4	Measured TMS/FSR of the curved mirror C2	19
5	Measured TMS/FSR of the curved mirror C3	19
6	Measured TMS/FSR of the curved mirror C4	20
7	Measured TMS/FSR of the curved mirror C5	20
8	Measured TMS/FSR of the curved mirror C6	21
9	Measured TMS/FSR of the curved mirror C7	21
10	Measured TMS/FSR of the curved mirror C8	22
11	Measured TMS/FSR of the curved mirror C9	22
12	Precession of the reflected beam due to axial asymmetry of a curved mirror .	24
13	Setup for curvature center measurement	24
14	Definition of the mirror angles	25
15	Geometrical analysis of the curvature center measurement.	25
16	Measurement of the reflected beam precession.	26
17	Graphical representation of the derived positions of the curvature minimum.	27
18	Horizontal wedge measurement	28
19	Vertical wedge measurement	28
20	Principle of the perpendicularity test.	31
21	The test setup for the prism perpendicularity.	32
22	Typical view of the autocollimator and the result analysis.	32
23	Coating A specification.	35
24	Coating B specification.	35
25	Coating C specification.	35
26	Coating D specification.	36
27	Coating E specification.	36
28	AR Coating ACD specification.	36
29	AR Coating BE specification.	36
30	Scattering measurement for the two flat OMC cavity mirrors	40

31	Scattering measurement for the two curved OMC cavity mirrors	41
32	Measured thicknesses of the PZTs	43
33	PZT assembly No.1 gluing sheet	46
34	PZT assembly No.2 gluing sheet	46
35	PZT assembly No.3 gluing sheet	46
36	PZT assembly No.4 gluing sheet	47
37	PZT assembly No.5 gluing sheet	47
38	PZT assembly No.6 gluing sheet	47
39	PZT assembly No.3 gluing sheet actual	48
40	PZT assembly No.4 gluing sheet actual	48
41	PZT assembly No.7~10 gluing sheet	49
42	PZT endurance test: Driving voltage monitor.	51
43	PZT endurance test: Teperature monitor setup.	52
44	Thermal vision of the PZTs before the actuation.	52
45	Thermal vision of the PZTs during the actuation.	52
46	Teperature change of the PZTs	53
47	Reverse voltage test of the PZT	53
48	Test result of DCPD SN:4, typical good diode performance	57
49	Test result of DCPD SN:1	58
50	Test result of DCPD SN:2	58
51	Test result of DCPD SN:3	58
52	Test result of DCPD SN:5	58
53	Test result of DCPD SN:6	58
54	Test result of DCPD SN:7	58
55	Test result of DCPD SN:8	59
56	Test result of DCPD SN:9	59
57	Test result of DCPD SN:10	59
58	Test result of DCPD SN:11	59
59	Test result of DCPD SN:12	59
60	Test result of DCPD SN:13	59
61	Measured quantities on the photodiode efficiency.	60

62	Reflectivity of IGHQEX3000	64
63	Reflectivity of C30665	64
64	Dark current measurement of the diodes	65
65	Dark Current Comparison with other similar photodiodes in hand	65
66	Quantum efficiency reduction after the air baking	68
67	Dark noise of C30665GH 07	69
68	Dark noise of IGHQEX3000 A1-23	69
69	Dark noise of IGHQEX3000 A1-25	69
70	Dark noise of IGHQEX3000 B1-01	69
71	Dark noise of IGHQEX3000 B1-16	70
72	Dark noise of IGHQEX3000 B1-22	70
73	Dark noise of IGHQEX3000 B1-23	70
74	Dark noise of IGHQEX3000 C1-03	70
75	Dark noise of IGHQEX3000 C1-05	70
76	Dark noise of IGHQEX3000 C1-07	70
77	Dark noise of IGHQEX3000 C1-08	71
78	Dark noise of IGHQEX3000 C1-09	71
79	Dark noise of IGHQEX3000 C1-10	71
80	Dark noise of IGHQEX3000 C1-11	71
81	Dark noise of IGHQEX3000 C1-12	71
82	Dark noise of IGHQEX3000 C1-14	71
83	Dark noise of IGHQEX3000 C1-17	72
84	Dark noise of IGHQEX3000 C1-21	72
85	Dark noise of IGHQEX3000 D1-08	72
86	Dark noise of IGHQEX3000 D1-10	72
87	Electrical diagrams for the high power illumination test	74
88	C30665 PD: dark current measurements after the high power beam illumination	75
89	C30665 PD: surface image after the high power beam illumination	75
90	IGHQEX3000 PD: dark current measurements after the high power beam illumination	76
91	IGHQEX3000 PD: surface image after the high power beam illumination	76

92	System diagram for the DCPD capacitance measurement	77
93	Capacitance measurements for IGHQEX3000 photodiodes	78
94	Capacitance measurements for C30665 photodiodes	78
95	Calibration of various power meters against aLIGO Pcal integrated sphere .	80
96	Optical setup for the OMC test.	83
97	Mode-matching telescope for the OMC cavity.	83
98	The actual setting of the mode matching telescope.	83
99	Beam profile measurement for the OMC cavity mode-matching.	84
100	Photo of the transission monitor CCD when the cavity is locked.	84
101	Photo of the reflection monitor CCD when the cavity is locked.	84
102	Electrical setup for the OMC test.	85
103	Measurements of the backscatter reflection	92
104	Measurement setup of the backscatter reflection (1)	94
105	Dependence of the detected backscattered power on the aperture size	94
106	Measurement setup of the backscatter reflection (2-1)	96
107	Measurement setup of the backscatter reflection (2-2)	96
108	Prism mirrors used for the backscatter reflection measurements	97
109	Prism mirrors used for the backscatter reflection measurements	97
110	Vibrational test of the OMC breadboard	102
111	Vibrational test of the OMC breadboard (high resolution)	102
112	Vibrational test of the OMC shaking DCPDs	103
113	Vibrational test of the OMC shaking QPDs	103
114	Vibrational test of the OMC shaking CMs	104
115	Vibrational test of the OMC shaking FMs	104
116	Vibrational test of the OMC shaking BSs and SMs	105
117	Vibrational test of the OMC shaking BDs	105
118	Mode analysis of the tombstone prism (first mode: 12.3 kHz)	106
119	Mode analysis of the tombstone prism (second mode: 16.9 kHz)	106
120	Mode analysis of the DCPD housing (first mode: 2.9 kHz)	107
121	Mode analysis of the DCPD housing (second mode: 4.1 kHz)	107
122	Mode analysis of the QPD housing (first mode: 6.0 kHz)	107

123	Mode analysis of the QPD housing (second mode: 8.2 kHz)	107
124	Mode analysis of the PZT mirror subassembly (first mode: 10.0 kHz)	108
125	Mode analysis of the PZT mirror subassembly (second mode: 14.6 kHz)	108
126	Mode analysis of the PZT mirror subassembly (third mode: 18.0 kHz)	108
127	Mode analysis of the PZT mirror subassembly (fourth mode: 22.5 kHz)	108
128	Mode analysis of the PZT mirror subassembly (fifth mode: 29.7 kHz)	108
129	Simulated transfer function of the PZT actuation bonded on the breadboard	109
130	OMC(001): Cavity absolute length (FSR) measurement with detuned locking	111
131	OMC(001): Cavity length (FSR) and finesse measurement with RFAM injection	111
132	OMC(001): Vertical TMS measurement with no PZT voltages applied.	113
133	OMC(001): Horizontal TMS measurement with no PZT voltages applied.	113
134	OMC(001): Higher-order modes distribution with no PZT voltages applied.	114
135	OMC(001): Dependence of the vertical and horizontal TMSs on the PZT voltage	115
136	OMC(001): Modelled coincidental resonances of the higher-order modes	115
137	OMC(001): Summary of the power budget test (left half)	117
138	OMC(001): PZT sweep voltages and the OMC resonances.	118
139	OMC(001): PZT AC responses	118
140	OMC(001): Image analysis for the DCPD1 shim height	119
141	OMC(001): Image analysis for the DCPD2 shim height	119
142	OMC(001): Image analysis for the QPD1 shim height	119
143	OMC(001): Image analysis for the QPD2 shim height	119
144	OMC(001): Arrangement of the QPD segments (beam view)	120
145	OMC(001): DCPD1 final spot position	121
146	OMC(001): DCPD1 reflection on the beam dump	121
147	OMC(001): DCPD2 final spot position	121
148	OMC(001): DCPD2 reflection on the beam dump	121
149	OMC(001): QPD1 final spot position	122
150	OMC(001): FM1 final spot position	122
151	OMC(001): FM2 final spot position	122
152	OMC(001): CM1 final spot position	123

153	OMC(001): CM2 final spot position	123
154	OMC(001): Balance mass distribution (upper)	123
155	OMC(002): Cavity absolute length (FSR) measurement with detuned locking	125
156	OMC(002): Cavity length (FSR) and finesse measurement with RFAM injection	125
157	OMC(002): Cavity finesse measurement with RFAM injection	126
158	OMC(002): Vertical TMS measurement with no PZT voltages applied. . . .	128
159	OMC(002): Horizontal TMS measurement with no PZT voltages applied. . .	128
160	OMC(002): Higher-order modes distribution with no PZT voltages applied. .	129
161	OMC(002): Dependence of the vertical and horizontal TMSs on the PZT voltages	130
162	OMC(002): Modelled coincidental resonances of the higher-order modes . . .	130
163	OMC(002): PZT sweep voltages and the OMC resonances.	132
164	OMC(002): PZT AC responses	132
165	OMC(002): Image analysis for the DCPD1 shim height	133
166	OMC(002): Image analysis for the DCPD2 shim height	134
167	OMC(002): Image analysis for the QPD1 shim height	134
168	OMC(002): Image analysis for the QPD2 shim height	135
169	OMC(002): Arrangement of the QPD segments (beam view)	135
170	OMC(002): DCPD1 final spot position	136
171	OMC(002): DCPD1 reflection on the beam dump	136
172	OMC(002): DCPD2 final spot position	136
173	OMC(002): DCPD2 reflection on the beam dump	136
174	OMC(002): QPD1 final spot position	137
175	OMC(002): QPD2 final spot position	137
176	OMC(002): FM1 final spot position	137
177	OMC(002): FM2 final spot position	137
178	OMC(002): CM1 final spot position	138
179	OMC(002): CM2 final spot position	138
180	OMC(002): CM1 burnt spot	139
181	OMC(003): Cavity absolute length (FSR) measurement with detuned locking	141
182	OMC(003): Cavity length (FSR) and finesse measurement with RFAM injection	142

183	OMC(003): Cavity finesse measurement with RFAM injection	142
184	OMC(003): Vertical TMS measurement with no PZT voltages applied. . . .	144
185	OMC(003): Horizontal TMS measurement with no PZT voltages applied. . .	144
186	OMC(003): Higher-order modes distribution with no PZT voltages applied. .	145
187	OMC(003): Dependence of the vertical and horizontal TMSs on the PZT voltages	146
188	OMC(003): Modelled coincidental resonances of the higher-order modes . . .	146
189	OMC(003): PZT sweep voltages and the OMC resonances.	148
190	OMC(003): PZT AC responses	148
191	OMC(003): Arrangement of the QPD segments (beam view)	149
192	OMC(003): DCPD1 final spot position	149
193	OMC(003): DCPD2 final spot position	149
194	OMC(002R2): Cavity absolute length (FSR) measurement with detuned locking	151
195	OMC(002R2): Cavity length (FSR) and finesse measurement with RFAM injection	151
196	OMC(002R2): Vertical TMS measurement with no PZT voltages applied. . .	153
197	OMC(002R2): Horizontal TMS measurement with no PZT voltages applied. .	153
198	OMC(002R2): Higher-order modes distribution with no PZT voltages applied.	154
199	OMC(002R2): Dependence of the vertical and horizontal TMSs on the PZT voltages	155
200	OMC(002R2): Modelled coincidental resonances of the higher-order modes .	155
201	OMC(002R2): Summary of the power budget test (right half)	157
202	OMC(002R2): PZT sweep voltages and the OMC resonances.	158
203	OMC(002R2): PZT AC responses	158
204	OMC(002R2): Arrangement of the QPD segments (beam view)	159
205	OMC(002R2): DCPD1 final spot position	159
206	OMC(002R2): DCPD1 reflection on the beam dump	159
207	OMC(002R2): DCPD2 final spot position	160
208	OMC(002R2): DCPD2 reflection on the beam dump	160
209	OMC(002R2): QPD1 reflection on the beam dump	160
210	OMC(002R2): QPD2 reflection on the beam dump	160
211	OMC(002): Balance mass distribution (lower)	161

212	OMC(004): Cavity absolute length (FSR) measurement with detuned locking	163
213	OMC(004): Cavity length (FSR) and finesse measurement with RFAM injection	163
214	OMC(004): Cavity finesse measurement with RFAM injection	164
215	OMC(004): Vertical TMS measurement with no PZT voltages applied. . . .	165
216	OMC(004): Horizontal TMS measurement with no PZT voltages applied. . .	165
217	OMC(004): Higher-order modes distribution with no PZT voltages applied. .	166
218	OMC(004): Dependence of the vertical and horizontal TMSs on the PZT voltages	167
219	OMC(004): Modelled coincidental resonances of the higher-order modes . . .	167
220	OMC(004): PZT sweep voltages and the OMC resonances.	170
221	OMC(004): PZT AC responses	170
222	OMC(004): Arrangement of the QPD segments (beam view)	171
223	OMC(004): DCPD1 final spot position	172
224	OMC(004): DCPD1 reflection on the beam dump	172
225	OMC(004): DCPD2 final spot position	172
226	OMC(004): DCPD2 reflection on the beam dump	172
227	OMC(004): QPD1 reflection spot position	173
228	OMC(004): QPD2 reflection spot position	173
229	OMC(004): FM1 final spot position	173
230	OMC(004): FM2 final spot position	173
231	OMC(004): CM1 final spot position	174
232	OMC(004): CM2 final spot position	174
233	DCPD dimensions	177
234	Definition of the parameters for the cavity axes and mirror alignment	178
235	Preamp SNs and arrangement at LLO	180
236	Preamp SNs and arrangement at LHO	180
237	OMC Wiring - diagram as built	180
238	OMC Wiring - diagram as built (OLD)	181
239	OMC Wiring - diagram as built (OLD)	181

List of Tables

1	Summary of the curvature radii of the C mirrors	18
2	Derived positions of the curvature minimum.	27
3	Result of the wedge angle measurement.	29
4	Perpendicularity measurement for the mounting prisms.	33
5	Perpendicularity measurement for the Mirror As.	33
6	Perpendicularity measurement for the Mirror Bs.	33
7	Perpendicularity measurement for the Mirror Es.	34
8	Mirror transmission measurement for Mirror A.	38
9	Mirror transmission measurement for Mirror C.	38
10	Mirror transmission measurement for Mirror E.	39
11	Mirror transmission measurement for Mirror B.	39
12	PZT actuator response and length-to-angle coupling	44
13	Measured impedances of the 3mm, 2mm, and 1mm photodiodes.	56
14	Dark noise/current measurement for the 3mm InGaAs photodiodes	57
15	Measurement of the quantum efficiencies for the DCPD photodiodes.	61
16	Estimated responsivities and quantum efficiencies of the DCPD photodiodes.	62
17	Responsivities and QEs of the high QE DCPDs and other PDs	67
18	The dimensions and masses of the OMC glass breadboards	79
19	OMC(001): Summary of the cavity geometry tests	110
20	OMC(001): Summary of the power measurement taken after final cleaning on 2013/6/2	116
21	OMC(001): Measurement results for the QPDs and the derived spot positions	120
22	OMC(002): Summary of the cavity geometry tests	124
23	OMC(002): Summary of the power measurement taken after final cleaning on 2013/9/17	131
24	OMC(002): Measurement results for the QPDs and the derived spot positions	135
25	OMC(003): Summary of the cavity geometry tests	140
26	OMC(003): Summary of the power measurement taken after final cleaning on 2014/7/2	143
27	OMC(003): Measurement results for the QPDs and the derived spot positions	149
28	OMC(002R2): Summary of the cavity geometry tests	150

29 OMC(002R2): Summary of the power budget test 156

30 OMC(002R2): Measurement results for the QPDs and the derived spot positions 159

31 OMC(004): Summary of the cavity geometry tests 162

32 OMC(004): Summary of the power budget test 168

33 OMC(004): Measurement results for the QPDs and the derived spot positions 171

34 List and location for OMC breadboards and Mounting Prisms 175

35 List and location for Mirror A & B 175

36 List and locations for Mirror C & PZTs 176

37 List and locations for Mirror E 176

1 Objective and scope

The Advanced LIGO Output Mode Cleaner (OMC) is a suspended glass optical cavity for filtering radio-frequency optical sidebands and higher-order modes in the output beam of the interferometer. The cavity optics, peripheral optics, suspension interface, photodiodes for signal readout, and interface for electrical connections are built on a single fused silica glass breadboard.

The goal of this report is to provide a one-stop documentation that describes various optical tests of the OMCs performed before they are installed at the sites.

The structure of this document is as follows:

- Section 2 describes various component tests that have been done before they were integrated to the OMC breadboard.
- Section 3 describes various tests for the integrated OMC cavity on the glass breadboard.
- Appendix describes additional information to keep the record of the optics inventory and installation information, as well as some results of useful calculations.

2 Test of individual optical components

2.1 Characterization of the curved mirrors

[External Link]

[LIGO-E1101088: aLIGO OMC Curved Optics Specification](#)

2.1.1 Curvature radii for the curved mirrors

Radii of curvature of the curved mirrors were evaluated by measuring a round-trip gouy phase of a fabry-perot cavity.

[External Link]

http://nodus.ligo.caltech.edu:8080/OMC_Lab/22

http://nodus.ligo.caltech.edu:8080/OMC_Lab/30

http://nodus.ligo.caltech.edu:8080/OMC_Lab/31

http://nodus.ligo.caltech.edu:8080/OMC_Lab/41

http://nodus.ligo.caltech.edu:8080/OMC_Lab/42

http://nodus.ligo.caltech.edu:8080/OMC_Lab/49

[Description]

The curved mirrors of the OMC are designed to have the radius of curvature of 2.5m. This number was necessary to be confirmed with a measurement. A Fabry–Perot cavity was formed by a curved mirror and a flat prism mirror of the OMC. The curvature of the curved

mirror was estimated from the ratio between the free spectral range (FSR) and the transverse mode spacing (TMS) of the cavity, assuming the flat mirror has negligibly small curvature.

[Experimental method]

The setup was built on the optical table at ATF. The optical and electrical setups are shown in Figure 1) and Figure 2), respectively. A Fabry–Perot cavity was formed by an OMC flat mirror (“A” coating) and a curved mirror (“C” coating). The cavity was locked with the PDH technique. The phase modulation was applied at 32.7MHz with a resonant EOM. The reflected light from the cavity was detected by a broadband photodetector (Thorlabs PDA255, BW \sim 50MHz). The output signal was demodulated at the LO frequency. Newport LB1005 Servo Box was used for the servo filter. The laser frequency was actuated with the laser fast PZT.

In order to measure the FSR and TMS of the cavity, the technique in [1] was used. The additional phase modulation was applied using an broadband EOM with the modulation frequency scanned by a network analyzer. The input beam of the cavity was misaligned in pitch or yaw. The broadband photodetector (BBPD: Newfocus 1801, BW: 125MHz, Si photodiode) is placed at the cavity transmission. The network analyzer measured the transfer function between the excitation to the BB EOM and the BBPD output. The transfer function exhibited the peaks associated with the transverse modes when the clipping is introduced to the BBPD.

The transfer function has a repetitive structure with the spacing by the FSR. In addition, the transfer function becomes symmetric with regard to the TEM00 resonances, because the phase modulation by an EOM introduces symmetric modulation sidebands to the carrier. For example, the peaks associated with the 1st-order higher-order modes, appears at $f = nf_{\text{FSR}} \pm f_{\text{TMS}}$. The FSR and the TMS can be obtained by measuring the frequency of the first three peaks for the 1st-order higher-order modes. Once f_{FSR} and f_{TMS} are obtained separately, the curvature of the curved mirror is obtained from the following formula, assuming the flat mirror has sufficiently large radius of curvature:

$$R_{\text{RoC}} = \frac{L}{1 - \cos^2(\pi f_{\text{TMS}}/f_{\text{FSR}})}$$

[Result]

The measured transfer functions are shown as Figures 3~11 together with the peak fitting data. Each peak was fitted with a Lorentzian $H(f)$:

$$H(f) = \frac{a_0}{\sqrt{1 + (f - f_0)^2/\gamma^2}},$$

where a_0 , f_0 , and γ are the fitting parameters.

The summary of the curvature measurement is found in Table 1. The average RoC is

$$\overline{R_{\text{RoC}}} = 2.575 \pm 0.005 \text{ [m]},$$

when C2, C7, C8 are excluded.

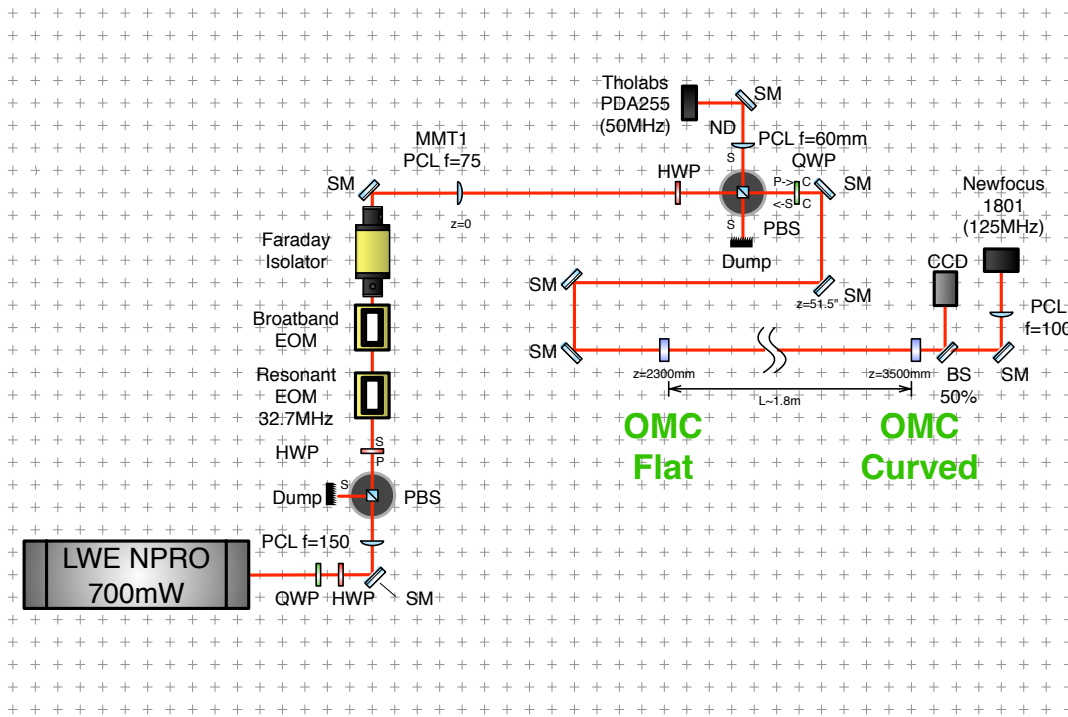


Figure 1: Optical setup for the mirror curvature measurement.

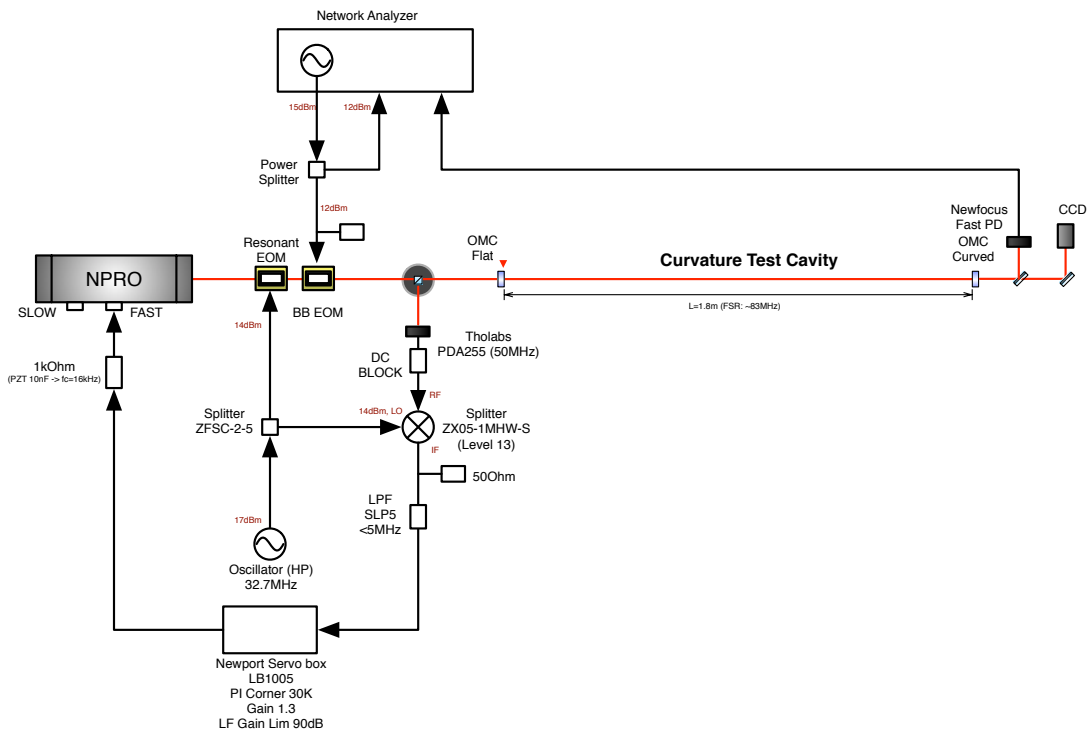


Figure 2: Electrical setup for the mirror curvature measurement.

Mirror serial	RoC [m]	note
C1	$2.57845 \pm 4.2 \times 10^{-5}$	
C2	$2.54363 \pm 4.9 \times 10^{-5}$	excluded
C3	$2.57130 \pm 6.3 \times 10^{-5}$	
C4	$2.58176 \pm 6.8 \times 10^{-5}$	
C5	$2.57369 \pm 9.1 \times 10^{-5}$	
C6	$2.57321 \pm 4.2 \times 10^{-5}$	
C7	$2.56244 \pm 4.0 \times 10^{-5}$	excluded
C8	$2.56291 \pm 4.7 \times 10^{-5}$	excluded
C9	$2.57051 \pm 6.7 \times 10^{-5}$	

Table 1: Summary of the curvature radii of the C mirrors

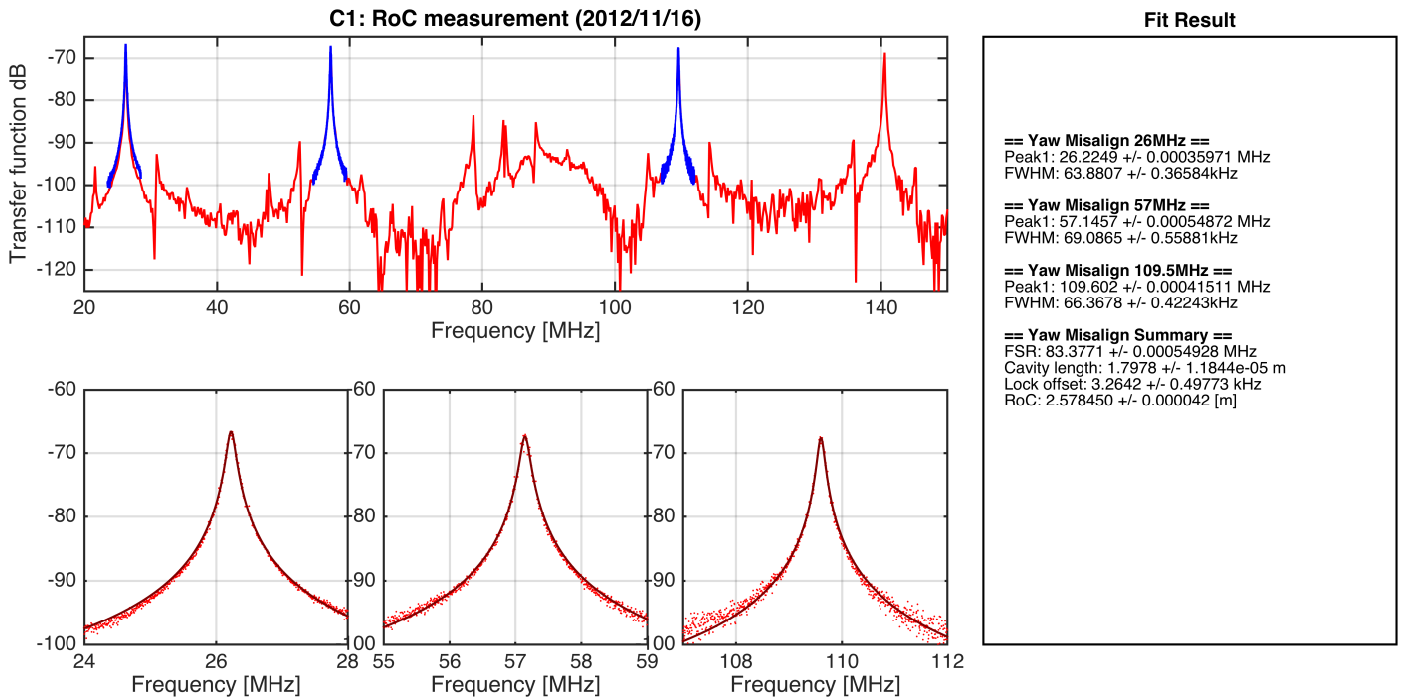


Figure 3: Measured TMS/FSR of the curved mirror C1

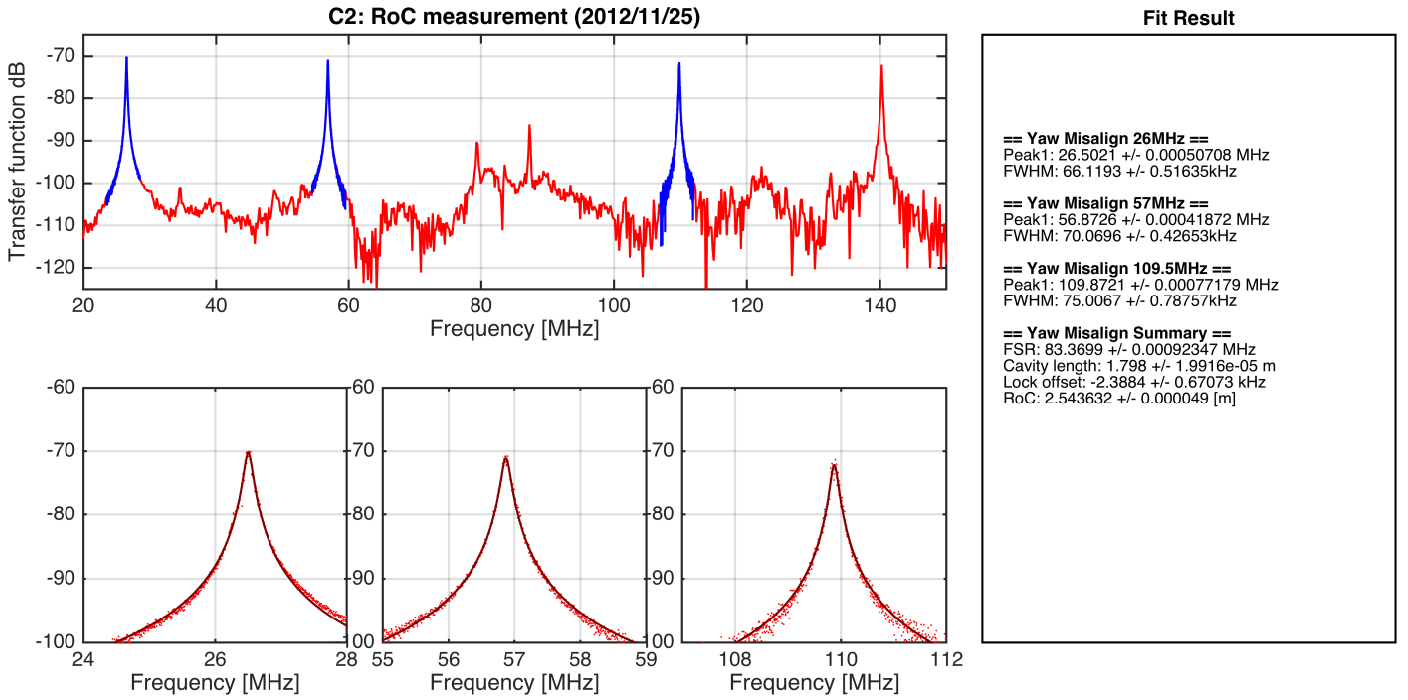


Figure 4: Measured TMS/FSR of the curved mirror C2

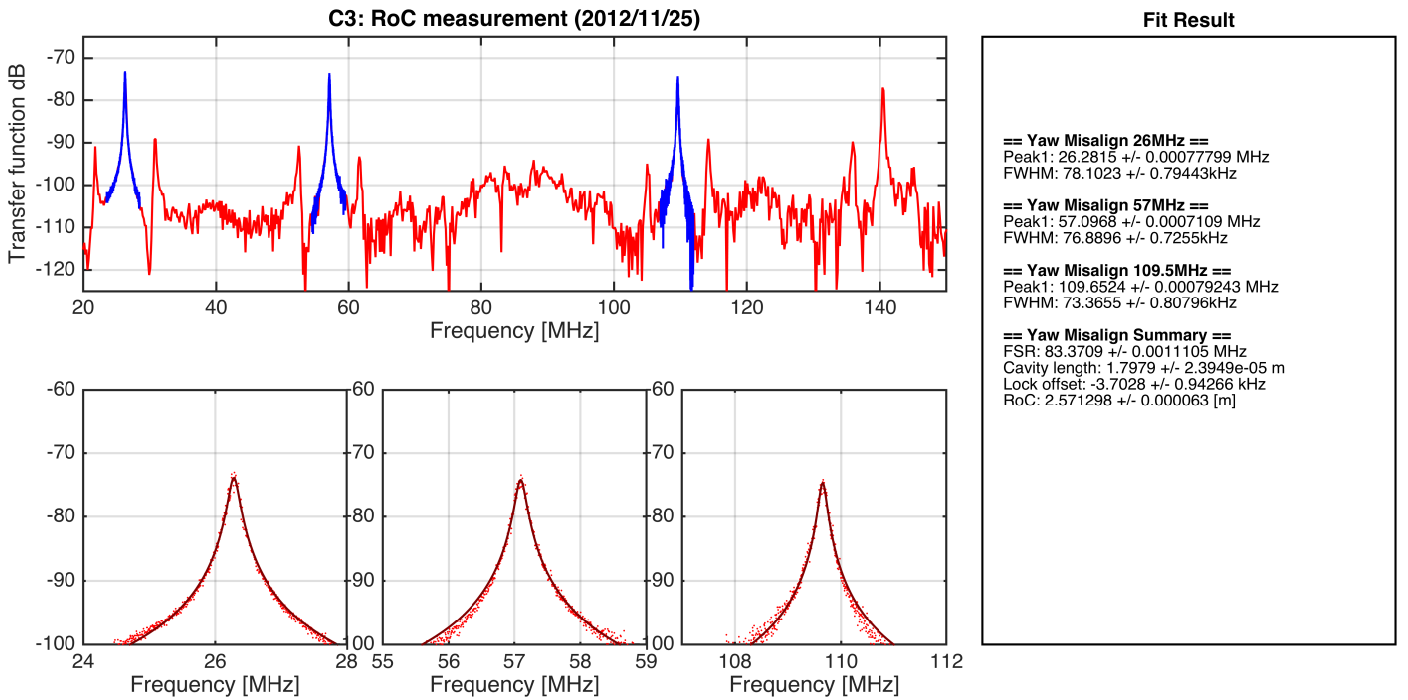


Figure 5: Measured TMS/FSR of the curved mirror C3

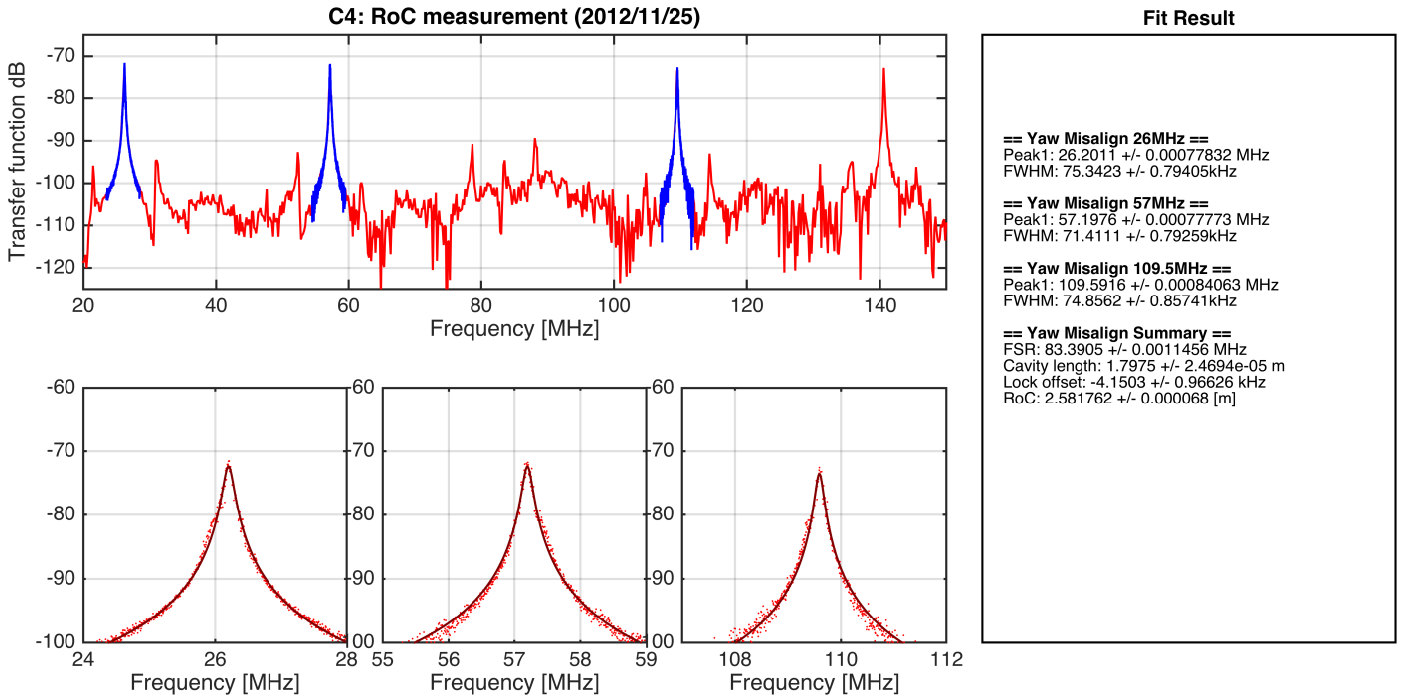


Figure 6: Measured TMS/FSR of the curved mirror C4

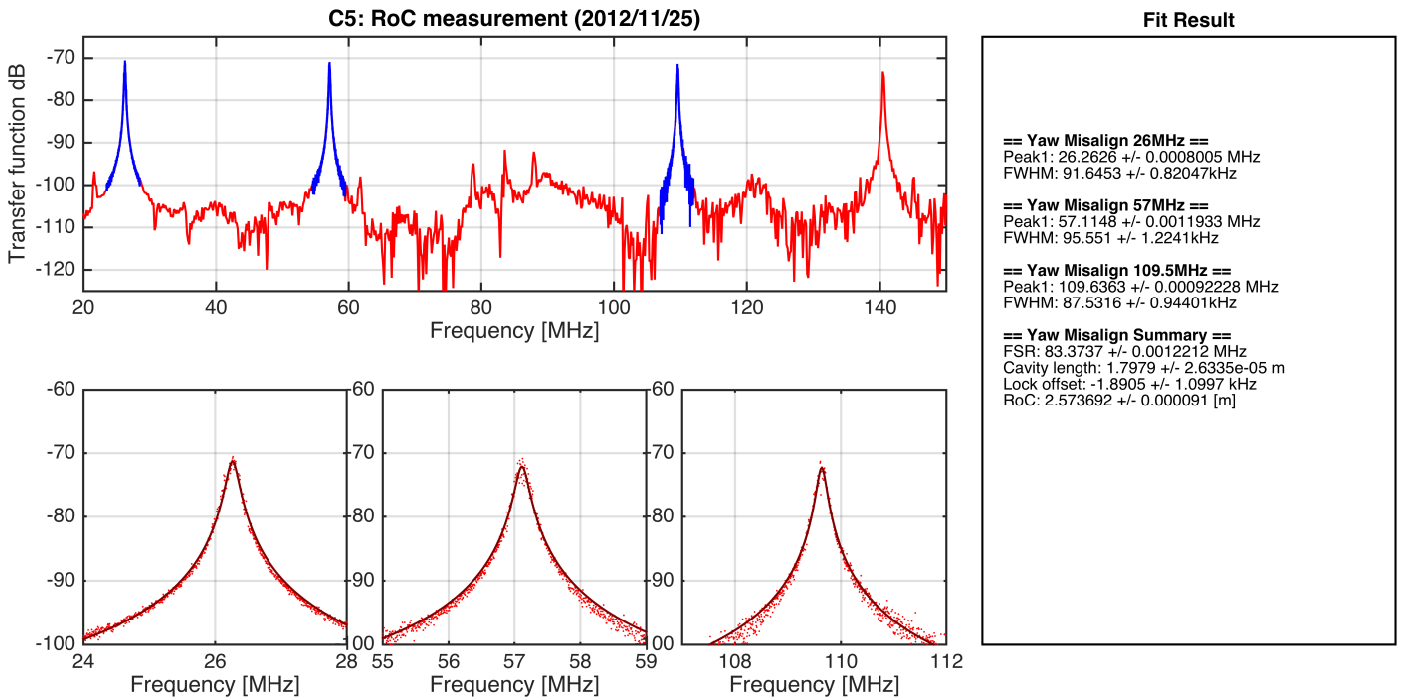


Figure 7: Measured TMS/FSR of the curved mirror C5

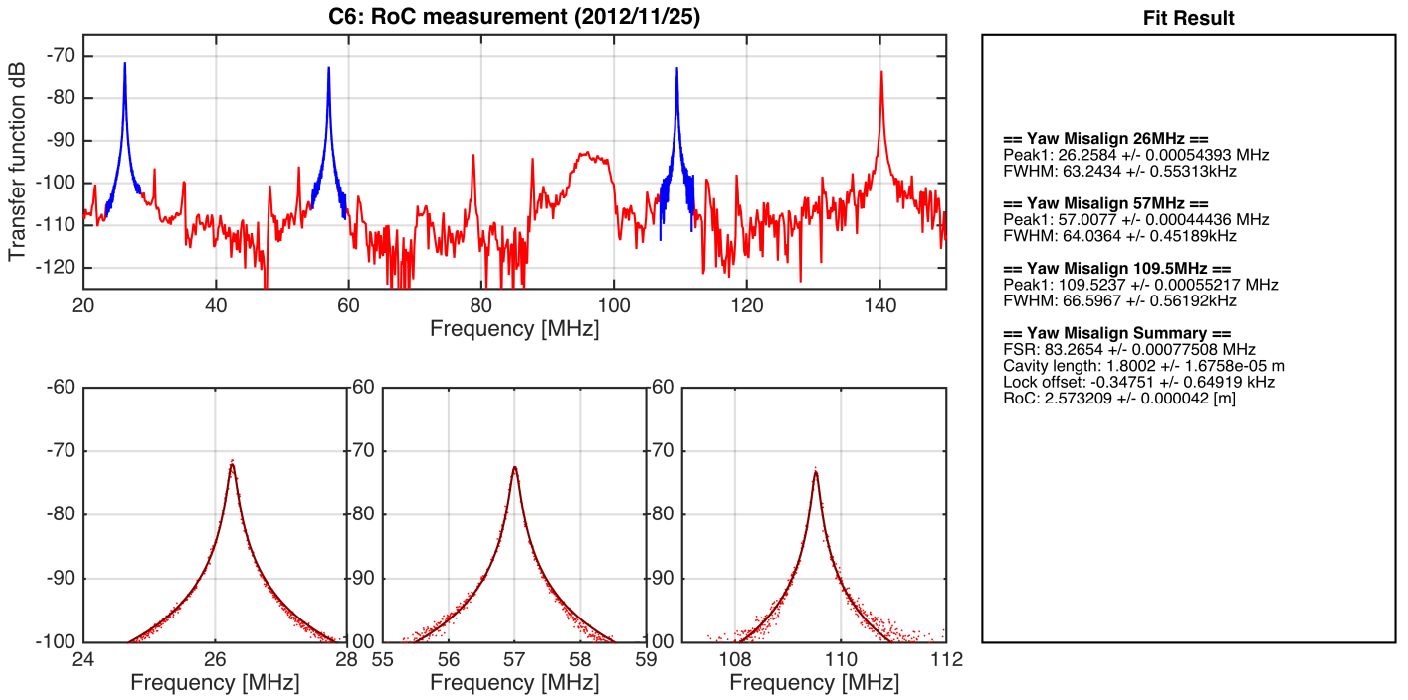


Figure 8: Measured TMS/FSR of the curved mirror C6

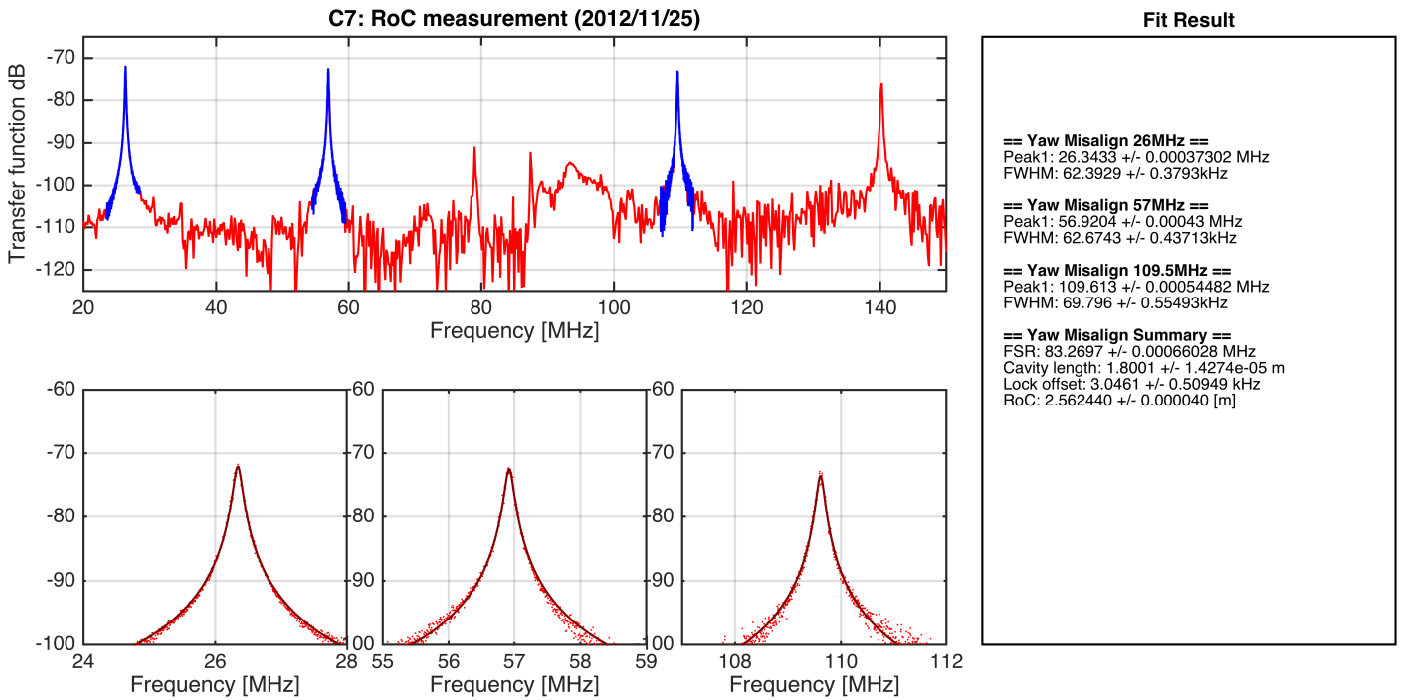


Figure 9: Measured TMS/FSR of the curved mirror C7

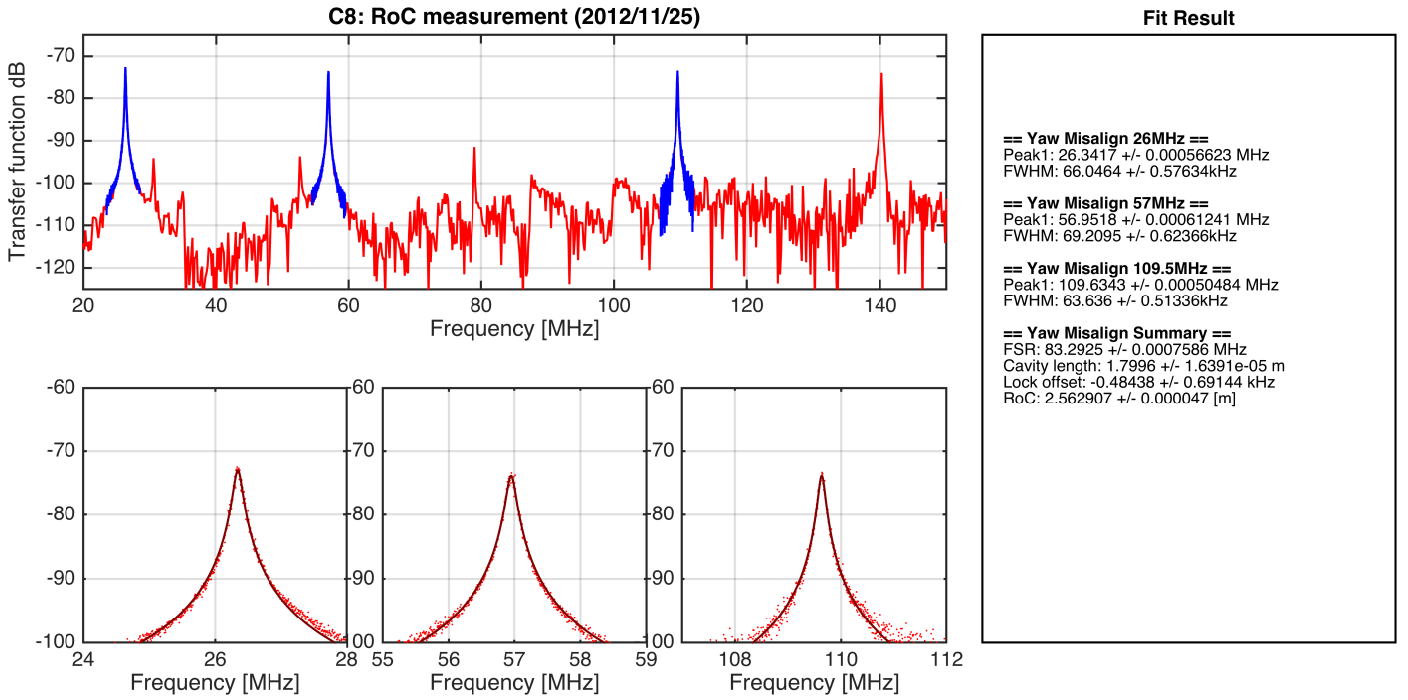


Figure 10: Measured TMS/FSR of the curved mirror C8

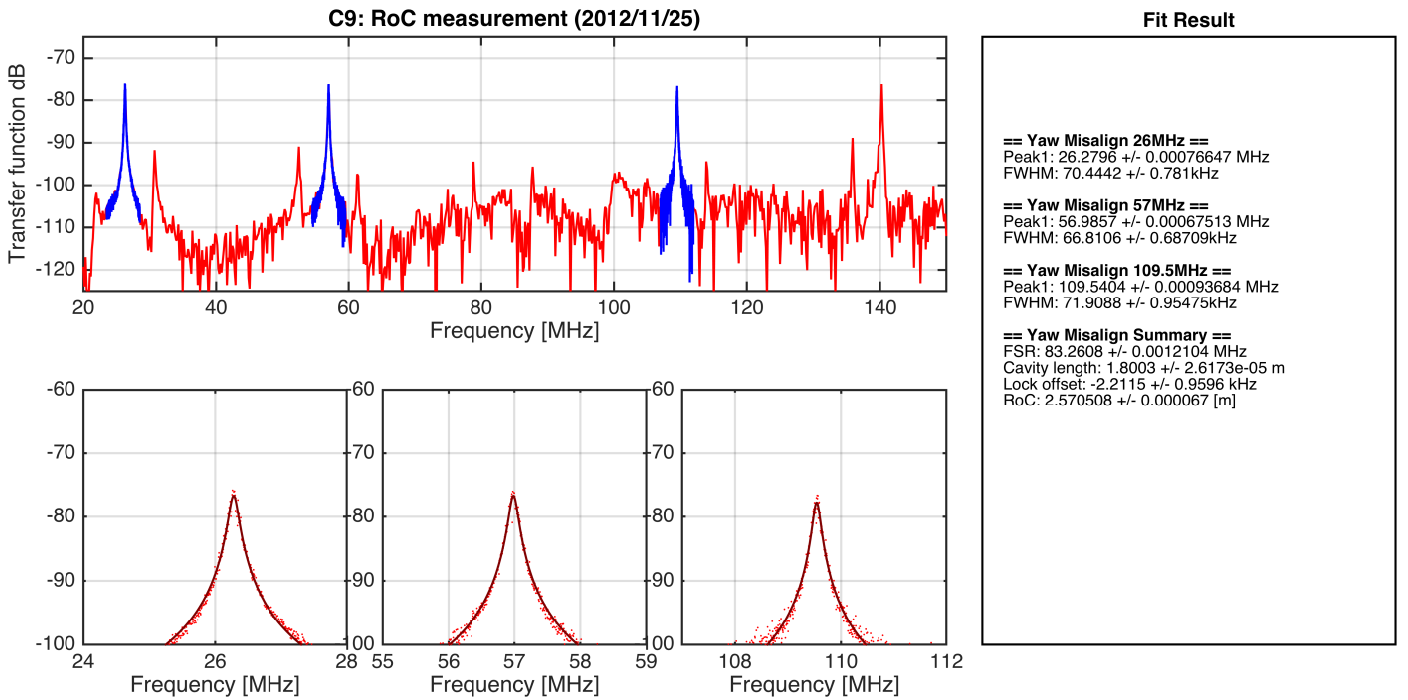


Figure 11: Measured TMS/FSR of the curved mirror C9

2.1.2 Thickness of the curved mirrors

[External Link]

http://nodus.ligo.caltech.edu:8080/OMC_Lab/50

[Description]

The curved mirror specification (E1101088) does not specify precise thickness of the curved mirror. We need to specify the position of the reflecting surface for the OMC cavity, we needed to know the thickness of the curved mirrors.

[Experimental method]

A micrometer gauge was used to measure the thickness of a curved mirror. Therefore this measurement has a risk to be destructive for the reflecting coating. Therefore, one of the worst mirrors in terms of the curvature (Section 2.1.1 was preselected for this measurement.

Took three points of the mirror edges separated by 120 degree to have some statistics.

[Result]

The curved mirror “C2” was used for this measurement.

Micrometer readings: (0.2478, 0.2477, 0.2477) in inch \implies (6.294, 6.292, 6.292) in mm

This gives us the thickness of 6.3mm.

2.1.3 Characterization of the curvature center

Locations of the curvature minimum on the OMC curved mirrors have been measured.

[External Link]

LIGO-D1300185: aLIGO OMC Curved Mirror Bonding Fixture Assembly
http://nodus.ligo.caltech.edu:8080/OMC_Lab/91

[Description]

When a curved mirror is misaligned, the location of the curvature center moves. We have to be aware of this effect because our curved mirror is going to be attached on a mounting prism (via a PZT) with the back surface of the mirror. This means that each curved mirror has inherent misalignment if the curvature minimum of the curved mirror is shifted from the center of the mirror. Since we have no ability to control mirror pitch angle once it is glued on the prism, the location of the curvature minimum should be characterized so that we can push all of the misalignment in the horizontal direction.

[Experimental method]

- Principle

When a curved mirror is completely axisymmetric (in terms of the mirror shape), any rotation of the mirror does not induce change on the axis of the reflected beam. If the curvature minimum deviates from the center of the mirror, the reflected beam suffer precession. As we want to precisely rotate the mirror, we use the gluing fixture for the PZT subassembly

(D1300185). In this method, the back surface of the curved mirror is pushed on the mounting prism, and the lateral position of the mirror is precisely defined by the fixture. As you rotate the mirror in clockwise viewing from the front, the spot moves in counter clockwise on the CCD

(Figure 12).

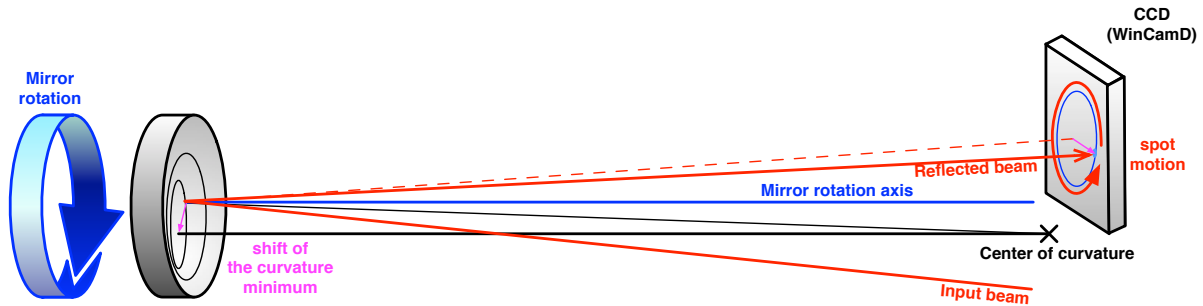


Figure 12: Precession of the reflected beam due to axial asymmetry of a curved mirror

- Setup and procedure

The measurement setup is shown in Figure 12. The mounting prism (#21) is placed on the gluing fixture. A curved mirror under the test is loaded in the fixture with no PZT, i.e. the back surface is aligned by the mounting prism. The fixing pressure is applied to the curved mirror by the front plate with spring loads. The mirror needs be pushed from the top at least once to seat on its defined position in the fixture. The incident beam is slightly slanted for the detection of the reflected spot. The beam is aligned to hit the center of the mirror as much as possible.

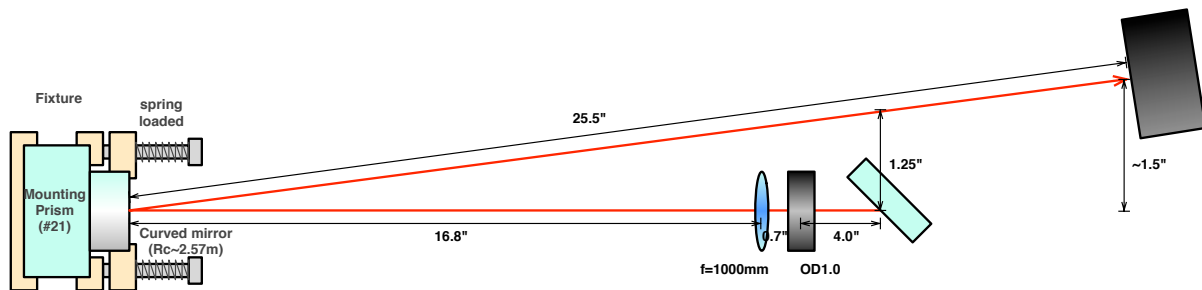


Figure 13: Setup for curvature center measurement

The position of the reflected spot on the CCD (WinCamD) is recorded, while the mirror is rotated 90 deg at once. The rotation of the mirror is defined as shown in Figure 14. The angle origin is defined by the arrow mark of the mirror and rotated in clockwise being viewed from the front face. The mirror is rotated 540 deg (8 points) to check reproducibility.

[Result]

Measured 8 points for each mirror is fitted by a circle. The fitting result provides the origin and radius of the circle, and the angle correspond to mirror angle of 0 deg.

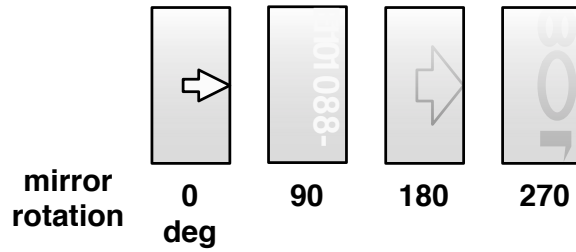


Figure 14: Definition of the mirror angles

The geometrical analysis of the measurement is shown in Figure 15. Here is the description of the symbols:

- d : distance of the curvature minimum and the mirror center (quantity to be derived)
- D : distance of the prove beam spot from the center of the mirror
- R : Radius of curvature of the mirror
- θ_R : angle of incidence/reflection

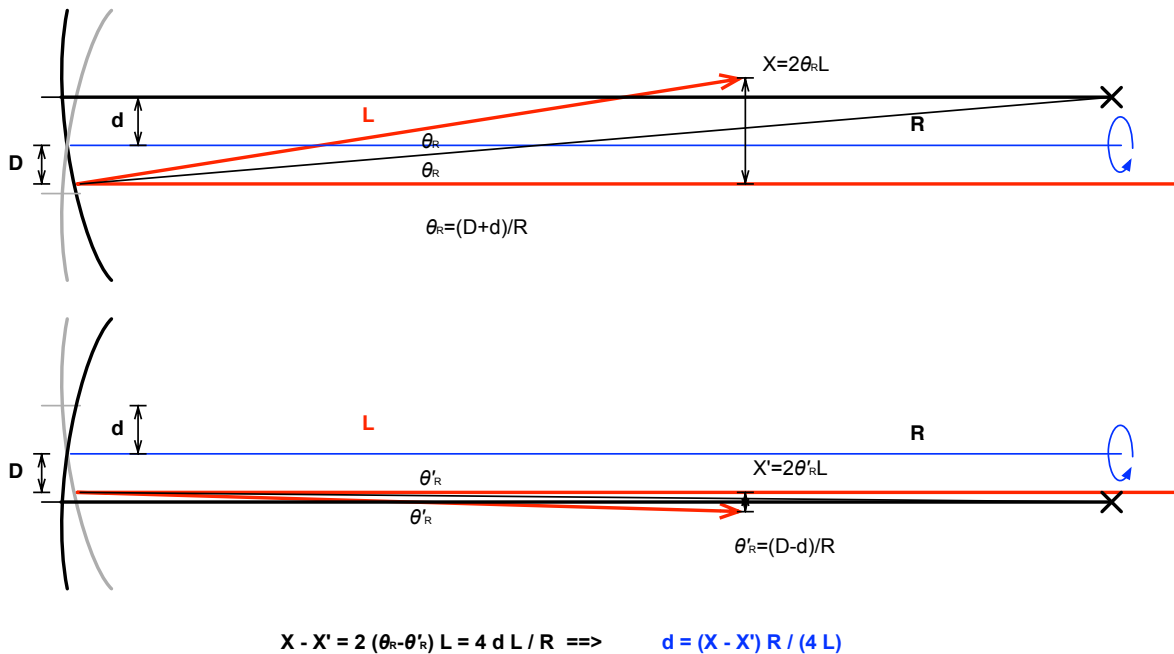


Figure 15: Geometrical analysis of the curvature center measurement. The upper figure shows the top view of the setup in the case when the curvature center is uppermost in the figure. The lower figure shows when the mirror is 180 deg rotated from the upper figure case.

The interesting consequence is that precession diameter $(X - X')$ on the CCD does not depend on the spot position on the mirror. This ensures the precision of the measurement.

In the measurement, the radius of the precession ($r = (X - X')/2$) is obtained. Therefore, we derive

$$d = \frac{rR}{2L}$$

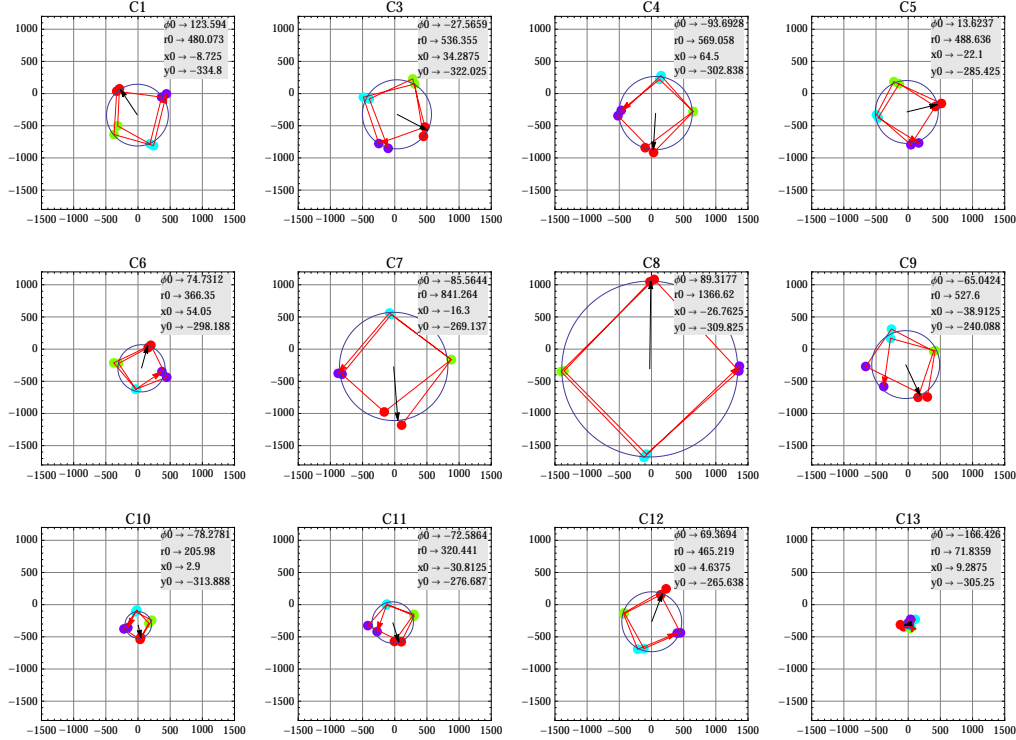


Figure 16: Measurement of the reflected beam precession. The units for the distance and angle is μm and deg.

The result of the analysis is found in Table 2. In the table, d is the distance of the curvature minimum from the mirror center, and ϕ is the angle of the minimum from the horizontal line at the center of the mirror.

2.2 Characterizations of the OMC prism mirrors

2.2.1 Wedge angle measurement

The wedge angles of the prism mirrors were measured with an autocollimator (“AC”) and a rotary stage.

[External Link]

LIGO-E1101086: OMC Optical Prisms

http://nodus.ligo.caltech.edu:8080/OMC_Lab/56

http://nodus.ligo.caltech.edu:8080/OMC_Lab/59

http://nodus.ligo.caltech.edu:8080/OMC_Lab/66

Datasheet: HPFS Fused Silica Standard Grade, Corning

[Description]

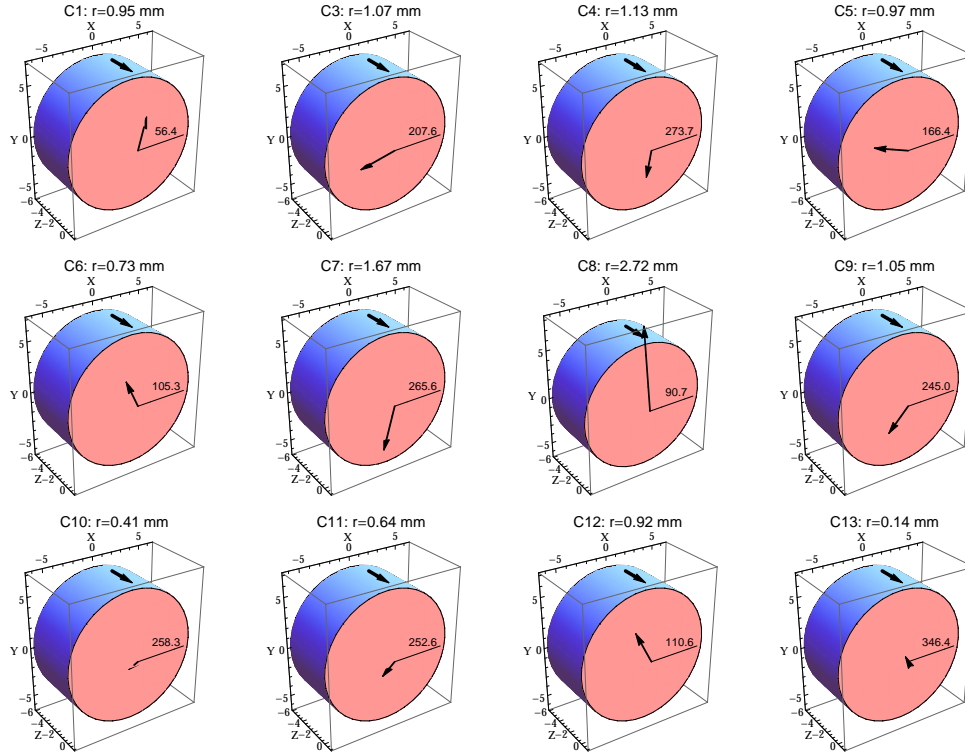


Figure 17: Graphical representation of the derived positions of the curvature minimum. The cylinder represents the curved mirror with an arrow mark at the top. The end of the arrow on the face represents the position of the curvature minimum.

Mirror serial	d [mm]	ϕ [deg]
C1	0.95	56.4
C3	1.07	207.6
C4	1.13	273.7
C5	0.97	166.4
C6	0.73	105.3
C7	1.67	265.6
C8	2.72	90.7
C9	1.05	245.0
C10	0.41	258.3
C11	0.64	252.6
C12	0.92	110.6
C13	0.14	346.4

Table 2: Derived positions of the curvature minimum.

The prism mirrors are wedged by 0.5 degree (30 arcmin). If the wedge angle is too much off from the specification, this may cause unexpected beam deflection. In order to check the wedge angle, the angle between the prompt and backside reflections were measured.

[Experimental method]

A prism mirror is set on a horizontal rotational stage. Realize the retroreflection for the front surface. Then realize the retroreflection for the back surface by rotating the stage. This angle difference α is related to the wedge angle θ_H with the following formula (see Figure 18):

$$\theta_H = \arcsin\left(\frac{\sin \alpha}{n}\right)$$

Here the refractive index is $n=1.462$ for green filter approximately at 500nm, according to the datasheet by Corning.

Horizontal wedge measurement

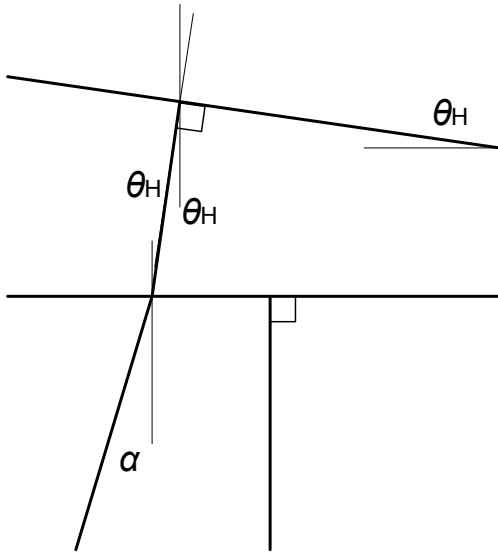


Figure 18: Horizontal wedge measurement: difference of the incident angle for retroreflection condition.

Vertical wedge measurement

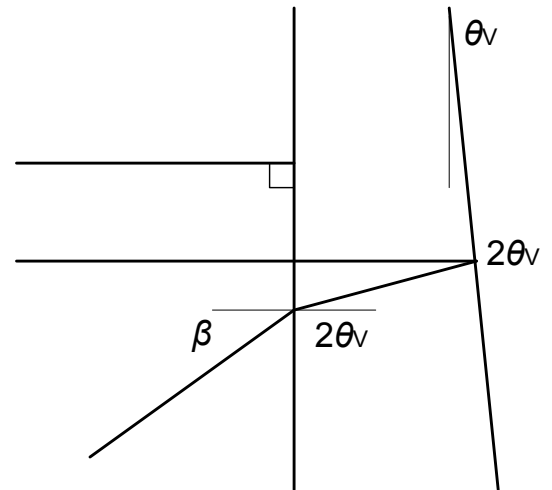


Figure 19: Vertical wedge measurement: difference between the front and back reflections.

There is no rotational adjustment in the vertical direction. Since the vertical wedge angle is expected to be small, it could be measured with the direct AC reading (Figure 19). Note that the AC is calibrated to show the angle that is required for the object to be rotated for making the view retroreflected. Therefore the direct reading angle is $\beta/2$ rather than β . The angle β and the wedge angle θ_V have the following relationship:

$$\theta_V = \frac{1}{2} \arcsin\left(\frac{\sin \beta}{n}\right)$$

Actual procedure is listed below:

Mirror Serial	α [deg]	β [arcmin]	θ_H [deg]	θ_V [deg]
A1	0.680	+0.0	0.465	+0.000
A2	0.800	-6.0	0.547	-0.034
A3	0.635	-1.6	0.434	-0.0091
A4	0.650	+0.0	0.445	+0.000
A5	0.655	+2.4	0.448	+0.014
A6	0.665	+3.0	0.455	+0.017
A7	0.635	+0.0	0.434	+0.000
A8	0.623	-0.4	0.426	-0.0023
A9	0.670	+2.4	0.458	+0.014
A10	0.605	+0.4	0.414	+0.0023
A11	0.640	+0.8	0.438	+0.0046
A12	0.625	-0.6	0.427	-0.0034
A13	0.630	+2.2	0.431	+0.013
A14	0.678	+0.0	0.464	+0.000
B1	0.665	+0.6	0.455	+0.0034
B2	0.615	+0.2	0.421	+0.0011
B3	0.620	+0.9	0.424	+0.0051
B4	0.595	+2.4	0.407	+0.014
B5	0.635	-1.8	0.434	-0.010
B6	0.640	+1.6	0.438	+0.0091
B7	0.655	+2.5	0.448	+0.014
B8	0.630	+2.8	0.431	+0.016
B9	0.620	-4.0	0.424	-0.023
B10	0.620	+1.2	0.424	+0.0068
B11	0.675	+3.5	0.462	+0.020
B12	0.640	+0.2	0.438	+0.0011
E1	0.672	+0.0	0.460	+0.000
E2	0.631	-0.3	0.432	-0.0017
E3	0.642	+0.0	0.439	+0.000
E4	0.659	+1.4	0.451	+0.0080
E5	0.695	+0.5	0.475	+0.0028
E6	0.665	-0.4	0.455	-0.0023
E7	0.652	+1.0	0.446	+0.0057
E8	0.675	+2.0	0.462	+0.011
E9	0.645	-2.4	0.441	-0.014
E10	0.640	+2.2	0.438	+0.013
E11	0.638	+1.6	0.436	+0.0091
E12	0.660	+1.6	0.451	+0.0091
E13	0.638	+0.8	0.436	+0.0046
E14	0.655	+0.4	0.448	+0.0023
E15	0.640	+1.4	0.438	+0.0080
E16	0.655	+0.6	0.448	+0.0034
E17	0.650	+0.8	0.445	+0.0046
E18	0.640	+2.4	0.438	+0.014

Table 3: Result of the wedge angle measurement.

- Prism mount: Thorlabs KM100P and PM3
- Rotational stage: Newport 481-A, 0.008deg (= 0.5 arcmin) resolution
- Attach the prism mount on the rotational stage. Mount the tombstone prism on a prism mount. the rotation stage.
- Locate the prism in front of the autocollimator.
- Find the retroreflected reticle in the view. Adjust the focus if necessary.
- Confirm that the rotation of the stage does not change the height of the reticle in the view. If it does, rotate the AC around its axis to realize it. This is to match the horizontal reticle to the rotation plane.
- Use the rotation stage and the alignment knobs to find the reticle at the center of the AC. Make sure the reticle corresponds to the front surface. **Record the micrometer reading.**
- Rotate the micrometer of the rotation stage until the retroreflected reticle for the back surface.
- There maybe the vertical shift of the reticle due to the vertical wedging. **Record the vertical shift.**
- **Record the micrometer reading.** Take a difference of the two micrometer readings.

[Result]

The measurement results are shown in Table 3. A2 prism showed a particularly big number but everything else actually showed a constant smaller number from the specification (0.5deg). This A2 prism should be excluded from the assembly. The mean and standard deviation excluding A2 are 0.441 ± 0.014 [deg]. This number should be reflected to the breadboard design. As far as we use the optics with the consistent wedge angle, the design of the breadboard is not affected.

2.2.2 Prism perpendicularity test

The perpendicularity of the prism optics were measured with an autocollimator.

[External Link]

http://nodus.ligo.caltech.edu:8080/OMC_Lab/63
http://nodus.ligo.caltech.edu:8080/OMC_Lab/64
http://nodus.ligo.caltech.edu:8080/OMC_Lab/65
http://nodus.ligo.caltech.edu:8080/OMC_Lab/369

[Description]

The OMC cavity optics have no internal adjustment for the pitch alignment because the two flat mirrors and the PZT subassemblies are glued on the breadboard directly. 10 arcsec (=2.8rad) of misalignment causes about 0.1mm shift of the beam. Therefore the front and bottom surfaces of the prisms have to have good perpendicularity. We set the requirement of the perpendicularity better than 30 arcsec. This should be confirmed.

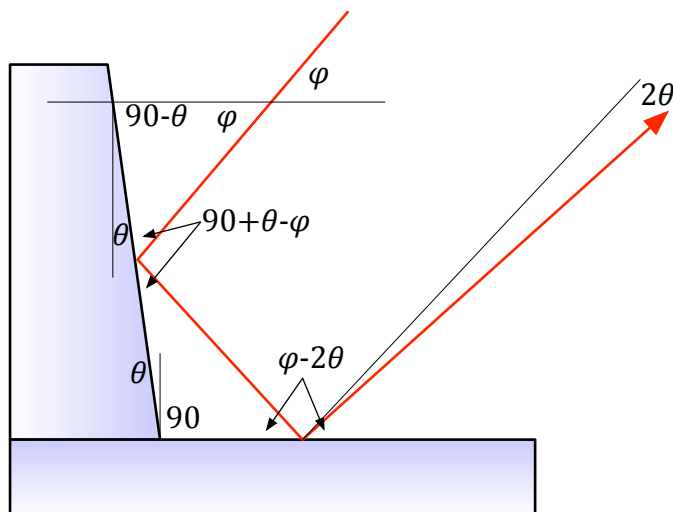


Figure 20: Principle of the perpendicularity test.

[Experimental method]

The perpendicularity of the prisms were checked with an autocollimator (AC).

Two orthogonally-joined surfaces form a 2D version of a corner cube, that retroreflects a beam towards the source regardless of the incident angle. When the joint has non-orthogonality of θ , the reflected image shows deviation from the retroreflection by 2θ (Figure 20). We can characterize this quantity with an autocollimator.

The schematic figure of the measurement setup is shown in Figure 21. In order to realize such a setup, the OMC prism optics were placed on an Al mirror. For ensuring the joint angle to be determined only by the optics, the surfaces of the joint were cleaned by Isopropanol every time when the mirror was placed. The AC illuminated the joint corner of the optics. The reflection from the optics was observed by the AC in order to determine the angle formed by the optics.

Typical view of the AC during the test is shown in Figure 22. When the image is retroreflected, only one horizontal line is observed in the view. If there is any deviation from the retroreflection, this horizontal line splits into two as the upper and lower halves have the angled wavefront by 4θ . The difference of the two horizontal bars in the view of the AC was calibrated in the angle. The deviation from the exact normal angle is a half of this measured angle between the two horizontal lines. The sign of the deviation can be determined by giving finger pressure on the mirror to tilt the prism.

[Result]

The results of the perpendicularity measurements are shown in Tables 4, 5, 6, and 7. Table 4 also lists the perpendicularity data, which has no sign, given from the manufacturer.

When the measured (and spec if exist) value shows the deviation from the normal angle less than 30 arcsec, it is indicated as “good”. The prisms only indicated as “good” should be used.

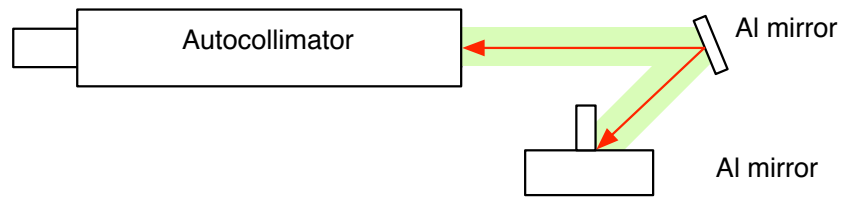
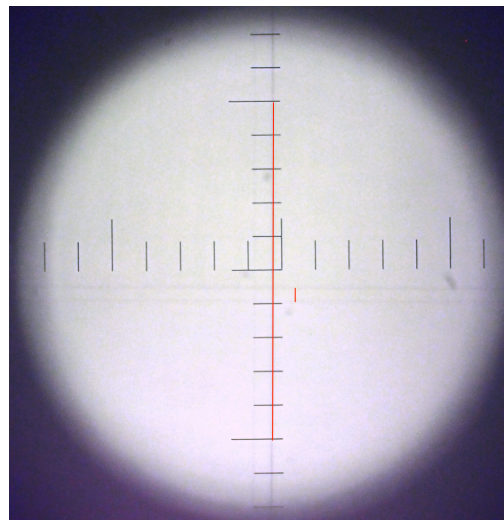
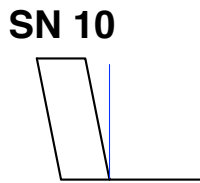


Figure 21: The test setup for the prism perpendicularity.



5.5709 vs 0.2222
= 0.3989 arcmin
= 0.01330 deg as the angle of two wavefront
 $\theta = +12.0$ arcsec

Figure 22: Typical view of the autocollimator and the result analysis.

SN #	Measurement in 2013		Measurement in 2019		Data Sheet [arcsec]	Note
	[div]	[arcsec]	[div]	[arcsec]		
10	0.399	12.0			29	good
11	0.220	6.6			16	good
16	0.191	5.7			5	good
20	-0.591	-17.7			5	good
21	-2.378	-71.3			15	
21	-1.7	-51.			15	
01	-0.5	-15.	-1.8	-54	52	
02	-2.5	-75.	-1.6	-48	48	
06	-1.0	-30.			15	good
07	1.7	51.			59	
12	-2.2	-66.	-1.8	-54	40	
13	-0.3	-9.			12	good
14	-2.8	-84.	-1.4	-42	27	
15	-2.5	-75.	-1.3	-39	50	
17	0.7	21.	+0.8	+24	48	
22	2.9	87.			63	

Table 4: Perpendicularity measurement for the mounting prisms. Requirement is the deviation of $< 30\text{arcsec}$.

SN #	Measurement in 2013		Measurement in 2019		Note	SN #	Measurement		Note
	[div]	[arcsec]	[div]	[arcsec]			[div]	[arcsec]	
A1	-0.5	-15.	+0.4	+12.	good	B1	-0.9	-27.	good
A3	0.5	15.	+0.8	+24.	good	B2	-0.6	-18.	good
A4	0.9	27.			good	B3	-0.9	-27.	good
A5	0.4	12.			good	B4	0.7	21.	good
A6	0.1	3.			good	B5	-1.1	-33.	
A7	0.0	0.			good	B6	-0.6	-18.	good
A8	0.0	0.			good	B7	-1.8	-54.	
A9	0.0	0.			good	B8	-1.1	-33.	
A10	1.0	30.	+0.6	+18.	good	B9	1.8	54.	
A11	0.3	9.	-0.25	-7.5	good	B10	1.2	36.	
A12	0.1	3.			good	B11	-1.7	-51.	
A13	0.0	0.			good	B12	1.1	33.	
A14	0.6	18.	+0.5	+15.	good				

Table 5: Perpendicularity measurement for the Mirror As.

Table 6: Perpendicularity measurement for the Mirror Bs.

SN #	Measurement [div]	Note [arcsec]	
E1	-0.8	-24.	good
E2	-0.8	-24.	good
E3	-0.2	-7.	good
E4	-0.5	-15.	good
E5	0.8	24.	good
E6	-1.0	-30.	good
E7	-0.2	-6.	good
E8	-0.8	-24.	good
E9	-1.0	-30.	good
E10	0.0	0.	good
E11	-1.0	-30.	good
E12	-0.3	-9.	good
E13	-0.8	-24.	good
E14	-1.0	-30.	good
E15	-1.2	-36.	
E16	-0.7	-21.	good
E17	-0.8	-24.	good
E18	-1.0	-30.	good

Table 7: Perpendicularity measurement for the Mirror Es.

2.2.3 Data sheet values for the mirror reflectivities and transmissivities

[External Link]

[LIGO-E1101095: Advanced LIGO Output Mode Cleaner Coating Specifications](#)

[Description]

Coating data sheets from G&H were inspected.

[Experimental method]

Estimate the coating specs from the data sheet. There are five HR surface coatings (A/B/C/D/E) and two AR coating runs (ACD for 4deg AOI and BE for 45deg AOI). From their wavelength dependence curves for transmission/reflection, the values are extracted.

[Result]

[HR coatings]

The coating spec from the vendor for HR coating A is shown in Figure 23. It shows the transmission of 7931 ppm.

The coating spec from the vendor for HR coating B is shown in Figure 24. It shows the transmission of 50.385%.

The coating spec from the vendor for HR coating C is shown in Figure 25. There seemed two coating runs and the vendor data shows the transmission of 51.48ppm and 48.40ppm.

The coating spec from the vendor for HR coating D is shown in Figure 26. It shows the transmission of 4089 ppm.

The coating spec from the vendor for HR coating E is shown in Figure 27. It shows the transmission of 7400 ppm.

[AR coatings]

The coating spec from the vendor for AR coating A/C/D is shown in Figure 28. There seemed three coating runs and the vendor data shows the reflection of 765, 585, and 439 ppm. The correspondence between which AR coating and which mirror are not specified.

The coating spec from the vendor for AR coating B/E is shown in Figure 29. There is no real specification but the vendor confirmed that the reflectivity was smaller than 0.1%.

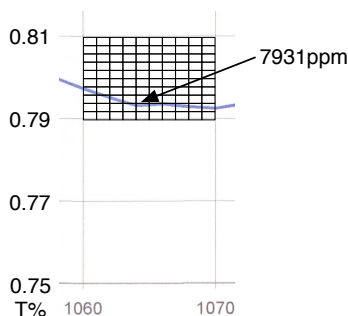


Figure 23: Coating A: Input/Output coupler, Side 1 HR, $T = 8300 \pm 800$ ppm @ 4 degrees AOI (best effort for ± 400 ppm)

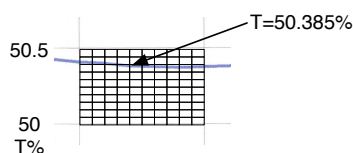


Figure 24: Coating B: Beam splitter, Side 1 50/50, $T = 50 \pm 2\%$ @ 45 degrees AOI

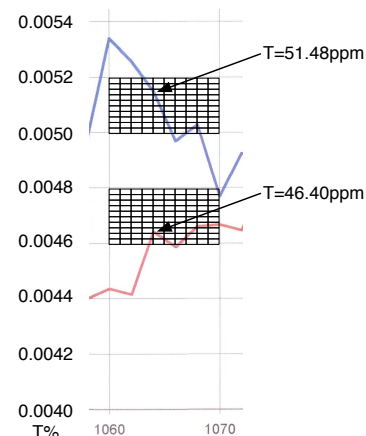


Figure 25: Coating C: High reflector, Side 1 HR, $T = 50 \pm 10$ ppm @ 4 degrees AOI

2.2.4 Measurement of the mirror transmissivities

[External Link]

http://nodus.ligo.caltech.edu:8080/OMC_Lab/96

http://nodus.ligo.caltech.edu:8080/OMC_Lab/100

http://nodus.ligo.caltech.edu:8080/OMC_Lab/112

http://nodus.ligo.caltech.edu:8080/OMC_Lab/114

LIGO-E1101095: Advanced LIGO Output Mode Cleaner Coating Specifications

[Description]

Power transmissions of the prism and curved mirrors were characterized.

[Experimental method]

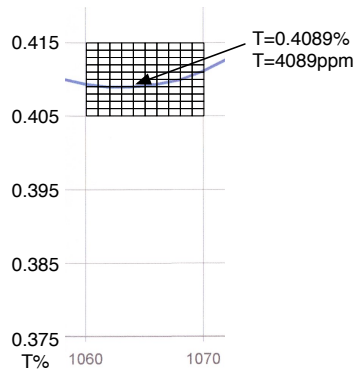


Figure 26: Coating D: Asymmetric output coupler, Side 1 HR, $T = 4150 \pm 400$ ppm @ 4 degrees AOI

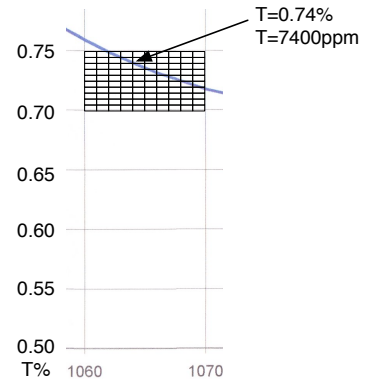


Figure 27: Coating E: High reflector, Side 1 HR, $T = 7500 \pm 2500$ ppm @ 45 degrees AOI

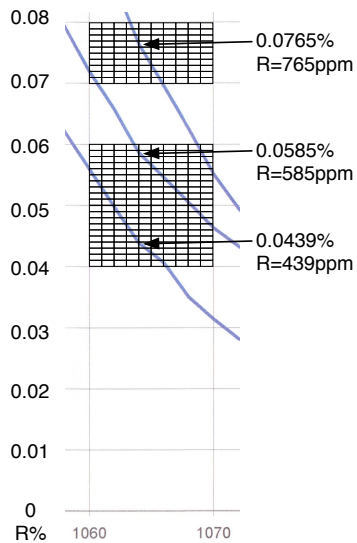


Figure 28: Coating ACD: Side 2 AR, $R < 0.1\%$, best effort < 100 ppm @ 4 degrees AOI

Theoretical 45° P-pol transmittance of AR witness is 99.2 %; measurement agreement indicates $R < 0.1\%$

Figure 29: Coating BE: Side 2 AR, $R < 0.1\%$, best effort < 100 ppm @ 45 degrees AOI

The measurement setup for the transmission measurement has been made at the output of the mode cleaning PM fiber.

- Made sure the output of the fiber was linearly polarized and has P-polarization by using a PBS. In fact it wasn't. Therefore the input and output fiber couplers were rotated to realize the linear P-polarization. Of course, this misaligns the input beam coupling to the fiber. Therefore some patient iteration was required.
- After some work, reasonable extinction ratio 10mW vs 100uW (100:1) with 11mW incidence. (It's curious what happened to the missing 0.9mW...)
- The P-pol (transmission) through the PBS goes into a prism mirror. The mirror is mounted on a prism mount supported by a rotational stage for precise angle adjustment. We limited the input power down to 5mW so that we can remove the attenuator on the power meter. The power meter output can depend on the position of my body. Therefore the lighting of the room had to be turned on in order to make the powermeter reading be stable.

[Result]

e.g. An example for an A mirror

- The offset of the power meter was -0.58uW
- The transmitted power for the normal incidence was 39.7uW with the incident 4.84mW.

$$[39.7 - (-0.58)]/[4.84 * 1000 - (-0.58)] * 10^6 = 8320\text{ppm}$$

- The transmitted power for the 4deg incidence was 38.0uW with the incident 4.87mW.

$$[38.0 - (-0.58)]/[4.87 * 1000 - (-0.58)] * 10^6 = 7980\text{ppm}$$

This number should be compared with the specification request for "Mirror A" (8300+/-800 ppm) and the data sheet spec (7931ppm).

The measurement results for the mirrors with 4-degree incidence are shown in Tables 8 and 9. The measurement results for the mirrors with 45-degree incidence are shown in Tables 10 and 11. Note that not all of E mirrors were inspected. None of the D mirrors were inspected.

Note on the mirror B measurements:

The initial B mirror measurements showed high number for the losses (1% ~ 3%). This inspired some investigation of the optical setup. The PBS to confine the polarization created a scattering halo around the main beam. This seemed a cause of distance dependent loss in the B mirror measurement. Therefore, the PBS was removed from the setup. Note that polarization ratio was 1:100 without the PBS. After the removal, the R&T measurement was redone. This time the loss distributed from 0.2% to 0.8% except for the one with 1.3%. Basically the loss of 0.25% is the quantization unit due to the lack of resolution.

The AR reflection was also measured for one of the B mirrors. There was a strong halo from the main specular reflection. Therefore the power from the AR reflection was measured at 0.5m distance from an iris to eliminate the halo. $33.6 \pm 0.2\mu\text{W}$ out of $39.10 \pm 0.05\text{mW}$ was observed. The offset was $-0.236\mu\text{W}$. This gives us the AR reflectivity of $865 \pm 5\text{ppm}$. This meets the spec requirement $R < 0.1\%$.

SN #	Power readings			Trans. [ppm]	Note
	Incident [mW]	Trans. [μ W]	Offset [μ W]		
A1	10.28	82.9	-0.205	8.08e3	
A2	—	—	—	—	@Fullerton
A3	10.00	83.2	-0.205	8.34e3	
A4	10.05	80.7	-0.205	8.05e3	
A5	9.94	81.3	-0.205	8.20e3	
A6	10.35	78.1	-0.205	7.57e3	
A7	10.35	77.8	-0.205	7.54e3	
A8	10.30	78.0	-0.205	7.60e3	
A9	10.41	84.1	-0.205	8.10e3	
A10	10.35	77.3	-0.205	7.49e3	
A11	10.33	77.9	-0.205	7.56e3	
A12	10.34	78.7	-0.205	7.63e3	
A13	10.41	85.4	-0.205	8.22e3	
A14	10.34	84.4	-0.205	8.18e3	

Table 8: Mirror transmission measurement for Mirror A. These numbers should be compared with the specification request (8300+/-800 ppm) and the data sheet spec (7931ppm).

SN #	Power readings			Trans. [ppm]	Note
	Incident [mW]	Trans. [μ W]	Offset [μ W]		
C1	10.30	0.2	-0.225	48.9	
C2	—	—	—	—	@Fullerton
C3	10.37	0.2	-0.191	41.6	
C4	10.35	0.2	-0.235	49.6	
C5	10.40	0.1	-0.235	35.9	
C6	10.34	0.1	-0.235	36.0	
C7	10.37	0.1	-0.229	35.9	
C8	10.41	0.2	-0.237	44.3	
C9	10.36	0.3	-0.230	54.8	
C10	10.39	0.3	-0.228	57.4	
C11	10.38	0.3	-0.209	56.6	
C12	10.28	0.2	-0.238	45.3	
C13	10.36	0.1	-0.234	39.8	

Table 9: Mirror transmission measurement for Mirror C. These numbers should be compared with the specification request (50+/-10 ppm) and the data sheet spec (51.48ppm or 46.40ppm, depending on the coating runs).

SN #	Power readings			Optical property		
	Incident [mW]	Trans. [μ W]	Refl [mW]	Trans [ppm]	Refl	Loss [ppm]
E4	13.65 ± 0.05	0.0915 ± 0.0005	13.50 ± 0.05	6703 ± 44	0.989 ± 0.005	0.004 ± 0.005
E12	13.75 ± 0.05	0.0978 ± 0.0005	13.65 ± 0.05	7113 ± 45	0.993 ± 0.005	0.000 ± 0.005
E16	13.90 ± 0.05	0.0975 ± 0.0005	13.30 ± 0.05	7014 ± 44	0.957 ± 0.005	0.036 ± 0.005

Table 10: Mirror transmission measurement for Mirror E. These numbers should be compared with the specification request (7500+/-2500 ppm) and the data sheet spec (7400ppm).

SN #	Power readings			Optical property		
	Incident [mW]	Trans. [μ W]	Refl [mW]	Trans	Refl	Loss
B1	39.10 ± 0.05	19.65 ± 0.05	19.25 ± 0.05	0.503 ± 0.001	0.492 ± 0.001	0.005 ± 0.002
B2	39.80 ± 0.05	19.90 ± 0.05	19.70 ± 0.05	0.500 ± 0.001	0.495 ± 0.001	0.005 ± 0.002
B3	13.87 ± 0.05	7.05 ± 0.05	6.55 ± 0.05	0.508 ± 0.004	0.472 ± 0.004	0.019 ± 0.005
B4	39.50 ± 0.05	19.70 ± 0.05	19.30 ± 0.05	0.499 ± 0.001	0.489 ± 0.001	0.013 ± 0.002
B5	39.50 ± 0.05	19.70 ± 0.05	19.50 ± 0.05	0.499 ± 0.001	0.494 ± 0.001	0.008 ± 0.002
B6	39.55 ± 0.05	19.50 ± 0.05	19.95 ± 0.05	0.493 ± 0.001	0.504 ± 0.001	0.003 ± 0.002
B7	40.10 ± 0.05	19.80 ± 0.05	20.20 ± 0.05	0.494 ± 0.001	0.504 ± 0.001	0.002 ± 0.002
B8	40.15 ± 0.05	19.80 ± 0.05	20.20 ± 0.05	0.493 ± 0.001	0.503 ± 0.001	0.004 ± 0.002
B9	40.10 ± 0.05	19.90 ± 0.05	19.90 ± 0.05	0.496 ± 0.001	0.496 ± 0.001	0.008 ± 0.002
B10	40.10 ± 0.05	19.70 ± 0.05	20.30 ± 0.05	0.491 ± 0.001	0.506 ± 0.001	0.002 ± 0.002
B11	40.20 ± 0.05	19.80 ± 0.05	20.20 ± 0.05	0.493 ± 0.001	0.502 ± 0.001	0.005 ± 0.002
B12	40.20 ± 0.05	19.90 ± 0.05	20.20 ± 0.05	0.495 ± 0.001	0.502 ± 0.001	0.002 ± 0.002

Table 11: Mirror transmission measurement for Mirror B. These numbers should be compared with the specification request (T=50+/-2 %) and the data sheet spec (T=50.385%). Note that only B3 was measured before the improvement of the measurement setup.

2.2.5 Mirror scattering measurement at Caltech

[Description]

Encountering the unexpected level of loss in the OMC cavity, the scattering measurement of the flat and curved cavity mirrors was performed at Caltech with full support of GariLynn Billingsley and Liyuan Zhang.

[Result]

The result of the measurement for the flat mirrors are shown in Figure 30. The result for the curved mirrors are shown in Figure 31.

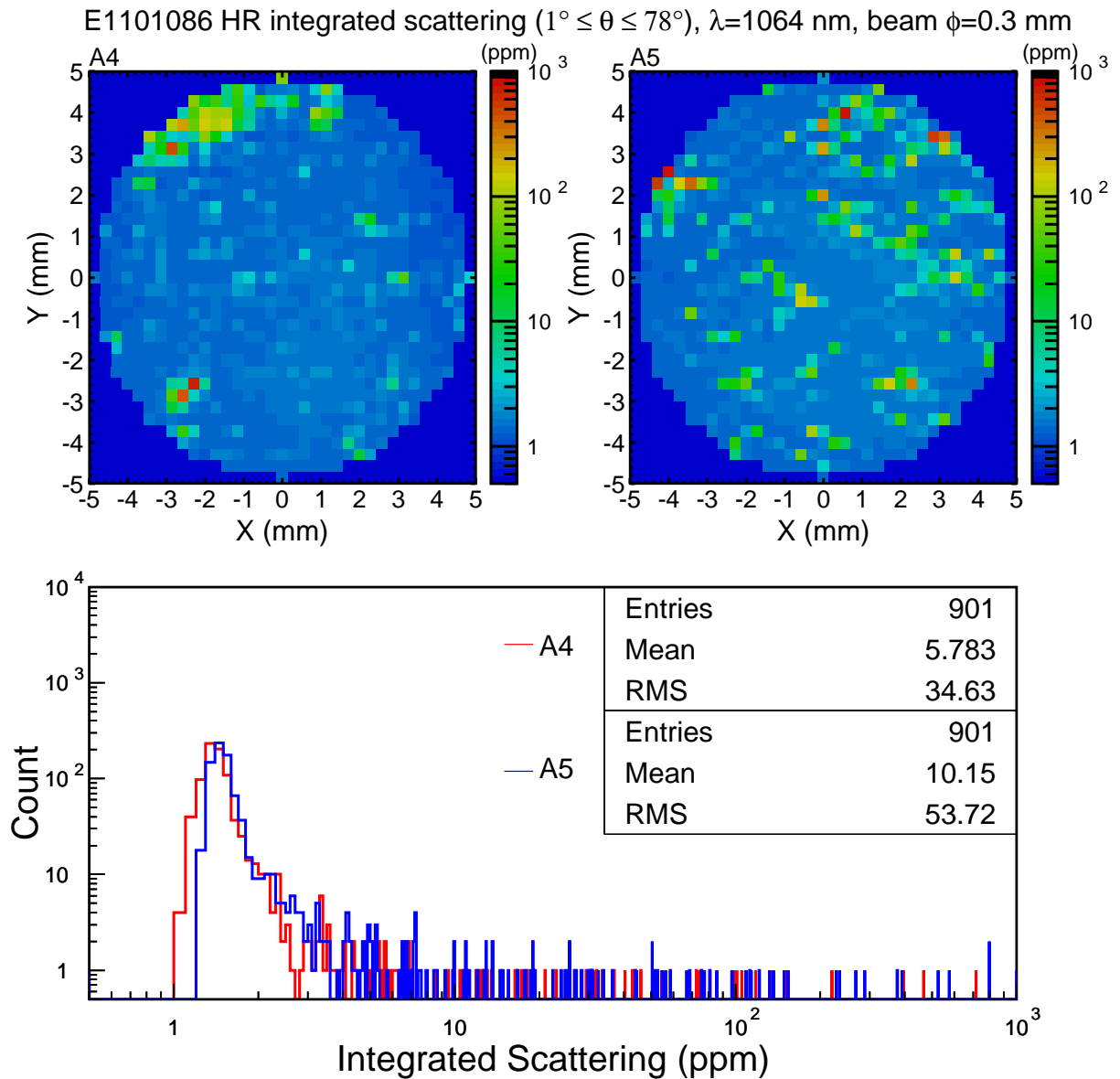


Figure 30: Scattering measurement for the two flat OMC cavity mirrors

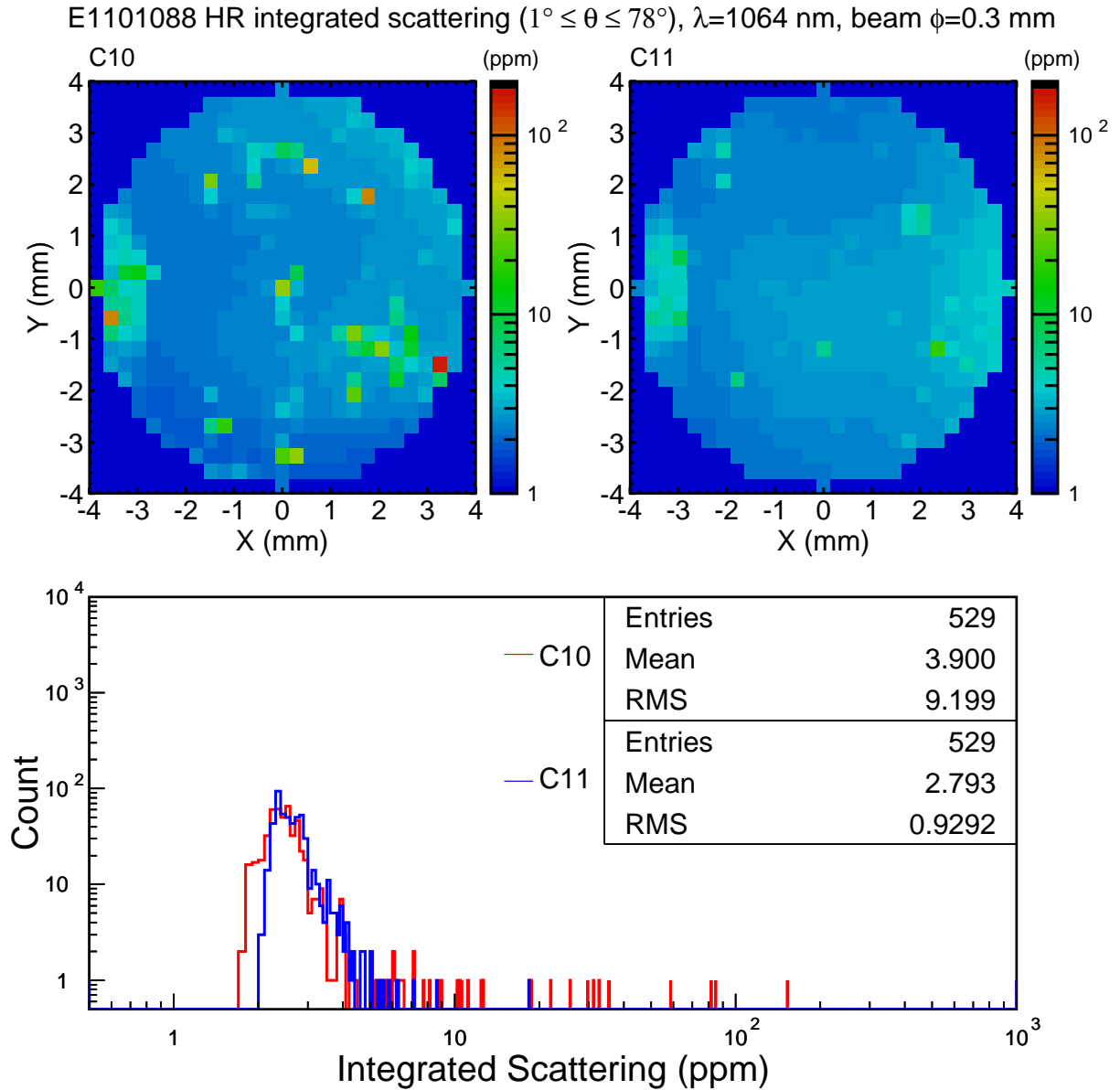


Figure 31: Scattering measurement for the two curved OMC cavity mirrors

2.2.6 Mirror scattering measurement at UC Fullerton

One mirror A and one curved mirror was sent to Joshua Smith at UC Fullerton for another scattering measurement. The below is the link to the poster posted in DCC.

[External Link]

[LIGO-G1301118: Scattered Light Measurements for Advanced LIGO's Output Mode-Cleaner Mirrors \(by A. Avila-Alvarez, et al.\)](#)

2.3 Characterization of the PZTs

The aLIGO OMCs cavity have two Noliac NAC2124. Characterization measurements of the OMC PZTs are described in this section.

[External Link]

[Noliac NAC2124](#)

2.3.1 PZT Wedge angle

[External Link]

http://nodus.ligo.caltech.edu:8080/OMC_Lab/53

[Description]

The thickness and the wedge angle of the Noliac PZTs were measured.

[Experimental method]

For each PZT, the thickness at six points along the ring was measured with a micrometer gauge. The orientation of the PZT was recognized by the wire direction and a black marking to indicate the polarity.

[Result]

The measured thicknesses of the PZTs are shown in Figure 32.

A least square fitting of these six points determines the most likely PZT plane. Note that the measured numbers are assumed to be the thickness at the inner rim of the ring as the micrometer can only measure the maximum thickness of a region and the inner rim has the largest effect on the wedge angle. The inner diameter of the ring is 9mm.

The measurements show all PZTs have thickness variation of 3 μm maximum.

The estimated wedge angles are distributed from 8 to 26 arcsec. The directions of the wedges seem to be random (i.e. not associated with the wires, for example)

As wedging of 30 arcsec causes at most $\sim 0.3\text{mm}$ spot shift of the cavity, the wedging of the PZTs is not critical by itself. Also, this number can be reduced by choosing the PZT orientations based on the estimated wedge directions.

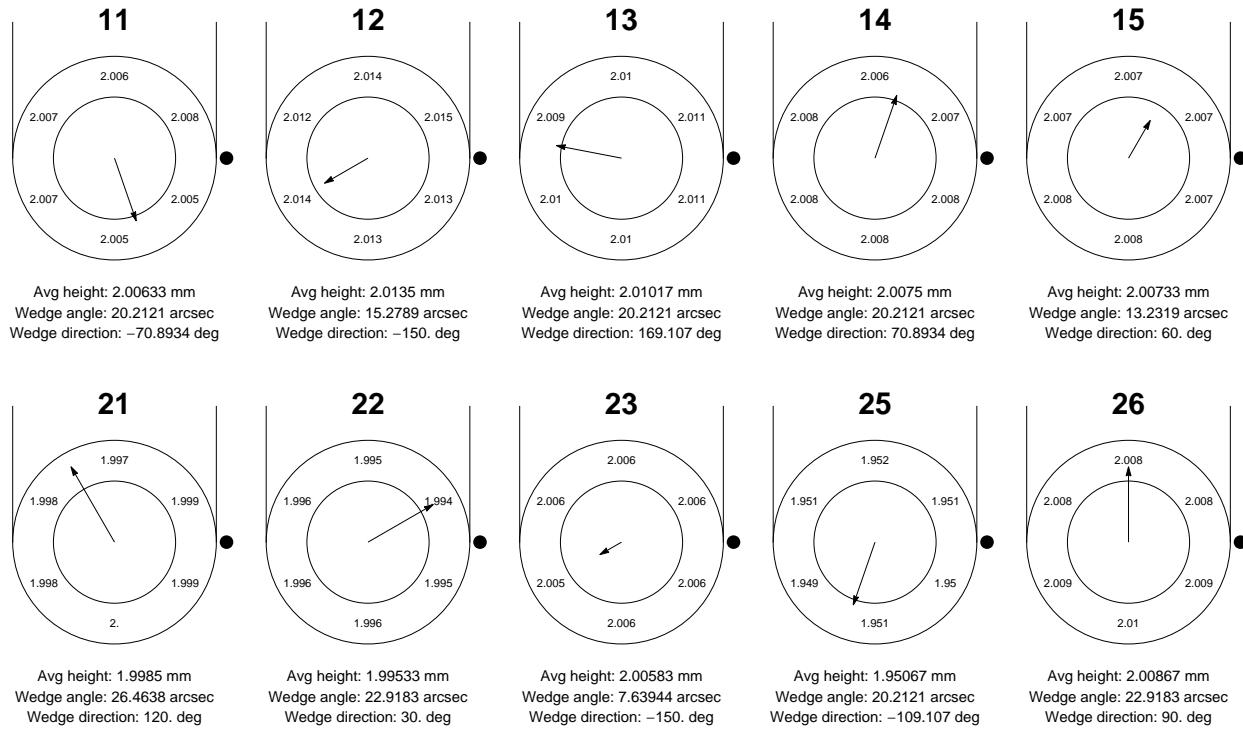


Figure 32: Measured thicknesses of the PZTs

2.3.2 PZT actuator DC response & length-to-angle coupling

[External Link]

http://nodus.ligo.caltech.edu:8080/OMC_Lab/102
aLIGO Wiki “PZT_testing”

[Description]

This is a measurement done by V. Frolov and R. DeRosa at LLO. This measurement characterized the PZTs actuation response at DC and length-to-angle coupling.

[Experimental method]

See their wiki page listed above.

[Result]

The result is summarized in Table 12. In the table, d is the distance of the curvature minimum from the mirror center, and ϕ is the angle of the minimum from the horizontal line at the center of the mirror.

2.3.3 Determination of the mirror arrangement for the PZT subassemblies

The combination and arrangement of a mounting prism, a PZT, and a curved mirror is determined for each PZT subassembly.

[External Link]

PZT #	Length [nm/V]	Angle [urad/um]	Location
11	14.5	17.6	PZT ASSY #8
12	13.8	17.8	PZT ASSY #9
13	11.2	25.0	PZT ASSY #7
14	14.5	6.6	OMC(003) CM1 (PZT ASSY #5)
15	12.5	10.6	OMC(003) CM2 (PZT ASSY #3)
21	14.5	9.7	OMC(002) CM1 (PZT ASSY #6)
22	13.8	28.8	PZT ASSY #10
23	14.5	6.8	OMC(001) CM2 (PZT ASSY #2)
24	18.5	51.7	Used for prototyping
25	17.1	13.8	OMC(002) CM2 (PZT ASSY #4)
26	14.5	6.6	OMC(001) CM1 (PZT ASSY #1)

Table 12: PZT actuator response and length-to-angle coupling

http://nodus.ligo.caltech.edu:8080/OMC_Lab/103

http://nodus.ligo.caltech.edu:8080/OMC_Lab/149

http://nodus.ligo.caltech.edu:8080/OMC_Lab/328

[Description]

The misalignment of the mirrors causes shift of the optical axis. Particularly, the vertical misalignment needs to be minimized, because the mirrors have no pitch adjustment. The pitch alignment of the prism mirrors were ensured with the perpendicularity measurement (Section 2.2.2).

However, the case for the curved mirrors is more complicated. It involves three components: a mounting prism, a PZT, and a curved mirror. The deviation of the curvature center for a curved mirror is equivalent with the misalignment. Therefore these misalignment needs to be minimized by carefully arranging these three components.

[Experimental method]

The vertical tilt of each of three components are individually assessed. The sign of the angle is defined such that the positive number means the horizontal beam is reflected so that it goes away from the breadboard surface.

- The prism angle was determined by the perpendicularity measurement by an autocollimator (Section 2.2.2).

- The angle of the PZT was determined by the wedge measurement (Section 2.3.1). If the wedge angle of θ_{PZT} in arcsec is at ϕ_{PZT} in deg, the resulting vertical angle is

$$\theta_V[\text{arcsec}] = \theta_{\text{PZT}} \sin \frac{\pi \phi_{\text{PZT}}}{180}$$

For simplicity of the construction, we limit the orientation of the PZT to 0 deg and 180 deg. In the 0 deg arrangement, the wires of the PZT goes away from the breadboard.

- The curvature center was measured as described in Section 2.1.3. Suppose the center of the curvature is located at the distance of d and angle of ϕ [deg], from the horizontal line

with the positive angle in CCW (cf. Figure 17). The vertical angle θ_V can be expressed as

$$\theta_V[\text{arcsec}] = \frac{180 \times 3600 \times d}{\pi R_{\text{RoC}}} \times \sin \frac{\pi(\phi - \phi_{\text{ROT}})}{180},$$

where R_{RoC} is the radius of curvature of the curved mirror, and ϕ_{ROT} is the rotation angle of the mirror in CW.

By adding these three quantities, the total vertical tilt is minimized.

[Result]

Such combinations to minimize the total vertical tilt are depicted in Figures 33 ~ 38.

For example, let's look at Figures 33.

- We use the mounting prism of #16. This has the vertical angle of +5.7arcsec.
- The PZT #26 has the wedge angle of 22.9arcsec at the angle 90deg (purely vertical). The PZT is rotated by 180 deg. Therefore the vertical angle by the PZT is -22.9arcsec.
- The C6 mirror has the curvature center at d of 0.73, mm and ϕ of 105 deg. When the mirror is rotated by 88 deg in CW, the curvature center is located at 17 deg from the horizontal line. This yields the vertical angle of +17.1arcsec.
- Therefore the total vertical angle is expected to be -0.1arcsec. That corresponds to the vertical beam shift of $1 \mu\text{m}$.
- The right most circle shows how the curved mirror should be rotated in the gluing fixture. The curved mirror has an arrow scribe. This is the reference for the curvature center measurement. Therefore we can rotate the mirror to realize the arrow angle shown as in the figure. Note that the figure shows the front face of the mirror.

Note:

During the assembly of the #3 and #4, the curved mirrors were rotated with mistakenly calculated values. Figures 39 ~ 40 show the actual expected vertical angles. They shows $-20 \sim -30$ arcsec. This corresponds to the beam shift of $25 \sim 37 \mu\text{m}$ closer to the breadboard.

Additional PZT subassemblies:

Upon the production of OMC(004), additional four PZT subassemblies were made. The combinations of these subassemblies are shown in Figure 41.

When the subassemblies were removed from the gluing fixtures, it was found that the fixtures and components were glued together (this is normal) and removed some glass/pzt pieces from the subassemblies (this is not normal in #1~#6). This made significant chipping on the subassembly #9 and unusable for the nominal use. The pictures can be found in the following elog entries.

http://nodus.ligo.caltech.edu:8080/OMC_Lab/331

http://nodus.ligo.caltech.edu:8080/OMC_Lab/332

http://nodus.ligo.caltech.edu:8080/OMC_Lab/333

http://nodus.ligo.caltech.edu:8080/OMC_Lab/334

http://nodus.ligo.caltech.edu:8080/OMC_Lab/335

Gluing sheet: OMC PZT subassembly #1

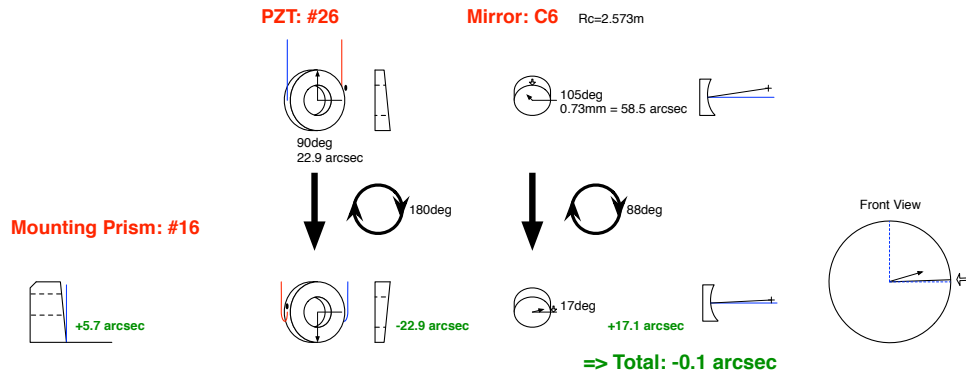


Figure 33: PZT assembly No.1 gluing sheet

Gluing sheet: OMC PZT subassembly #2

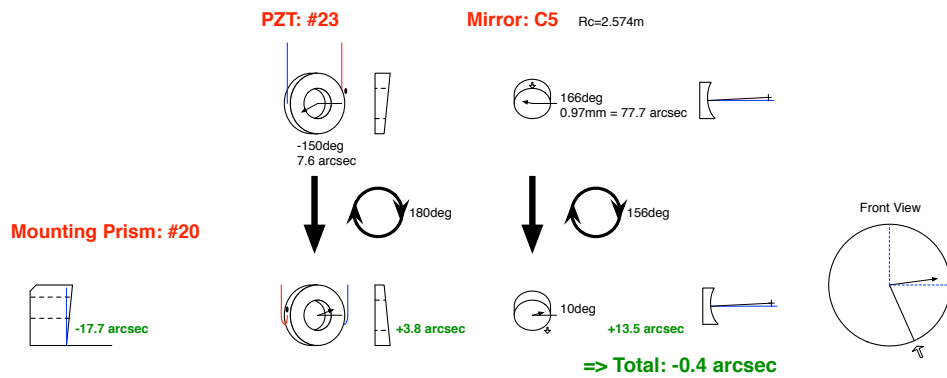


Figure 34: PZT assembly No.2 gluing sheet

Gluing sheet: OMC PZT subassembly #3

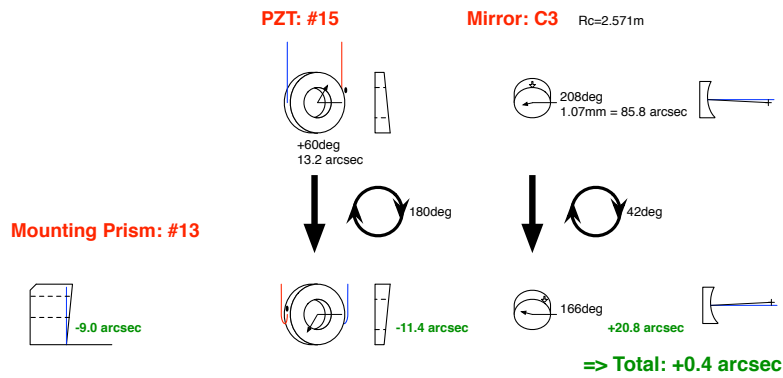


Figure 35: PZT assembly No.3 gluing sheet

Gluing sheet: OMC PZT subassembly #4

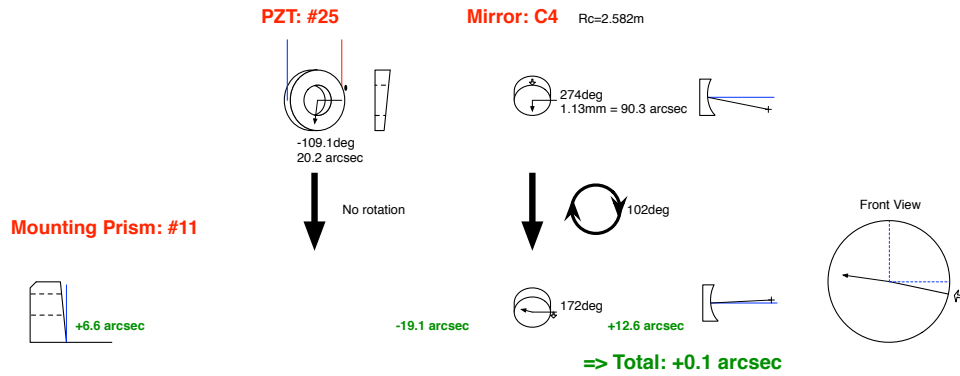


Figure 36: PZT assembly No.4 gluing sheet

Gluing sheet: OMC PZT subassembly #5

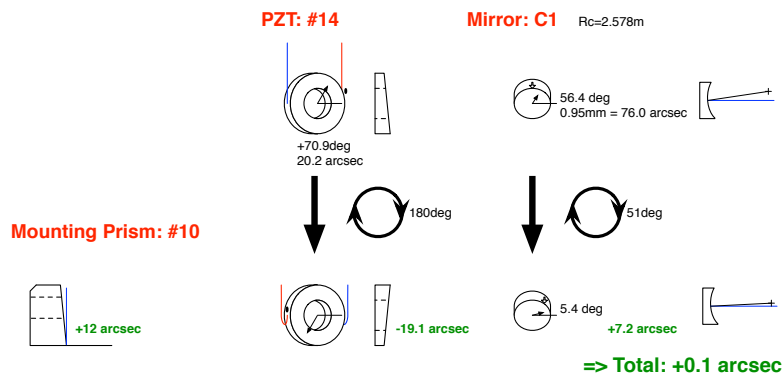


Figure 37: PZT assembly No.5 gluing sheet

Gluing sheet: OMC PZT subassembly #6

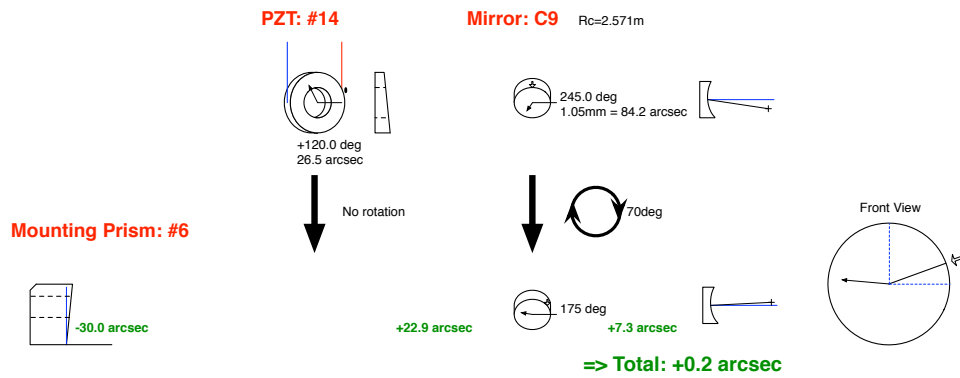


Figure 38: PZT assembly No.6 gluing sheet

Gluing sheet: OMC PZT subassembly #3 (actual)

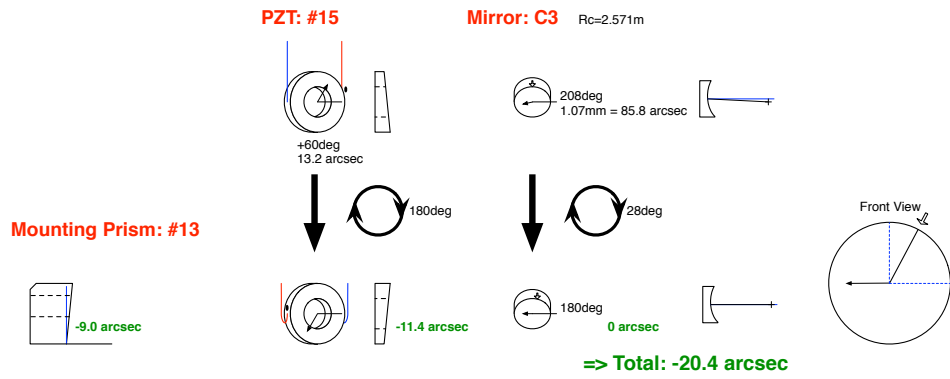


Figure 39: PZT assembly No.3 gluing sheet actual

Gluing sheet: OMC PZT subassembly #4 (actual)

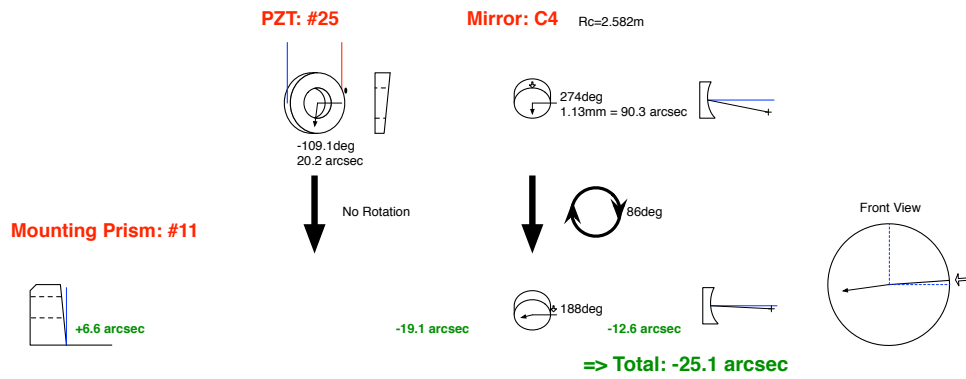


Figure 40: PZT assembly No.4 gluing sheet actual

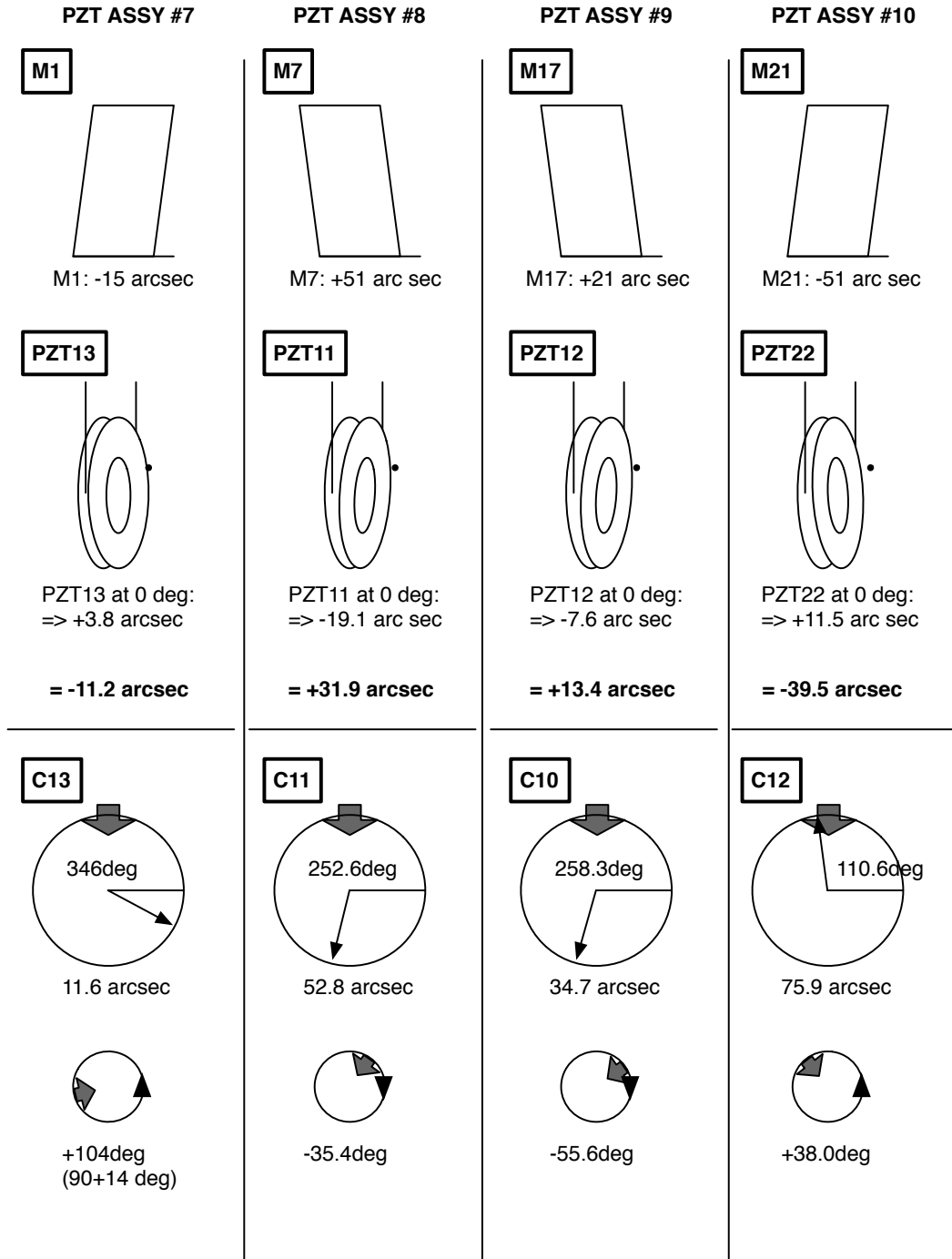


Figure 41: PZT assembly No.7~10 gluing sheet

2.3.4 PZT endurance test 1: High repetition test

[External Link]

http://nodus.ligo.caltech.edu:8080/OMC_Lab/156

http://nodus.ligo.caltech.edu:8080/OMC_Lab/336

http://nodus.ligo.caltech.edu:8080/OMC_Lab/337

Reliability, Noliac

[Description]

In response to the failure of one of the PZTs on OMC(001) at Livingston ([LLO aLOG:8366](#)), we have been taking place an endurance test of the four PZT sub-assemblies in prior to their being glued on the glass breadboard.

According to the technical note by Noliac, the common mode of PZT failure is degradation of the impedance due to cyclic actuation (like 10^7 times) with over voltage. Therefore our procedure of the test to actuate the PZTs at least 10^7 times with half voltage of the nominal operating voltage (i.e. nominal 200V) and check the degradation of the impedance.

[Experimental method]

- Driving signal

For driving the PZT, a thorlabs HV amp was used. A source signal of 3.5 V_{pp} with an offset of 1.7 V was produced by DS345 function generator. This signal turned to a sinusoidal signal between 0 and 100V in conjunction with the gain of 15 at the HV amp.

The maximum driving frequency is determined by the current supply limit of the HV amp (60mA). The capacitance of each PZT is 0.47 μ F. If we decide to cycle the signal for 4 PZTs in parallel, the maximum frequency achievable without inducing voltage drop is 100Hz. This yields the test period of 28 hours in order to achieve 10^7 cycles.

- Initial impedance diagnosis

To check the initial state of the PZTs, a DC voltage of 100V was applied via 1kOhm output resistance. Note that this output resistance is used only for the impedance test. For each PZTs, both side of the resistor showed 99.1V for all measurement by a digital multimeter (i.e. no measurable voltage difference). Assuming the minimum resolution (0.1V) of the multimeter, the lower limit of the resistance for each PZT was 1MOhm before the cycling test.

- Failure detection

In order to detect any impedance drop of the PZTs, the driving signal is monitored on the oscilloscope via a 1:10 probe. If there is any significant impedance drop, the driver can't provide the driving current correctly. This can be found by the deviation of the driving voltage from the reference trace on the oscilloscope (Figure 42).

- Temperature monitor

Because of the loss angle of the PZT capacitance, heating of the PZTs is expected. In order to check the temperature rise, an IR Viewer (FLIR) was used. We did not take care of

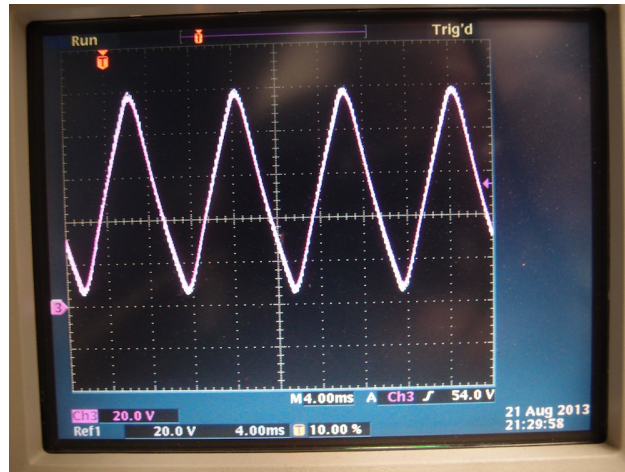


Figure 42: PZT endurance test: Driving voltage monitor.

careful calibration for the PZT emissivity as what we want was a rough estimation of the temperature.

[Result]

The temperature change of the PZT was tracked for an hour (below). Fitting of the points indicated that the temperature rise is 2.3 degC and the time constant of 446 sec. This level of temperature rise is totally OK. Note that the fitting function was $T = 27.55 - 2.31 \exp(-t/446)$.

For the 1st day, the actuation was applied for 70 minutes (i.e. 4.2×10^5 cycles). No sign of degradation was observed.

For the 2nd and 3rd day, the actuation was continuously applied for about 28 hours. This yielded total 10.65 Mcycles. **No sign of degradation was observed.**

Upon making OMC(004), the four new PZT subassemblies were tested in the same way. They showed no impedance change after 7.6 Mcycles.

2.3.5 PZT endurance test 2: Reverse voltage test

This is a test of the PZTs to make sure small (10V) reverse voltage does not break the PZTs.

[External Link]

http://nodus.ligo.caltech.edu:8080/OMC_Lab/157

[Description]

At the Livingston site, we decided to use one of the two OMC PZTs, which is still alive, for the HV and LV actuation. The HV actuation is limited to 0 to 100V while the LV actuation is 10Vdc with 1Vpp fast dithering. This means that a reverse voltage upto 10.5V will be applied to the PZT at the worst case.

From the technical note of Noliac, this level of reverse voltage does not induce polarization

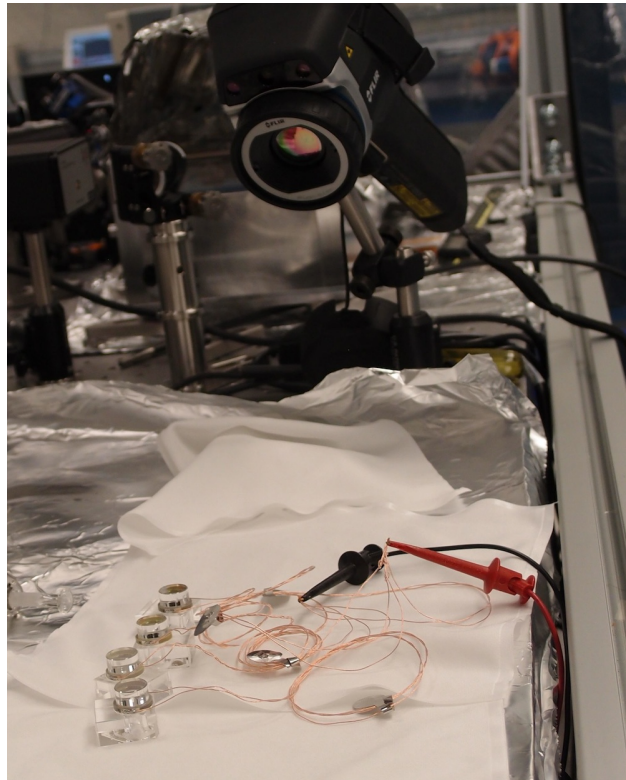


Figure 43: PZT endurance test: Teperature monitor setup.



Figure 44: Thermal vision of the PZTs before the actuation.



Figure 45: Thermal vision of the PZTs during the actuation.

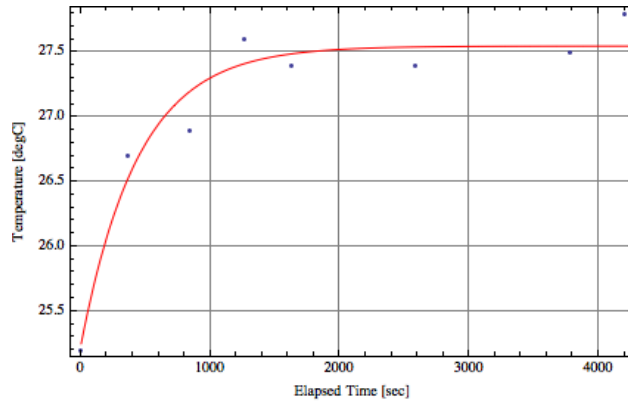


Figure 46: Teperature change of the PZTs

of the PZT. The test is to ensure the PZT is not damaged or degraded by this small reverse voltage.

[Experimental method]

HV and LV drives are simultaneously applied. (See Figure 47)

HV drive: Thorlabs HV amp (G=15) driven with DS345 function generator (3.5Vpp+1.7Vdc, 0.1Hz). This provides 0~100V signal at 0.1Hz. The hot side of the potential is connected to the positive side of the PZT.

LV drive: Phillips function generator (1Vpp at 1kHz +9.5Vdc offset). The driving frequency is limited by the current output of the function generator. The hot side of the potential is connected to the negative side of the PZT.

These drives shares the common ground.

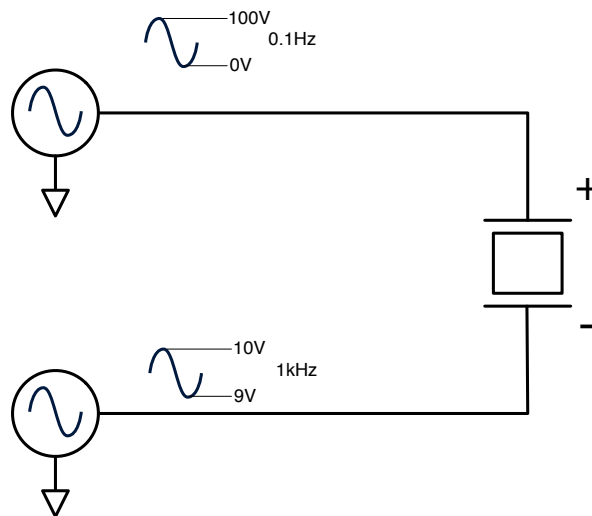


Figure 47: Reverse voltage test of the PZT

[Result]

Firstly, the spare PZTs were used for the test.

The actuation voltage has been applied for 48 hours and 52 minutes, which corresponds to 17600 and 176M cycles for the 0.1Hz and 1kHz drives, respectively.

After the actuation test, the impedance of the PZTs were measured. When 100Vdc was applied via a 1kOhm resistor, 0V (0.001V resolution) was detected across the 1kOhm resistor. This corresponds to the upper limit of the 1MOhm resistance.

Then, the PZT subassemblies were tested.

After the same actuation for 39.5 hours, no impedance change was detected.

Thus it was concluded that the PZT were unchanged after the reverse voltage test.

2.4 Photodiode and photodetector test

2.4.1 DCPD diode test

[External Link]

http://nodus.ligo.caltech.edu:8080/OMC_Lab/73

LIGO-T1100208: Photodiodes Pulse Damage Testing - status report, a.k.a. “Totally Awesome Diode Blasting Experiment”, Frank Seifert

LIGO-T1300321: OMC DCPD Test Result - InGaAs PD C30665GH

[Description]

The photodiodes for the OMC DCPDs are the photodiodes that the gravitational wave signals will eventually appear. Therefore they have to be carefully selected and characterized.

[Experimental method]

Measurement setup was inherited from the diode blasting experiment (see above T1100208). Here is the brief description.

- The dark current was measured with a sourcemeter (Keithley 2635A Sorce meter).
- The RF impedance was measured with a network analyzer (Agilent 4395A Network Analyzer + 43961A RF impedance test adapter)
- The dark noise was measured with a low noise current amplifier (FEMTO DLPCA-200) and FFT analyzer (Stanford Research SR785).

Some remarks on the setup:

- For the dark noise measurement, the lid of the die-cast case should also contact to the box for better shielding. This made the 60Hz lines almost completely removed, although unknown 1kHz harmonics remains.
- The diode characteristics with the impedance kit was measured between 10MHz and 100MHz.

- The impedance of the diodes could not be obtained when Frank’s measurement box was used. The cables between the diode and the network analyzer was too long to allow precise impedance measurement. Instead, the diode impedances were measured directly on the impedance measurement kit at the network analyzer. With this setup, the reverse bias voltage of 5V was applied on the network analyzer.

[Result]

- Impedance measurement

For comparison, 1mm and 2mm diameter photodiodes brought from the 40m lab were also tested. In total, 30 photodiodes were measured. The breakdown of the tested diodes are as follows:

- 3mm InGaAs photodiodes: C30665GH, Serial 1~13.
- 2mm InGaAs photodiodes: C30642G, Serial 20~29.
- 1mm InGaAs photodiodes: C30641GH, Serial 30~36.

The photodiode impedances are listed as Table 13. The DCPDs employ 3mm photodiodes. The PD #1~#13 showed basically identical performance in terms of the impedance.

- Dark current / dark noise measurement

Table 14 shows the result of the dark noise and current measurement for the 3mm InGaAs photodiodes. The dark current is represented at the value at 5V reverse bias. The dark noise is represented by the average between 1 Hz and 10 Hz, and between 200 Hz and 290 Hz.

Three out of 13 PDs showed abnormal dark current or noise and rejected for the use for the OMC purpose.

Typical performance of a “good” diode is shown in Figures 48. The measured data for the other PDs are attached as Figures 49~60. The same figures are also available in T1300321 (linked above).

Diode	LIGO Serial	Vendor Serial	R_s [Ω]	C_d [pF]	Source
C30665GH	1	0782	8.3	219.9	Peter King
C30665GH	2	1139	9.9	214.3	Peter King
C30665GH	3	0793	8.5	212.8	Peter King
C30665GH	4	0732	7.4	214.1	Peter King
C30665GH	5	0791	8.4	209.9	Peter King
C30665GH	6	0792	8.0	219.0	Peter King
C30665GH	7	0787	9.0	197.1	Peter King
C30665GH	8	0790	8.4	213.1	Peter King
C30665GH	9	0781	8.2	216.9	Peter King
C30665GH	10	0784	8.2	220.0	Peter King
C30665GH	11	1213	10.0	212.9	40m
C30665GH	12	1208	9.9	216.8	40m
C30665GH	13	1209	10.0	217.5	40m
C30642G	20	2484	12.0	99.1	40m, EG&G
C30642G	21	2487	14.2	109.1	40m, EG&G
C30642G	22	2475	13.5	91.6	40m, EG&G
C30642G	23	6367	9.99	134.7	40m, ?
C30642GH	24	1559	8.37	94.5	40m, Perkin-Elmer
C30642GH	25	1564	7.73	94.5	40m, Perkin-Elmer
C30642GH	26	1565	8.22	95.6	40m, Perkin-Elmer
C30642GH	27	1566	8.25	94.9	40m, Perkin-Elmer
C30642GH	28	1568	7.83	94.9	40m, Perkin-Elmer
C30642GH	29	1575	8.32	100.5	40m, Perkin-Elmer
C30641GH	30	8983	8.19	25.8	40m, Perkin-Elmer
C30641GH	31	8984	8.39	25.7	40m, Perkin-Elmer
C30641GH	32	8985	8.60	25.2	40m, Perkin-Elmer
C30641GH	33	8996	8.02	25.7	40m, Perkin-Elmer
C30641GH	34	8997	8.35	25.8	40m, Perkin-Elmer
C30641GH	35	8998	7.89	25.5	40m, Perkin-Elmer
C30641GH	36	9000	8.17	25.7	40m, Perkin-Elmer

Table 13: Measured impedances of the 3mm, 2mm, and 1mm photodiodes.

Diode P/N	LIGO Serial	Vendor Serial	Dark Current @5V[nA]	Dark Noise		Note
				1-10 Hz _{AVG} [pA/√Hz]	200-290 Hz _{AVG} [pA/√Hz]	
C30665GH	1	0782	6.74	6.504	1.452	Too high D.N.
C30665GH	2	1139	5.19	2.031	0.205	Too high D.N.
C30665GH	3	0793	4.83	1.473	0.269	OK
C30665GH	4	0732	2.19	0.051	0.107	good
C30665GH	5	0791	2.33	0.048	0.115	good
C30665GH	6	0792	2.76	0.077	0.111	good
C30665GH	7	0787	2.01	0.223	0.143	OK
C30665GH	8	0790	5.87	0.911	0.177	OK
C30665GH	9	0781	1131.96	0.011	0.005	Broken
C30665GH	10	0784	2.09	0.062	0.111	good
C30665GH	11	1213	3.48	0.674	0.128	OK
C30665GH	12	1208	2.19	0.076	0.096	good
C30665GH	13	1209	2.15	0.077	0.097	good

Table 14: Dark noise/current measurement for the 3mm InGaAs photodiodes

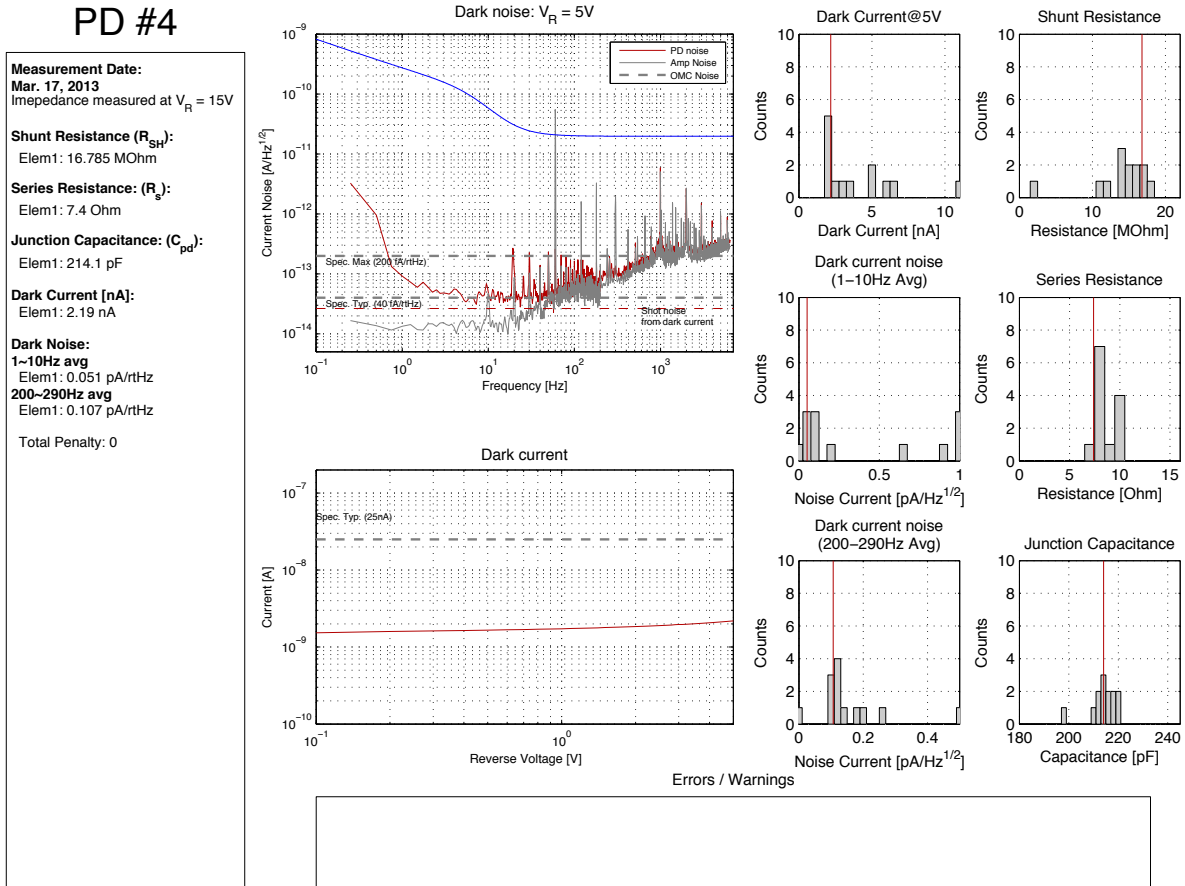


Figure 48: Test result of DCPD SN:4, typical good diode performance

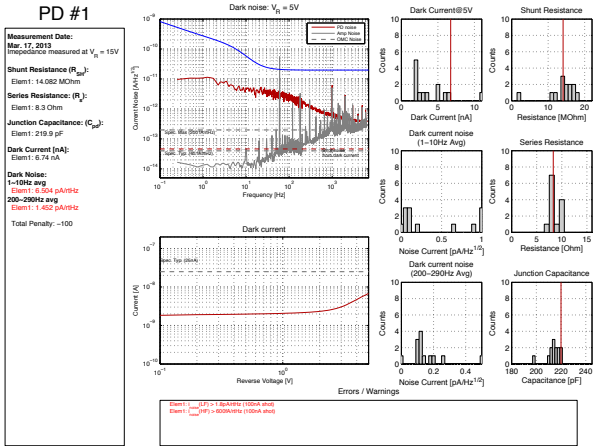


Figure 49: Test result of DCPD SN:1

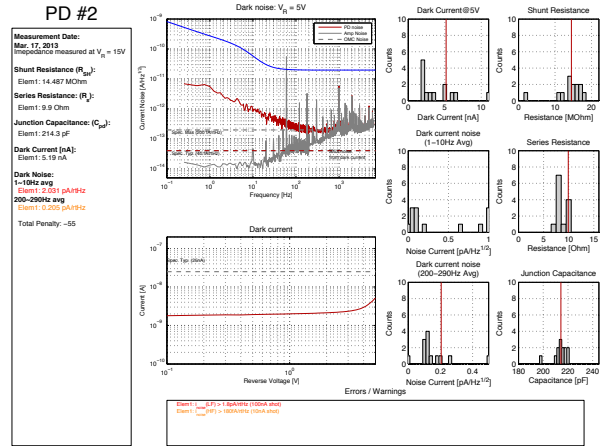


Figure 50: Test result of DCPD SN:2

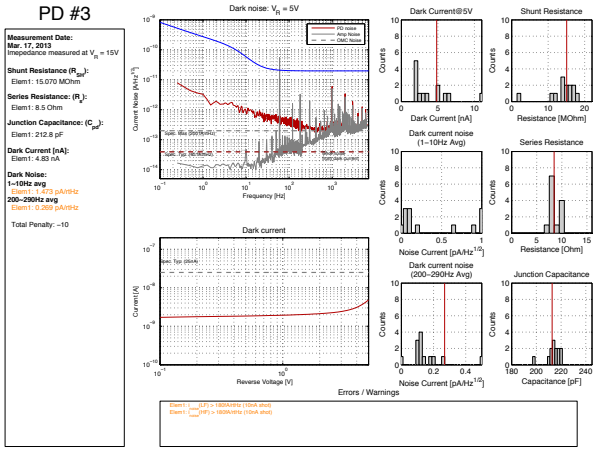


Figure 51: Test result of DCPD SN:3

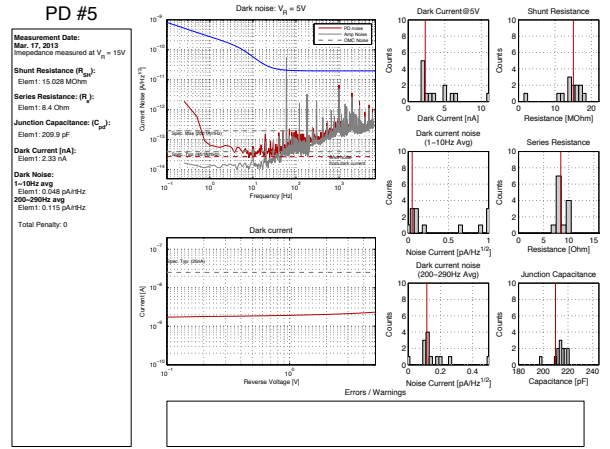


Figure 52: Test result of DCPD SN:5

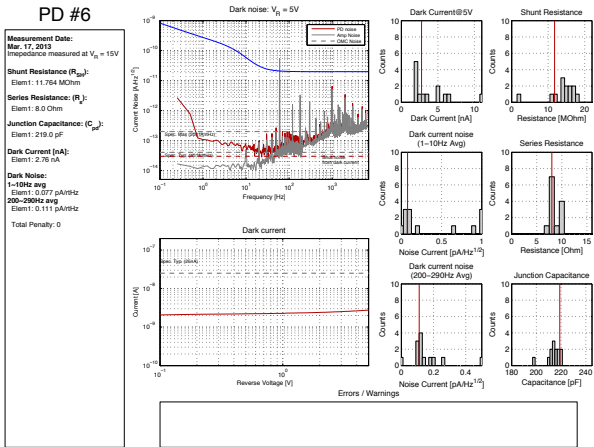


Figure 53: Test result of DCPD SN:6

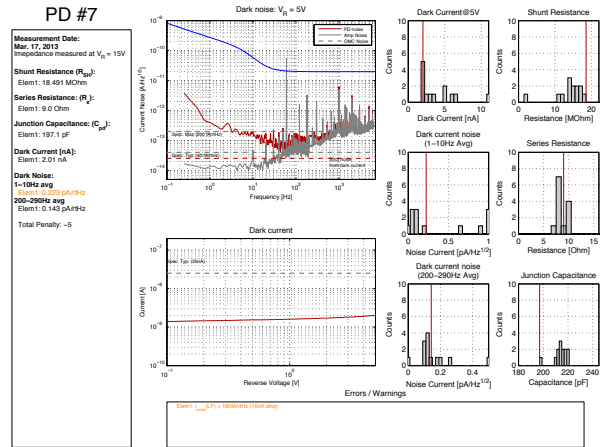


Figure 54: Test result of DCPD SN:7

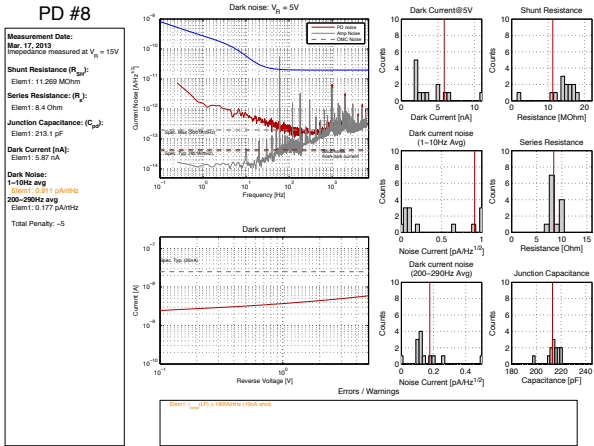


Figure 55: Test result of DCPD SN:8

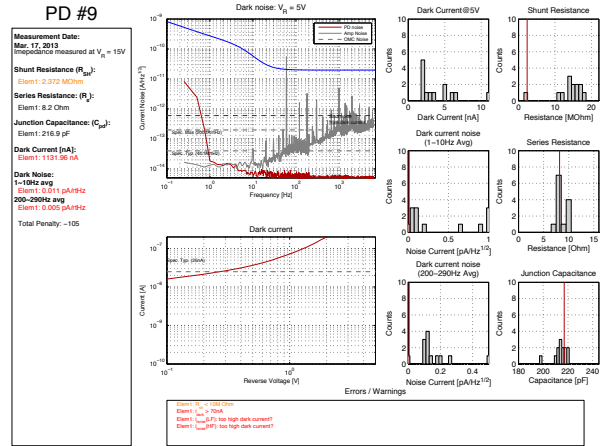


Figure 56: Test result of DCPD SN:9

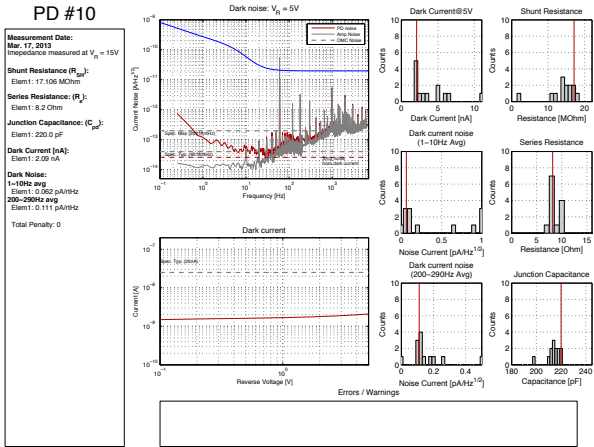


Figure 57: Test result of DCPD SN:10

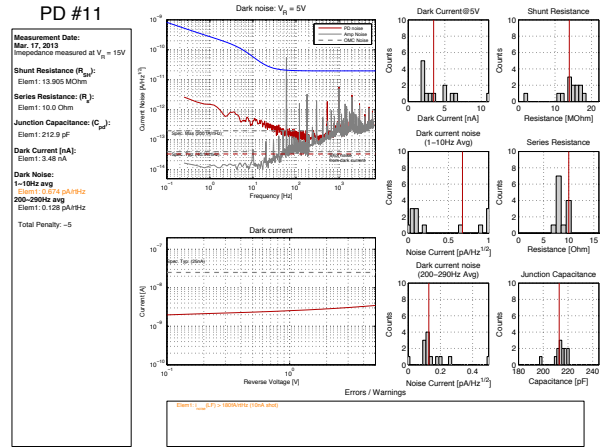


Figure 58: Test result of DCPD SN:11

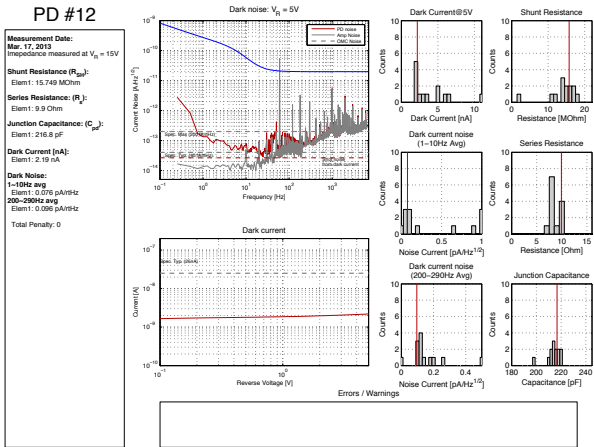


Figure 59: Test result of DCPD SN:12

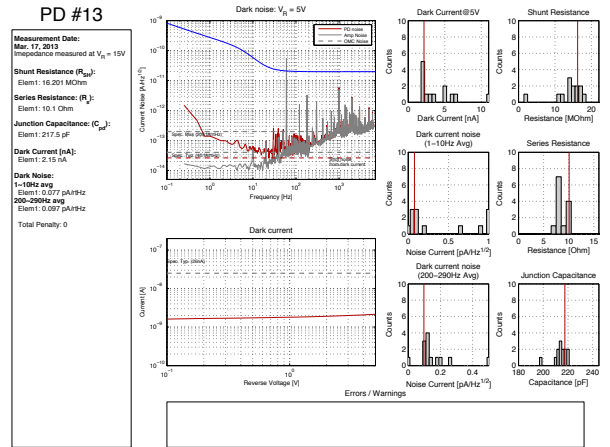


Figure 60: Test result of DCPD SN:13

2.4.2 DCPD diode response test

[External Link]

http://nodus.ligo.caltech.edu:8080/OMC_Lab/78

LHO iLog Aug 24, 2009

LLO iLog Sep 5, 2009

LIGO-T0900420: H1 OMC DC PDs

[Description]

The responsivities (i.e. quantum efficiencies) of the C30665GH diodes were measured.

[Experimental method]

The photodiode under test was reverse-biased by FEMTO DLPCA-200, transimpedance amplifier (TIA). The diode pin 1 (anode) was connected to the signal input of the amplifier. The diode pin 2 (cathode) was the shield side of the amplifier input and was set to be +5V. The pin 3 (case) was left open. The amplifier gain was 10^3V/A .

P-polarized light is focused on the diode. The diode angle was adjusted to be the incident angle of 10 deg with a rotation stage. The diodes had their glass windows on. Therefore this significantly reduces the quantum efficiency. The output from the TIA V_{out} , the power of the incident beam P_{inc} and the prompt reflection $P_{\text{refl,prompt}}$, and the total reflected power from the photodiode $P_{\text{refl,total}}$, are measured (Figure 61). The power measurements have been done with Thorlabs S130C, **which has the measurement uncertainty of $\pm 7\%$ at 1064nm.**

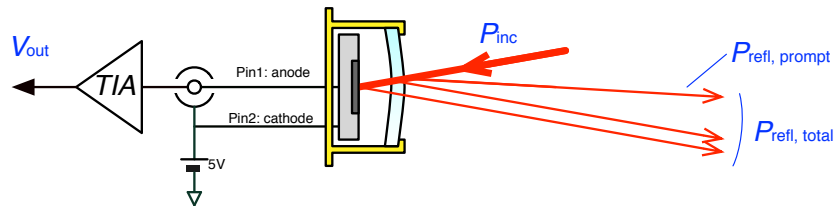


Figure 61: Measured quantities on the photodiode efficiency.

[Result]

The raw results of the measurements are shown in Table 15. From the numbers, some properties of the photodiodes are extracted.

- R_{ON} , Responsivity with the glass window on:

$$R_{\text{ON}} = \frac{V_{\text{out}}}{G_{\text{TIA}} P_{\text{inc}}} \text{ [A/W] } ,$$

where G_{TIA} is the transimpedance of the TIA ($1\text{k}\Omega$).

LIGO SN	Vendor SN	Power measurements [mW]			PD output
		P_{inc}	$P_{\text{ref},\text{total}}$	$P_{\text{ref},\text{prompt}}$	V_{out} [V]
1	0782	12.82 ± 0.02	1.168	0.404	9.161 ± 0.0005
2	1139	12.73 ± 0.02	0.937	0.364	9.457 ± 0.0005
3	0793	12.67 ± 0.02	1.272	0.383	9.114 ± 0.001
4	0732	12.71 ± 0.02	1.033	0.393	9.307 ± 0.0005
5	0791	12.69 ± 0.02	1.183	0.401	9.107 ± 0.005
6	0792	12.65 ± 0.02	1.306	0.395	9.031 ± 0.01
7	0787	12.67 ± 0.02	1.376	0.411	9.059 ± 0.0005
8	0790	12.63 ± 0.01	1.295	0.420	9.079 ± 0.0005
9	0781	12.67 ± 0.02	1.091	0.384	9.208 ± 0.0005
10	0784	12.70 ± 0.01	1.304	0.414	9.088 ± 0.001
11	1213	12.64 ± 0.01	1.152	0.416	9.286 ± 0.0005
12	1208	12.68 ± 0.02	1.057	0.419	9.365 ± 0.001
13	1209	12.89 ± 0.01	1.047	0.410	9.386 ± 0.001

Table 15: Measurement of the quantum efficiencies for the DCPD photodiodes. P_{inc} : Incident power on a photodiode. $P_{\text{ref},\text{total}}$: Total reflected power from a photodiode. $P_{\text{ref},\text{prompt}}$: The reflected power in a first spot. V_{out} [V]: PD output voltage with a transimpedance of $10^3[\Omega]$.

- η_{ON} , Quantum efficiency with the glass window on:

$$\eta_{\text{ON}} = R_{\text{ON}} \times \frac{hc}{e\lambda} ,$$

where h and e are the Planck constant and the electron charge, respectively. λ is the wavelength of the laser.

- R_{OFF} , Estimated responsivity when the glass window is removed:

$$R_{\text{OFF}} = \frac{V_{\text{out}}}{G_{\text{TIA}} P_{\text{inc}} (1 - P_{\text{ref},\text{prompt}}/P_{\text{inc}})^2} \text{ [A/W]} ,$$

This assumes two glass reflections are reflected with the same reflectivities.

- η_{OFF} , Estimated quantum efficiency with the glass window off:

$$\eta_{\text{OFF}} = R_{\text{OFF}} \times \frac{hc}{e\lambda} .$$

Table 16 shows the summary of these values for the DCPD photodiodes. Note that the quantum efficiency of the diodes are distributed around 90%.

2.4.3 Dependence of the photodiode response on the incident angle

[External Link]

LIGO-T1100564: E.G.&G. Photodiode angular response (S. Waldman)

[Description]

LIGO SN	Vendor SN	With window				Without window			
		R_{ON} [A/W]		Q.E. η_{ON}		R_{OFF} [A/W]		Q.E. η_{OFF}	
1	0782	0.715	± 0.001	0.833	± 0.001	0.762	± 0.001	0.8877	± 0.0015
2	1139	0.743	± 0.001	0.866	± 0.002	0.787	± 0.001	0.9174	± 0.0015
3	0793	0.719	± 0.001	0.838	± 0.001	0.765	± 0.001	0.8913	± 0.0015
4	0732	0.732	± 0.001	0.853	± 0.001	0.780	± 0.001	0.9087	± 0.0015
5	0791	0.718	± 0.001	0.836	± 0.002	0.765	± 0.001	0.8919	± 0.0016
6	0792	0.714	± 0.001	0.832	± 0.002	0.761	± 0.001	0.8865	± 0.0018
7	0787	0.715	± 0.001	0.833	± 0.001	0.764	± 0.001	0.8901	± 0.0015
8	0790	0.7188	± 0.0006	0.8376	± 0.0006	0.7691	± 0.0006	0.8964	± 0.0008
9	0781	0.727	± 0.001	0.847	± 0.001	0.773	± 0.001	0.9006	± 0.0015
10	0784	0.7156	± 0.0006	0.8340	± 0.0006	0.7646	± 0.0006	0.891	± 0.0008
11	1213	0.7347	± 0.0006	0.8562	± 0.0006	0.7855	± 0.0006	0.9153	± 0.0008
12	1208	0.739	± 0.001	0.861	± 0.002	0.790	± 0.001	0.9204	± 0.0016
13	1209	0.7282	± 0.0006	0.8487	± 0.0006	0.7768	± 0.0006	0.9054	± 0.0008

Table 16: Estimated responsivities and quantum efficiencies of the DCPD photodiodes.

It's worth to mention that there is a document by S. Waldman about measured angular response of 2mm InGaAs photodiodes distributed by EG&G (i.e. = Perkin Elmer = Excelitas).

Note that the aLIGO OMC PDs have the AOI of ~ 10 deg. The AOI is well within the central flat region according to the document.

2.4.4 DCPD preamp test

[External Link]

[LIGO-E1600013: OMC DCPD characterization for aLIGO transition \(W.Z. Korth, K. Arai\)](#)

[Description]

At L1 and H1, we transitioned the eLIGO OMC DCPD preamps for aLIGO use. This document summarizes the electrical performance of these preamps. Refer the external link for the details.

2.4.5 High QE DCPD diode test

[External Link]

[LIGO-E1600013: aLIGO OMC: Handling procedure for high quantum efficiency photodiodes](#)
[LIGO-D1500487: Photodiode Transport and Handling Fixture](#)

[Description]

Based on the quantum efficiency defect of C30665 photodiodes (Table 16), LIGO asked Fraunhofer HHI via Laser Components to produce custom high Q.E. photodiodes that has the same dimentions (Section B)and pinouts. This photodiode (now commercially available

as IGHQEXxxxx¹ is supposed to have Q.E. of 99%. The following sections describe the characteristic of the photodiodes.

E1600013 describes the handling procedure of the photodiodes based on the following background. A special care is necessary for handling of the photodiodes because they are expensive and precious products that were customly ordered and not off-the-shelf. The custom photodiodes are particularly prone to be damaged by ESD shock, according to the manufacturer. For easier handling, the photodiode transport and handling fixture D1500487 was designed.

Also it turned out that the manufacturer used Eccobond CE3103WLV and EPO-TEK H70E-4 in this batch of the photodiodes. These adhesives are not LIGO-approved ones. Therefore, a careful procedure for the outgassing reduction is necessary as well as performance check before and after the bake process.

2.4.6 High QE DCPD reflectivity test

[Description]

The reflectivity of IGHQEX3000 was measured and compared with the one for C30665.

[Experimental method]

The incident beam was adjusted to have P-polarization. The High QE PDs loaded on the fixture was mounted on a rotation stage. Defined the retroreflection of the beam as 0 deg. The angle of incidence (AOI) of the beam was scanned from -45 deg to $+45$ deg. The power of the reflected and incident beams were measured everytime the AOI was changed. During the measurement, the PD legs were always shorted by clean PD plugs.

[Result]

Figure 62: The reflectivity of IGHQEX3000 was measured as low as 0.25% at AOI of ~ 0 deg. The reflectivity is lower than 1% within AOI of ± 40 deg.

Figure 63: The reflectivity of C30665 was measured to be 11% at AOI of ~ 0 deg. As the angle increased, the reflectivity went down.

2.4.7 High QE DCPD dark current measurement

[External Link]

http://nodus.ligo.caltech.edu:8080/OMC_Lab/251

[Description]

Dark current of the HQE PD and other PDs were measured.

[Experimental method]

The measurement was performed with a KEITHLEY sourcemeter SMU2450. The source

¹https://www.lasercomponents.com/de/?embedded=1&file=fileadmin/user_upload/home/Datasheets/diverse-photodiodes/hqe-photodiodes.pdf&no_cache=1

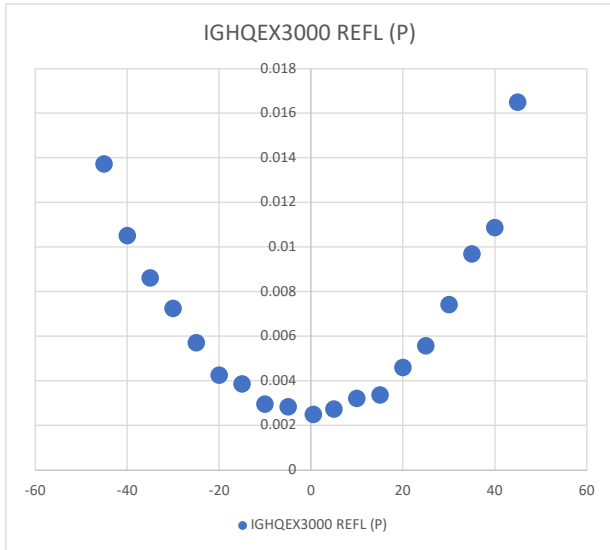


Figure 62: Reflectivity of IGHQEX3000

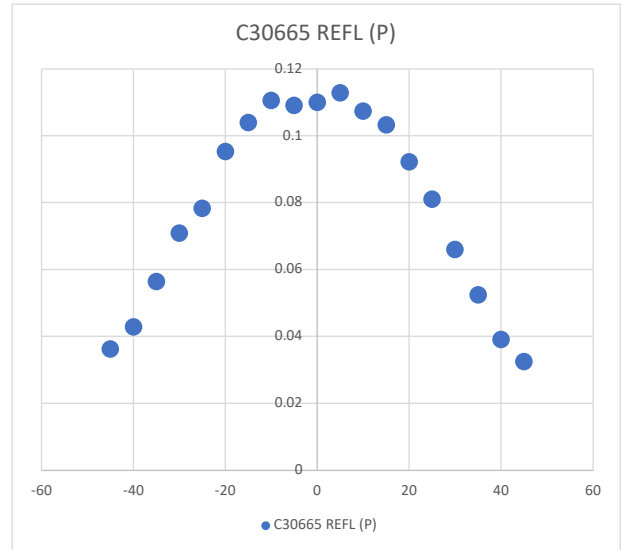


Figure 63: Reflectivity of C30665

voltage was supplied from the unit and the resulting current was sensed by the unit. It is important to set the current limit (e.g. 0.1 mA) to prevent from the damaging the photodiodes with an accidental forward voltage.

[Result]

The result is shown in Fig. 64. Most of the PDs showed the dark current of $\sim 3\text{nA}$ at the bias of 15 V. C1-05 and C1-07 showed higher dark current at high V region. We should avoid using them for the aLIGO purpose. Note that the PD names are not readable in the figure, but it is ok as they are almost identical.

As a comparison, the dark current of a C30655 (serial #10) was measured. Considering a DC current due to an ambient light (although the PD was covered), the typical dark current of IGHQEX3000 seemed higher than the one of C30655 #10 at 15V while it was lower at the low bias region.

Taking an advantage of having the setup, the same measurement was performed for the Laser Components PDs found in ATF. They were named #1 and #2. #1 has full-length legs while #2 has truncated ones. It was already reported that they showed significantly high dark current (See Fig. 65).

2.4.8 High QE DCPD responsibility measurement

[External Link]

http://nodus.ligo.caltech.edu:8080/OMC_Lab/254

http://nodus.ligo.caltech.edu:8080/OMC_Lab/255

[Description]

The responsibilities of the high QE DCPDs were measured. The quantum efficiency of the

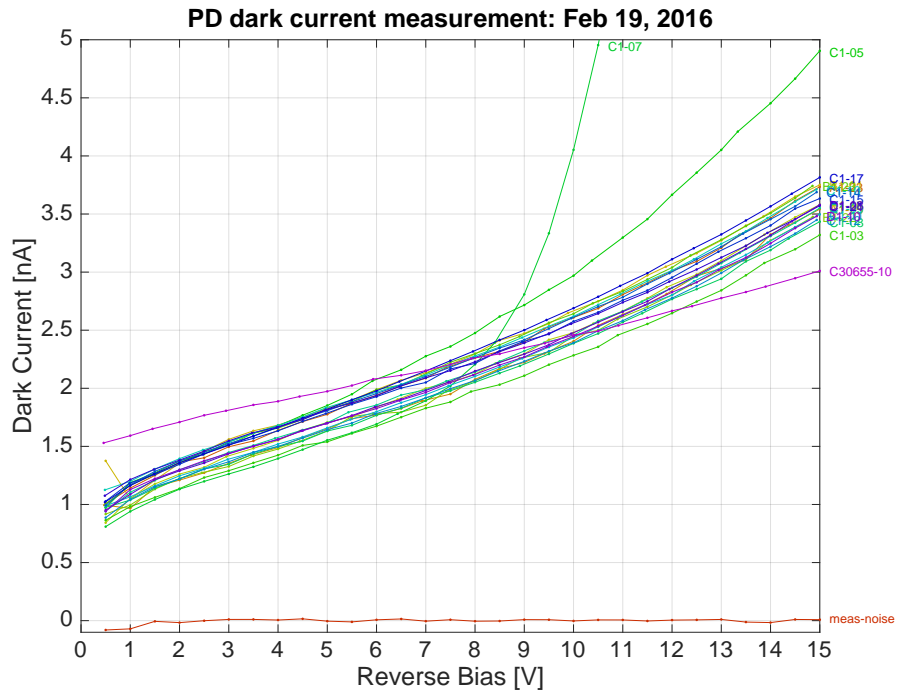


Figure 64: Dark current measurement of the diodes

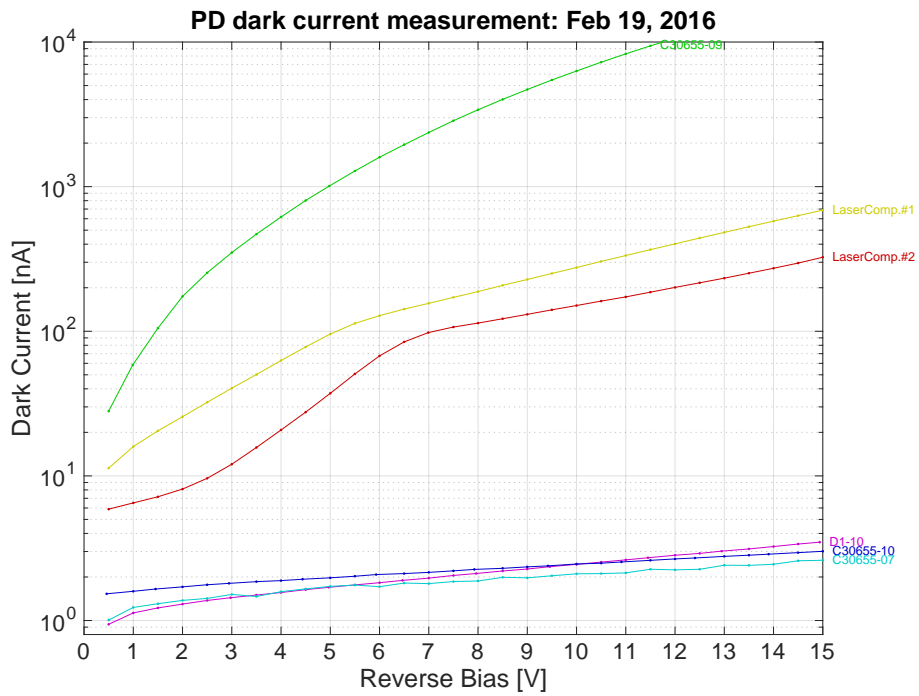


Figure 65: Dark Current Comparison with other similar photodiodes in hand

PDs were estimated from the responsibilities.

[Experimental method]

A PD in a PD fixture was setup to the beam with the AOI of about 10 deg. The beam has P-polarization and the gaussian radius of 0.5mm. The photocurrent was amplified by FEMTO's preamp DLPCA-200 with the transimpedance gain of $10^3\Omega$. The reverse bias was set to be 6 V. The output voltage was read by a digital voltage meter. The incident power was measured with Ophir RM9C with chopper. This powermeter has the systematic error of $\pm 5\%$ so it is hard to pin down the absolute QE of the PDs. Main purpose is to compare the QE with the conventional photodiodes.

The responsivity R and the quantum efficiency η has a linear relationship:

$$\eta = R \frac{h\nu}{e} = R \frac{hc}{e\lambda} . \quad (1)$$

For $\lambda = 1064 \text{ nm}$, $R=0.858$ gives the QE of the unity.

[Result]

First of all, the transimpedance of the current preamp was calibrated. KEITHLEY 2450 was used as a calibrated current source. It has the current source accuracy of $0.020\% + 1.5\mu\text{A}$ at 10 mA range. This corresponds to the error of $3\mu\text{A}$ ($= 0.05\%$) for 6 mA DC current. So, the current error of KEITHLEY 2450 was totally negligible.

The output of the current preamp at $10^3\Omega$ setting was 6.0023 V when -6.000 mA current was applied. i.e. $R_{\text{trans}} = 1000.4 \pm 0.5\Omega$. This is a negligible level.

The measured responsibilities and QEs are shown in Table 17. The QEs are shown to be 98~99%, however the difficult to pin down the accuracy due to the 5% accuracy of the power meter. The difference of the QEs between the high QE DCPDs and the conventional C30665 with no glass window was 5~6%.

2.4.9 Effect of air-baking on high QE DCPD

[External Link]

http://nodus.ligo.caltech.edu:8080/OMC_Lab/259

<https://ics-redux.ligo-la.caltech.edu/JIRA/browse/Bake-8047>

[Description]

Possible reduction of the QE was observed after air-bake at 75degC.

[Result]

The QE of the photodiodes after air bake was tested. According to the ICS entry (see above link), the PDs were air baked at 75degC for 48 hours.

The PDs were brought to the OMC lab to check if there is any change in terms of the performance after the baking.

- Dark current: No change observed

PD Type	SN	Case	Responsivity [A/W]	Quantum Efficiency	Measurement Date
IGHQEX3000	A1-23	A1	0.849 ± 0.001	0.990 ± 0.002	March 18, 2016
IGHQEX3000	A1-25	A2	0.856 ± 0.001	0.998 ± 0.001	March 18, 2016
IGHQEX3000	B1-01	A3	0.850 ± 0.001	0.990 ± 0.001	March 24, 2016
IGHQEX3000	B1-16	A4	0.847 ± 0.001	0.987 ± 0.001	March 18, 2016
IGHQEX3000	B1-22	B1	0.850 ± 0.001	0.990 ± 0.001	March 18, 2016
IGHQEX3000	B1-23	B2	0.845 ± 0.001	0.985 ± 0.001	March 18, 2016
IGHQEX3000	C1-03	B3	0.848 ± 0.001	0.989 ± 0.001	March 18, 2016
IGHQEX3000	C1-08	C2	0.844 ± 0.001	0.984 ± 0.001	March 18, 2016
IGHQEX3000	C1-09	C3	0.844 ± 0.001	0.984 ± 0.001	March 18, 2016
IGHQEX3000	C1-10	C4	0.844 ± 0.001	0.983 ± 0.001	March 18, 2016
IGHQEX3000	C1-11	D1	0.845 ± 0.001	0.985 ± 0.001	March 18, 2016
IGHQEX3000	C1-12	D2	0.846 ± 0.001	0.986 ± 0.001	March 18, 2016
IGHQEX3000	C1-14	D3	0.845 ± 0.001	0.984 ± 0.001	March 18, 2016
IGHQEX3000	C1-17	E1	0.850 ± 0.001	0.990 ± 0.001	March 18, 2016
IGHQEX3000	C1-21	E2	0.848 ± 0.001	0.988 ± 0.001	March 18, 2016
IGHQEX3000	D1-08	E3	0.845 ± 0.001	0.984 ± 0.001	March 18, 2016
IGHQEX3000	D1-10	E4	0.850 ± 0.001	0.990 ± 0.001	March 18, 2016
IGHQEX3000	C1-05	F1	0.842 ± 0.001	0.981 ± 0.001	March 24, 2016
IGHQEX3000	C1-07	F2	0.852 ± 0.001	0.993 ± 0.002	March 24, 2016
C30665	07	H2	0.799 ± 0.001	0.931 ± 0.002	March 18, 2016
IG17X3000Gi	LC1	H4	0.704 ± 0.001	0.821 ± 0.001	March 18, 2016
IG17X3000Gi	LC2	H3	0.744 ± 0.001	0.867 ± 0.001	March 18, 2016

Table 17: Responsivities and QEs of the high QE DCPDs and other PDs

- Dark noise: No noise increase observed
- Quantum efficiency: Probably reduced by 0.6%.

Figure 66 shows the result of the QE measurement. The QEs of the baked ones (A1-23 and A1-25) and the reference were measured. Since the reference PD has not been baked, this gives us the size of the systematic effect. The both high QE PDs showed the reduction of the QEs while the reference showed the reduction of only $\sim 0.1\%$. The net reduction of the QE for A1-23 was estimated to be 0.3% . Note that the previous measurement of 99.8% for A1-25 seemed too high and dubious.

Another evidence was that now the beam spots on these air-baked-PDs are clearly visible using an IR viewer when the PDs were illuminated with a 1064-nm beam. Usually it is difficult to see the spot on the PD. The spot on the reference PD was still dark. So this difference was very obvious. I was afraid that something has been deposited on the surface of the photosensitive element. The surface of the diodes looked still very clean when they were checked with a green LED flash light.

This reduction of the QE can be mitigated by cleaning the PD element by first contact while the process is quite delicate.

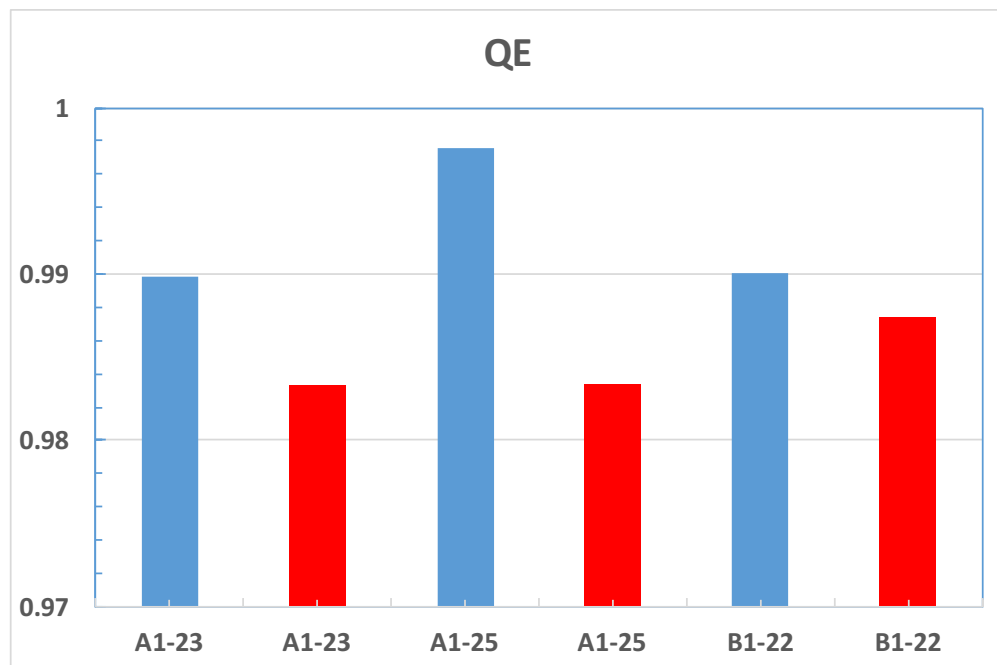


Figure 66: Quantum efficiency reduction after the air baking

2.4.10 High QE DCPD dark noise measurement

[External Link]http://nodus.ligo.caltech.edu:8080/OMC_Lab/256

http://nodus.ligo.caltech.edu:8080/OMC_Lab/260

[Description]

The dark noise of the high QE DCPDs was measured.

[Experimental method]

PDs were mounted with the PD transportation fixture. The lid of the fixture was closed to keep the PDs away from the ambient light. The photocurrent was sensed by a DLCPA-200 preamp with the gain of $10^7 \Omega$. With this gain setting the amplifier bandwidth is supposed to be 50 kHz. The reverse-bias voltage of 10 V was applied through DLCPA-200.

[Result]

The dark noise of C30665 was also measured to make it as a reference data for comparison. The dark noise of the high QE PDs are sufficiently low dark current noise levels compared with the noise level of the DCPD preamp. The measurement was limited by the input noise (ADC) noise of the FFT analyzer as the line noise coupling was too big.

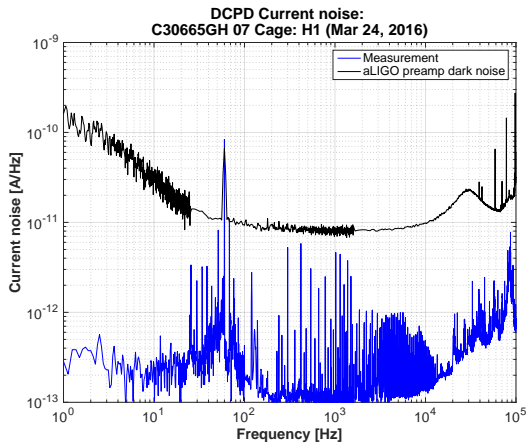


Figure 67: Dark noise of C30665GH 07

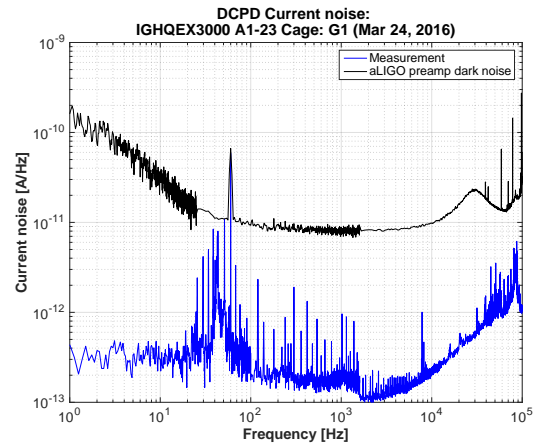


Figure 68: Dark noise of IGHQEX3000 A1-23

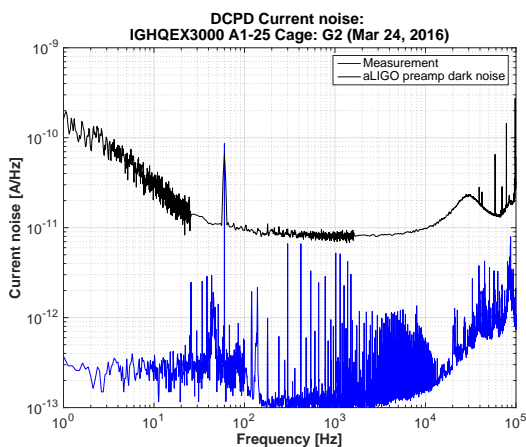


Figure 69: Dark noise of IGHQEX3000 A1-25

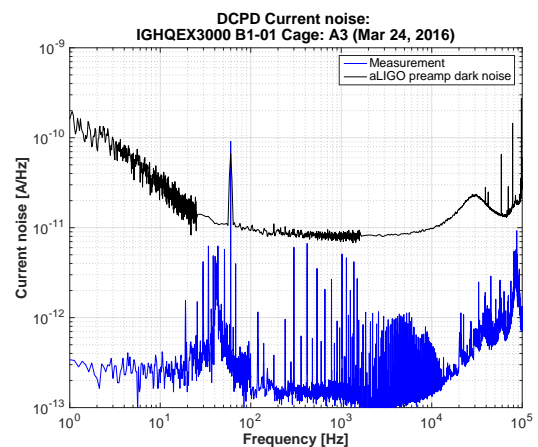


Figure 70: Dark noise of IGHQEX3000 B1-01

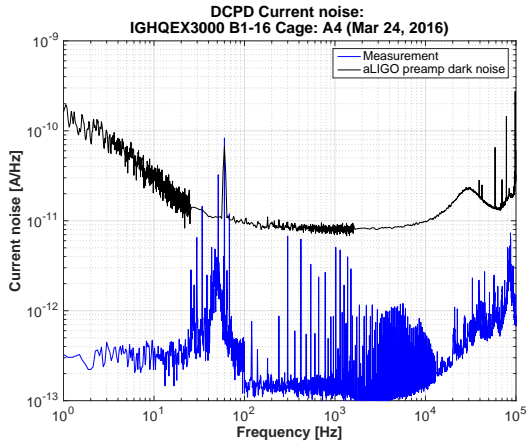


Figure 71: Dark noise of IGHQEX3000 B1-16

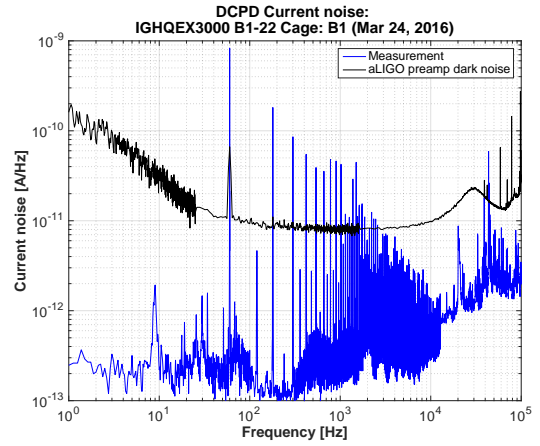


Figure 72: Dark noise of IGHQEX3000 B1-22

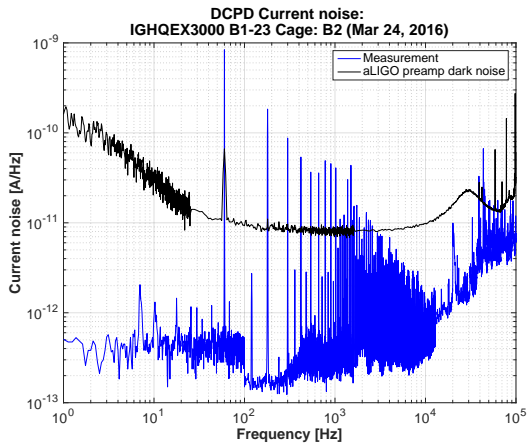


Figure 73: Dark noise of IGHQEX3000 B1-23

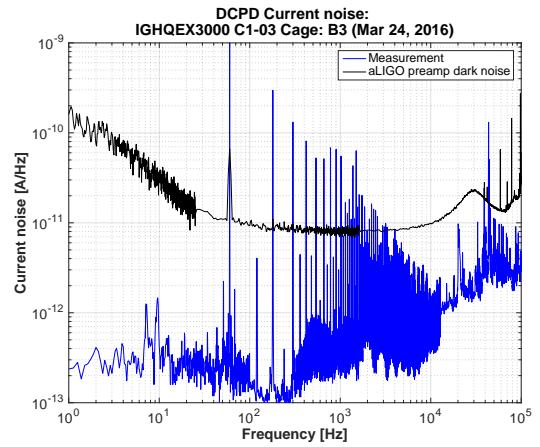


Figure 74: Dark noise of IGHQEX3000 C1-03

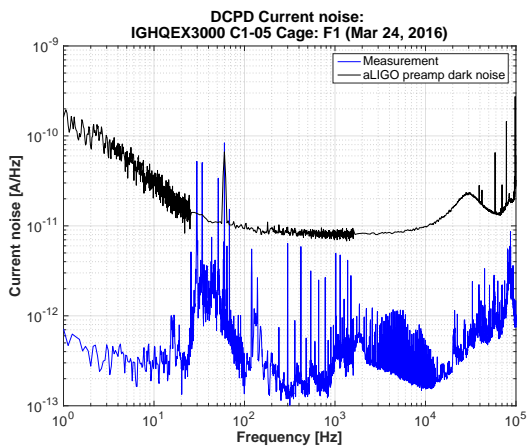


Figure 75: Dark noise of IGHQEX3000 C1-05

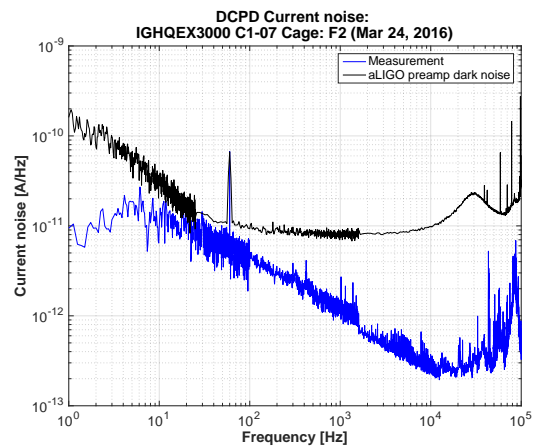


Figure 76: Dark noise of IGHQEX3000 C1-07

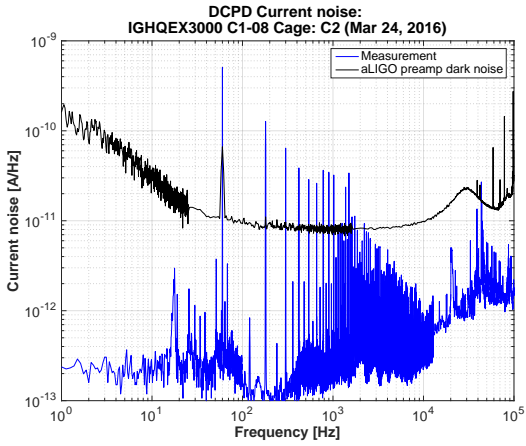


Figure 77: Dark noise of IGHQEX3000 C1-08

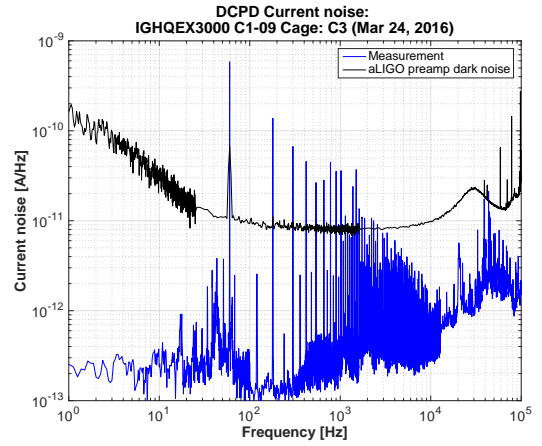


Figure 78: Dark noise of IGHQEX3000 C1-09

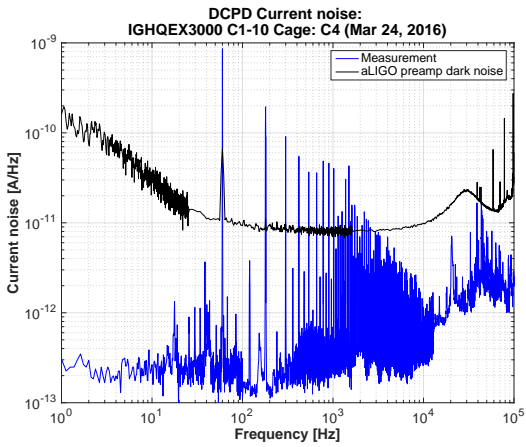


Figure 79: Dark noise of IGHQEX3000 C1-10

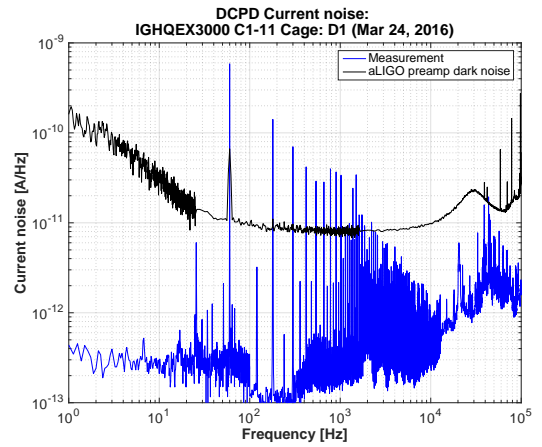


Figure 80: Dark noise of IGHQEX3000 C1-11

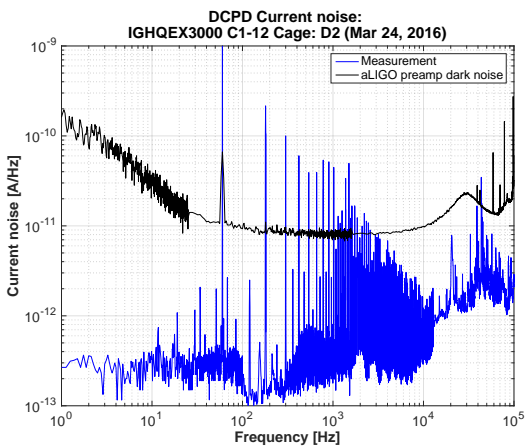


Figure 81: Dark noise of IGHQEX3000 C1-12

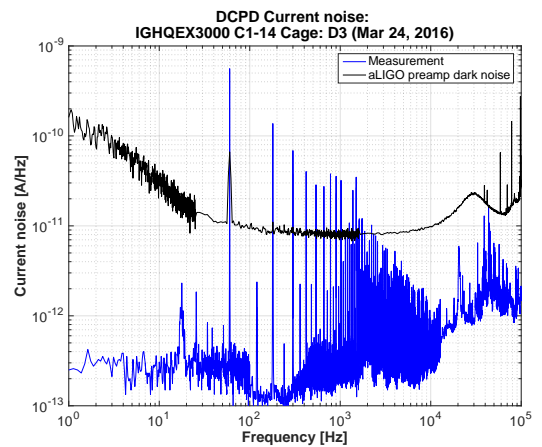


Figure 82: Dark noise of IGHQEX3000 C1-14

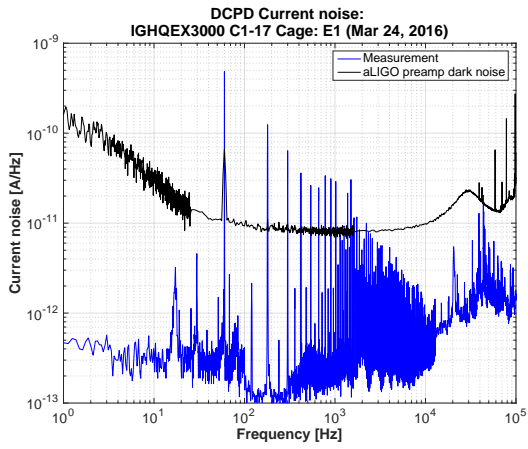


Figure 83: Dark noise of IGHQEX3000 C1-17

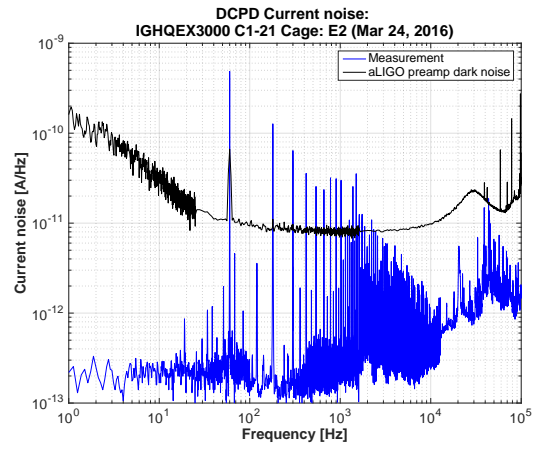


Figure 84: Dark noise of IGHQEX3000 C1-21

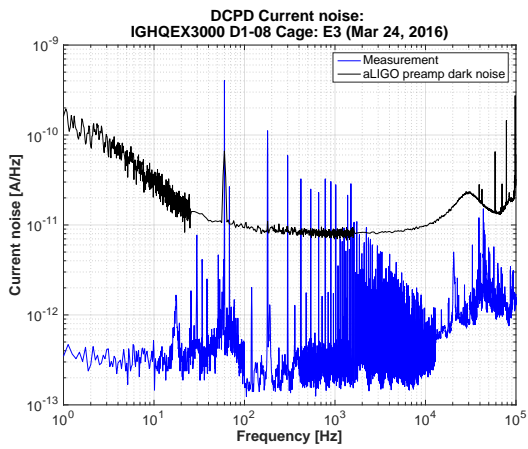


Figure 85: Dark noise of IGHQEX3000 D1-08

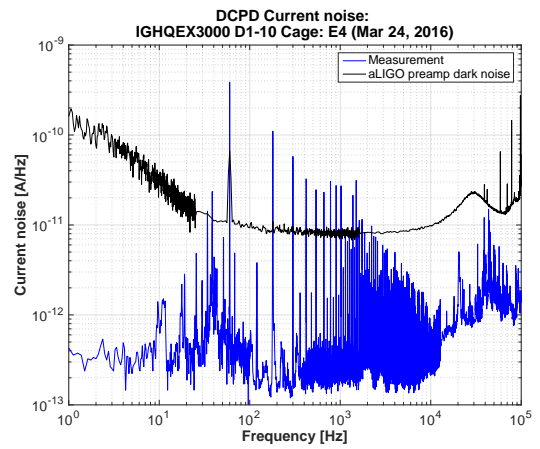


Figure 86: Dark noise of IGHQEX3000 D1-10

2.4.11 High QE high power exposure test

[External Link]

http://nodus.ligo.caltech.edu:8080/OMC_Lab/363

http://nodus.ligo.caltech.edu:8080/OMC_Lab/365

http://nodus.ligo.caltech.edu:8080/OMC_Lab/366

[Description]

The DCPD photodiodes were exposed to high power beam to check the damage threshold.

[Experimental method]

The PD under the test was exposed to the beam with the optical power from ~ 1 mW to ~ 300 mW. After each illumination, the dark current and the dark noise level were measured. Also the photo image of the PD surface was taken each time under the illumination of a green LED flashlight for visibility.

Figure 87(A) shows the electrical setup for the illumination test. The reverse bias voltage of 12 V was applied to mimic the aLIGO setup. The actual bias voltage across the photodiode gets reduced as the photocurrent increases. Above the photocurrent of 30 mA, the bias voltage is effectively zero and the PD is expected to work in the photovoltaic mode.

Figure 87(B) shows the electrical setup for the dark current/noise measurement.

[Result]

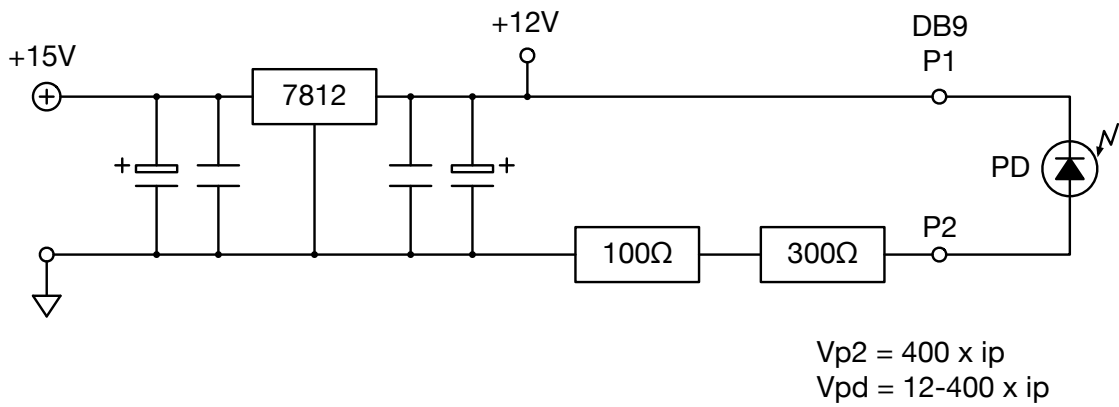
Firstly, an Excelitas C30665 PD (SN07, Cap removed, Case H2) was to the beam with the optical power of 1.4 mW to 334 mW.

- No significant change of the dark current after each illumination. (Figure 88)
- No significant change of the dark noise after each illumination. The amp gain of 10^7 was used. (Figure 88)
- No visible change of the surface observed. (Figure 89)

Secondly, a Laser Components IGHQEX3000 (Cage B2: SN B1-23) was exposed to the beam with the optical power from 1.6 mW to 332 mW.

- No significant change of the dark current after each illumination. (Figure 90)
- No significant change of the dark noise after each illumination. The amp gain of 10^8 was used. (Figure 90)
- No visible change of the surface observed. (Figure 91)

A) Illumination setup



B) Dark current / dark noise setup

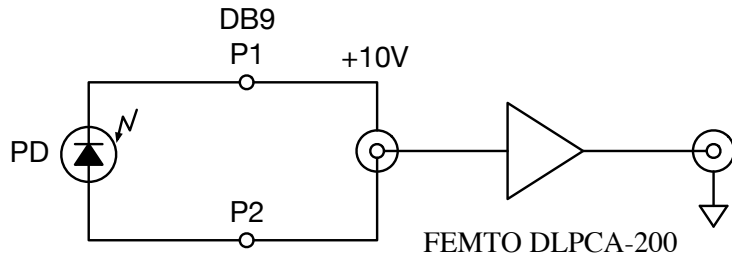


Figure 87: Electrical diagrams for the high power illumination test

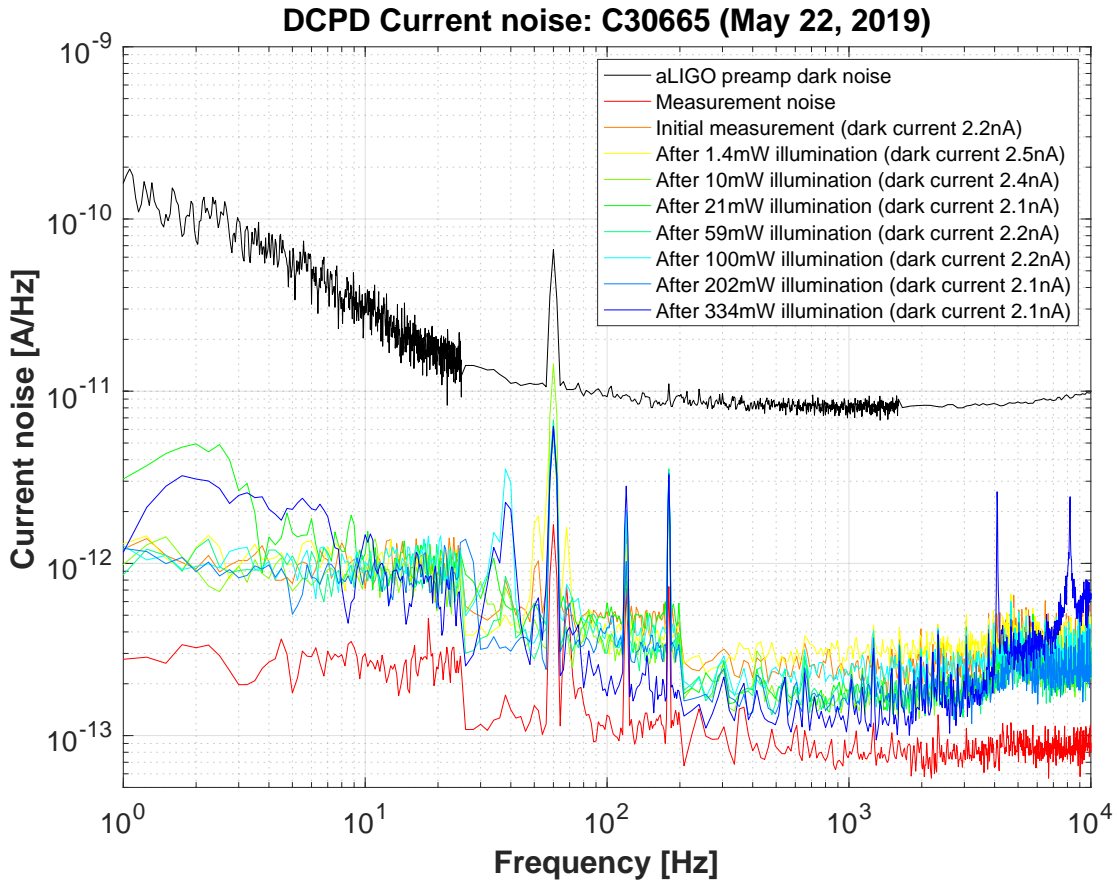


Figure 88: C30665 PD: dark current measurements after the high power beam illumination

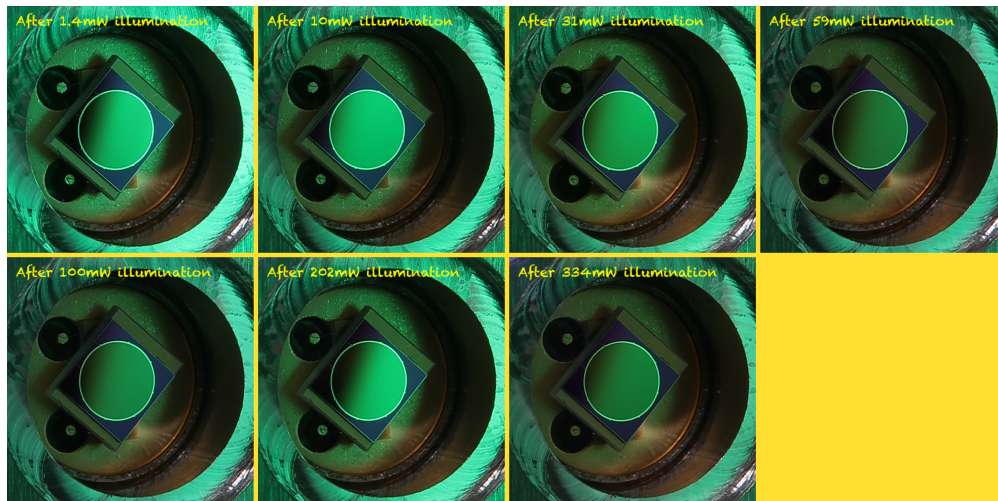


Figure 89: C30665 PD: surface image after the high power beam illumination

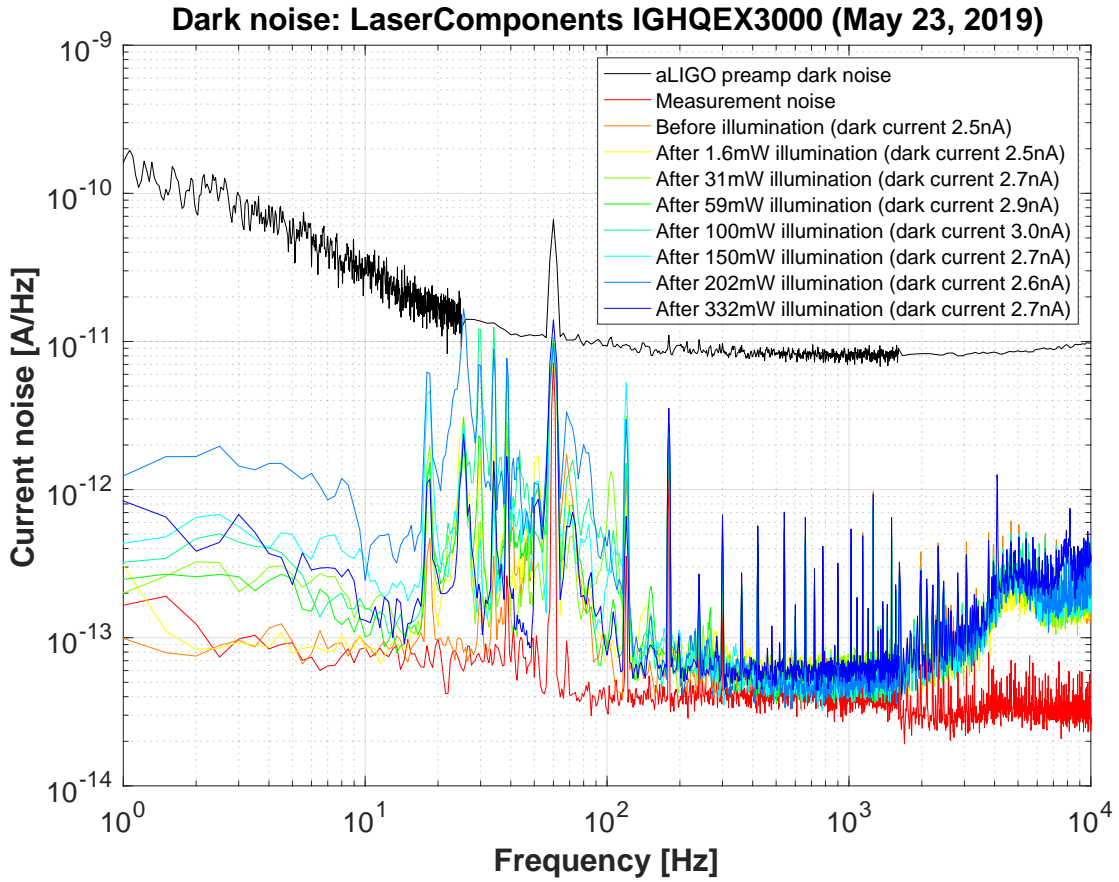


Figure 90: IGHQEX3000 PD: dark current measurements after the high power beam illumination

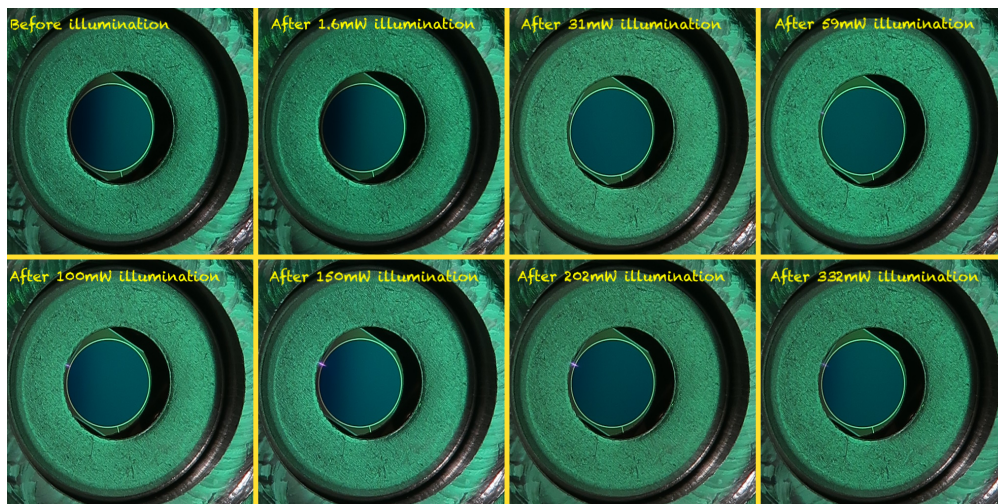


Figure 91: IGHQEX3000 PD: surface image after the high power beam illumination

2.4.12 High QE DCPD capacitance measurement

[External Link]

http://nodus.ligo.caltech.edu:8080/OMC_Lab/409

http://nodus.ligo.caltech.edu:8080/OMC_Lab/410

[Description]

The capacitances of the high QE DCPDs were measured using SR720 LCR meter.

[Experimental method]

Figure 92 shows the system diagram for the PD capacitance measurement. The reverse-bias voltage was applied via DS335. This can produce a voltage offset up to 10 V. A gain of +2 opamp circuit was inserted so that a bias of up to +15V can be produced. The capacitance of a photodiode was measured with SR720 LCR meter with a probe. DS335 and SR720 were controlled from PC/Mac via serial connections.

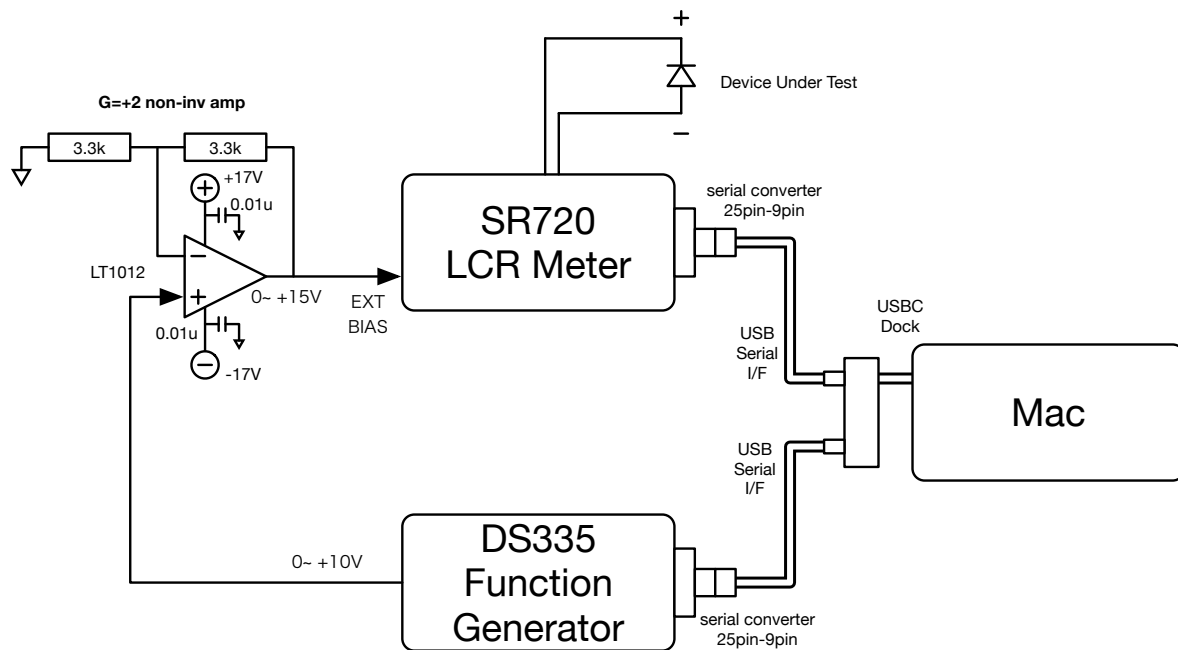


Figure 92: System diagram for the DCPD capacitance measurement

[Result]

Figure 93 shows the measured capacitances of the high QE PDs as a function of the reverse bias voltage. The capacitance at no bias is 500 pF, which is reduced to the half at the bias of 2 V. It reaches ~ 200 pF at 15 V.

Figure 94 shows the comparison of the capacitances between high QE PDs and the conventional C30665. C30665 PDs nominally show lower capacitance.

2.5 Miscellaneous measurements

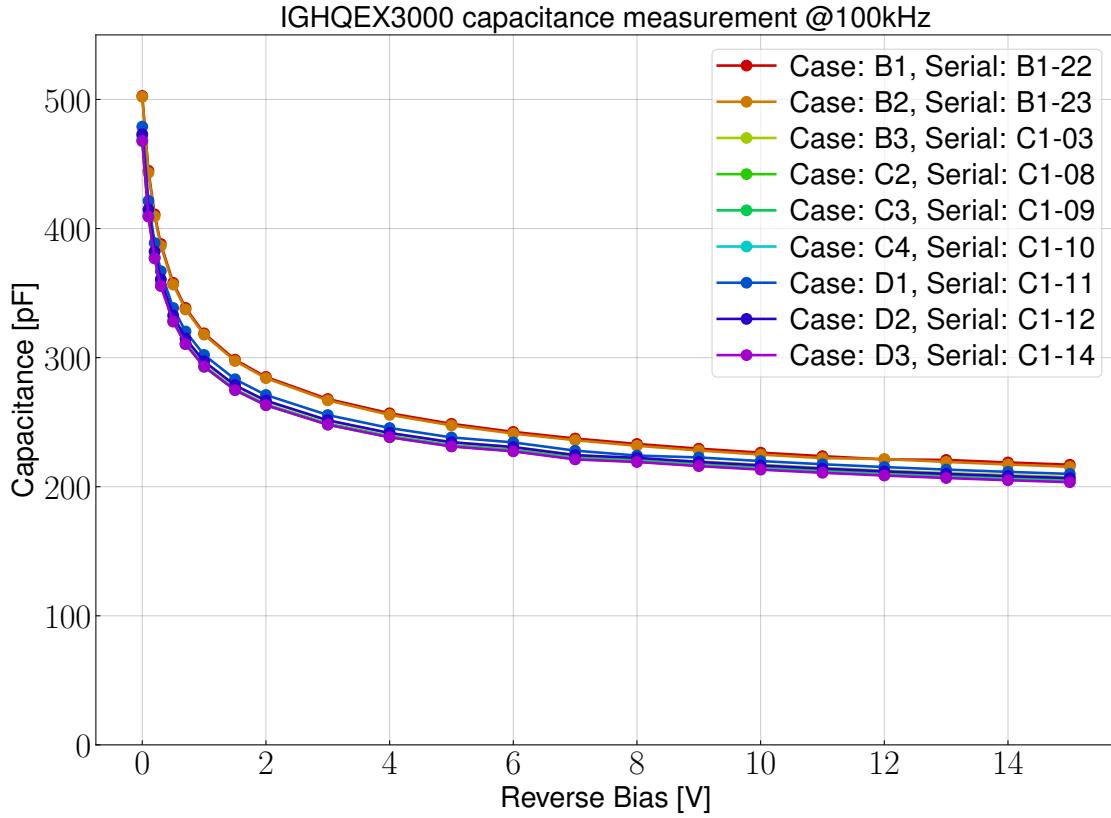


Figure 93: Capacitance measurements for IGHQEX3000 photodiodes

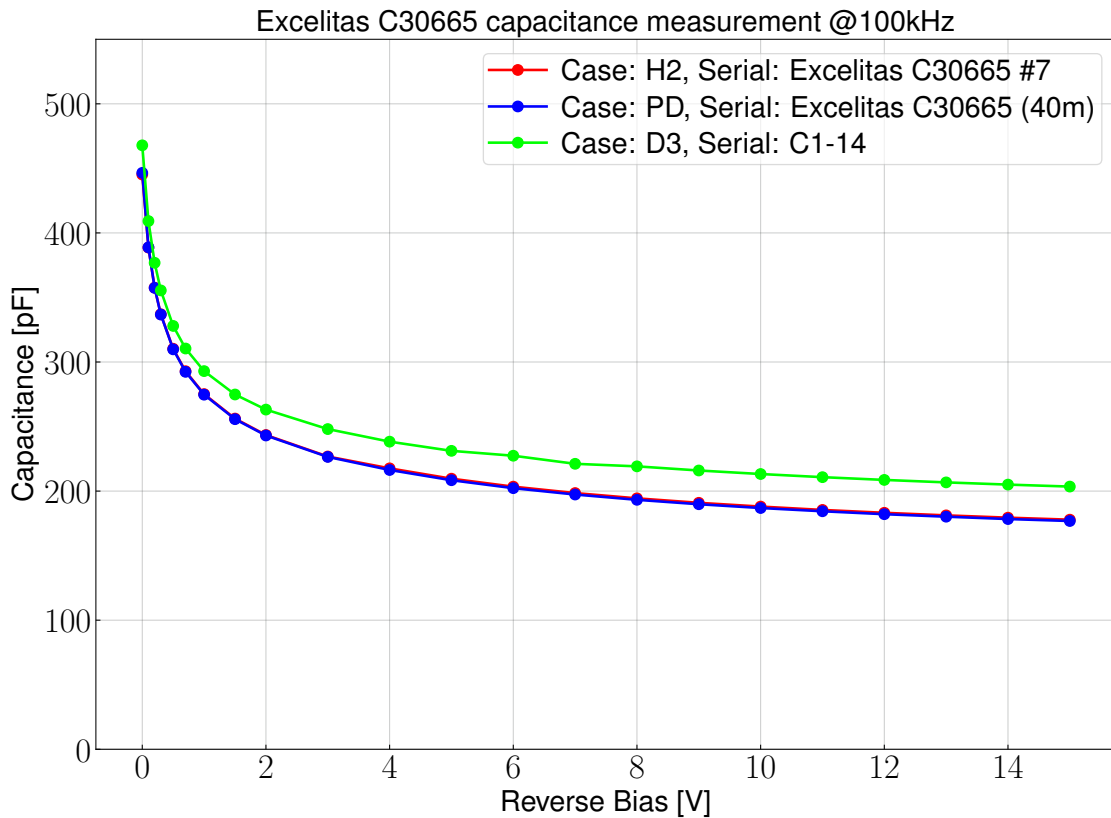


Figure 94: Capacitance measurements for C30665 photodiodes

2.5.1 Breadboard size measurement

[External Link]

http://nodus.ligo.caltech.edu:8080/OMC_Lab/27

[Description]

The OMC glass breadboards were inspected. The size and mass of them were measured.

[Experimental method]

The scale of the 40m bake lab (max 60kg, min resolution of 1g) was brought and used. The dimensions were measured by a huge caliper which was brought from Downs.

[Result]

Results are shown in Table. 18

Height measurements were made twice, once at each end.

S/N 01, 03, 04 look pretty similar. They should be the primary candidates.

S/N #	Mass [g]	Length [mm]	Width [mm]	Height [mm]	Notes
01	6146	449.66	149.85	41.42, 41.42	OMC(001)
02	6126	449.66	149.97	41.32, 41.32	OMC(002)
03	6143	449.76	149.98	41.39, 41.43	
04	6139	449.78	149.81	41.40, 41.40	OMC(003)
05	6132	449.76	150.03	41.27, 41.31	corner chip, front-bottom-left*
06	6138	449.84	149.71	41.42, 41.42	OMC(004)

Table 18: The dimensions and mass of the OMC glass breadboards. * Orientation of the chipping is relative to "front" face, i.e. long-short face with S/N on it, with S/N upright.

2.5.2 UV epoxy thickness

http://nodus.ligo.caltech.edu:8080/OMC_Lab/62

[Description]

Thickness of the UV epoxy was measured upon gluing test with UV-cure epoxy Optocast 3553-LV-UTF-HM.

The thickness of a pair of fused silica substrates (no coating) was measured without any glue. The total thickness before the gluing was 12.658 mm.

Then the UV epoxy was applied and the UV light was illuminated for curing. The thickness after the gluing was 12.663 mm. This indicates the glue thickness is $5 \pm 1 \mu\text{m}$.

2.5.3 Power meter calibration

S130C calibration: 0.975 ± 0.001

S410C calibration: 0.982 ± 0.005

S144C calibration: 0.9851 ± 0.0009

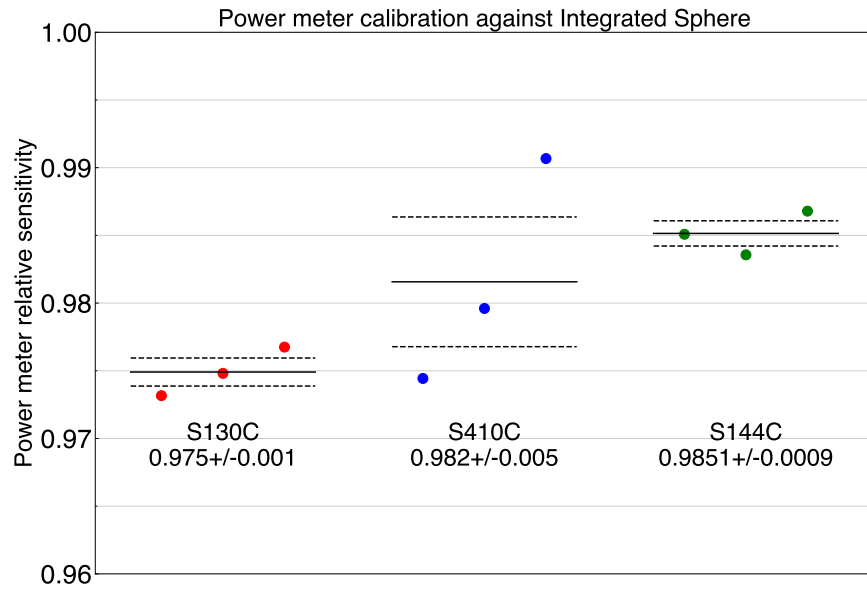


Figure 95: Calibration of various power meters against aLIGO Pcal integrated sphere

3 Test of the integrated OMC breadboards

During the OMC building, the parameters of the cavity geometry was necessary to be continuously monitored. In addition, various parameters of the OMC breadboards needed to be characterized after the assembly.

These tests of the integrated OMC have been done using a cavity locking setup built in the OMC lab at Caltech. This section explains the setup and the tests performed there.

In the following sections, the measurement items and methods are explained. In the subsequent sections, then the measurement results for each OMC will be presented.

The results of the OMC tests can be found in the referenced sections here. Here, brief descriptions of the unit history are also included.

OMC(001) Section 3.10:

- The original OMC installed to LLO on 6/18/2013.
- This OMC was unmounted from the OMCS on 9/8/2022.
- It turned out that the black glass beam dump had melted marks.
- It was then shipped to Caltech for forensic study.

OMC(002) Section 3.11:

- The original OMC installed to LHO on 11/18/2013.
- On 7/27/2016, LHO suffered from inability to lock the OMC because of the damage of one of the curved mirrors.
- The unit was uninstalled from HAM6 on 7/27/2016.
- It was shipped back to Caltech for forensic study and repair.

OMC(003) Section 3.12:

- The OMC unit for the 3rd IFO.
- It was completed on 7/15/2014.
- Upon the failure of OMC(002) at Hanford, the unit was shipped to LHO and installed in HAM6 on 8/4/2016.

OMC(002) Rev2 Section 3.13:

- The damaged OMC(002) got CM1 removed and a replacement mirror was attached in-situ. Luckily, the unit showed very good resonant structure and decided to be used as a legitimate spare.
- LLO claimed that their OMC(001) indicates reduction in the optical transmission. This unit was sent to LLO as a replacement.

OMC(004) Section ??:

- The place holder for the 4th unit.

3.1 Experimental setup

The test setup is similar to the one in Section 2.1.1. The setup has been built on the optical table at Room 056 in West Bridge, Caltech.

The schematic diagram of the optical setup is shown in Figure 96. The main difference from the RoC measurement setup is listed below:

- The input mode to the cavity was confined by a polarization-maintaining single-mode fiber (Thorlabs P3-1064PM-FC-5). Each fiber end has a collimation lens (Thorlabs CFC-2X-C) on a fiber mount (Thorlabs K6X) so that we can easily mode-match the input beam to the fiber, as well as the output from the fiber to the OMC.
- The input beam to the OMC cavity was elevated by a periscope to the optical height of the OMC cavity on the transport fixture.
- The photodetector for the PDH locking was replaced with PDA100CF, instead of PDA255. In addition, the transmission RF detector was replaced with Newfocus 1611FS (InGaAs, 1GHz BW), instead of 1801FS (Si, 125MHz BW).
- The reflection and transmission of the OMC cavity were monitored by CCDs.
- After the production of the first three OMCs, the resonant EOM was removed and the BB EOM provides the PDH modulation too. The modulation frequency of the EOM was tuned to be ~ 26 MHz so that it provides the maximum I-phase demodulated signal. In this new setup, a low noise AF preamp was added right after the demodulator LPF. Also, a low noise RF amp was added to the RF PD at the transmission.
- The reflected beam of the PBS after the fiber output was guided to Thorlabs PDA100A for the power monitoring. This is crucial for the precise power budgeting to track down the incident power drift.

The OMC itself was mounted on the transport fixture. The transport fixture was rigidly mounted on the optical table so that the OMC cavity does not shift during assembling and testing.

Mode-matching of the input beam to the OMC cavity was the crucial part of this optical setup in order to make the power budget measurement precise. The mode-matching telescope is consist of two plano-convex lenses ($f = 35$ mm and $f = 125$ mm). The distances of the lenses from the fiber coupler is shown in 97. This mode-matching telescope resulted the beam profile as shown in 99. This mode-matching solution was estimated to have the mode-matching of 99.8%. The actual beam had the mode-matching of about 99%, which seemed not limited by the second-order higher-order mode (Figure 101). Since the mode-matching telescope was built on a separate sub-breadboard (Figure 98), the same mode-matching quality of the beam can be reproduced by maintaining the optics on this sub-breadboard including the fiber and the coupler.

The electrical setup is shown in Figure 102. For the measurement of the FSR and TMS of the cavity, the technique in Section 2.1.1 was used again. Therefore the electrical setup is

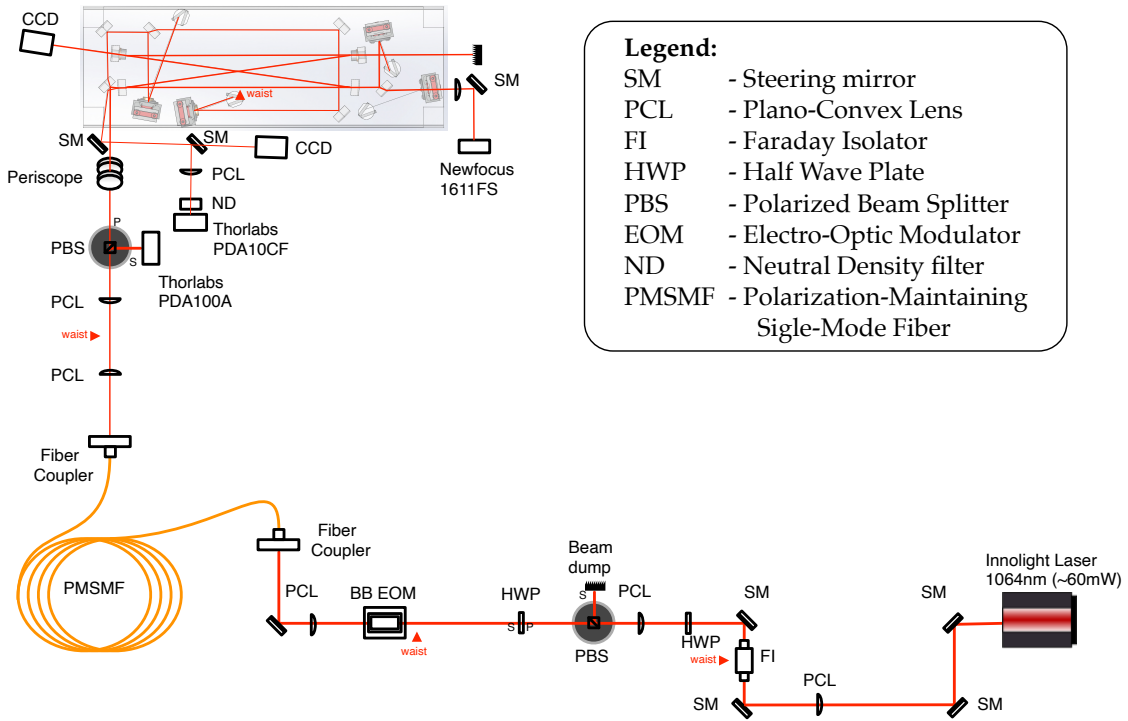


Figure 96: Optical setup for the OMC test.

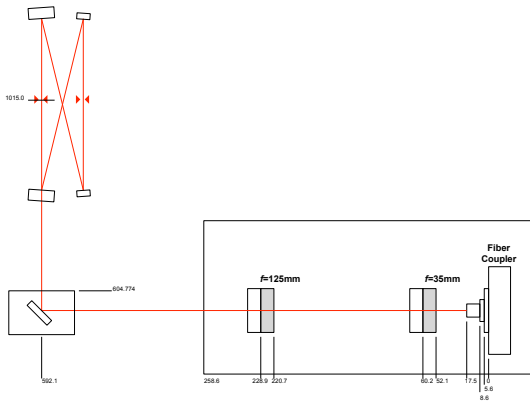


Figure 97: Mode-matching telescope for the OMC cavity. The small numbers indicates the distance of the optics from the body of the fiber coupler in the unit of mm. The waist is located at the distance of 1015.0 mm.

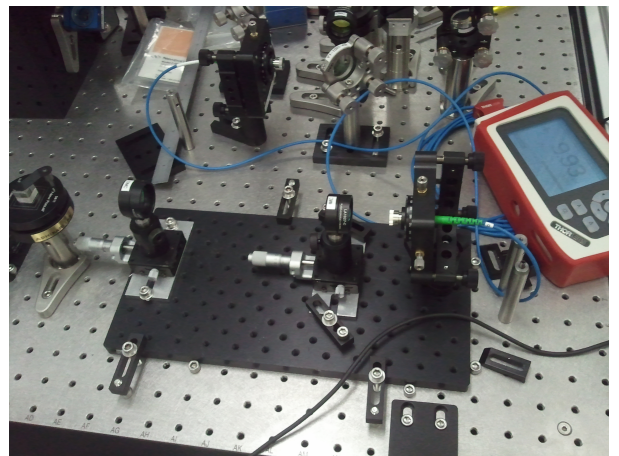


Figure 98: The actual setting of the mode matching telescope.

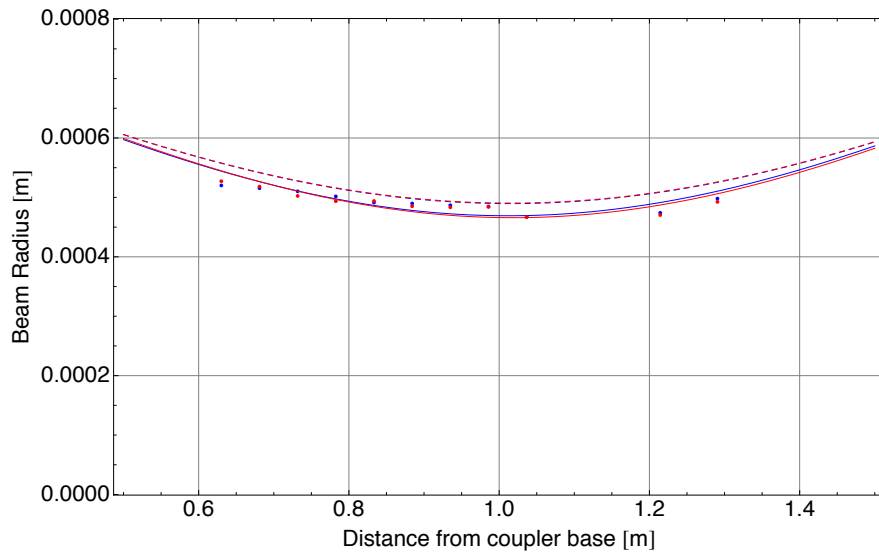


Figure 99: Beam profile measurement for the OMC cavity mode-matching. The blue and red dots indicate the measured horizontal and vertical beam radius. The solid lines indicate the estimated mode profile with curve fitting. The dashed lines indicate the calculated OMC modes.

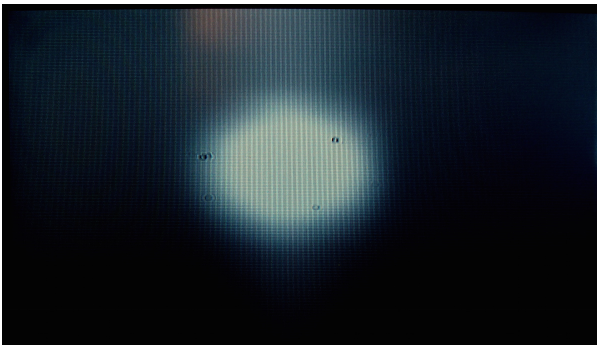


Figure 100: Photo of the transmission monitor CCD when the cavity is locked.

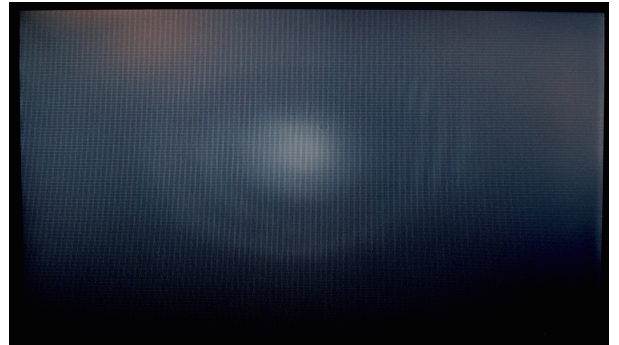


Figure 101: Photo of the reflection monitor CCD when the cavity is locked.

basically same as the one in the RoC measurement (Figure 2) with some improvement of the components. Particularly, the cavity is now just locked with laser PZT via a high-voltage driver.

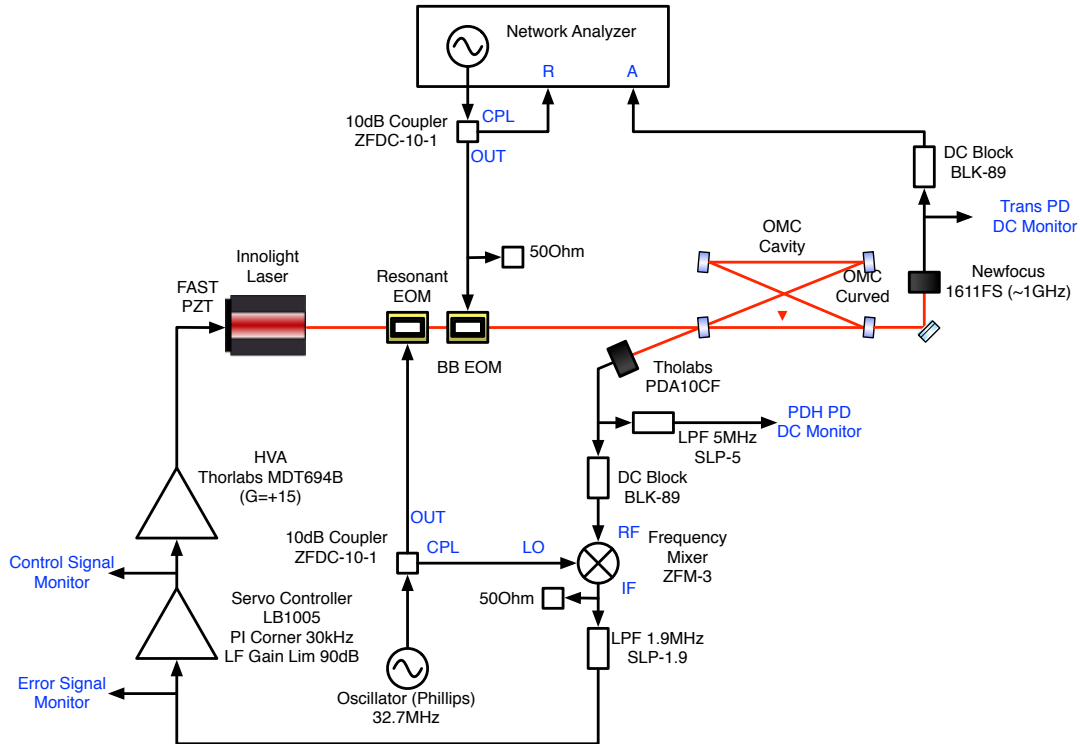


Figure 102: Electrical setup for the OMC test.

3.2 Cavity geometry test

3.2.1 Cavity absolute length measurement with detuned locking

[Description]

When a cavity is locked with an error signal offset, the detuning imposes frequency-modulation to amplitude-modulation (FM-AM) conversion. This conversion does not happen when the modulation frequency is at the free spectral range. Therefore the transfer function from the phase modulation at an EOM to amplitude modulation at the transmission RF PD has a dip at the FSR. This effect is described in [1].

[Experimental method]

This test has been done with the following procedure:

- Lock the OMC cavity and maximize the transmission by aligning the input beam. Align the transmission and reflection PDs too.
- Adjust the input signal offset of the LB1005 servo module.

- Measure the transfer function between R channel (modulation signal for the BB EOM) and A channel (transmission PD RF). The twin-peak structure should be present at around 265MHz (or 262MHz for OMC(002)).
- Adjust the offset so that the structure is maximized.

The cavity FSR can be determined by fitting the dip in the transfer function. The fitting function is

$$f(a, f_0, \phi, dT, f) = a e^{-i2\pi f dT} (f - e^{i\phi} f_0) , \quad (2)$$

where f is the variable (frequency) and the others are fitting parameters: f_0 corresponds to the FSR. The other parameters a, ϕ, dT are related to an amplitude, a complex constant offset, and a time delay of the measurement.

3.2.2 Cavity length and finesse measurement with RFAM injection

[Description]

Another technique to characterize the cavity length is the amplitude modulation injection. The similar measurement can be done with the injection of the frequency shifter carrier using an AOM. In our case, the frequency shifter AOM was broken, and the AM injection technique was needed.

[Experimental method]

When the input polarization to the EOM is rotated, the actuation on the EOM produces voltage dependent birefringence. This is converted to the amplitude modulation via polarization optics between the EOM and the OMC. Therefore the EOM works as the AM injector.

One problem of this technique is that this RFAM cause the offset in the PDH signal as the polarization was rotated before the EOM for the PDH signal. If we have the offset in the PDH locking, this causes FM-AM conversion around the FSR frequency and confuses the response of the AM injection method. The PDH offset was cancelled by the input offset of the servo filter so that the line width of the response is minimized.

[Result]

The measured transfer function was fitted by the following model function:

$$f(a, f_{\text{FSR}}, F, dT, f) = a \left[\frac{1 - r(F)}{1 - r(F)e^{-i2\pi f/f_{\text{FSR}}}} \right]^2 e^{-i2\pi f dT} , \quad (3)$$

where $r(F)$ is the inverse function of

$$F = \frac{\pi\sqrt{r}}{1-r}, 0 < r < 1. \quad (4)$$

f is the variable (frequency) and the others are fitting parameters. f_{FSR} and F correspond to the FSR and the finesse of the cavity. The other parameters a, dT are related to an amplitude, and a time delay of the measurement.

3.2.3 Transverse-mode spacing measurement

[Description]

The transverse mode spacing of the OMC cavity was measured. The vertical and horizontal modes have different TMSs as expected. It was found that the TMSs depend on the PZT voltages.

[Experimental method]

Similarly to the measurement in Section 2.1.1, the transverse mode spacing (TMS) of each OMC cavity was measured. Because of the intrinsic astigmatism of the ring cavity, the TMSs for the vertical and horizontal directions were measured independently.

It was also found that the TMS is dependent on the PZT voltage. This is probably due to the three dimensional deformation of the ring PZT with the voltage applied (See https://nodus.ligo.caltech.edu:8081/OMC_Lab/314). The TMSs in both directions were measured with each PZT voltage swept from 0V to 200V with 50V increment.

[Result]

The measured transfer function has three peaks associated with the 1st order modes. Each peak was fitted by the following function:

$$f(a_R, a_I, f_0, \Gamma, dT, f) = (a_R + i a_I) e^{-i2\pi f dT} \frac{\Gamma}{\Gamma + i(f - f_0)} \quad (5)$$

where f is the variable (frequency) and the others are fitting parameters. f_0 and Γ correspond to the peak frequency and the half line width. The other parameters a_R, a_I, dT are related to the real and imaginary part of the amplitude, and a time delay of the measurement.

3.3 Power budget

[Description]

The transmission performance and the optics transmissivities were estimated from the power measurements.

[Experimental method]

The transmission performance and mode matching ratio of an OMC cavity can be estimated from the cavity's visibility and the amount of incident and transmitted light. The OMC cavity uses the same optics for the input and output mirrors so that the cavity becomes critically coupled. This means that the reflectivity of the cavity to the mode-matched beam is negligibly small in the approximation with a small optical loss. Therefore, the visibility well represents the measurement of the mode matching ratio. The cavity transmission performance can then be obtained by comparing the mode-matched light power with the transmitted light power. The dissipated optical power is explained by the optical loss.

If the cavity finesse is additionally given, this represents the roundtrip reflectivity of the cavity. If the reflectivity of the curved mirrors are assumed to be the unity, the transmission

from the curved mirrors are incorporated in the optical loss and this gives the reflectivity for the input and output mirrors. This information makes the estimation of the mode matching even improved.

When the transmitted power from the curved mirrors are given, we will be able to estimate the transmittance of the curved mirrors.

In total, what we want to measure is:

- OMC incident light power: P_{INC}
- OMC transmitted light power from FM2: P_{FM2}
- OMC transmitted light power from CM1: P_{CM1}
- OMC transmitted light power from CM2: P_{CM2}
- OMC reflected light power in volt (cavity locked): $V_{\text{REFL-LOCKED}}$
- OMC reflected light power in volt (cavity unlocked): $V_{\text{REFL-UNLOCKED}}$
- Cavity finesse: \mathcal{F}

We want to incorporate the presense of the input beam splitter (BS1). The actual cavity incident power P_{in} is given as:

$$P_{\text{in}} = (1 - T_{\text{BS1}})P_{\text{INC}} \quad , \quad (6)$$

where T_{BS1} is the power transmissivity of BS1 (E coating), which is 7400 ppm (see Section 2.2.3).

The incident beam power to the cavity (P_{in}) can be split into the mode-matched (coupled) and mode-mismatched (junk) light power (P_{coupled} and P_{junk} , *respectively*). i.e.,

$$P_{\text{in}} = P_{\text{coupled}} + P_{\text{junk}} \quad (7)$$

When the cavity mirror amplitude reflectivities and transmissivities for FM1, FM2, CM1, and CM2 are defined as $(r_1, t_1), (r_2, t_2), (r_3, t_3), (r_4, t_4)$, respectively, the cavity finesse is defined as:

$$\mathcal{F} = \frac{\pi\sqrt{r}}{1-r} \quad , \quad (8)$$

where $r = r_1 r_2 r_3 r_4$ is the roundtrip reflectivity of the cavity. r_i and t_i have the following relationship using the average loss per mirror A :

$$r_i^2 + t_i^2 + A = 1 \quad (i = 1, 2, \dots, 4). \quad (9)$$

The amplitude reflectivity of the cavity, the transmissivity of the cavity with regard to FM2, CM1, and CM2 can be described as

$$r_{\text{cav}} = -r_1 + \frac{t_1^2 r}{r_1(1-r)} \quad (10)$$

$$t_{\text{cav}2} = \frac{t_1 t_2}{1-r} \quad (11)$$

$$t_{\text{cav}3} = \frac{t_1 r_2 t_3}{1-r} \quad (12)$$

$$t_{\text{cav}4} = \frac{t_1 r_2 r_3 t_4}{1-r} \quad (13)$$

By solving these equation (numerically) under the additional condition of $r_2 = r_1$, we obtain P_{junk} , r_2 , r_3 , r_4 , and A .

The mode matching ratio η_{MM} is obtained by

$$\eta_{\text{MM}} = P_{\text{couple}}/P_{\text{in}} \quad (14)$$

The cavity (only) transmissivity is $t_{\text{cav}2}^2$ and thus the total OMC throughput and the total optical loss of the OMC are

$$\eta_{\text{OMC}} = (1 - T_{\text{BS}1})t_{\text{cav}2}^2 \quad (15)$$

$$A_{\text{OMC}} = 1 - \eta_{\text{OMC}} \quad (16)$$

In the actual measurement, we also need to subtract the dark offset of the power meters and the photodetectors. All the measurements should be measured together with the value of the power reference photodetectors to compensate the short term power drift.

3.4 PZT characterization

3.4.1 PZT response: DC scan

[Description]

The displacement of each PZT was calibrated using the cavity resonances and the voltage applied to the PZT.

[Experimental method]

Each PZT was swept by applying 1Hz triangular voltage from 0V to 10V on Thorlabs' HV amplifier (MDT694B). The amplifier gain was $G = 15$. Nominally about four TEM00 peaks were observed in a sweep between 0 and 10V.

Mark the input voltages where the peaks were. Each peak was mapped on the corresponding fringe among four. i.e., each peak was separated by 532 nm. The effect of non-zero AOI is 0.2% and negligible here. Then the multiple slopes (up and down) were fitted with a liner function separately to obtain the slope.

3.4.2 PZT response: AC scan

[Description]

The frequency response of each PZT was measured with the locked cavity.

[Experimental method]

Lock the OMC cavity with the fast laser actuation. Each PZT was shaken with an FFT analyzer for transfer function measurements. No bias voltage was applied.

The displacement data was obtained from the laser fast feedback. Since the control UGF was above 30 kHz, the data was valid at least up to 30 kHz. The over all calibration of the each curve was then adjusted so that it agrees with the DC response of the PZTs (as shown above).

3.5 Photodiode alignment

3.5.1 DCPD/QPD shim height adjustment

[Description]

The shim thickness was adjusted to have the beam hit the center of the PD as much as possible.

[Experimental method]

Attach a dummy PD disk on a PD housing. Approximately align the housing so that the beams can be seen right next to the center hole of the dummy disks. Take the CCD image of the housing so that the image analysis can tell us how much the beam is away from the center of the disk. The increment of the shim height is 0.25 mm. Therefore the miscentering in the height is 0.125 mm in the worst case.

3.5.2 QPD housing alignment

[Description]

The QPD alignment was adjusted using the aligned beam to the cavity and the 4ch transimpedance amplifier.

[Experimental method]

First of all, the reflection from a QPD should be directed to the beam dump. While keeping this condition, the QPD housing is adjusted to have the beam as much as possible, by looking at the output of the QPDs.

Attach the test cable for the QPD on the QPD housing. The other side of the cable is a DB9 connector which can be connected to a QPD transimpedance amplifier. The transimpedance of the circuit has the gain of 1 kV/A. As this board ([D1001974](#)) does not have X/Y/SUM outputs, a custom circuit was made.

Record the incident power to the QPD, X/Y/SUM outputs, as well as the output for each

segment. When the X/Y signals are normalized with the incident power, the normalized values represents the spot displacement with the following relationship:

$$V_{\text{normalized}} = \text{erf} \left(\frac{\sqrt{2}d}{w} \right) , \quad (17)$$

where d and w are the distance of the spot from the center and the beam radius.

Adjust the QPD housing, until the horizontal displacement is less than a 100 μm .

3.5.3 DCPD housing alignment / DCPD&QPD photos

[Description]

DCPD housing is aligned and take the CCD images of the spot on all the photodiodes.

[Experimental method]

The alignment of a DCPD housing is adjusted so that the beam hits the center of the actual PD. The reflection from the DCPD should be nicely dumped with the beam dump.

Once the alignment is done, take the photographs of the spot on the DCPDs and QPDs. The photodiode housings are no longer moved. They are supposed to be the reference for the DCPD/QPD alignment from this point.

3.6 Misc measurements

3.6.1 Weight

[External Link]

http://nodus.ligo.caltech.edu:8080/OMC_Lab/144

[Description]

Upon the installaiton of OMC(001), we measured the various weight related to the OMC.

[Result]

- OMCS suspension cage and the OMCS transportation box: 250.8 lb
- OMCS transportation box: 150.2 lb
- \Rightarrow OMCS suspension cage: 100.6 lb = 45.63 kg
- Metal (dummy) OMC breadboard: 7.26 kg
- Glass OMC and transportation fixture: 16.382 kg
- Transportation fixture only: 9.432 kg
- *Rightarrow* Glass OMC weight = 6.95 kg
- Added mass: 300 g \Rightarrow 7.25 kg

3.7 Backscatter measurement 1

[External Link]

http://nodus.ligo.caltech.edu:8080/OMC_Lab/207

http://nodus.ligo.caltech.edu:8080/OMC_Lab/208

http://nodus.ligo.caltech.edu:8080/OMC_Lab/209

<https://alog.ligo-la.caltech.edu/aLOG/index.php?callRep=61478>

[Description]

The backscattering reflectivity of an OMC was measured.

[Experimental method]

Figure 103 a): Insert a BS before the OMC input. Measure the backreflected power that shows up at the reflection port of the BS. Estimate the backscatter reflectivity from the measurement.

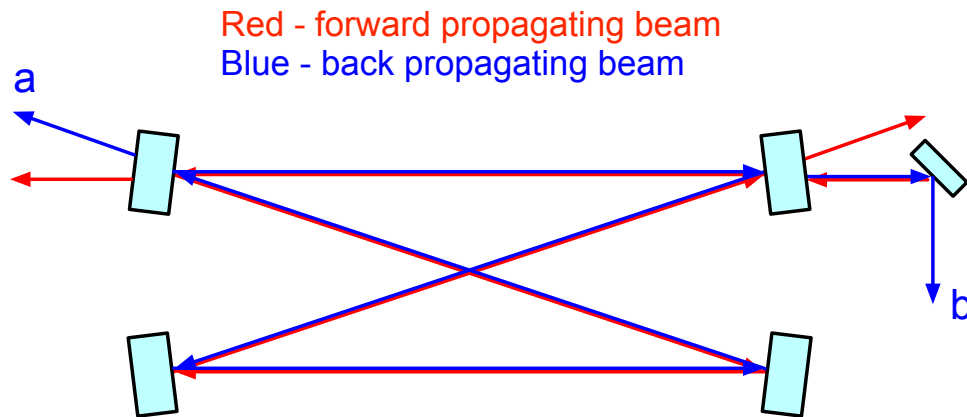


Figure 103: Measurements of the backscatter reflection. Method 1: measurement using a beamsplitter. Method 2: measurement of the transmitted power of the back propagating mode.

- A CVI 45P 50:50 BS was inserted in the input beam path. The backward propagating beam was reflected by the BS. The reflected beam power was measured with a powermeter. This BS was tilted from the nominal 45 deg so that the reflection of the input beam is properly dumped. This yielded the reflectivity of the BS deviated from 45deg.
- The powermeter was aligned with the beam retroreflected from the REFL PD and the iris in the input path. The iris was removed during the measurement as it causes a significant scatter during the measurement. Note that no visible spot was found at the powermeter side no matter whether the cavity was either locked or not.
- The beam dump for the forward going beam, the beamsplitter, and the mirrors on the periscope were cleaned.

- The power meter was heavily baffled with anodized Al plates and Al foils. This reduced many spurious contributions from the REFL path and the input beam path. Basically, the power meter should not see any high power path.
- The REFL path was rebuilt so that the solid angle of the PD was reduced.
- The power meter is now farther back from the BS to reduce the exposed solid angle to the diffused light

[Result]

Summary

OMC(003) was tested and the backscatter reflectivity of $0.71 \pm 0.01\text{ppm}$ was measured.

Measurement

- Input beam power: $P_{\text{in}} = 12.3 \pm 0.001 \text{ mW}$
- Sampling beamsplitter reflectivity: $R_{\text{BS}} = 0.549 \pm 0.005$
- The reflected power measured with the OMC locked $P_{\text{back}} = 4.8 \pm 0.05 \text{ nW}$
- See Figure 104 for the detailed setup. Note that the aperture size of the iris before the power meter was $\sim 5.5 \text{ mm}$ in diameter.

The backscatter reflectivity is then estimated

$$R_{\text{back}} = \frac{P_{\text{back}}}{R_{\text{BS}}P_{\text{in}}} \quad (18)$$

$$= 0.71 \pm 0.01\text{ppm} \quad . \quad (19)$$

Aperture size test

In order to see if the detected power is diffused light or not, the dependence of the detected light power on the aperture size was measured. Note that the dark offset was nulled during the measurement.

The measured backreflection power as a function of the aperture size was converted to the power density (Fig. 105).

This result means that the detected power is concentrated at the central area of the aperture. Note that the vertical axis is logarithmic. If the detected power is coming from a diffused beam, the power density should be uniform. Therefore this result strongly suggests that the detected power is not a diffused beam but a reflected beam from the OMC.

According to this result, the aperture size of 2.6mm in radius (5.5mm in diameter) was determined for the final reflected power measurement.

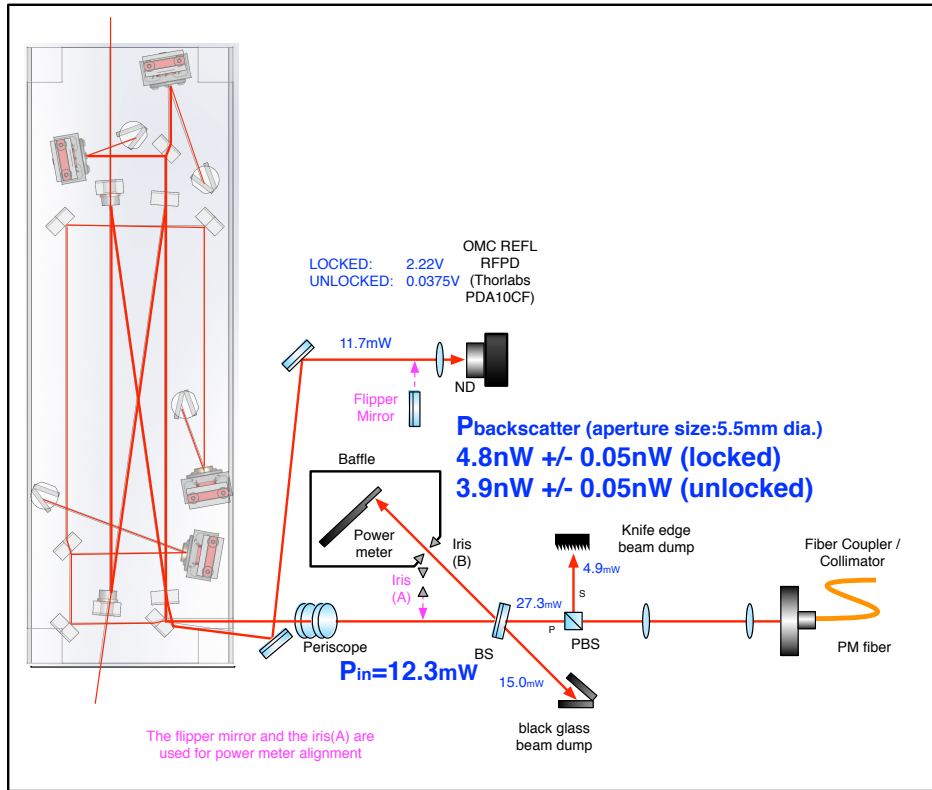


Figure 104: Measurement setup of the backscatter reflection (1)

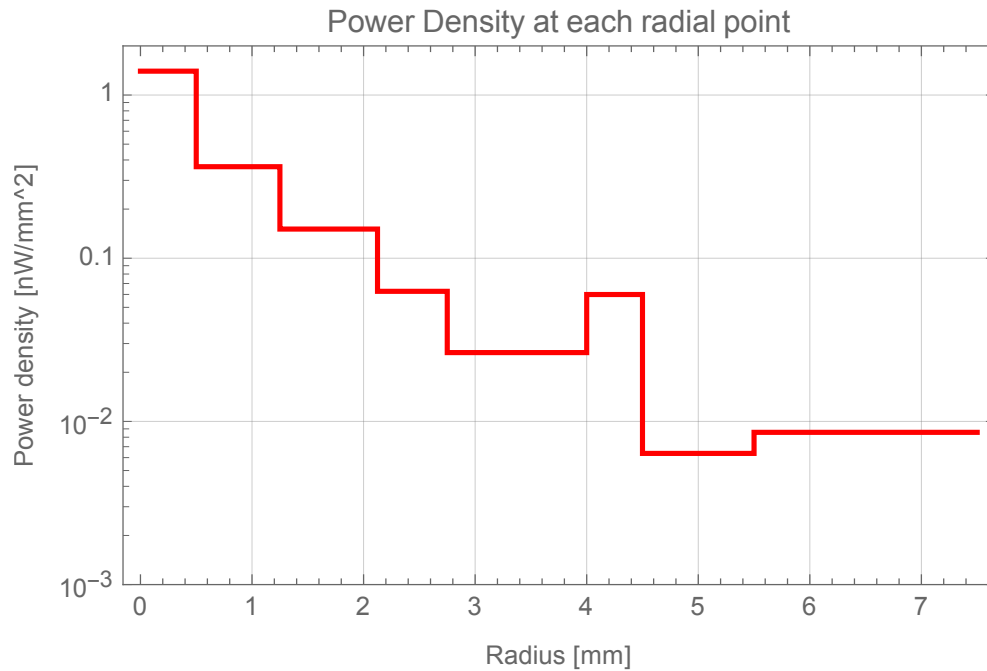


Figure 105: Dependence of the detected backscattered power on the aperture size

3.8 Backscatter measurement 2

[External Link]

http://nodus.ligo.caltech.edu:8080/OMC_Lab/422

<https://alog.ligo-la.caltech.edu/aLOG/index.php?callRep=61478>

[Description]

Another method to characterize the backscattering reflectivities of OMC(001) and OMC(002R2). T. Cullen joined the work at LLO.

[Experimental method]

Figure 103 b): Assume the OMC cavity is the main source of the backscatter reflection. Measure the optical power ratio of the forward-propagating and back-propagating modes of the OMC cavity. Estimate the backreflectivity of the OMC from the incident power and the mode matching ratio.

- Place a small deflecting mirror at the transmission.
- Place a flat mirror at the deflected transmission. When the alignment of this mirror is adjusted to retroreflect the beam, most of the beam goes through the cavity. Therefore the alignment can be optimized using one of the CM mirror transmission power.
- This condition allows us to locate the power meter at the reverse-propagating spot of the transmission (Fig. 106).
- Place a black glass beam dump for the main (bright) transmission so that this does not disturb the weak power measurement for the back propagating mode. (Fig. 107).
- Now the power meter is receiving the counter-propagating beam power. Turn off the room light and place an anodized Al baffle as shown in Figure 107). Move the baffle to block only the beam of the back-propagating mode. Hit the power meter null button, then move the baffle out. Record the power meter reading.
- Now measure the power of the deflected main transmission. This tells us the power ratio between the forward- and back-propagating beams.
- Remove the small deflecting mirror and measure the power of the main transmission. This tells us the reflectivity of the small mirror. We assumed that the OMC is symmetric and the same amount goes back to the input path. The reflectivity can be calculated from this amount and the incident power multiplied with the mode matching ratio.

Figure 108 shows the two types of deflecting mirrors. The flat rectangle mirror was used in the test at Caltech. Later at LLO, we found that it is not easy to steer the both forward- and back-propagating beams picked off with no clipping of both beams. Therefore we decided to use the vertical steering at LLO employing the triangular prism. Figure 109 shows how the vertically steered beams were guided to the power meter.

[Result]

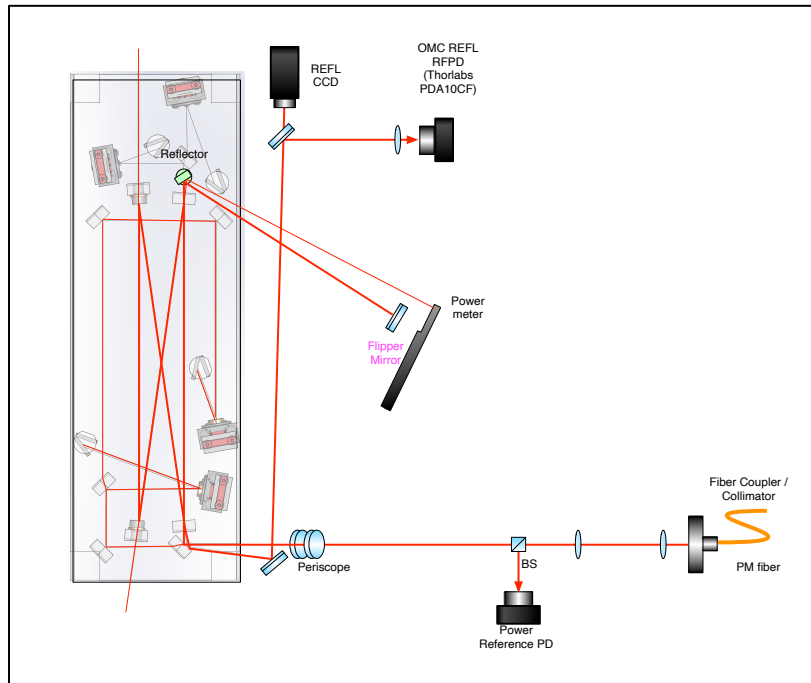


Figure 106: Measurement setup of the backscatter reflection (2-1)

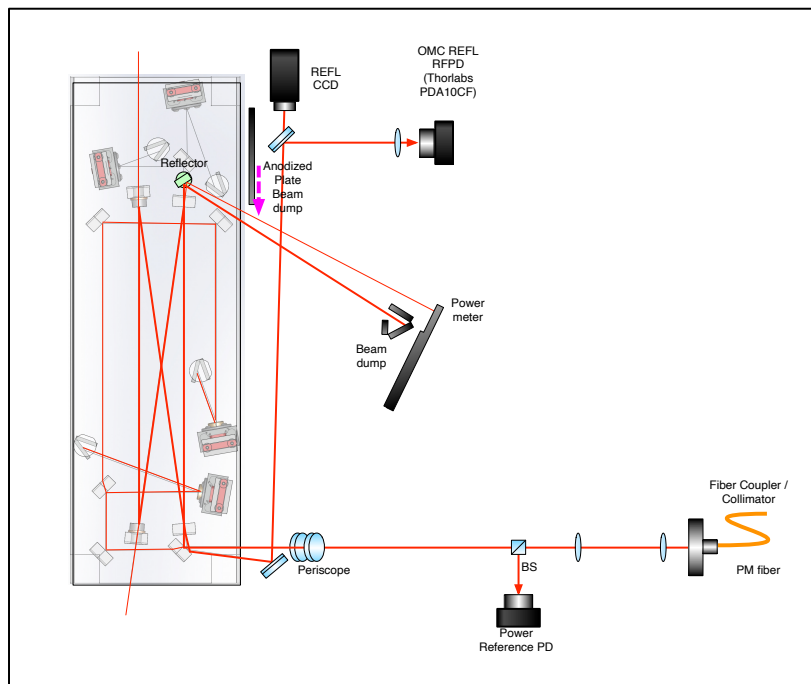


Figure 107: Measurement setup of the backscatter reflection (2-2)

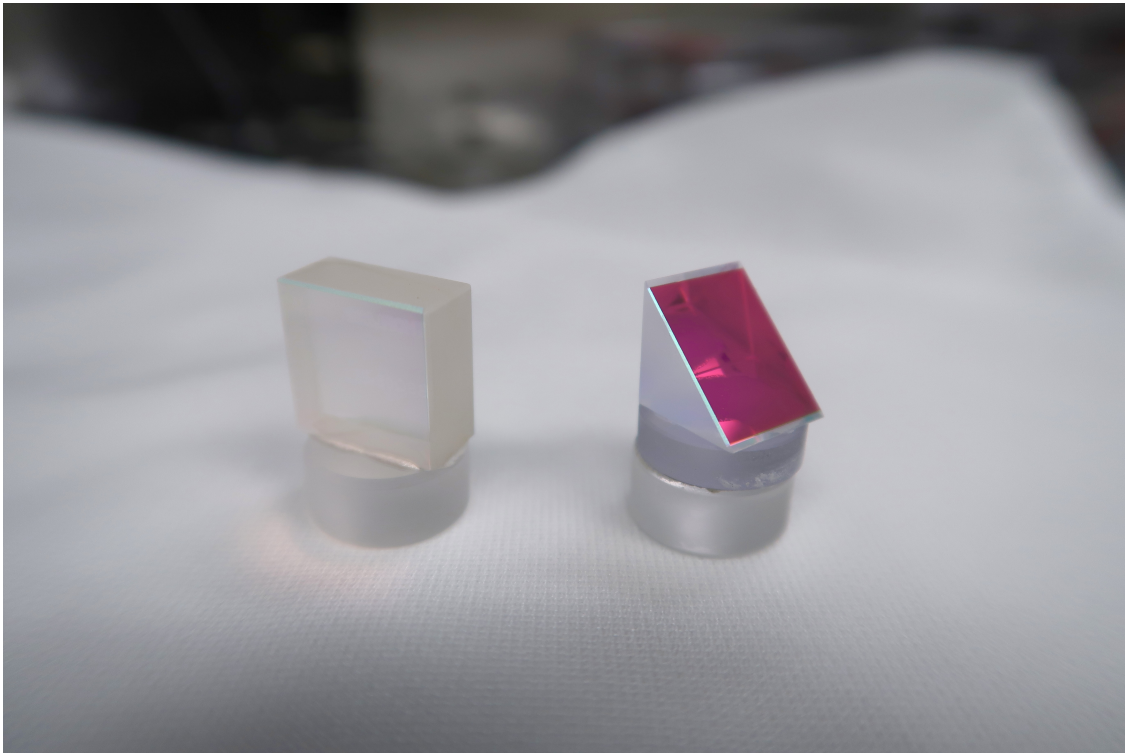


Figure 108: Prism mirrors used for the backscatter reflection measurements

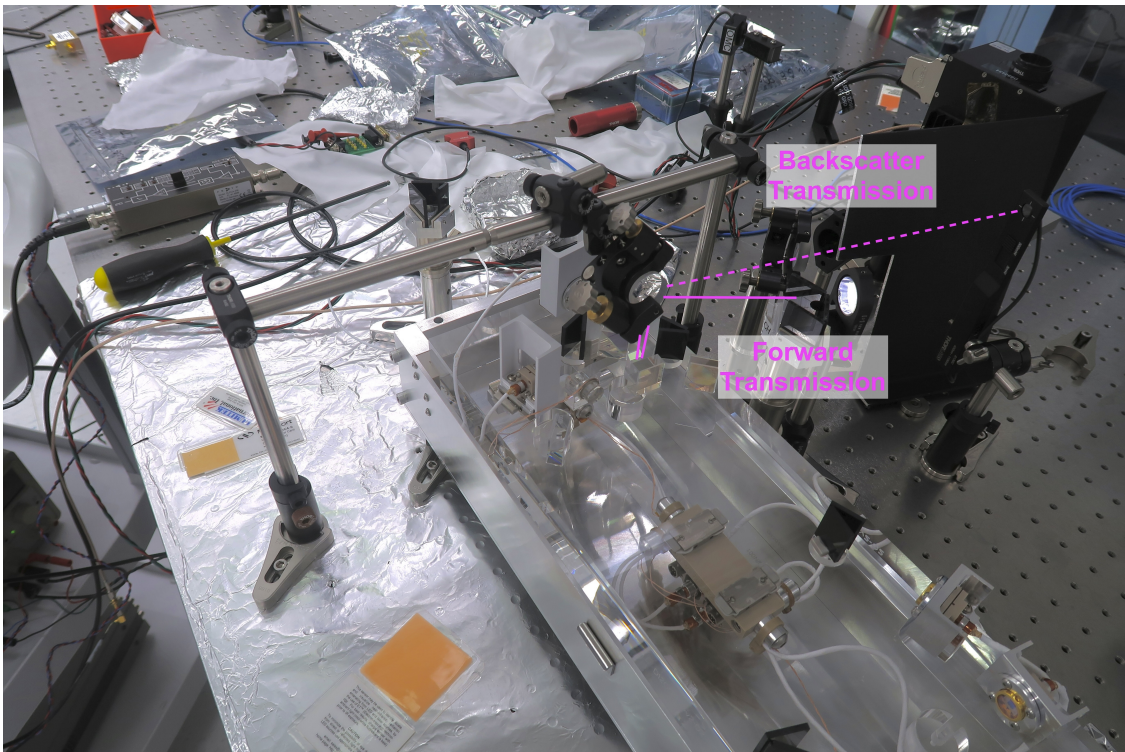


Figure 109: Prism mirrors used for the backscatter reflection measurements

The following tests are carried out with OMC(002R2). At LLO OMC(001) was also tested.

Result of the test at Caltech (2022/6/22):

- Measured power for the back-propagating mode: $P_{\text{back}} = 53.3 \pm 0.6 \text{ nW}$
- Measured power for the forward-propagating mode: $P_{\text{forward}} = 84.0 \pm 0.1 \text{ nW}$
- Direct measurement of the OMC transmission: $P_{\text{rmtrans}} = 96.6 \pm 0.1 \text{ mW}$.

The prism reflectivity was $R_{\text{prism}} = P_{\text{forward}}/P_{\text{trans}} = 0.870$

The cavity transmission for the matched beam was $T_{\text{cav}}R_{\text{inputBS}} = 0.963$, where T_{cav} was measured on the same day and the first OMC BS reflectivity $R_{\text{inputBS}} = (1 - 7400 \text{ ppm})$. This leads the incident resonant TEM₀₀ power on the OMC cavity to be $P_{\text{rmtrans}}/(T_{\text{cav}}R_{\text{inputBS}}) = 100.3 \text{ mW}$.

$$R_{\text{back}} = \frac{P_{\text{back}}R_{\text{inputBS}}}{R_{\text{prism}}} / \left(\frac{P_{\text{trans}}}{T_{\text{cav}}R_{\text{inputBS}}} \right) \quad (20)$$

$$= 0.606 \pm 0.007 \text{ ppm} \quad (21)$$

Results of the test at LLO

OMC(001) (2022/9/16)

- Mode Matching: 0.9613 ± 0.0003
- OMC Throughput: 0.947 ± 0.006
- Take1
 - The back-propagating beam transmission: $17 \pm 1 \text{ nW}$
 - The forward-propagating beam transmission: $34.14 \pm 0.5 \text{ mW}$
 - The incident power to the OMC : $38.85 \pm 0.5 \text{ mW}$
 - **Backscatter reflectivity: $0.47 \pm 0.03 \text{ ppm}$**
- Take2
 - The back-propagating beam transmission: $18 \pm 1 \text{ nW}$
 - The forward-propagating beam transmission : $34.10 \pm 0.5 \text{ mW}$
 - The incident power to the OMC : $39.45 \pm 0.5 \text{ mW}$
 - **Backscatter reflectivity: $0.50 \pm 0.03 \text{ ppm}$**

OMC(002R2) (2022/9/19)

- Mode Matching: 0.9638 ± 0.0002

- Throughput: 0.975 ± 0.004
- Take1: Rejected
- Take2
 - The back-propagating beam transmission: 11 ± 0.5 nW
 - The forward - propagating beam transmission : 36.2 ± 0.5 mW
 - The incident power to the OMC : 40.15 ± 0.5 mW
 - **Backscatter reflectivity: 0.29 ± 0.01 ppm**
- Take3
 - The back-propagating beam transmission: 16 ± 0.5 nW
 - The forward - propagating beam transmission : 35.5 ± 0.5 mW
 - The incident power to the OMC : 40.1 ± 0.5 mW
 - **Backscatter reflectivity: 0.44 ± 0.02 ppm**

3.9 Vibrational property

3.9.1 Vibrational test of the OMC breadboard

[External Link]

http://nodus.ligo.caltech.edu:8080/OMC_Lab/210

http://nodus.ligo.caltech.edu:8080/OMC_Lab/211

<https://alog.ligo-la.caltech.edu/aLOG/index.php?callRep=8674>

<https://alog.ligo-la.caltech.edu/aLOG/index.php?callRep=10554>

[Description]

The body mode and other resonant modes of the OMC assembly was tested

Motivation

Zach's LLO OMC(001) characterization (see [LLO ALOG 8674](#) revealed that the OMC length signals have the forest of spikes at 400-500Hz and 1kHz regions. He tried to excite these peaks assuming they were coming from mechanical systems. It was hard to excite them with the OMC PZT, but actuating the OMCS slightly excited them (see [LLO ALOG 10554](#)).

Because the OMC length control loop can't suppress these peaks due to their high frequency and high amplitude, they limit the OMC residual RMS motion. This may cause the coupling of the OMC length noise into the intensity of the transmitted light. We want to eventually suppress or eliminate these peaks.

By this vibration test we want to:

- confirm whether the peaks are coming from the OMC or not.
- identify what is causing the peaks if they are originated from the OMC

- correct experimental data for comparison with FEA

[Experimental method]

- Used OMC(003) for the test.
- Place a NOLIAC PZT on the object to be excited.
- Look at the actuation signal for the OMC locking to find the excited peaks.
- Added some vibration isolation. Four 1/2" rubber legs were added between the OMC bread board and the transport fixture (via Al foils). In order to keep the beam height same, 1/2" pedestal legs were removed.
- The HEPA filter at the OMC side was stopped to reduce the excitation of the breadboard. It was confirmed that the particle level for 0.3 μm was still zero only with the other HEPA filter.

[Result]

Summary

- The OMC breadboard has a body-mode resonance at 1.2 kHz. The resonant freq may be chagned depending on the additional mass and the boundary condition.
- There is no forest of resonances at around 1kHz. A couple of resonances It mainly starts at 5 kHz.
- The PZT mirrors (CM1/CM2) have the resonance at 10kHz as I saw in the past PZT test.

Breadboard

The mode at 1.1kHz was most eminently excited (red curve in Fig. 110). Like in the later cases, the structures above 5 kHz were also excited.

The result of the high resolution measurement is shown in Figure 111.

The 1.1-kHz mode was suspected to be the bending mode of the breadboard. To confirm this, metal blocks (QPD housing and a 4" pedestal rod) were added on the breadboard to change the load. This actually moved (or damped) the 1.1-kHz mode (blue curve in Fig. 110).

DCPD / QPD

See Figrues 112 and 113.

Vibration on the DCPDs and QPDs mainly excited the modes above 2 3kHz. Some excitation of the breadboard mode at 1.1kHz was also seen.

CM1/CM2 (PZT mirrors)

See Figure 114.

Basically excitation was dominated by the PZT mode at 10 kHz. Some spurious resonances were seen at 4~5 kHz but it was believed that they were associated with the weight placed on the excitation PZT.

FM1/FM2 and peripheral prism mirrors (BSs and SMs)

The modes of the FMs are seen ~8 or 12 kHz (Fig. 115). I believe they were lowered by the weight for the measurement. In any case, the mode frequency is quite high compared to our frequency region of interest.

As the prism resonance is quite high, the excitation is directly transmitted to the breadboard (Fig. 116). Therefore the excitation of the non-cavity mirrors caused similar effect to the excitation on the breadboard. In fact what we can see from the plot is excitation of the 1.1-kHz body mode and many high frequency resonances.

Beam dumps

See Figure 117. This is also similar to the case of the peripheral mirrors.

3.9.2 FEM analysis of the resonant modes for the components

[External Link]

http://nodus.ligo.caltech.edu:8080/OMC_Lab/213

http://nodus.ligo.caltech.edu:8080/OMC_Lab/218

[Description]

FEM analysis was run on COMSOL to confirm the resonances of the mechanical components.

[Result]

- **Tombstone Prism:**
 - Fundamental mode: 12.3 kHz (Fig. 118).
 - Secondary mode: 16.9 kHz (Fig. 119).
- **DCPD Housing:**
 - Fundamental mode: 2.9 kHz (Fig. 120).
 - Secondary mode: 4.1 kHz (Fig. 121).
- **QPD Housing:**
 - Fundamental mode: 6.0 kHz (Fig. 122).

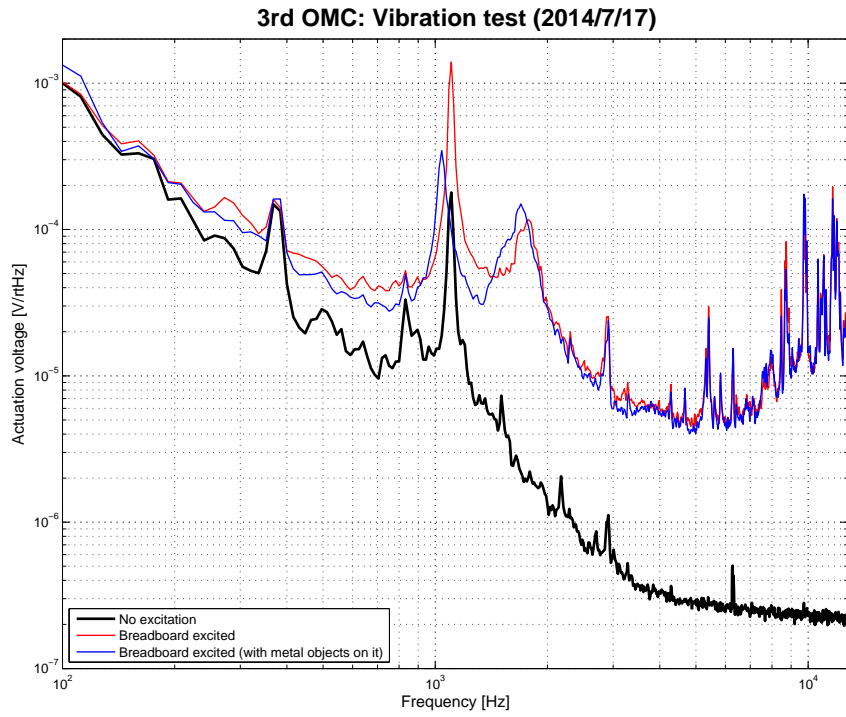


Figure 110: Vibrational test of the OMC breadboard

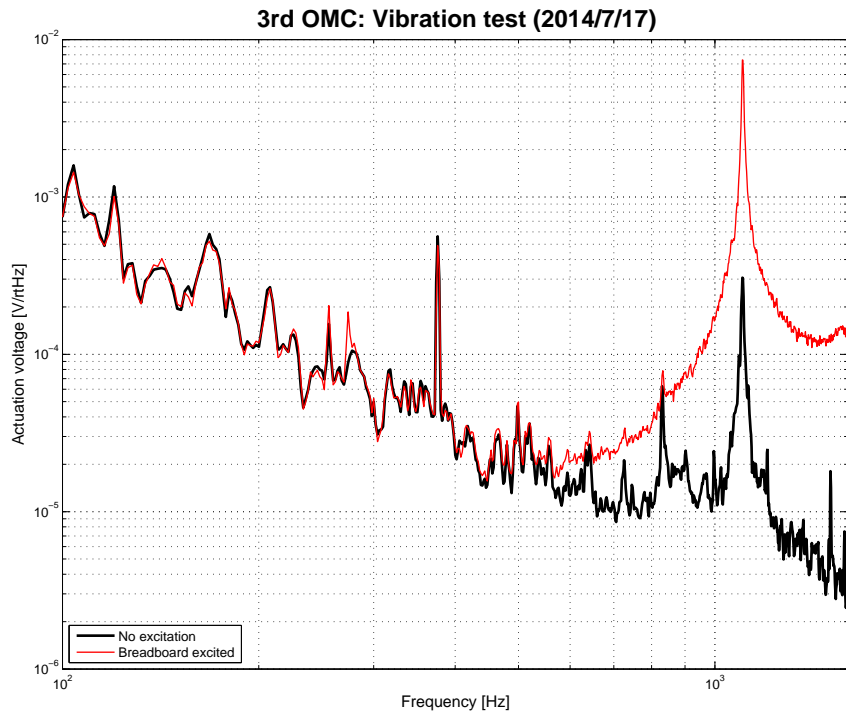


Figure 111: Vibrational test of the OMC breadboard (high resolution)

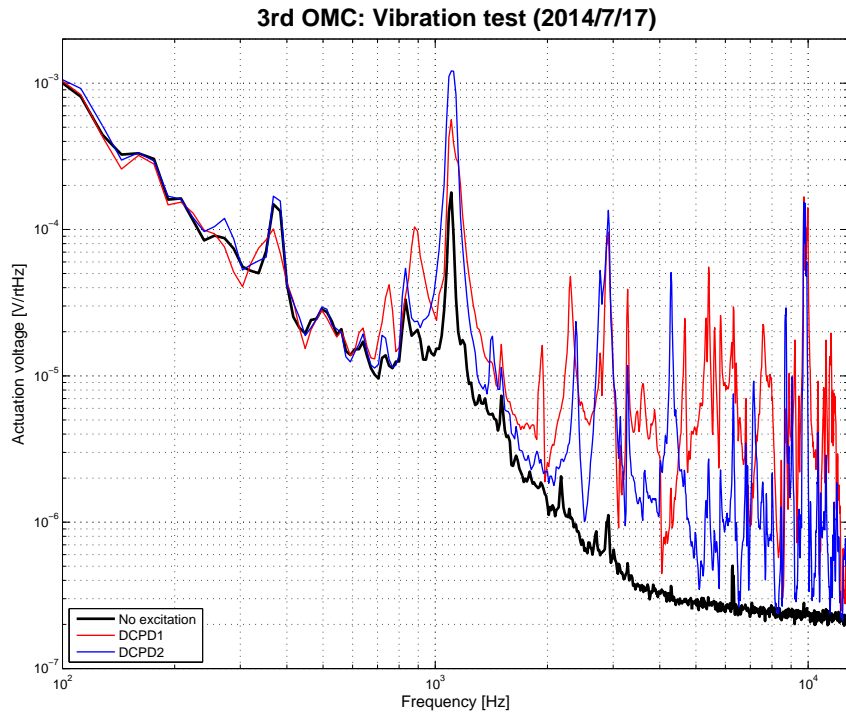


Figure 112: Vibrational test of the OMC shaking DCPDs

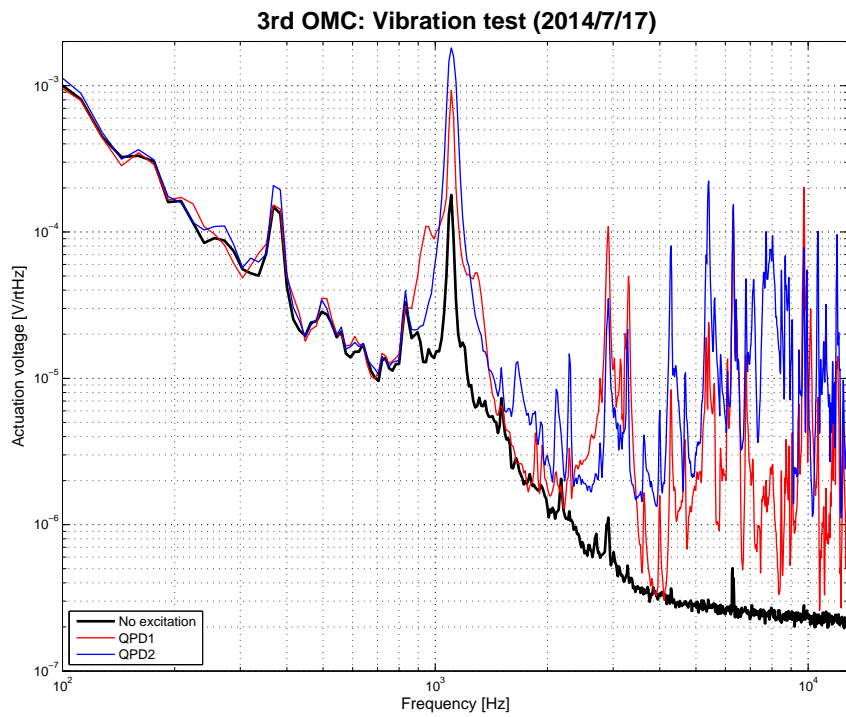


Figure 113: Vibrational test of the OMC shaking QPDs

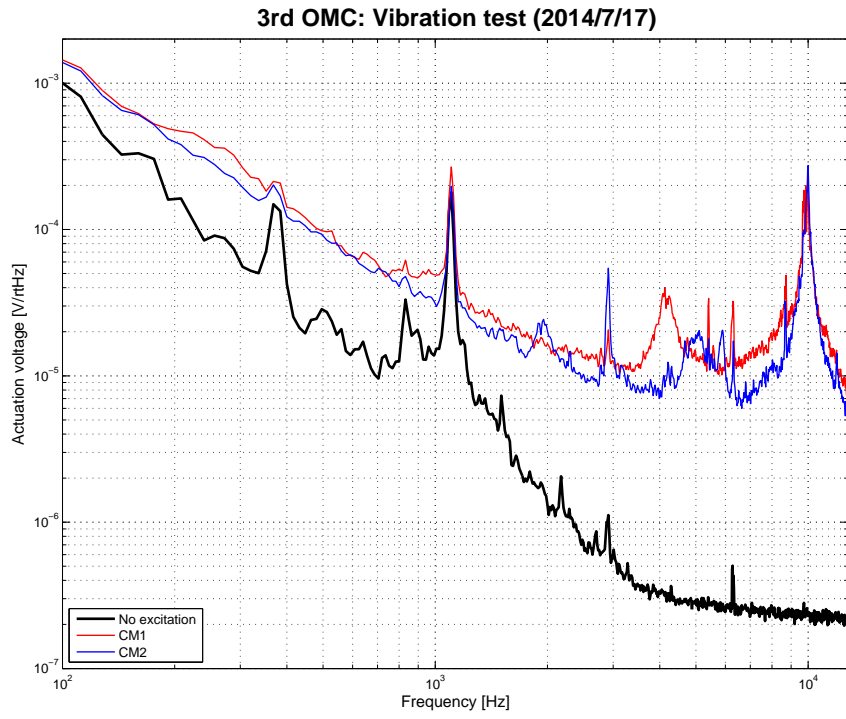


Figure 114: Vibrational test of the OMC shaking CMs

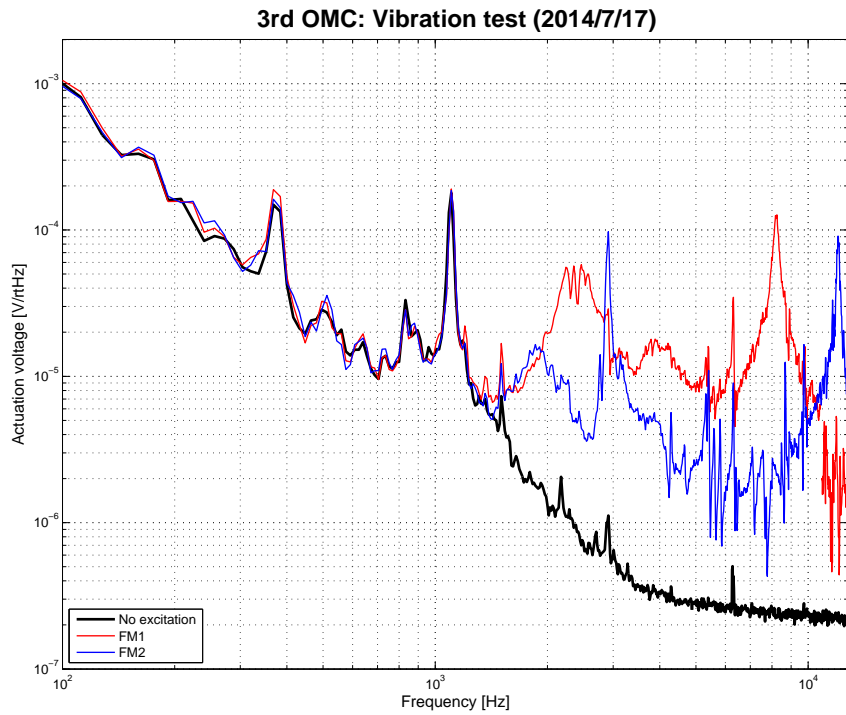


Figure 115: Vibrational test of the OMC shaking FMs

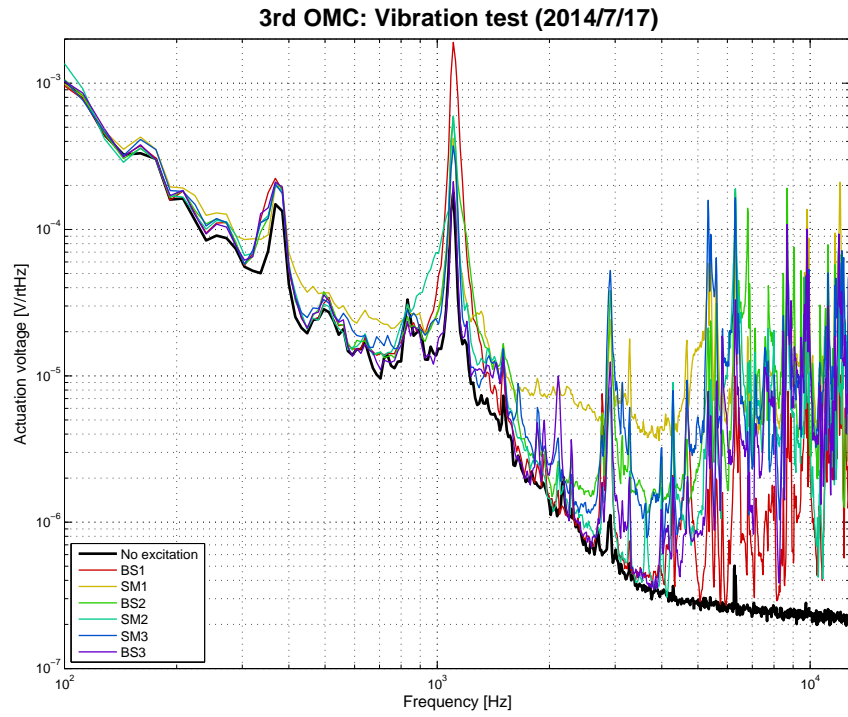


Figure 116: Vibrational test of the OMC shaking BSs and SMs

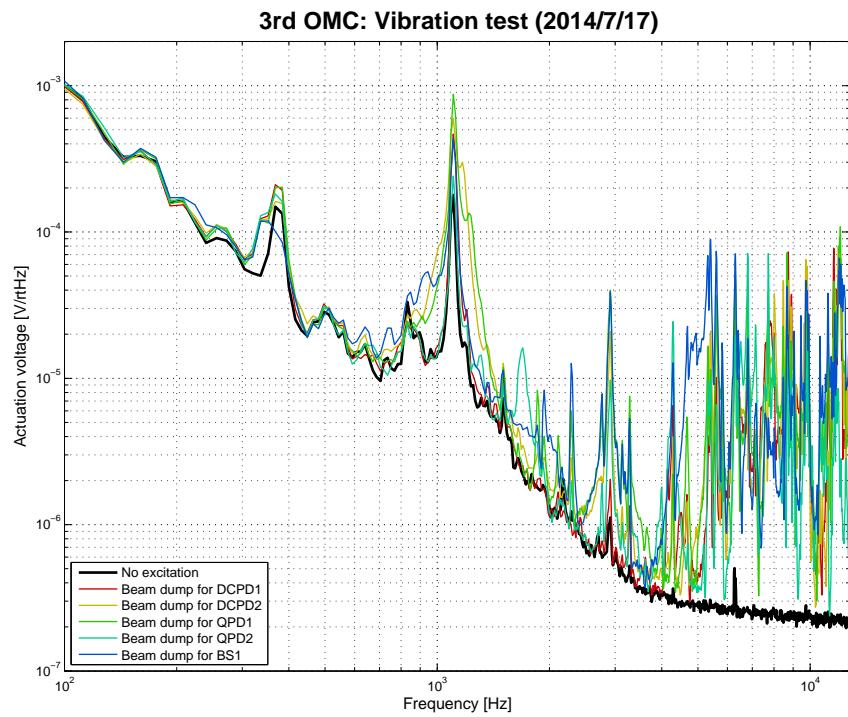


Figure 117: Vibrational test of the OMC shaking BDs

– Secondary mode: 8.2 kHz (Fig. 121).

- **PZT mirror subassembly:** Eigenmodes which involves large motion of the tombstone. In deed 10-kHz mode is not the resonance of the PZT-mirror joint, but the resonance of the tombstone.
 - 10.0 kHz (Fig. 124).
 - 14.6 kHz (Fig. 125).
 - 18.0 kHz (Fig. 126).
 - 22.5 kHz (Fig. 127).
 - 29.7 kHz (Fig. 128).

Then, the transfer function of the PZT actuation was simulated (Fig. 129). In order to simulate the PZT motion, boundary loads on the two sides of the PZT were applied with opposite signs. The 10-kHz peak appeared as the resonance of the tombstone that dominates the mirror motion. At 12 kHz, the PZT extension and the backaction of the tombstone cancels each other and the net displacement of the mirror becomes zero.

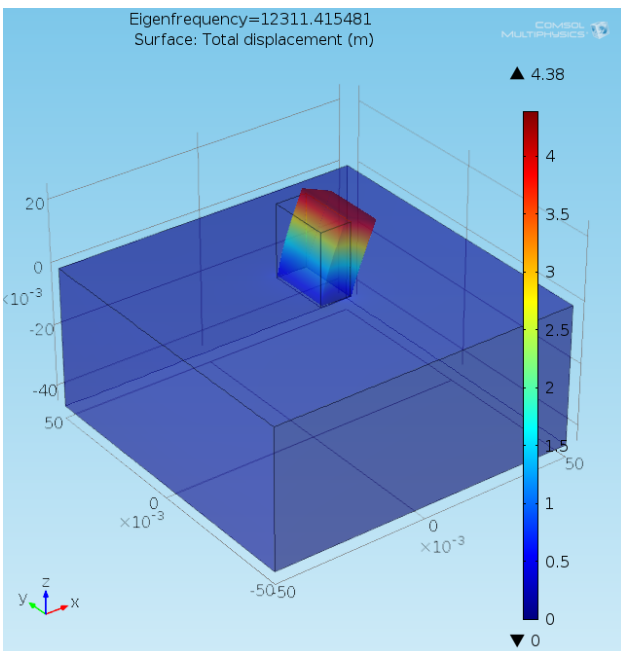


Figure 118: Mode analysis of the tombstone prism (first mode: 12.3 kHz)

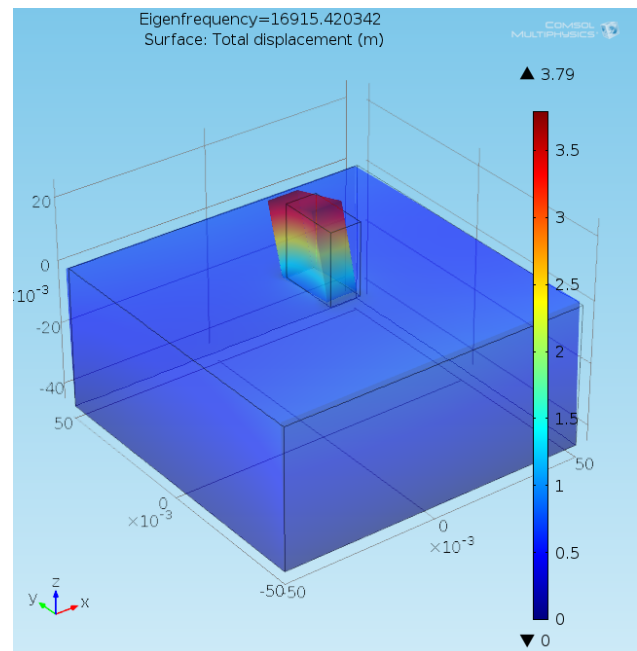


Figure 119: Mode analysis of the tombstone prism (second mode: 16.9 kHz)

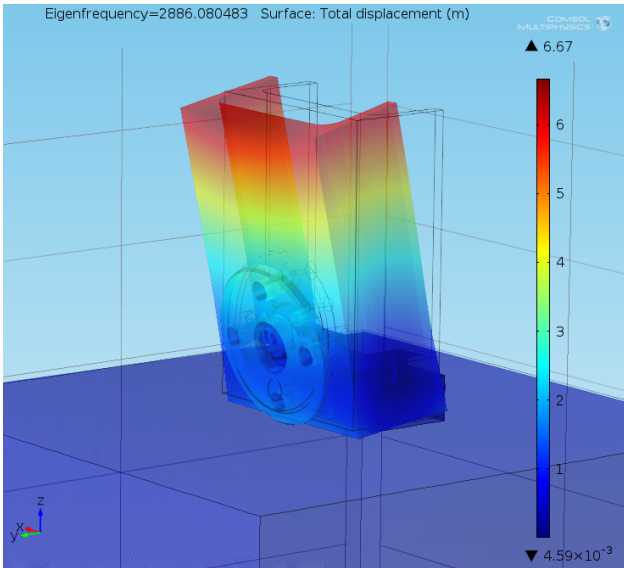


Figure 120: Mode analysis of the DCPD housing (first mode: 2.9 kHz)

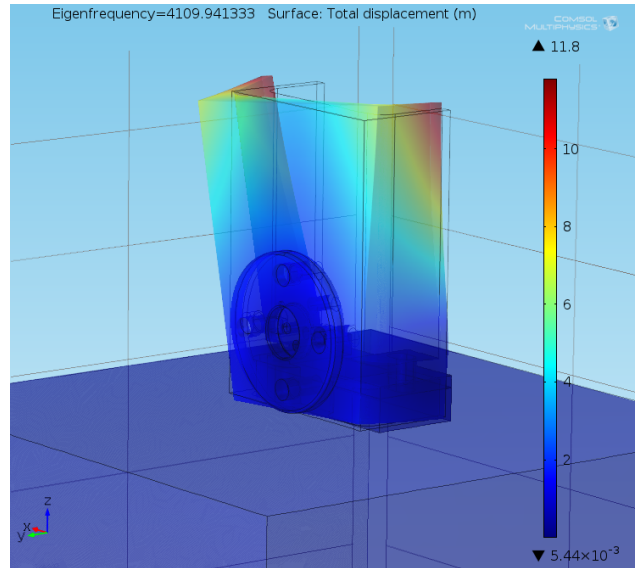


Figure 121: Mode analysis of the DCPD housing (second mode: 4.1 kHz)

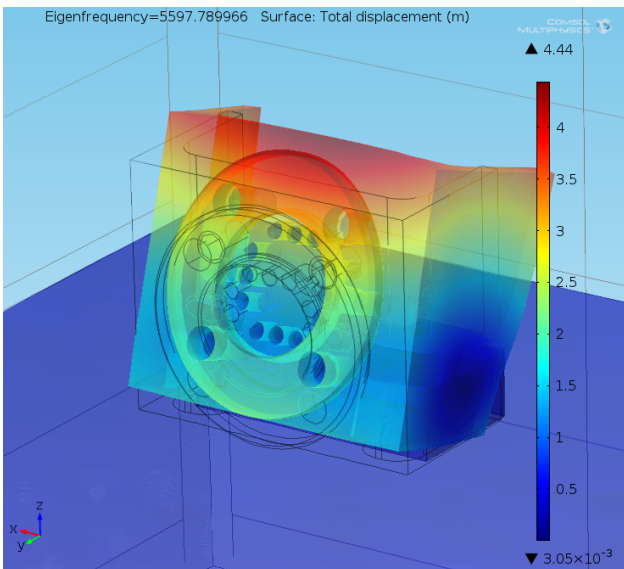


Figure 122: Mode analysis of the QPD housing (first mode: 6.0 kHz)

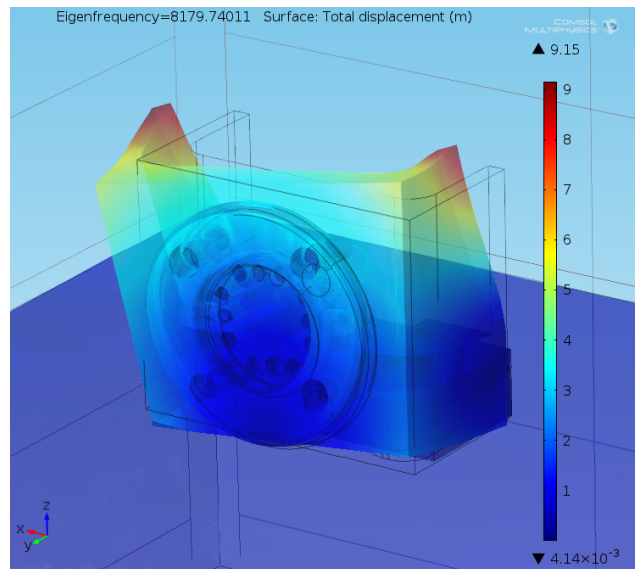


Figure 123: Mode analysis of the QPD housing (second mode: 8.2 kHz)

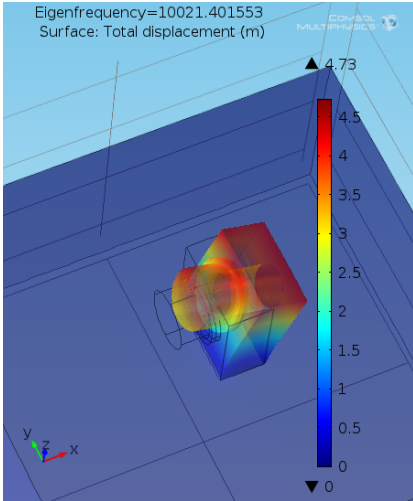


Figure 124: Mode analysis of the PZT mirror subassembly (first mode: 10.0 kHz)

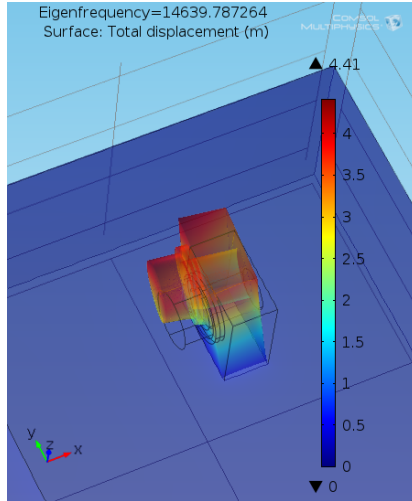


Figure 125: Mode analysis of the PZT mirror subassembly (second mode: 14.6 kHz)

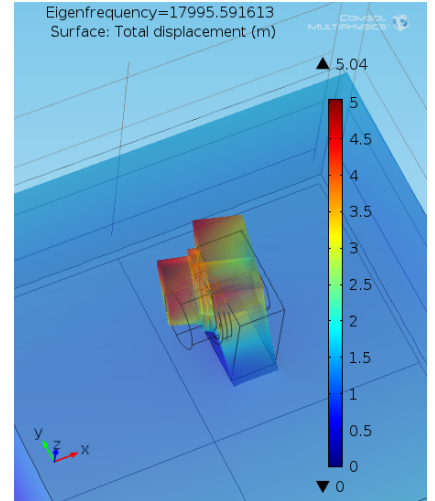


Figure 126: Mode analysis of the PZT mirror subassembly (third mode: 18.0 kHz)

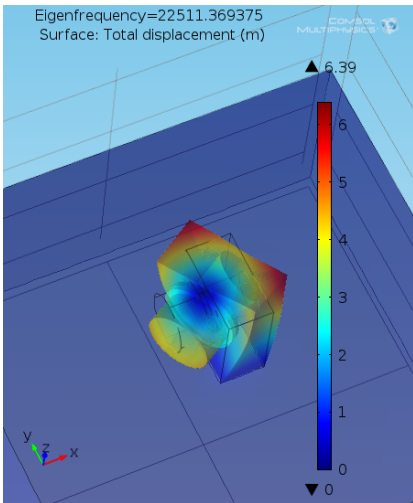


Figure 127: Mode analysis of the PZT mirror subassembly (fourth mode: 22.5 kHz)

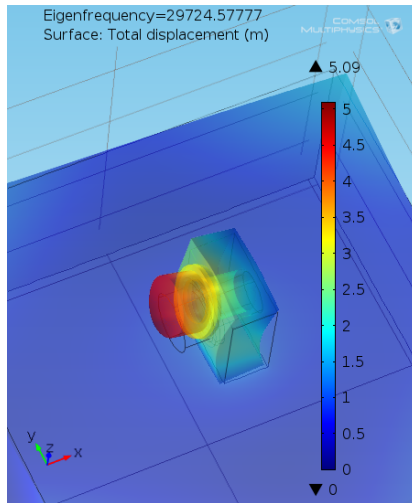


Figure 128: Mode analysis of the PZT mirror subassembly (fifth mode: 29.7 kHz)

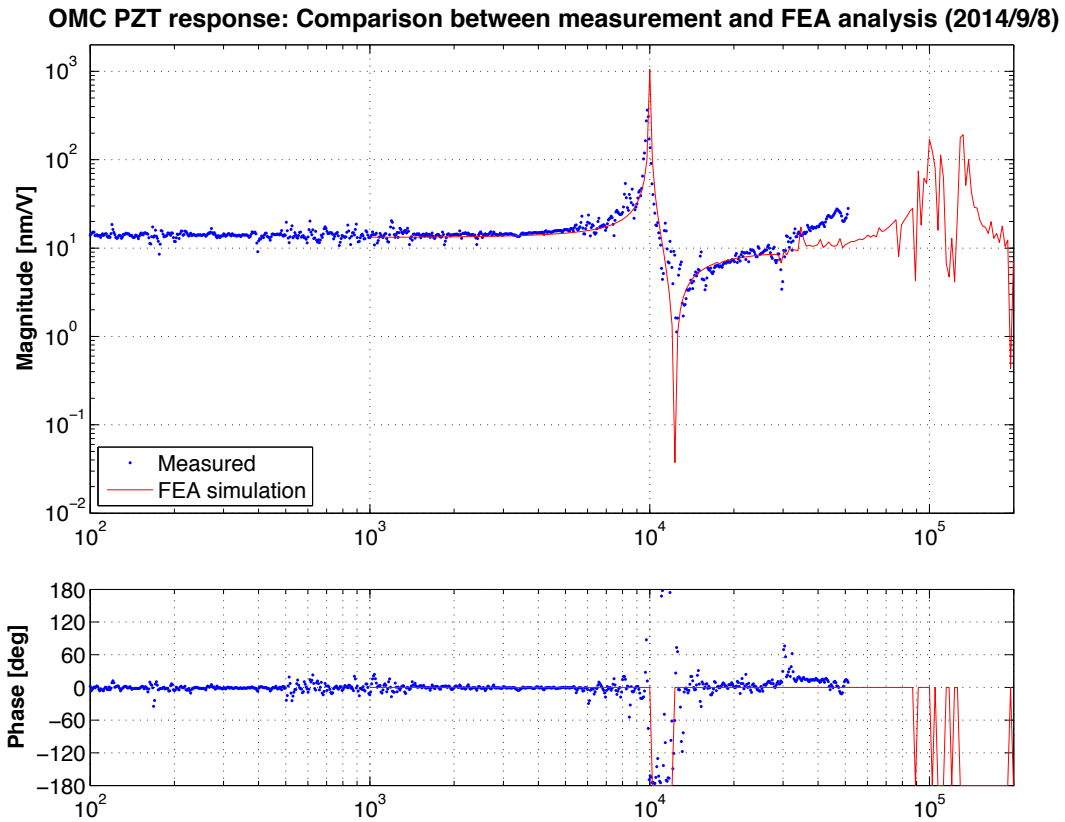


Figure 129: Simulated transfer function of the PZT actuation bonded on the breadboard. The simulated transfer function of the PZT actuation bonded on the breadboard. The simulation result (red) was compared with the measurement (blue). They show good agreement.

3.10 Test results for OMC(001)

3.10.1 Summary of the OMC(001) tests

[Description]

The table shows the summary of the OMC(001) optical test results. The detailed results are shown in the following sections.

FSR (detuned locking)			
FSR	264.967	± 0.002	[MHz]
Cavity roundtrip length	1.131433	± 0.000007	[m]
FSR & Finesse (RFAM injection)			
FSR	264.9694	± 0.0003	[MHz]
Cavity roundtrip length	1.131423	± 0.000001	[m]
Finesse	405.3	± 0.3	
TMS			
TMS (Vertical)	57.9406	± 0.0003	[MHz]
	0.218669	± 0.000001	[FSR]
TMS (Horizontal)	58.0498	± 0.0003	[MHz]
	0.219081	± 0.000001	[FSR]
Total Optical Loss (2013/6/2)			
OMC unit throughput	0.972	± 0.004	
OMC optical loss	0.028	± 0.004	
PZT response			
PZT1:	13.2418	± 0.0003	[nm/V]
PZT2:	12.92	± 0.01	[nm/V]

Table 19: OMC(001): Summary of the cavity geometry tests

3.10.2 Cavity absolute length measurement with detuned locking

[Description]

See Section 3.2.1 for the details of the measurement method.

The transfer function and the measurement results are shown in Figure 130.

3.10.3 Cavity length and finesse measurement with RFAM injection

[Description]

See Section 3.2.2 for the details of the measurement method.

The transfer function and the measurement results are shown in Figure 131.

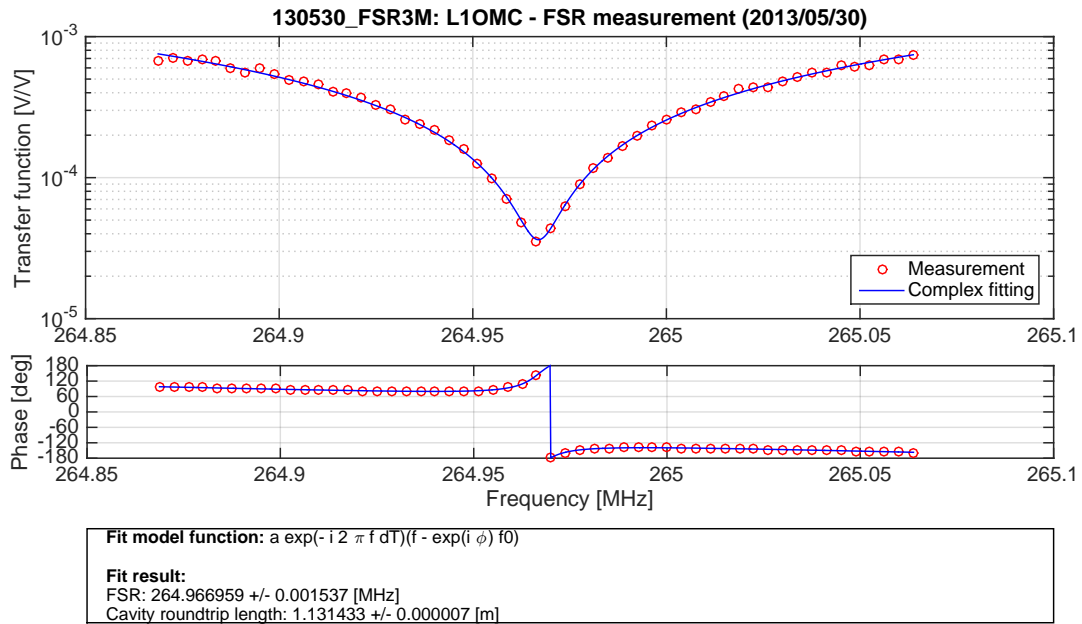


Figure 130: OMC(001): Cavity absolute length (FSR) measurement with detuned locking

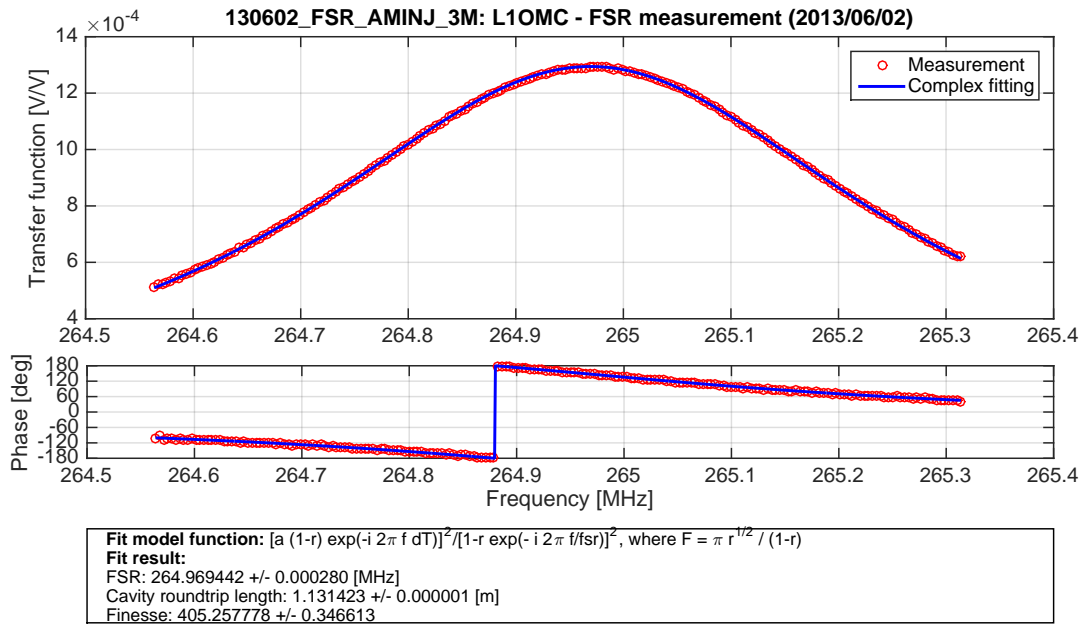


Figure 131: OMC(001): Cavity length (FSR) and finesse measurement with RFAM injection

3.10.4 Transverse-mode spacing measurement

[External Link]

http://nodus.ligo.caltech.edu:8080/OMC_Lab/134

[Description]

See Section 3.2.3 for the details of the measurement method.

The transfer functions and the measurement results are shown in Figures 132 and 133. They show the TMS measurements and results in vertical and horizontal modes, respectively.

Figure 134 shows the higher-order modes distribution when no PZT voltages are applied. This plot shows how the higher-order modes (order number in the vertical axis) of the carrier and RF sidebands are distributed within a single FSR (the horizontal axis). For the RF sidebands, f_1 sidebands (± 9.0099055 MHz) and f_2 sidebands ($5 \times f_1 = \pm \sim 45$ MHz), as well as (± 3.125 MHz) are shown.

From this plot, the closest near miss with the TEM_{00} carrier resonance is the 9th-order modes of +9 MHz sideband. The next is the 19th order modes of the -45 MHz sideband.

The problem is that the HOM resonant frequency shifts when the PZT voltages are applied, and thus the HOM resonance distribution also changes.

To assess the impact of the PZT voltages, the dependence of TMSs on the voltages on PZT1 and PZT2 were measured (Fig. 135). Since the dependence was approximately linear, a TMS in a unit of FSR was fitted with a linear function. When we define a TMS as

$$\frac{\nu_{\text{TMS}}}{\nu_{\text{FSR}}} = P_0 + P_1 V_{\text{PZT1}} + P_2 V_{\text{PZT2}} , \quad (22)$$

the parameters for each TMS were estimated to be

Vertical TMS :

$$P_0 = 0.21886 \pm 2 \times 10^{-5}$$

$$P_1 = -9.61 \times 10^{-6} \pm 2 \times 10^{-7}$$

$$P_2 = -9.55 \times 10^{-6} \pm 2 \times 10^{-7}$$

Horizontal TMS :

$$P_0 = 0.21924 \pm 2 \times 10^{-5}$$

$$P_1 = -1.07 \times 10^{-5} \pm 3 \times 10^{-7}$$

$$P_2 = -1.06 \times 10^{-5} \pm 3 \times 10^{-7}$$

Using the modelled TMSs as functions of the PZT voltages, we can predict which HOMs are coming into the TEM_{00} carrier resonance. Figure 136) shows the case for PZT1 but the situation is almost identical for PZT2 according to Figure. 135). The most lowest order one is the 9th-order modes of the +9-MHz sideband that are resonant between 50 V and 80 V for the PZT voltage. At high voltage range various modes come into the resonance and we should avoid it. Below 35 V, the 23rd-order modes of the -9 -MHz are resonant. This seems less harmful considering the high number for the order. In conclusion, it is safe to keep the total PZT voltage as low as possible for this OMC.

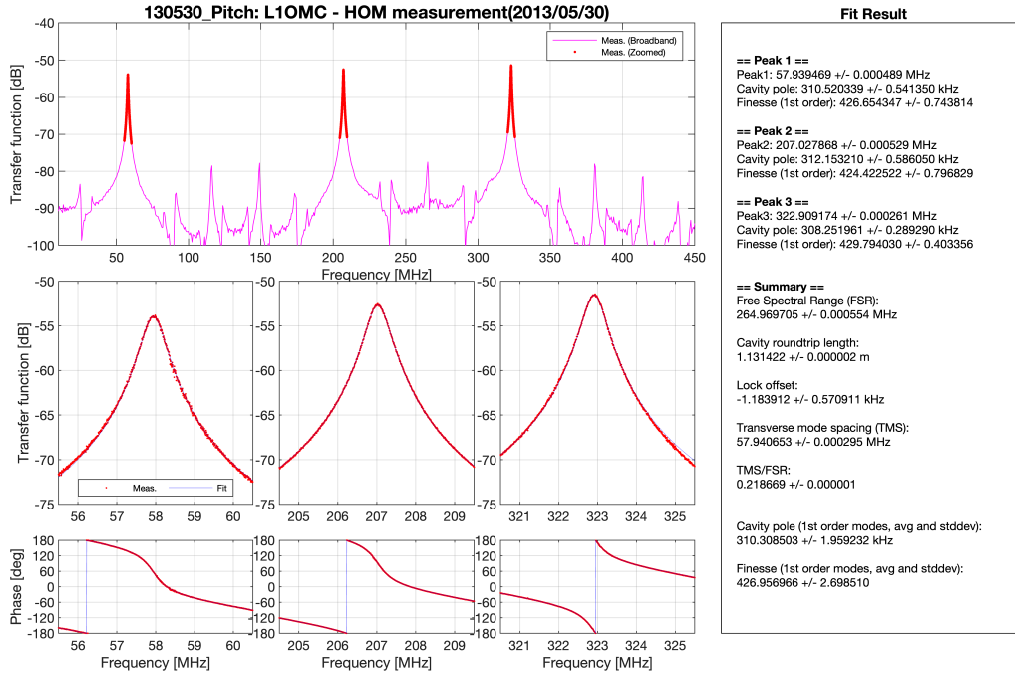


Figure 132: OMC(001): Vertical TMS measurement with no PZT voltages applied.

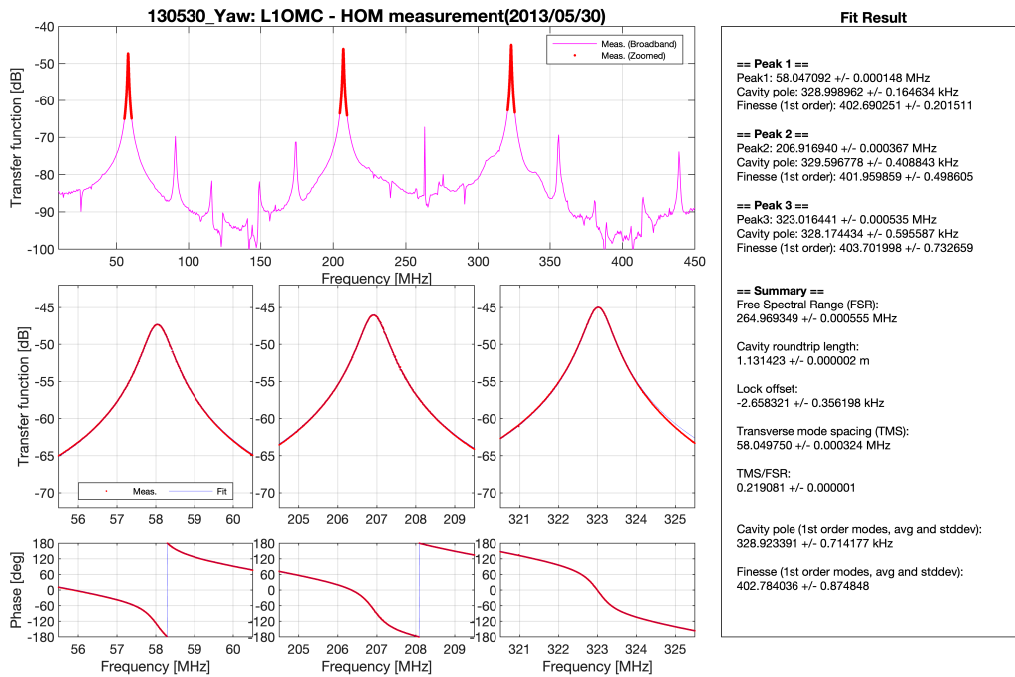


Figure 133: OMC(001): Horizontal TMS measurement with no PZT voltages applied.

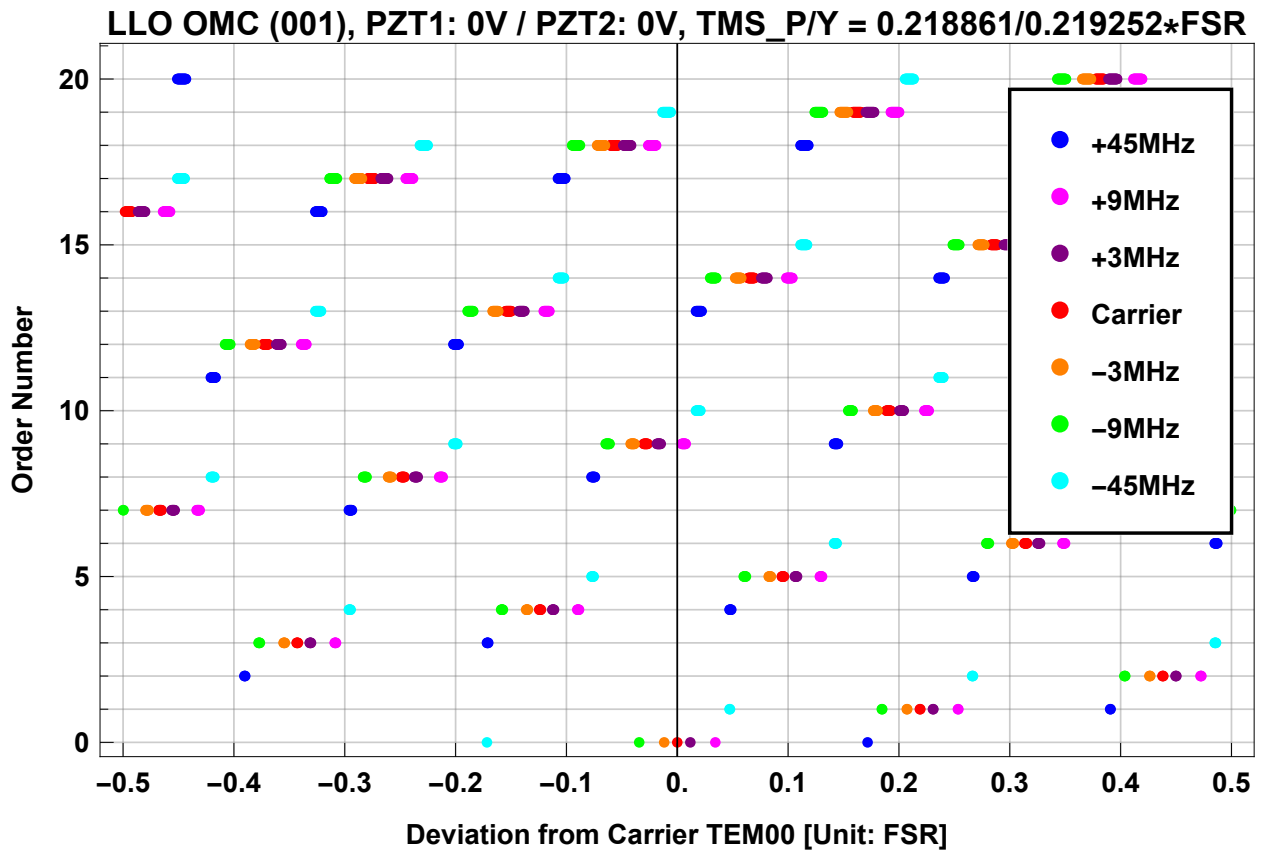


Figure 134: OMC(001): Higher-order modes distribution with no PZT voltages applied.

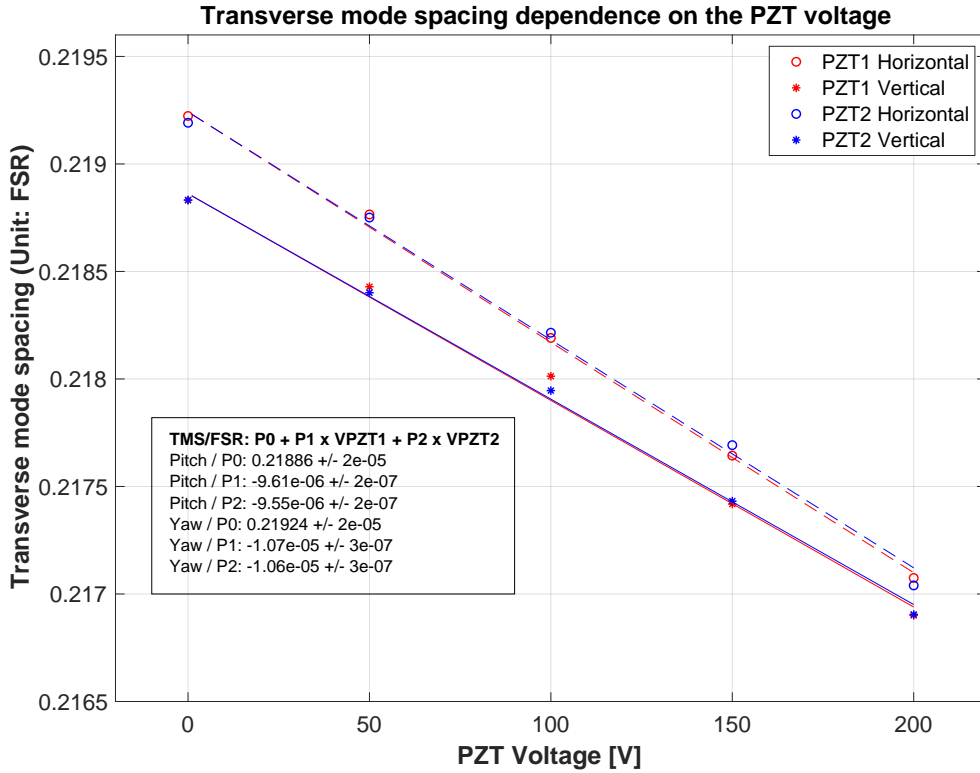


Figure 135: OMC(001): Dependence of the vertical and horizontal TMSs on the PZT voltages. The TMSs are expressed in the unit of FSR.

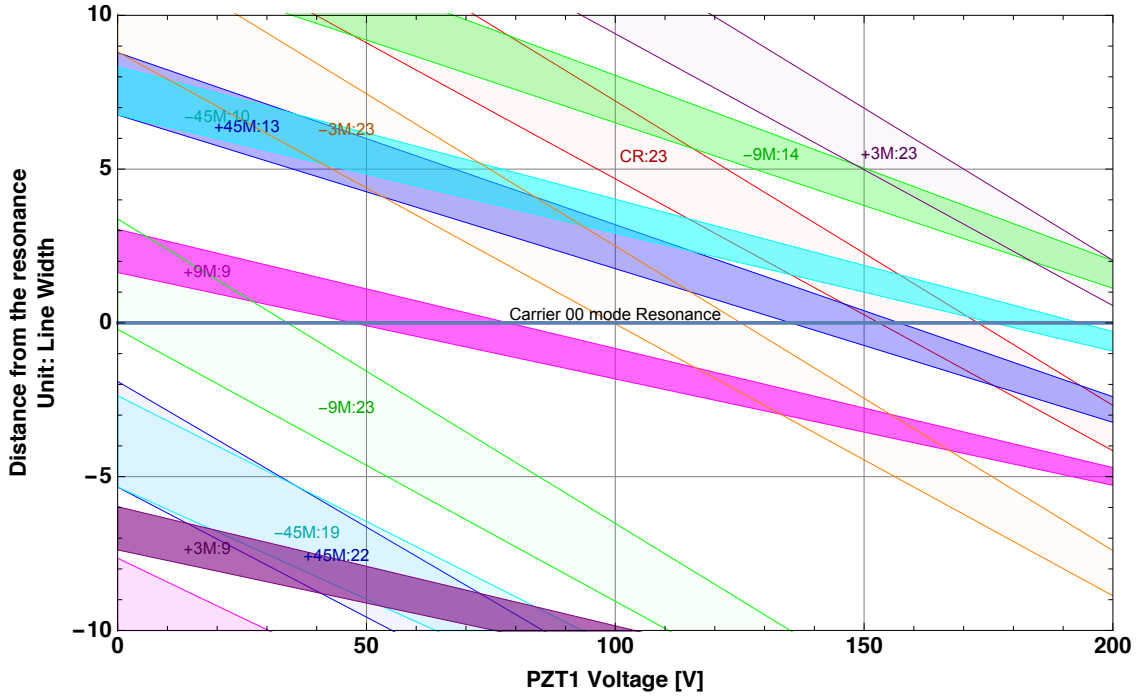


Figure 136: OMC(001): Modelled coincidental resonances of the higher-order modes as the PZT voltages scanned.

3.10.5 Power budget for OMC(001)

[External Link]

http://nodus.ligo.caltech.edu:8080/OMC_Lab/135

<https://alog.ligo-la.caltech.edu/aLOG/index.php?callRep=61515>

<https://alog.ligo-la.caltech.edu/aLOG/index.php?callRep=61552>

[Description]

Summary of the measurement on 2013/6/2 is shown in Table 20.

LLO observed the increased loss of the OMC over the years. In 2022 September, this unit was extracted from HAM6 ². The power budget test performed on the extracted unit (before and after FirstContact cleaning) are shown at the left half of Figure 137. T. Cullen joined the characterization work at LLO.

Assumptions			
Finesse	403.79		
Input BS transmission	7400		ppm
Derived Values			
Roundtrip reflectivity	0.9922		
Power: OMC incident	38.40	±0.05	mW
Power: Cavity incident	38.12	±0.05	mW
Power: Coupled to the cavity	37.80	±0.05	mW
Power: Junk light at the cavity	0.318	±0.002	mW
Mode Matching	0.9916	± 0.00005	
Cavity power reflectivity	0.00011	±0.00004	
Cavity power transmission	0.979	±0.004	
OMC unit throughput	0.972	±0.004	
OMC optical loss	0.028	±0.004	
Loss per mirror	20	±8	ppm
FM1/FM2 transmission	7670	±20	ppm
CM1 transmission	41.4	±0.6	ppm
CM2 transmission	42.8	±0.6	ppm

Table 20: OMC(001): Summary of the power measurement taken after final cleaning on 2013/6/2

3.10.6 PZT response DC/AC

[External Link]

http://nodus.ligo.caltech.edu:8080/OMC_Lab/148

²<https://alog.ligo-la.caltech.edu/aLOG/index.php?callRep=61398>

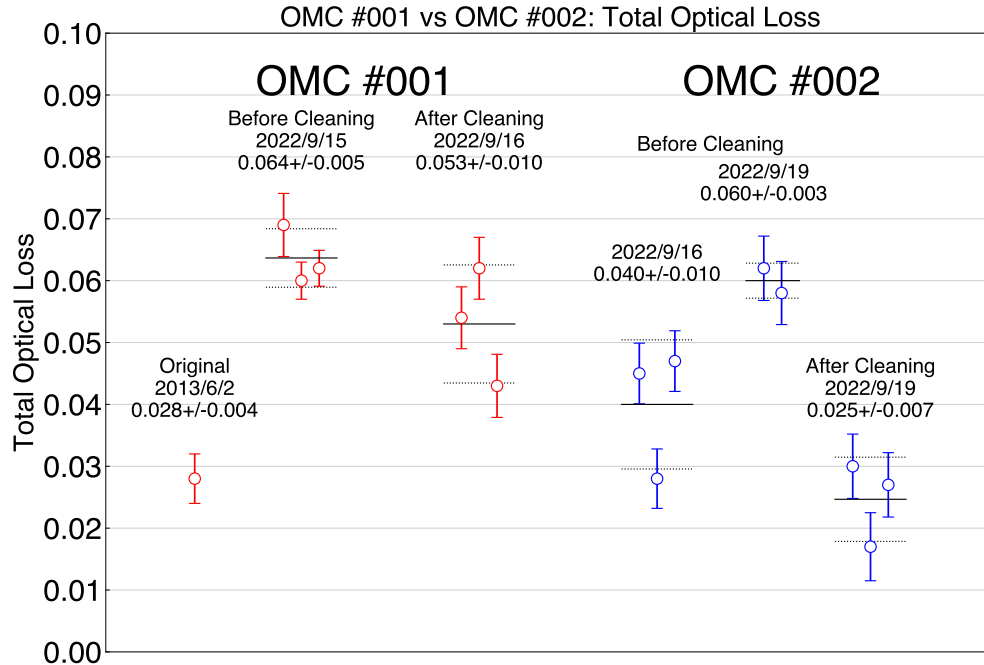


Figure 137: OMC(001): Summary of the power budget test (left half)

[Description]

Figures 138 and 139 show DC and AC responses of the PZTs. Estimated DC responses were

- **PZT1:** $13.2418 \pm 0.003 \text{ nm/V}$
- **PZT2:** $12.92 \pm 0.01 \text{ nm/V}$

Note that OMC(001) has one of the PZT not functioning any more. The link: <https://alog.ligo-la.caltech.edu/aLOG/index.php?callRep=8366>

3.10.7 DCPD/QPD shim height adjustment

[External Link] 1st trial: http://nodus.ligo.caltech.edu:8080/OMC_Lab/120

Final: http://nodus.ligo.caltech.edu:8080/OMC_Lab/121

Invar threaded shims glued on the glass brackets: http://nodus.ligo.caltech.edu:8080/OMC_Lab/125

[Description]

Determined shim heights: (0.085mm for the glue height)

- DCPD1: $1.50 \text{ mm} + 0.085 \text{ mm} \Rightarrow$ Beam 0.084mm too high
- DCPD2: $1.50 \text{ mm} + 0.085 \text{ mm} \Rightarrow$ Beam 0.023mm too high
- QPD1: $1.25 \text{ mm} + 0.085 \text{ mm} \Rightarrow$ Beam 0.001mm too low
- QPD2: $1.25 \text{ mm} + 0.085 \text{ mm} \Rightarrow$ Beam 0.155mm too low

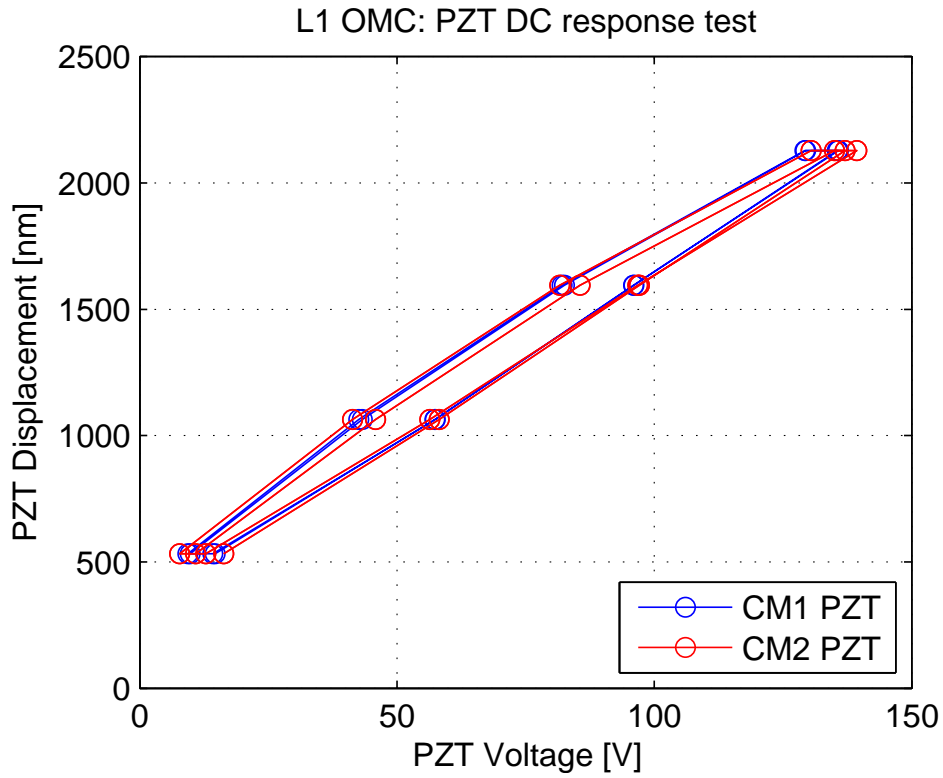


Figure 138: OMC(001): PZT sweep voltages and the OMC resonances.

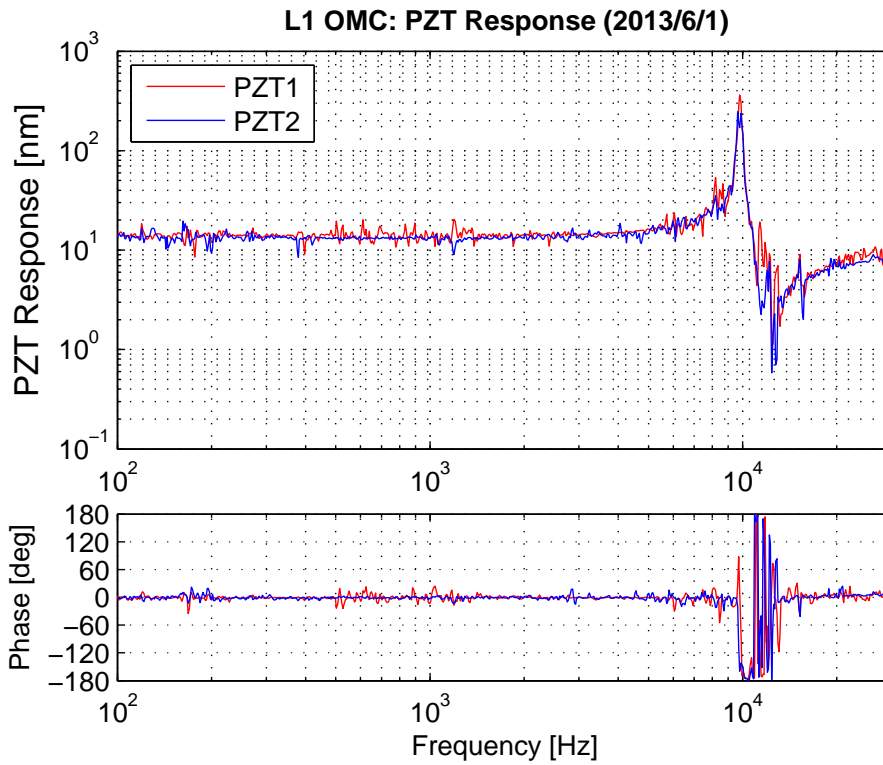
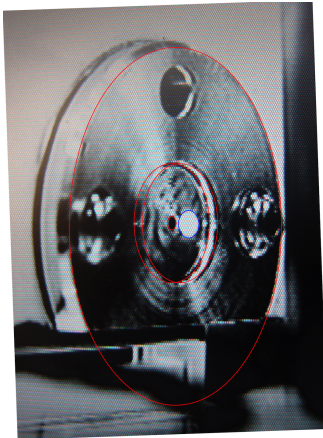


Figure 139: OMC(001): PZT AC responses. The DC gain was adjusted to match the DC scan result.



DCPD1 (BS Transmission)
SHIM: 1.75mm

HOLE
 Hole Height in the picture: 11.5897
 Hole Vert size in the picture: 0.6901
 => Hole center pos in the pic: 11.9348

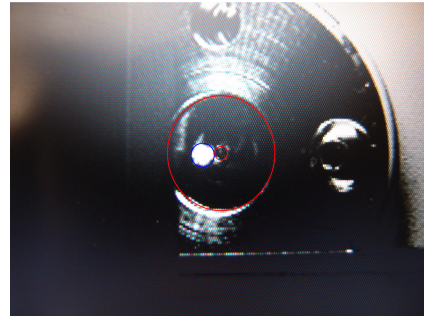
VS

BEAM
 Beam height in the picture: 11.2807
 Beam Vert size in the picture: 1.4193
 => Beam center pos in the pic: 11.9904

Conversion: 0.6901 = 1.016mm (40mil)
 => Beam 0.081mm too low

Shim 1.75mm + Glue 0.085mm
 => Beam 0.166mm too low (negligible)
 Shim 1.50mm + Glue 0.085mm
 => Beam 0.084mm too high (negligible)

Figure 140: OMC(001): Image analysis for the DCPD1 shim height



DCPD2 (BS Reflection)
SHIM: 1.75mm

HOLE
 HPOS: 10.9936
 HSIZ: 0.9628
 CPOS: 11.475

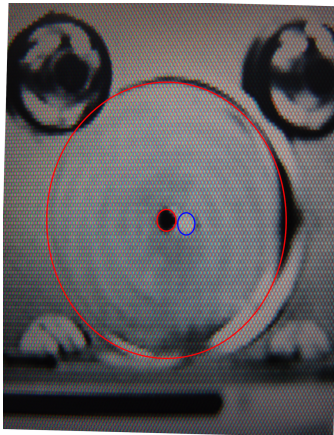
VS

BEAM
 HPOS: 10.7772
 HSIZ: 1.667
 CPOS: 11.6107

Conversion: 0.9628 = 1.016mm (40mil)
 => Beam 0.141mm too low

Shim 1.75mm + Glue 0.085mm
 => Beam 0.226mm too low
 Shim 1.50mm + Glue 0.085mm
 => Beam 0.024mm too high

Figure 141: OMC(001): Image analysis for the DCPD2 shim height



QPD1 (BS Reflection)
SHIM: 1.5mm

HOLE
 HPOS: 10.6364
 HSIZ: 1.1138
 CPOS: 11.1933

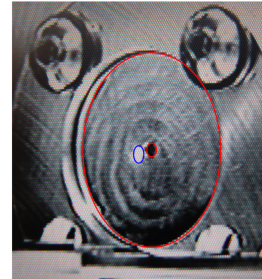
VS

BEAM
 HPOS: 10.8086
 HSIZ: 1.1391
 CPOS: 11.3782

Conversion: 1.1138 = 1.016mm (40mil)
 => Beam 0.165mm too low

Shim 1.25mm + Glue 0.085mm
 => Beam 0.001mm too low (perfect)

Figure 142: OMC(001): Image analysis for the QPD1 shim height



QPD2 (BS Transmission)
SHIM: 1.5mm

HOLE
 HPOS: 8.6946
 HSIZ: 0.7956
 CPOS: 9.0924

VS

BEAM
 HPOS: 8.8429
 HSIZ: 1.0078
 CPOS: 9.3468

Conversion: 0.7956 = 1.016mm (40mil)
 => Beam 0.320mm too low

Shim 1.25mm + no sphere
 => Beam 0.070mm too low

Shim 1.25mm + Glue 0.085mm
 => Beam 0.155mm too low (not negligible but OK)

Figure 143: OMC(001): Image analysis for the QPD2 shim height

3.10.8 QPD alignment

[External Link]

http://nodus.ligo.caltech.edu:8080/OMC_Lab/133

[Description]

See Table 21 for the result.

QPD#	QPD1		QPD2	
Diode#	#43		#38	
Incident power	84.7	[μ W]	86.2	[μ W]
Sum Out	56	[mV]	61	[mV]
Vertical Out	-6.8	[mV]	10	[mV]
Horizontal Out	4.2	[mV]	8.8	[mV]
SEG1	-17	[mV]	-15	[mV]
SEG2	-14.5	[mV]	-11	[mV]
SEG3	-11	[mV]	-15	[mV]
SEG4	-13	[mV]	-20	[mV]
Spot position X^a	+25	[μ m]	+46	[μ m]
Spot position Y^b	-42	[μ m]	+46	[μ m]
Responsivity	0.66	[A/W]	0.71	[A/W]
Q.E.	0.77		0.82	

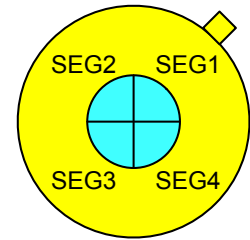


Table 21: OMC(001): Measurement results for the QPDs and the derived spot positions

^apositive = more power on SEG1 and SEG4

^bpositive = more power on SEG3 and SEG4

Figure 144: OMC(001): Arrangement of the QPD segments (beam view)

3.10.9 Alignment / beam spot photos

[Description]

Collection of the spot photos for the DCPDs, DCPD reflections, QPDs (QPD2 photo missing), FMs, and CMs.

3.10.10 Balance Mass Distribution

Figure 154 (upper) shows the mass distribution when this OMC was installed to LLO in 2013 June.

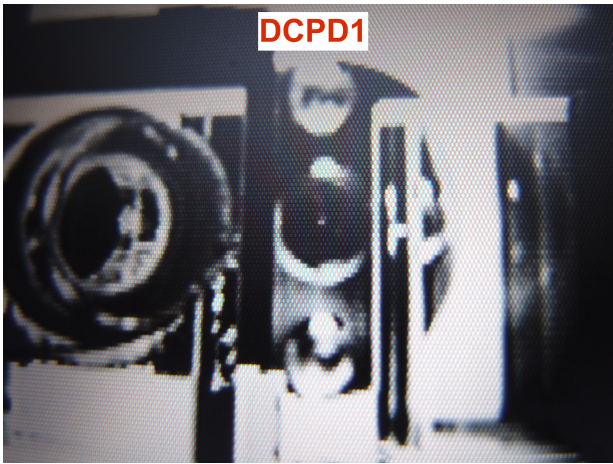


Figure 145: OMC(001): DCPD1 final spot position

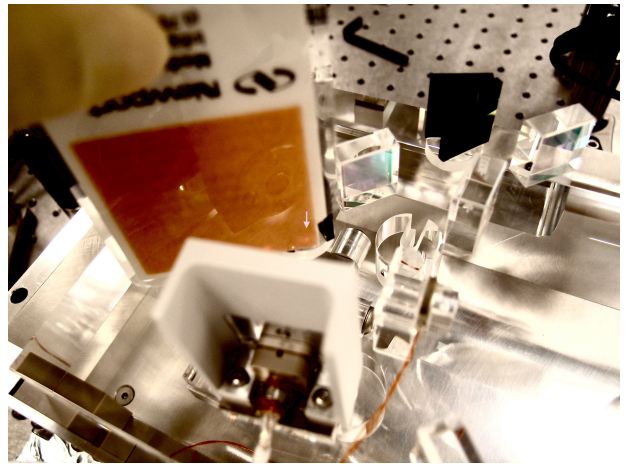


Figure 146: OMC(001): DCPD1 reflection on the beam dump



Figure 147: OMC(001): DCPD2 final spot position

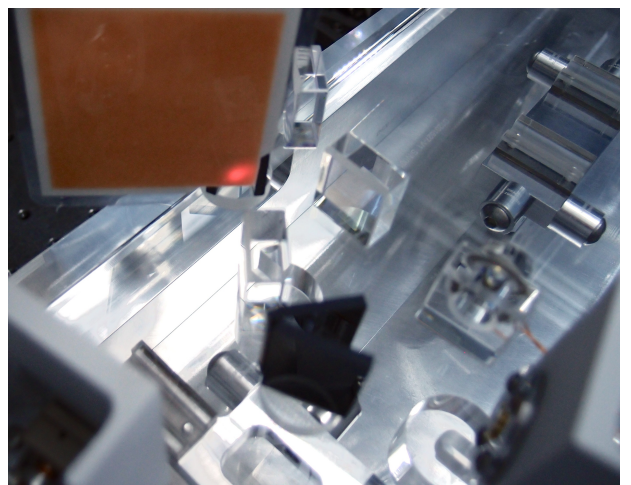


Figure 148: OMC(001): DCPD2 reflection on the beam dump

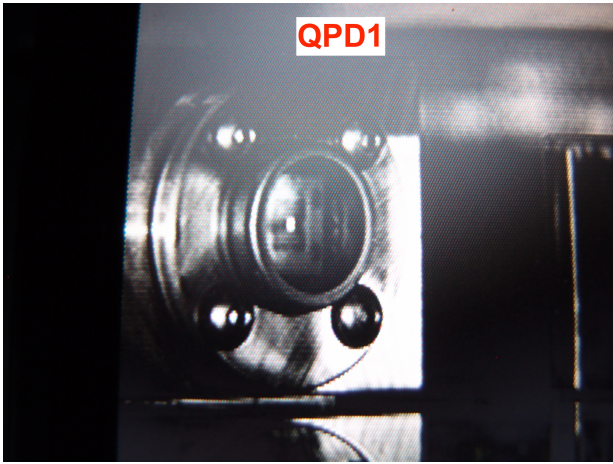


Figure 149: OMC(001): QPD1 final spot position

QPD2 spot photo missing

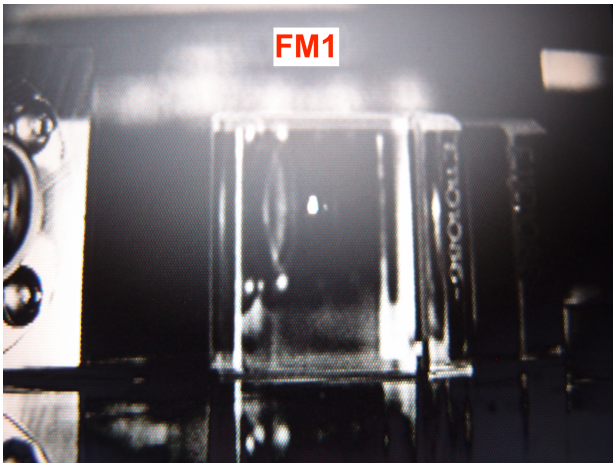


Figure 150: OMC(001): FM1 final spot position

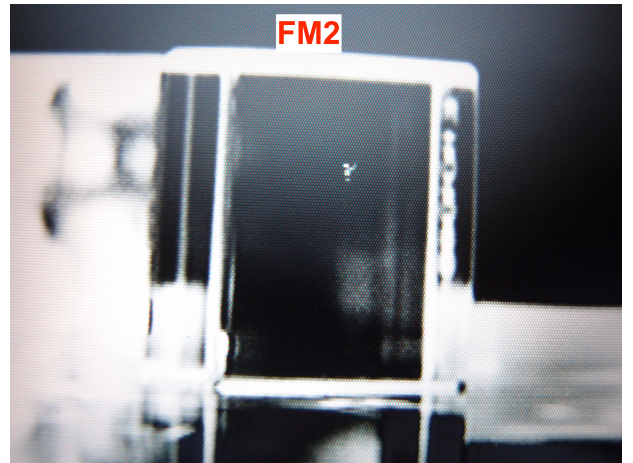


Figure 151: OMC(001): FM2 final spot position

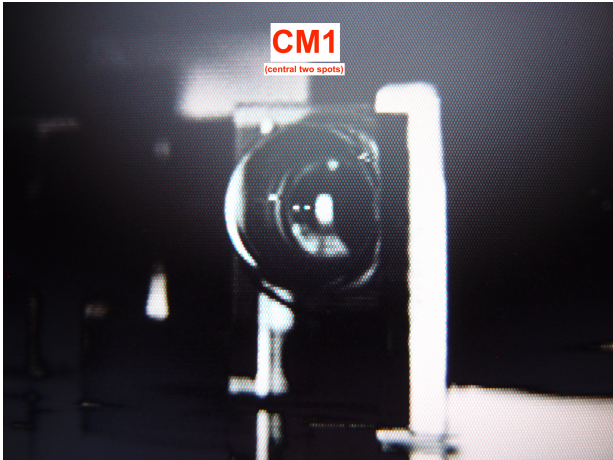


Figure 152: OMC(001): CM1 final spot position

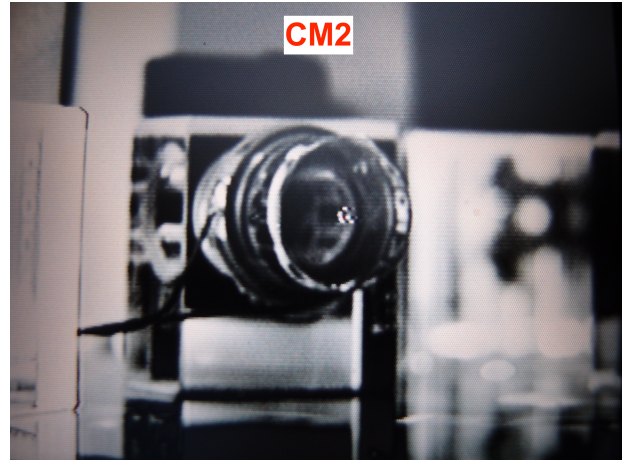


Figure 153: OMC(001): CM2 final spot position

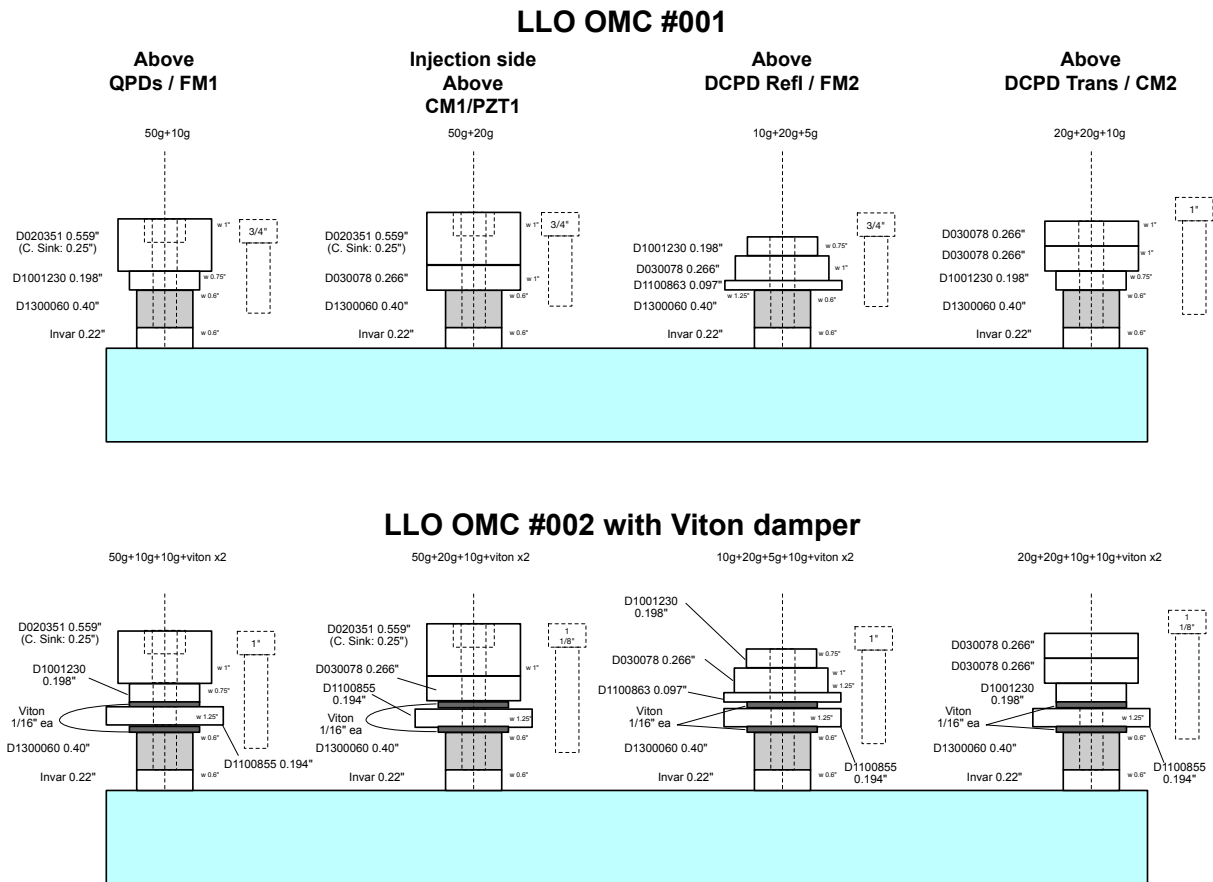


Figure 154: OMC(001): Balance mass distribution (upper)

3.11 Test results for OMC(002)

3.11.1 Summary of the OMC(002) tests

The table shows the summary of the OMC(002) optical test results. The detailed results are shown in the following sections.

The problem of the OMC (002) was that the PZT subassembly was not baked before the cavity assembly. Because the mirror curvature seemed so different from the case of OMC (001), the cavity FSR was changed to compensate the issue. Post gluing bake made the PZT bonding stress changed, and the RoC seemed reverted to more normal value.

FSR (detuned locking)			
FSR	261.710	± 0.003	[MHz]
Cavity roundtrip length	1.14552	± 0.00001	[m]
FSR & Finesse (RFAM injection)			
FSR	261.7104	± 0.0003	[MHz]
Cavity roundtrip length	1.145512	± 0.000001	[m]
Finesse	373.1	± 0.6	
TMS			
TMS (Vertical)	57.5948	± 0.0008	[MHz]
	0.220064	± 0.000003	[FSR]
TMS (Horizontal)	57.7457	± 0.0003	[MHz]
	0.220654	± 0.000001	[FSR]
Total Optical Loss (2013/9/17)			
OMC unit throughput	0.931	± 0.002	
OMC optical loss	0.069	± 0.002	
PZT response			
PZT1:	11.6	± 0.1	[nm/V]
PZT2:	12.4	± 0.1	[nm/V]

Table 22: OMC(002): Summary of the cavity geometry tests

3.11.2 Cavity absolute length measurement with detuned locking

[Description]

See Figure 155.

3.11.3 Cavity length and finesse measurement with RFAM injection

[Description]

See Figures 156 and 157.

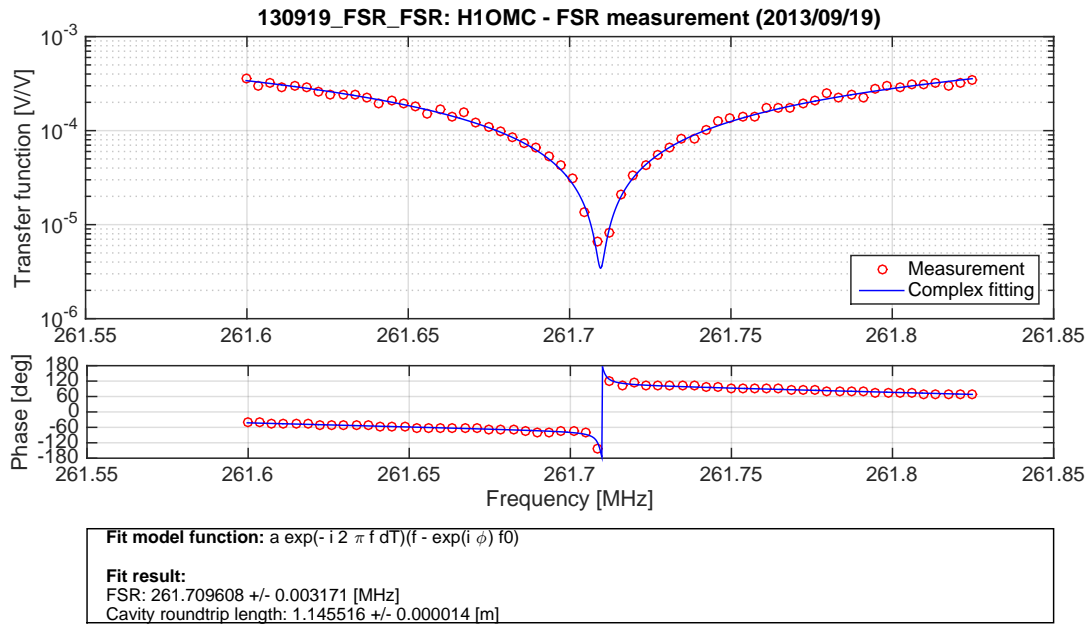


Figure 155: OMC(002): Cavity absolute length (FSR) measurement with detuned locking

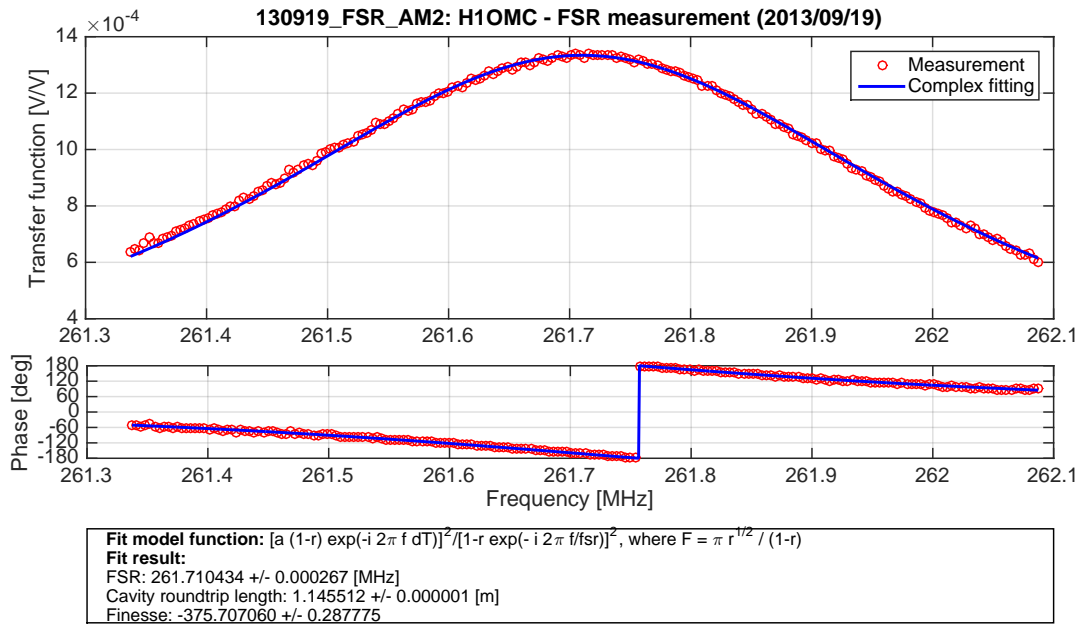


Figure 156: OMC(002): Cavity length (FSR) and finesse measurement with RFAM injection

H1OMC – FSR/Finesse measurement with AM injection (2013/09/19)

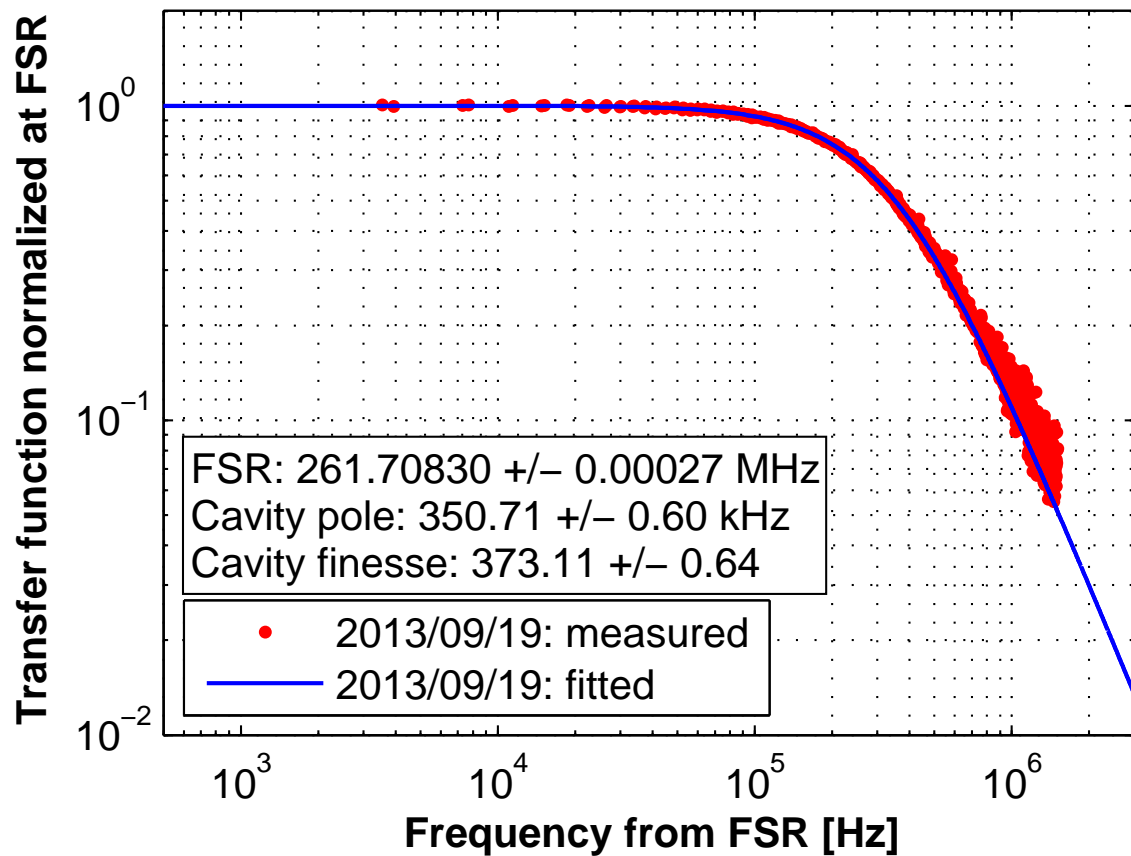


Figure 157: OMC(002): Cavity finesse measurement with RFAM injection

3.11.4 Transverse-mode spacing measurement

[Description]

See Figures 158 and 159 for the transfer functions and the estimated TMSs.

Figure 160 shows that the 9th-order and 18th-order modes potentially cause the problem of the coincident resonance.

The dependence of TMSs on the PZT voltages is shown in Figure. 161). The dependence model is expressed as

$$\frac{\nu_{\text{TMS}}}{\nu_{\text{FSR}}} = P_0 + P_1 V_{\text{PZT1}} + P_2 V_{\text{PZT2}} , \quad (23)$$

the parameters for each TMS were estimated to be

Vertical TMS :

$$P_0 = 0.22013 \pm 6 \times 10^{-5}$$

$$P_1 = -1.45 \times 10^{-5} \pm 5 \times 10^{-7}$$

$$P_2 = -1.55 \times 10^{-5} \pm 6 \times 10^{-7}$$

Horizontal TMS :

$$P_0 = 0.22072 \pm 4 \times 10^{-5}$$

$$P_1 = -1.38 \times 10^{-5} \pm 3 \times 10^{-7}$$

$$P_2 = -1.56 \times 10^{-5} \pm 3 \times 10^{-7}$$

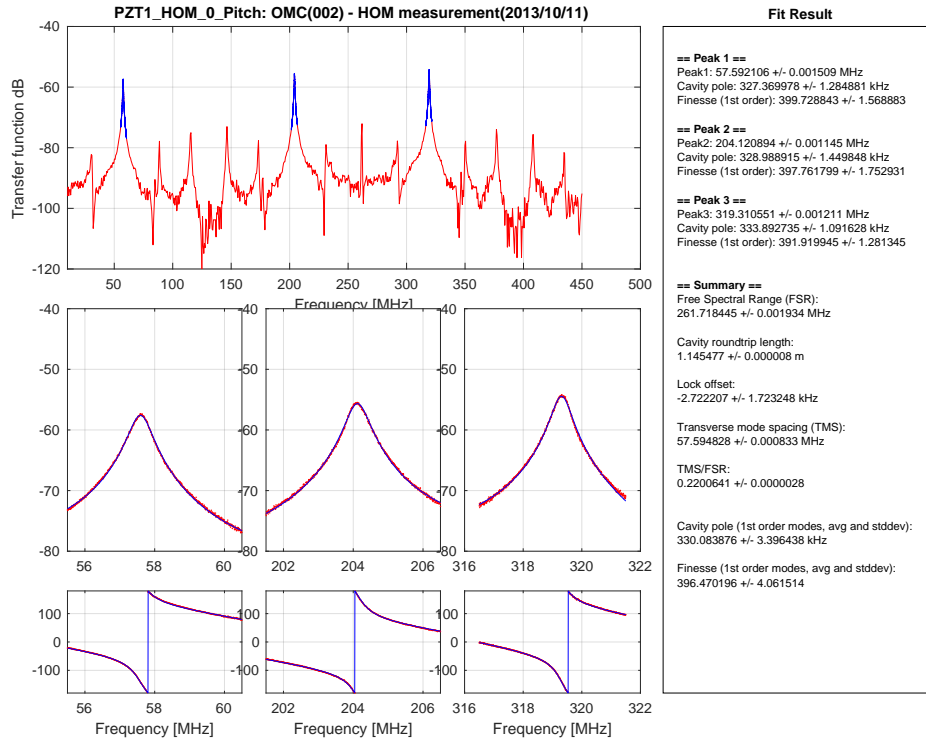


Figure 158: OMC(002): Vertical TMS measurement with no PZT voltages applied.

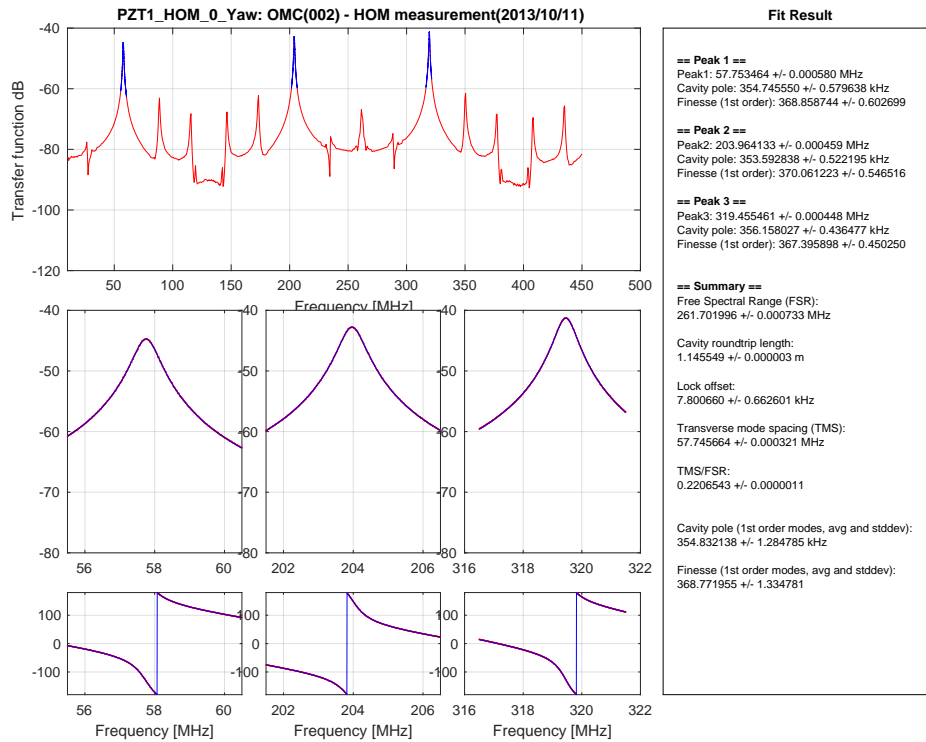


Figure 159: OMC(002): Horizontal TMS measurement with no PZT voltages applied.

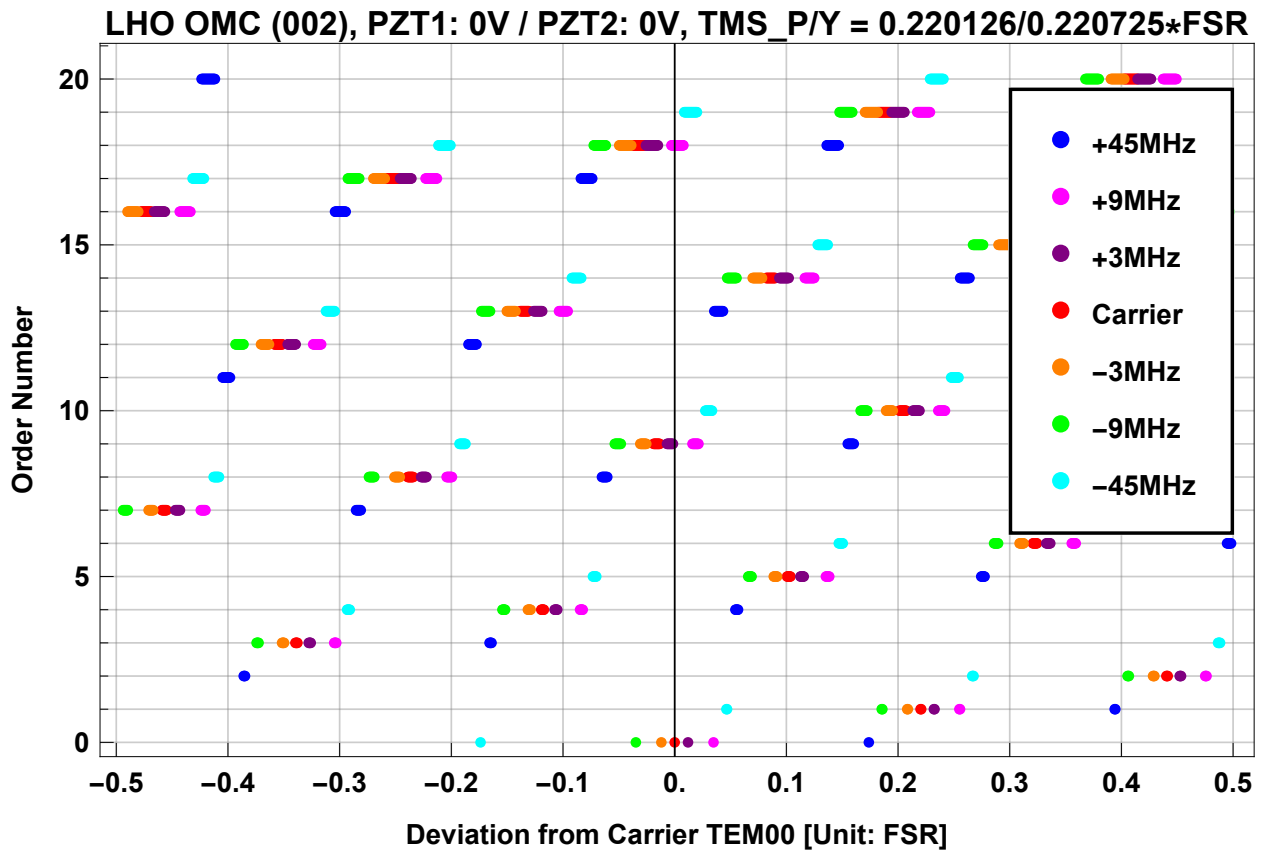


Figure 160: OMC(002): Higher-order modes distribution with no PZT voltages applied.

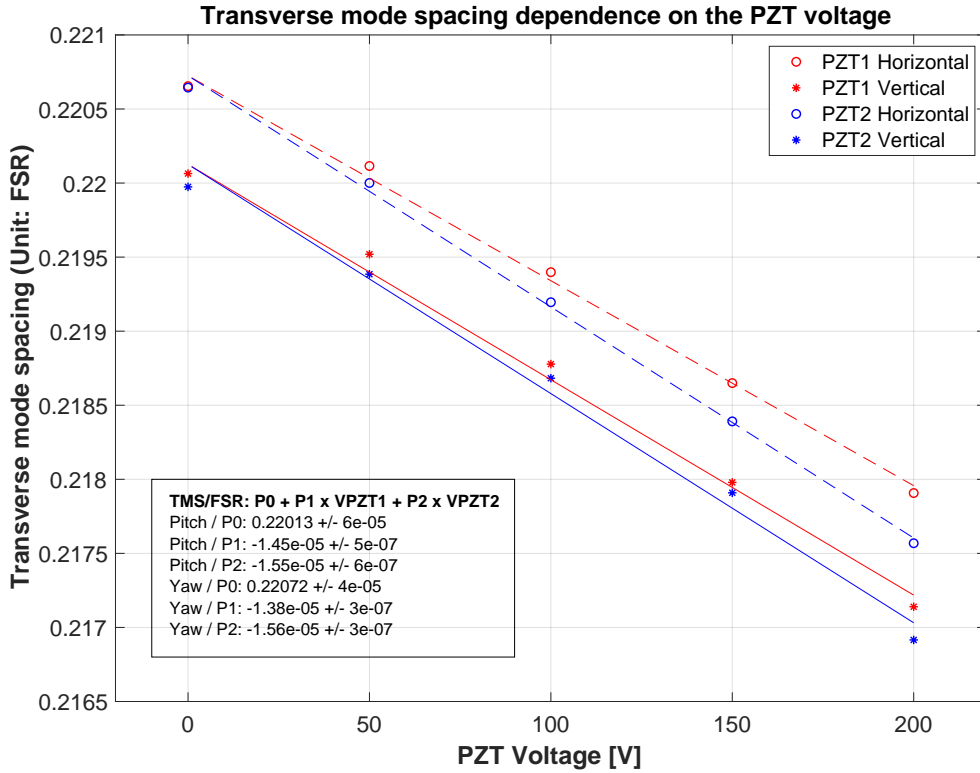


Figure 161: OMC(002): Dependence of the vertical and horizontal TMSs on the PZT voltages. The TMSs are expressed in the unit of FSR.

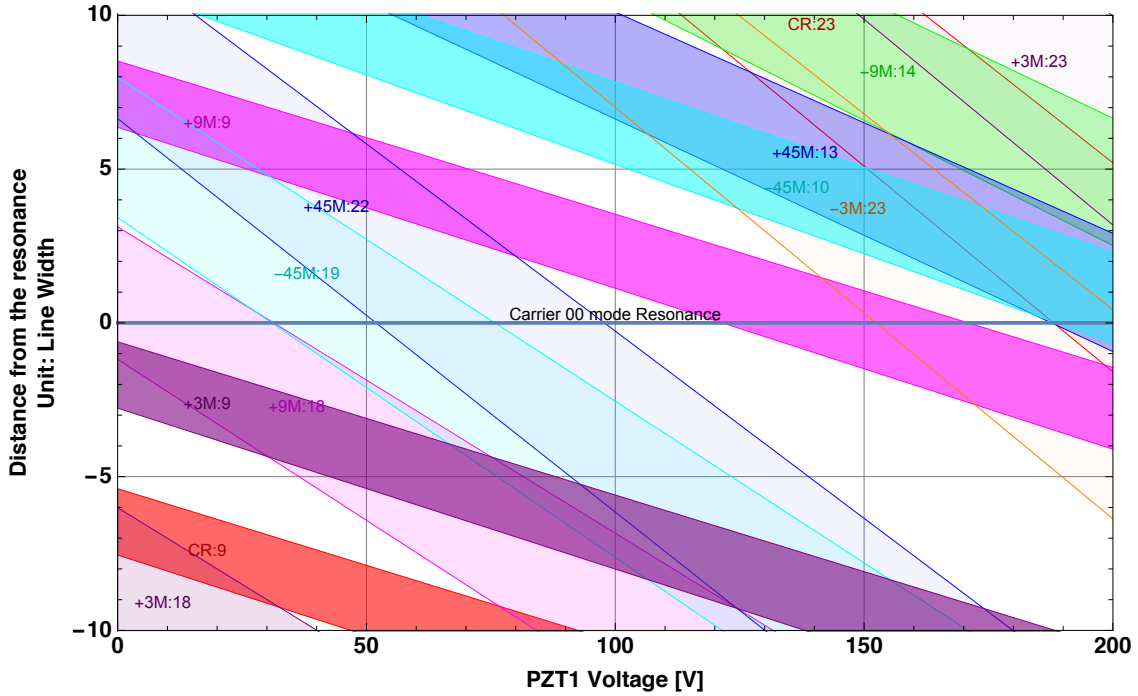


Figure 162: OMC(002): Modelled coincidental resonances of the higher-order modes as the PZT voltages scanned.

3.11.5 Power budget for OMC(002)

[External Link]

http://nodus.ligo.caltech.edu:8080/OMC_Lab/170

[Description]

Summary of the measurement on 2013/9/17 is shown in Table 23.

Assumptions			
Finesse	373.114		
Input BS transmission	7400		ppm
Derived Values			
Roundtrip reflectivity	0.9916		
Power: OMC incident	35.40	± 0.07	mW
Power: Cavity incident	35.14	± 0.07	mW
Power: Coupled to the cavity	34.75	± 0.07	mW
Power: Junk light at the cavity	0.390	± 0.004	mW
Mode Matching	0.9889	± 0.0001	
Cavity power reflectivity	0.0010	± 0.0001	
Cavity power transmission	0.938	± 0.002	
OMC unit throughput	0.931	± 0.002	
OMC optical loss	0.069	± 0.002	
Loss per mirror	111	± 5	ppm
FM1/FM2 transmission	8121	± 9.1	ppm
CM1 transmission	42.5	± 0.3	ppm
CM2 transmission	42.5	± 0.3	ppm

Table 23: OMC(002): Summary of the power measurement taken after final cleaning on 2013/9/17

3.11.6 PZT response DC/AC

[External Link]

http://nodus.ligo.caltech.edu:8080/OMC_Lab/148

[Description]

Figures 163 and 164 show DC and AC responses of the PZTs. Estimated DC responses were

- **PZT1:** $11.6 \pm 0.1 \text{ nm/V}$
- **PZT2:** $12.4 \pm 0.1 \text{ nm/V}$

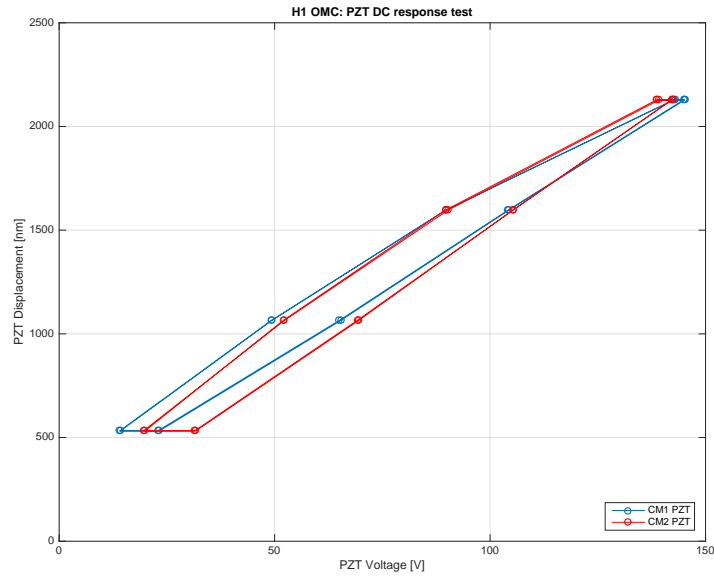


Figure 163: OMC(002): PZT sweep voltages and the OMC resonances.

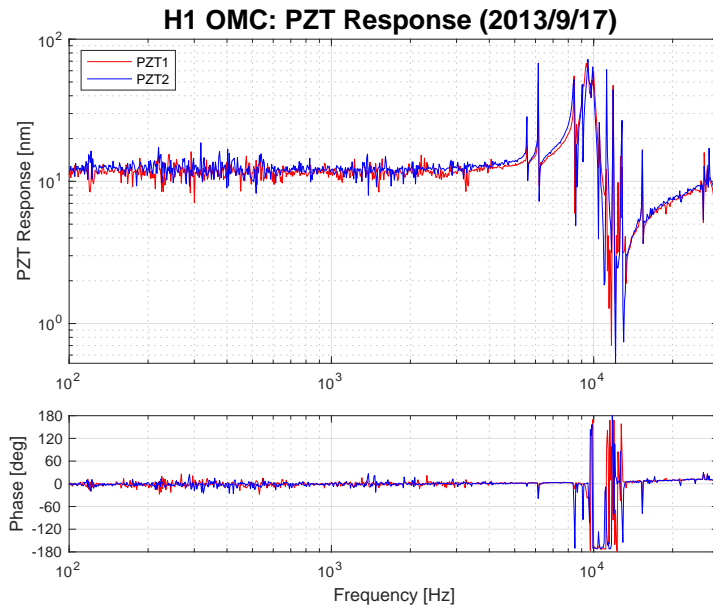


Figure 164: OMC(002): PZT AC responses. The DC gain was adjusted to match the DC scan result.

3.11.7 DCPD/QPD shim height adjustment

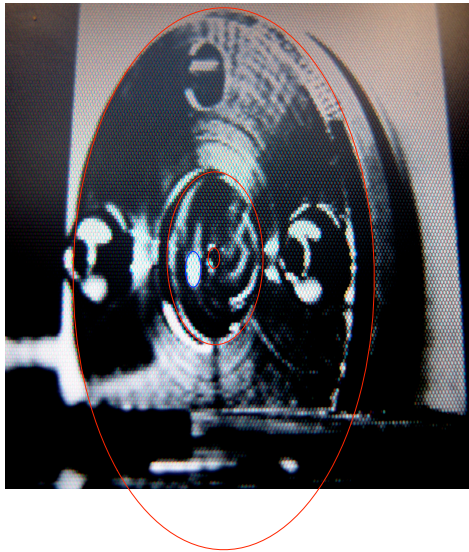
[External Link]

Final: http://nodus.ligo.caltech.edu:8080/OMC_Lab/163

[Description]

Determined shim heights: (0.085mm for the glue height)

- DCPD1: 1.50mm shim \Rightarrow Beam 0.038mm too low
- DCPD2: 1.25mm shim \Rightarrow Beam 0.026mm too low. Shortage of 1.25mm shim *rightarrow* 1.50mm shim used. Beam 0.276mm too low.
- QPD1: 1.75mm shim \Rightarrow Beam 0.056mm too low
- QPD2: 1.5mm shim \Rightarrow Beam 0.118mm too low \rightarrow 1.25mm shim used. Beam 0.132mm too high.



**DCPD1 (BS Transmission Side / without BS)
Glass Mount + 2mm SHIM (D1201467-3)**

HOLE

Hole Height in the picture: 10.643
Hole Vert size in the picture: 0.8229
 \Rightarrow Hole center pos in the pic: 11.0545

VS

BEAM

Beam height in the picture: 10.7892
Beam Vert size in the picture: 1.4213
 \Rightarrow Beam center pos in the pic: 11.4999

Conversion: $0.8229 = 1.016\text{mm}$ (40mil)

\Rightarrow Beam 0.541mm too low

\Rightarrow with 1.5mm shim, the beam will be 0.038mm too low

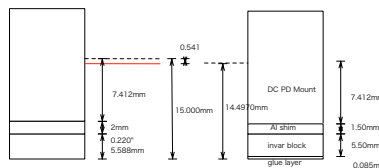


Figure 165: OMC(002): Image analysis for the DCPD1 shim height

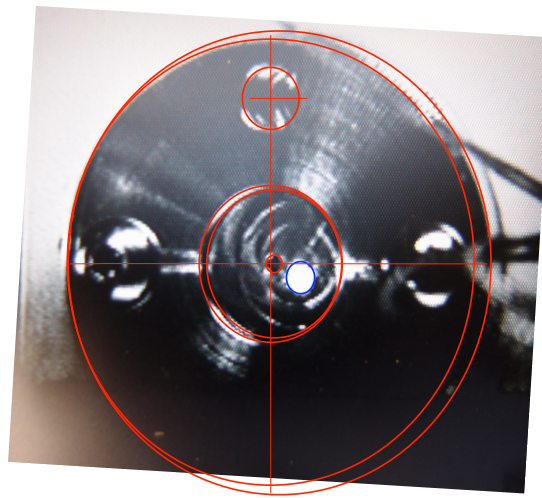
3.11.8 QPD alignment

[External Link]

http://nodus.ligo.caltech.edu:8080/OMC_Lab/172

[Description]

See Table 24.



**DCPD1 (BS Transmission Side / without BS)
Glass Mount + 2mm SHIM (D1201467-3)**

HOLE
Hole Height in the picture: 11.6269
Hole Vert size in the picture: 0.7584
=> Hole center pos in the pic: 12.0061

VS

BEAM
Beam height in the picture: 11.9085
Beam Vert size in the picture: 1.3766
=> Beam center pos in the pic: 12.5968

Conversion: 0.7584 = 1.016mm (40mil)

=> Beam 0.779mm too low

=> with 1.25mm shim, the beam will be 0.026mm too low

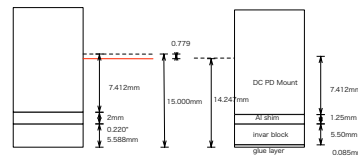
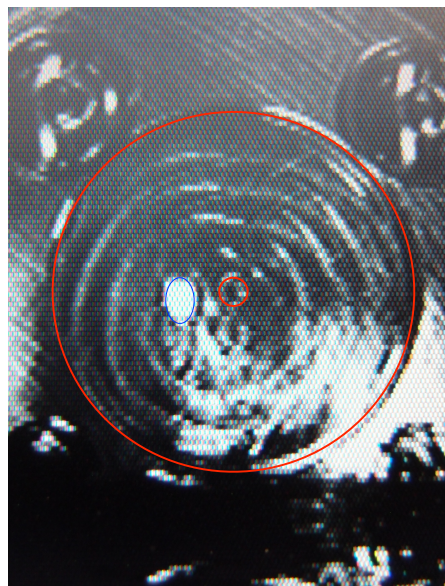


Figure 166: OMC(002): Image analysis for the DCPD2 shim height



**QPD1 (BS Reflection)
SHIM: 2mm**

HOLE
HPOS: 8.8612
HSIZ: 1.0262
CPOS: 9.3743

VS

BEAM
HPOS: 8.8612
HSIZ: 1.6607
CPOS: 9.6916

Conversion: 1.0262 = 1.016mm (40mil)

=> Beam 0.309mm too low

=> with 1.75mm shim, the beam will be 0.056mm too low

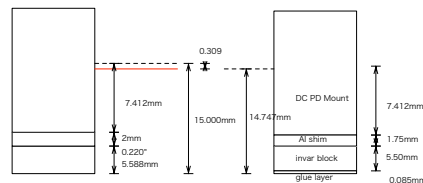


Figure 167: OMC(002): Image analysis for the QPD1 shim height

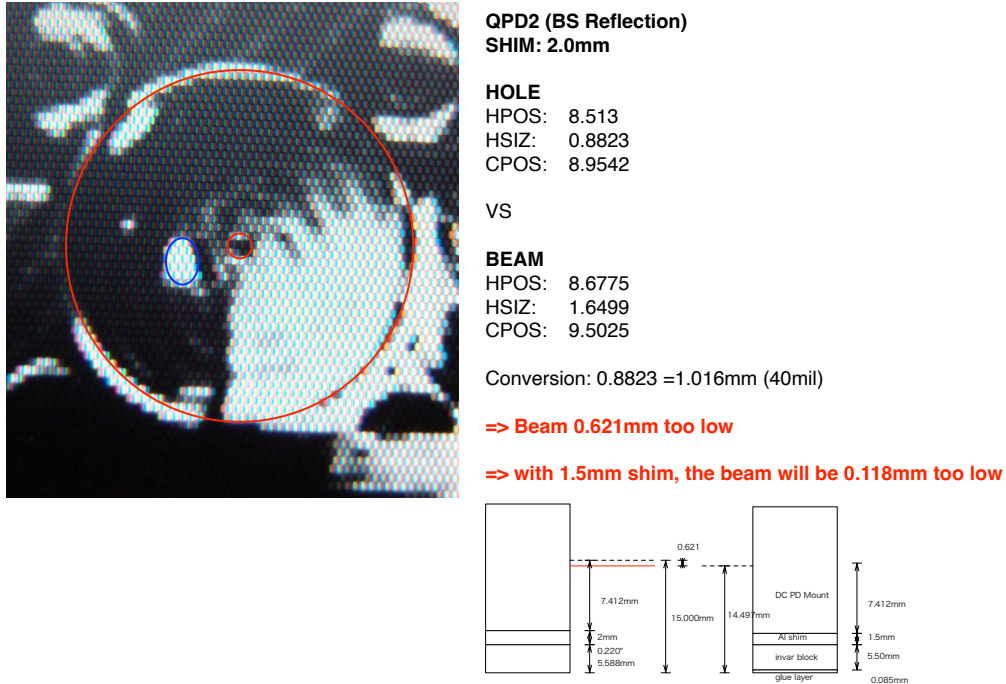


Figure 168: OMC(002): Image analysis for the QPD2 shim height

QPD#	QPD1		QPD2	
Diode#	#44		#46	
Incident power	125.7	[μ W]	126.4	[μ W]
Sum Out	80.1	[mV]	78.9	[mV]
Vertical Out	3.4	[mV]	0.0	[mV]
Horizontal Out	-23.7	[mV]	-26	[mV]
SEG1	-15.6	[mV]	-13.2	[mV]
SEG2	-13.1	[mV]	-13.3	[mV]
SEG3	-29.0	[mV]	-26.4	[mV]
SEG4	-23.2	[mV]	-26.3	[mV]
Spot position X ^a	-13	[μ m]	-0.8	[μ m]
Spot position Y ^b	+93	[μ m]	+107	[μ m]
Responsivity	0.64	[A/W]	0.62	[A/W]
Q.E.	0.74		0.73	

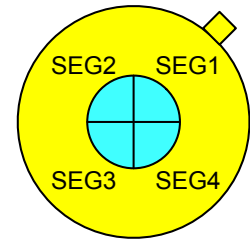


Figure 169: OMC(002): Arrangement of the QPD segments (beam view)

Table 24: OMC(002): Measurement results for the QPDs and the derived spot positions

^apositive = more power on SEG1 and SEG4

^bpositive = more power on SEG3 and SEG4

3.11.9 Alignment / beam spot photos

[Description]

Collection of the spot photos for the DCPDs, DCPD reflections, QPDs (QPD2 photo miss-

ing), FMs, and CMs.



Figure 170: OMC(002): DCPD1 final spot position

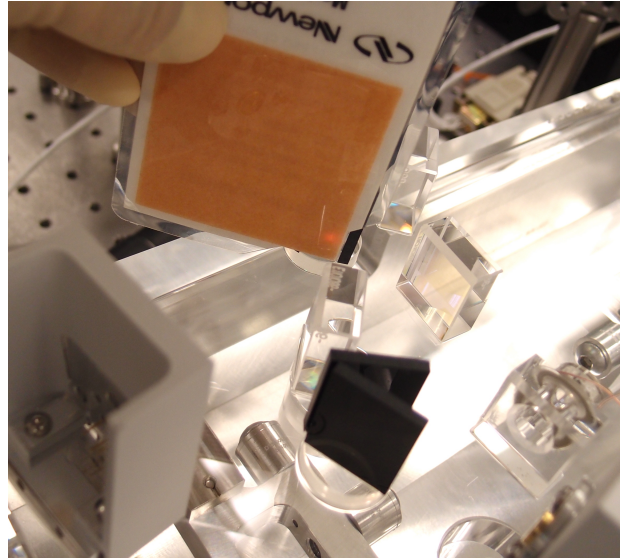


Figure 171: OMC(002): DCPD1 reflection on the beam dump

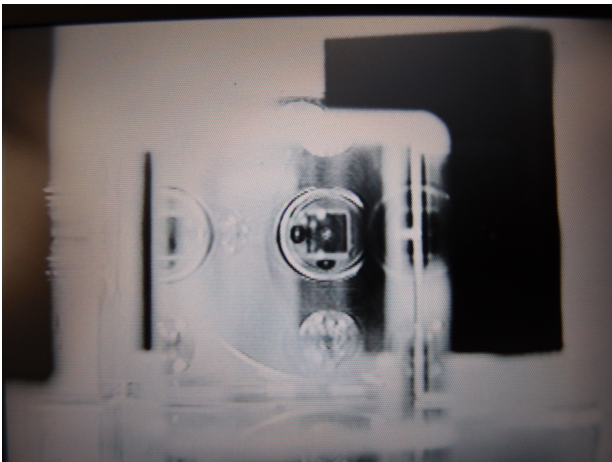


Figure 172: OMC(002): DCPD2 final spot position



Figure 173: OMC(002): DCPD2 reflection on the beam dump

3.11.10 Forensic study of the damaged OMC(002)

[External Link]

<https://alog.ligo-wa.caltech.edu/aLOG/index.php?callRep=28683>

<https://alog.ligo-wa.caltech.edu/aLOG/index.php?callRep=28840>

Forensic study by the CIT team [E1600268](#)

[Description]

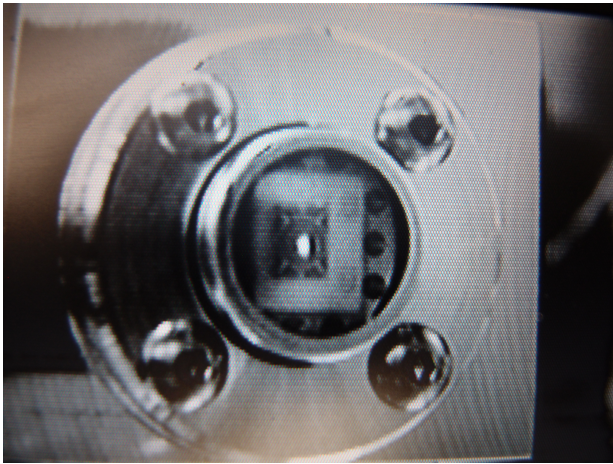


Figure 174: OMC(002): QPD1 final spot position

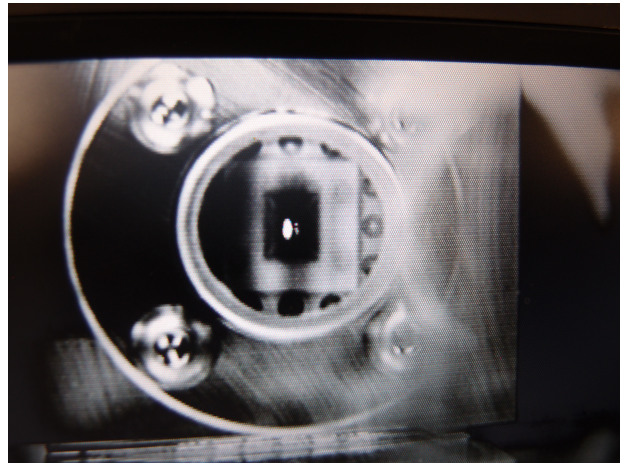


Figure 175: OMC(002): QPD2 final spot position

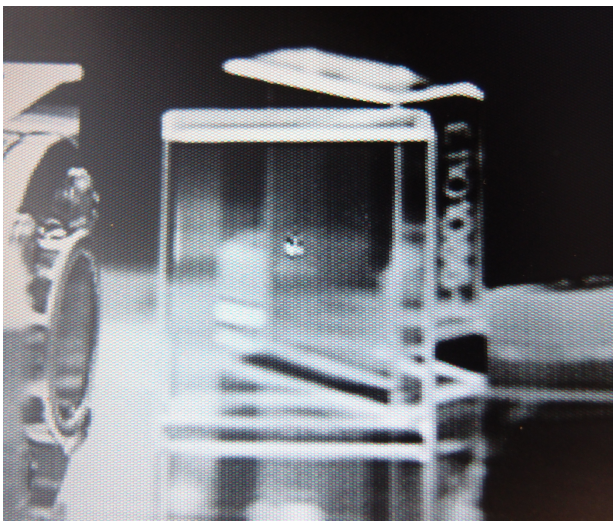


Figure 176: OMC(002): FM1 final spot position



Figure 177: OMC(002): FM2 final spot position



Figure 178: OMC(002): CM1 final spot position

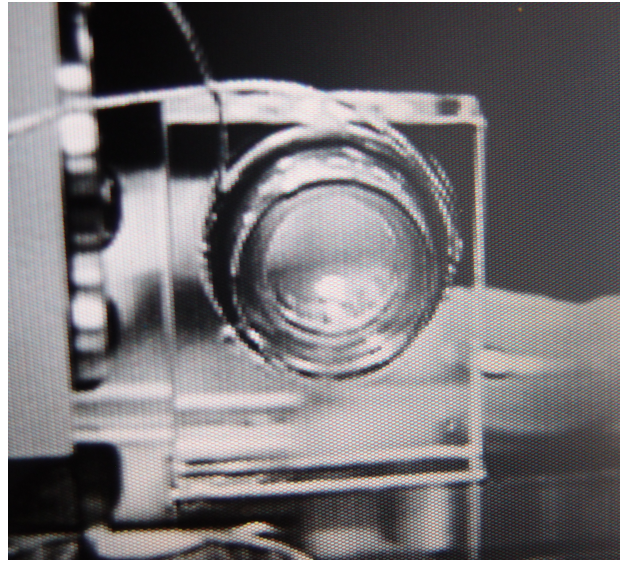


Figure 179: OMC(002): CM2 final spot position

After the vent of HAM6 at LHO in 2016 April, the fast shutter trigger was not properly restored. This resulted in the OMC(002), as well as other optics in HAM6, being exposed to high power pulses of IFO lock losses. On July 27th, 2016, a lock loss eventually caused one of the OMC curved mirror failed.

In the above LHO ALOG thread (28683~), Stefan evaluated the optical pulse OMC has received ³. According to his analysis, the pulse that made the failure reached more than 160W for the duration of about 30msec. This corresponds to the pulse energy of $> 5\text{ J}$ and the peak power density was $> 400\text{ W/mm}^2$ and the energy density of $> 12\text{ J/mm}^2$. This seemed a typical lock loss pulse and was not a particularly strong one. Daniel pointed out that in the ALOG 28840 that the pressure rises of HAM6 were observed during the lock losses. The forensic study carried out at Caltech was summerized in E1600268.

³<https://alog.ligo-wa.caltech.edu/aLOG/index.php?callRep=28701>

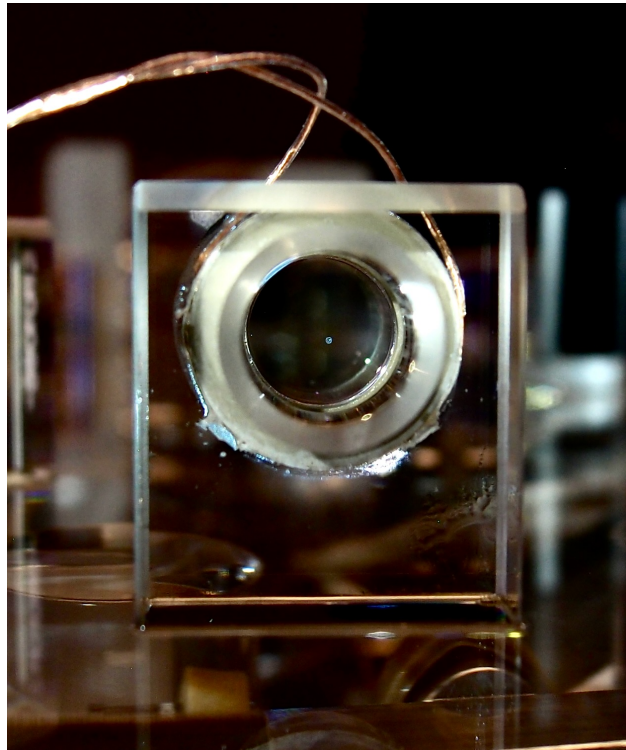


Figure 180: OMC(002): CM1 burnt spot (a white circle at the center of the mirror): forensic study after the failure in 2016

3.12 Test results for OMC(003)

3.12.1 Summary of the OMC(003) tests

[Description]

The table shows the summary of the OMC(003) optical test results. The detailed results are shown in the following sections.

FSR (detuned locking)			
FSR	264.819	± 0.001	[MHz]
Cavity roundtrip length	1.132065	± 0.000004	[m]
FSR & Finesse (RFAM injection)			
FSR	264.8119	± 0.0003	[MHz]
Cavity roundtrip length	1.132096	± 0.000001	[m]
Finesse	399.7	± 0.3	
TMS			
TMS (Vertical)	57.8435	± 0.0004	[MHz]
	0.218430	± 0.000001	[FSR]
TMS (Horizontal)	58.1377	± 0.0003	[MHz]
	0.219539	± 0.000001	[FSR]
Total Optical Loss (2014/7/2)			
OMC unit throughput	0.957	± 0.004	
OMC optical loss	0.043	± 0.004	
PZT response			
PZT1:	11.31	± 0.04	[nm/V]
PZT2:	12.73	± 0.02	[nm/V]

Table 25: OMC(003): Summary of the cavity geometry tests

3.12.2 Cavity absolute length measurement with detuned locking

[Description]

See Figure 181.

3.12.3 Cavity length and finesse measurement with RFAM injection

[Description]

See Figures 182 and 183.

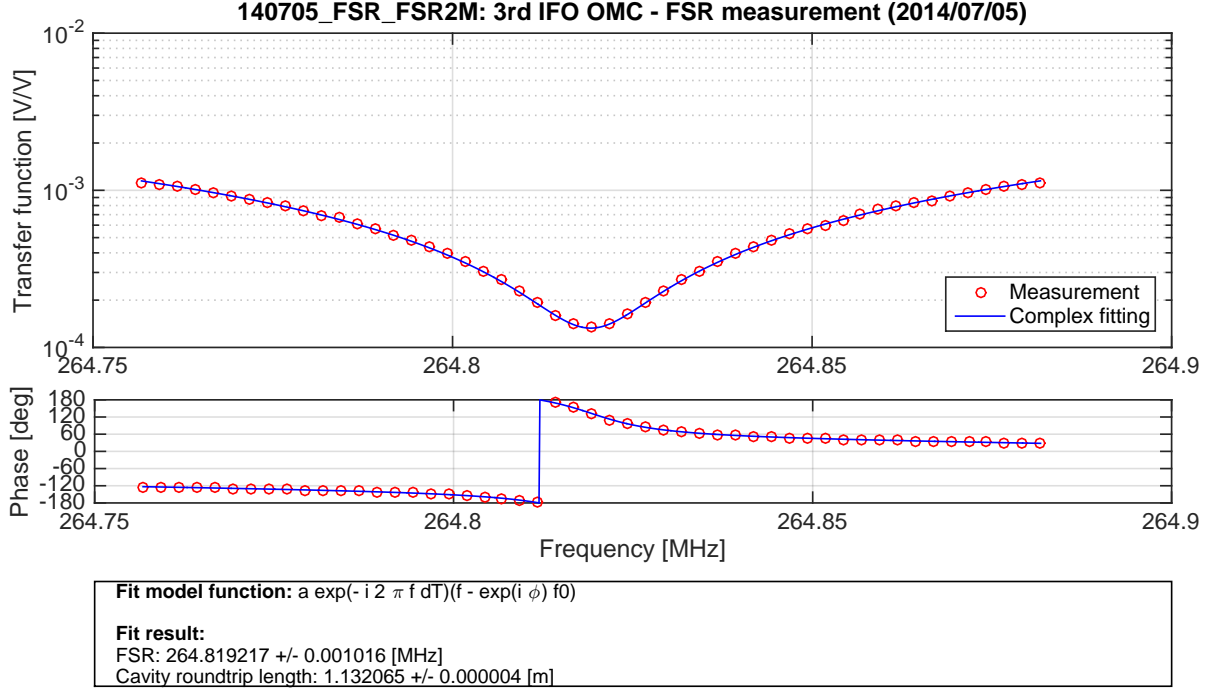


Figure 181: OMC(003): Cavity absolute length (FSR) measurement with detuned locking

3.12.4 Transverse-mode spacing measurement

[Description]

See Figures 184 and 185 for the transfer functions and the estimated TMSs.

Figure 186 shows that the 9th-order and 19th-order modes potentially cause the problem of the coincident resonance.

The dependence of TMSs on the PZT voltages is shown in Figure. 187). The dependence model is expressed as

$$\frac{\nu_{\text{TMS}}}{\nu_{\text{FSR}}} = P_0 + P_1 V_{\text{PZT1}} + P_2 V_{\text{PZT2}} , \quad (24)$$

the parameters for each TMS were estimated to be

Vertical TMS :

$$P_0 = 0.21843 \pm 5 \times 10^{-5}$$

$$P_1 = -6.47 \times 10^{-6} \pm 6 \times 10^{-7}$$

$$P_2 = -6.61 \times 10^{-6} \pm 6 \times 10^{-7}$$

Horizontal TMS :

$$P_0 = 0.21939 \pm 7 \times 10^{-5}$$

$$P_1 = -9.41 \times 10^{-6} \pm 7 \times 10^{-7}$$

$$P_2 = -1.17 \times 10^{-5} \pm 7 \times 10^{-7}$$

The prediction of the coincident resonance of the higher-order modes are shown in Fig-

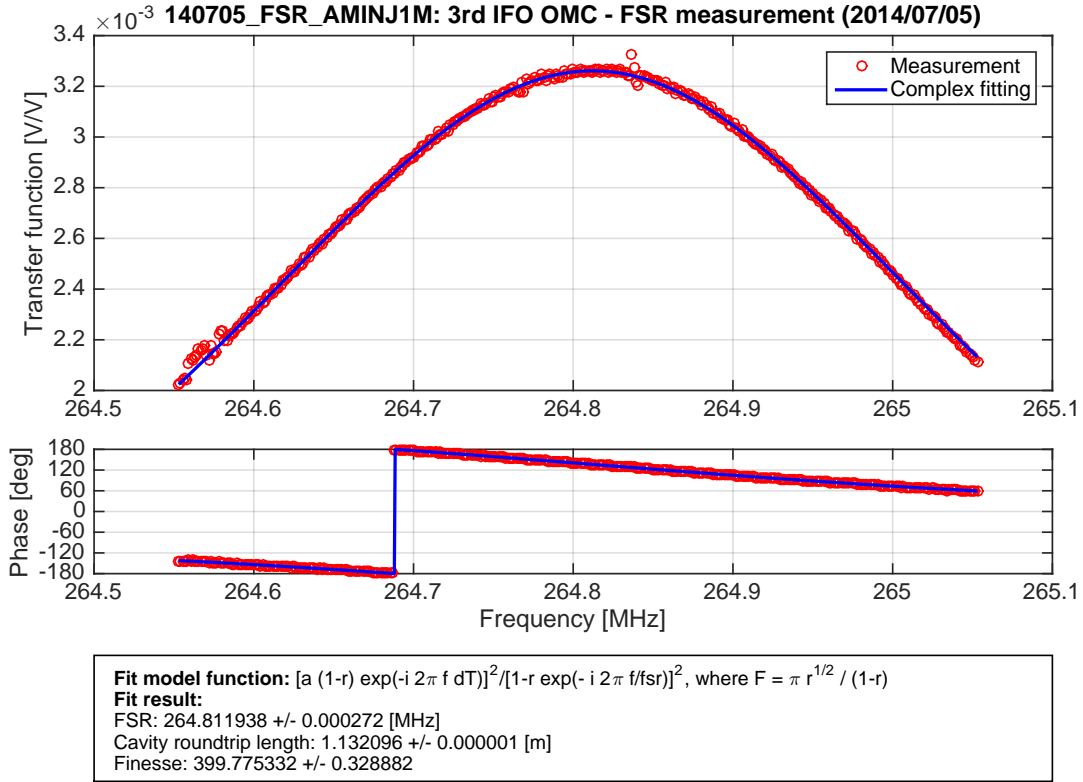


Figure 182: OMC(003): Cavity length (FSR) and finesse measurement with RFAM injection

3rd OMC – FSR/Finesse measurement with AM injection (2014/07/05)

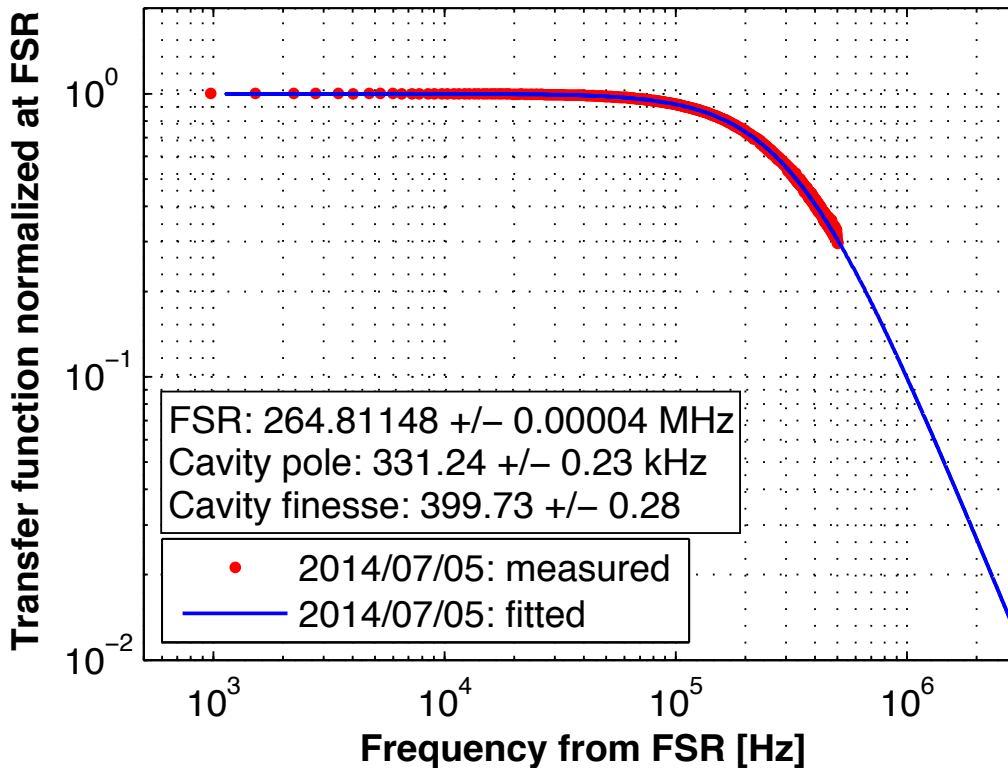


Figure 183: OMC(003): Cavity finesse measurement with RFAM injection
page 142

ure 188). It was predicted that the 9th-order modes of the +9MHz sideband is coincidentally resonant. Some of the 23rd-order modes are also resonant, but it is expected to be less problematic due to their high order number. Pushing the voltage higher has also a risk to have one of the 45MHz modes, which could be stronger, to come into the resonance.

This coincidental resonance of the 9th-order modes was actually observed at LHO⁴⁵

3.12.5 Power budget for OMC(003)

[External Link]

http://nodus.ligo.caltech.edu:8080/OMC_Lab/197

[Description]

Summary of the measurement on 2014/7/2 is shown in Table 26.

Assumptions			
Finesse	399.73		
Input BS transmission	7400		ppm
Derived Values			
Roundtrip reflectivity	0.9922		
Power: OMC incident	34.80	±0.1	mW
Power: Cavity incident	34.54	±0.1	mW
Power: Coupled to the cavity	33.90	±0.1	mW
Power: Junk light at the cavity	0.641	±0.003	mW
Mode Matching	0.9814	± 0.00009	
Cavity power reflectivity	0.00032	±0.00009	
Cavity power transmission	0.965	±0.005	
OMC unit throughput	0.957	±0.005	
OMC optical loss	0.043	±0.005	
Loss per mirror	49.2	±10	ppm
FM1/FM2 transmission	7689	±20	ppm
CM1 transmission	41.7	±0.3	ppm
CM2 transmission	42.9	±0.3	ppm

Table 26: OMC(003): Summary of the power measurement taken after final cleaning on 2014/7/2

3.12.6 PZT response DC/AC

[External Link]

⁴<https://alog.ligo-wa.caltech.edu/aLOG/index.php?callRep=29395>

⁵<https://alog.ligo-wa.caltech.edu/aLOG/index.php?callRep=29817>

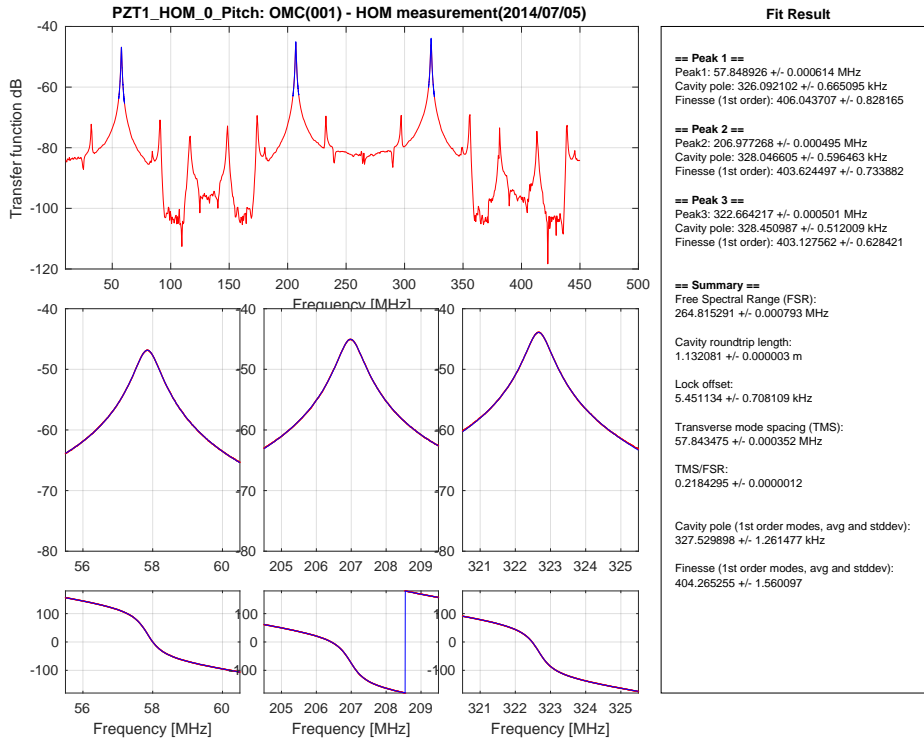


Figure 184: OMC(003): Vertical TMS measurement with no PZT voltages applied.

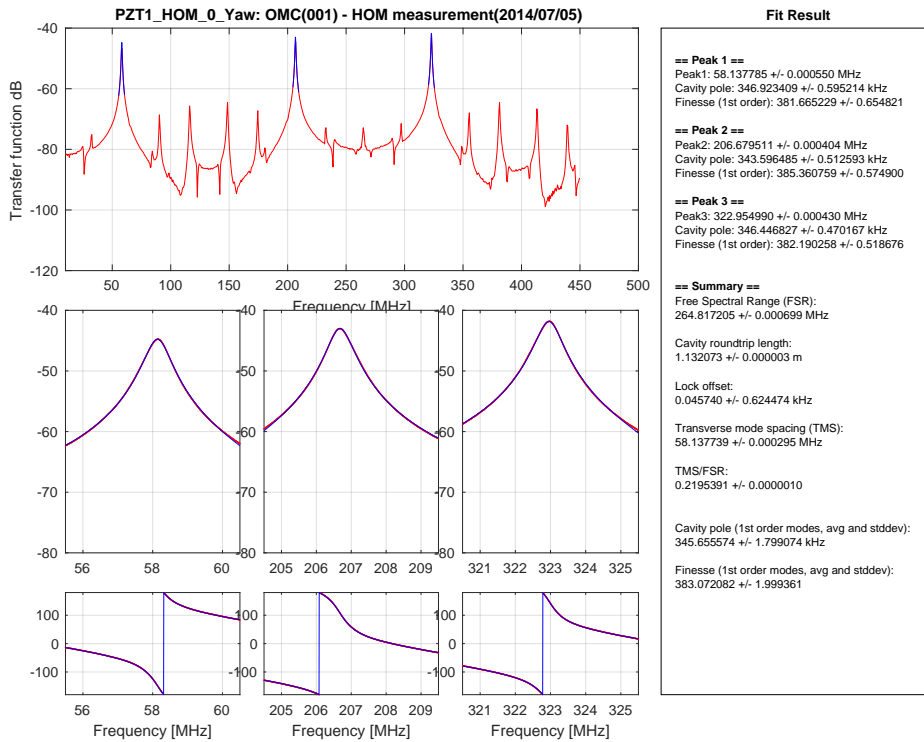


Figure 185: OMC(003): Horizontal TMS measurement with no PZT voltages applied.

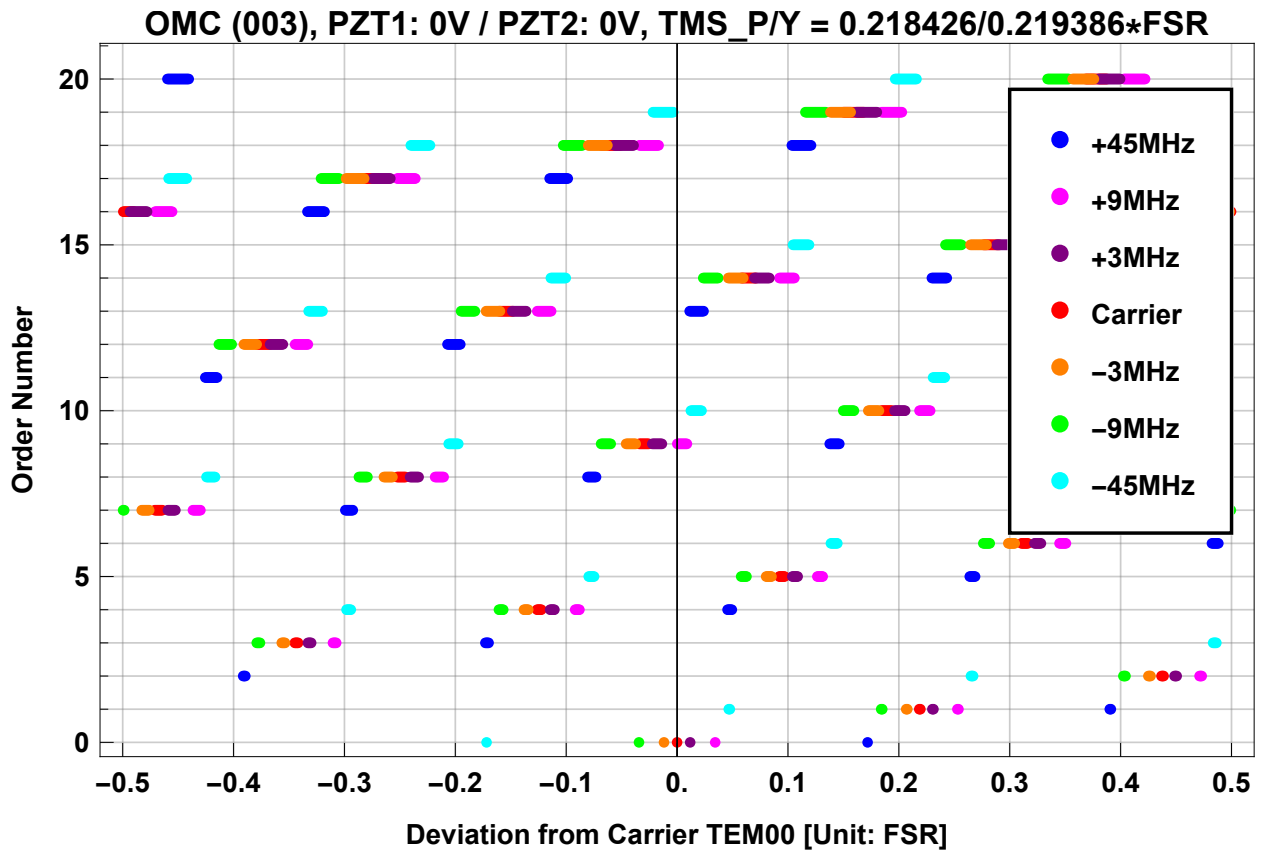


Figure 186: OMC(003): Higher-order modes distribution with no PZT voltages applied.

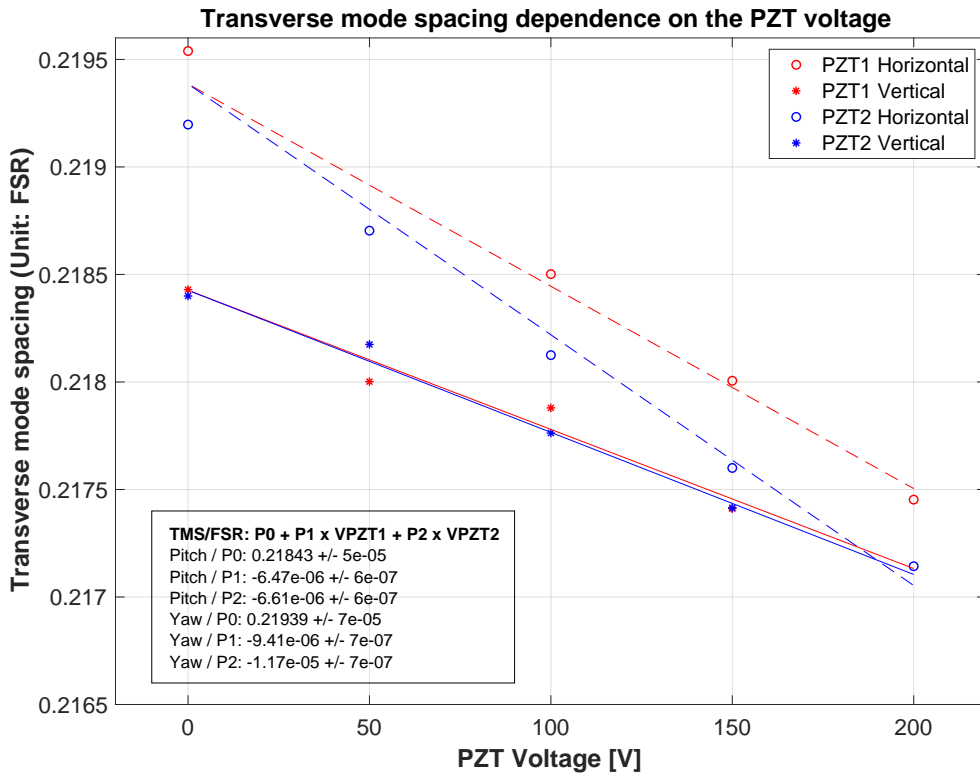


Figure 187: OMC(003): Dependence of the vertical and horizontal TMSs on the PZT voltages. The TMSs are expressed in the unit of FSR.

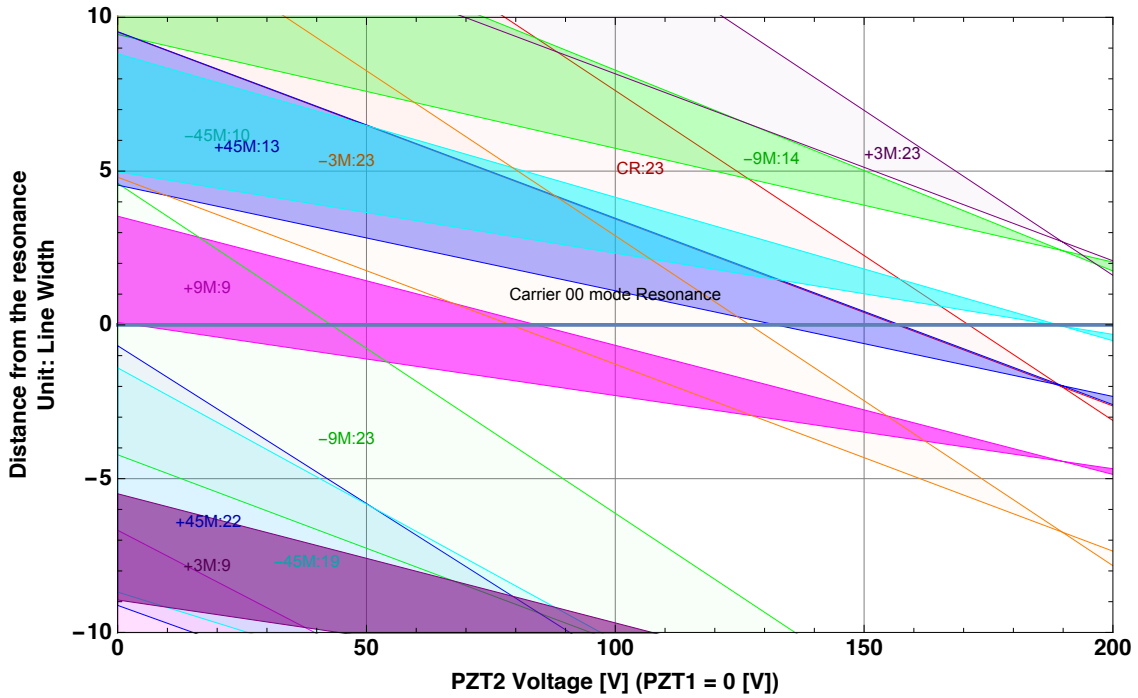


Figure 188: OMC(003): Modelled coincidental resonances of the higher-order modes as the PZT voltages scanned.

http://nodus.ligo.caltech.edu:8080/OMC_Lab/202

[Description]

Figures 189 and 190 show DC and AC responses of the PZTs. Estimated DC responses were

- **PZT1:** $11.31 \pm 0.04\text{nm/V}$
- **PZT2:** $12.73 \pm 0.02\text{nm/V}$

3.12.7 DCPD/QPD shim height adjustment

[External Link]http://nodus.ligo.caltech.edu:8080/OMC_Lab/206

[Description]

Determined shim heights:

- DCPD1: 1.00mm
- DCPD2: 1.00mm
- QPD1: 1.25mm
- QPD2: 1.25mm

3.12.8 QPD alignment

[External Link]

http://nodus.ligo.caltech.edu:8080/OMC_Lab/205

[Description]

See Table 27

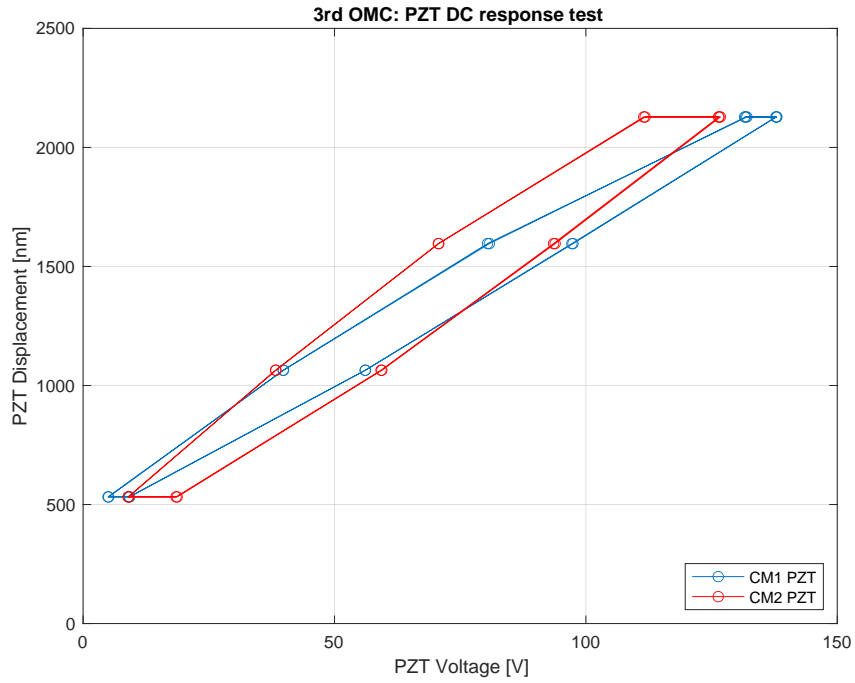


Figure 189: OMC(003): PZT sweep voltages and the OMC resonances.

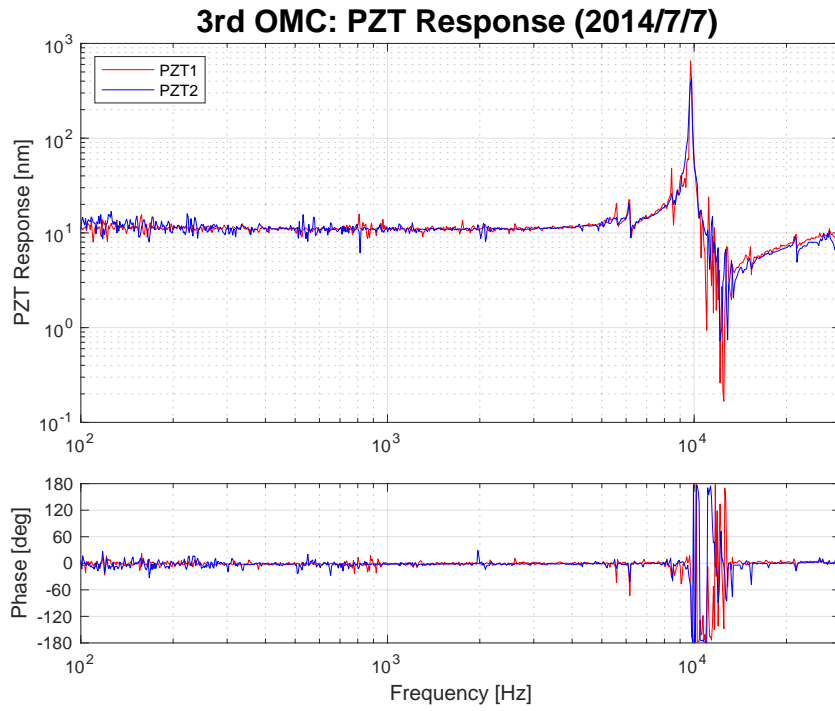


Figure 190: OMC(003): PZT AC responses. The DC gain was adjusted to match the DC scan result.

QPD#	QPD1		QPD2	
Diode#	#50		#51	
Incident power	110.1	[μ W]	116.5	[μ W]
Sum Out	77.0	[mV]	82.5	[mV]
Vertical Out	-24.0	[mV]	-8.8	[mV]
Horizontal Out	4.2	[mV]	9.0	[mV]
SEG1	-11.6	[mV]	-16.0	[mV]
SEG2	-12.6	[mV]	-18.0	[mV]
SEG3	-25.2	[mV]	-24.4	[mV]
SEG4	-21.4	[mV]	-21.4	[mV]
Spot position X ^a	-21	[μ m]	-19	[μ m]
Spot position Y ^b	+102	[μ m]	+47	[μ m]
Responsivity	0.70	[A/W]	0.71	[A/W]
Q.E.	0.82		0.83	

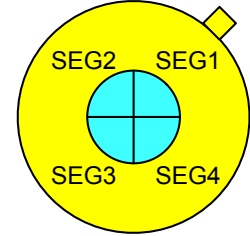


Table 27: OMC(003): Measurement results for the QPDs and the derived spot positions

^apositive = more power on SEG1 and SEG4

^bpositive = more power on SEG3 and SEG4

Figure 191: OMC(003): Arrangement of the QPD segments (beam view)

3.12.9 Alignment / beam spot photos

[Description]

Beam spot photos for DCPD1 and DCPD2



Figure 192: OMC(003): DCPD1 final spot position

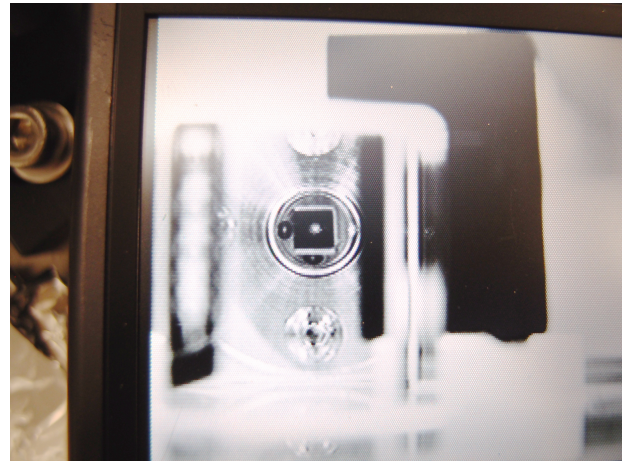


Figure 193: OMC(003): DCPD2 final spot position

3.13 Test results for OMC(002R2)

3.13.1 Summary of the OMC(002R2) tests

[Description]

The table shows the summary of the OMC(002R2) optical test results. The detailed results are shown in the following sections. From the OMC(002), CM1 and the PZT on CM1 were replaced. So the optical parameters were expected to be changed. Luckily, the measured optical parameters still matched with the OMC requirements. Therefore this OMC was stored as a legit spare and then decided to be installed as the 2nd OMC for LLO in 2022.

FSR (detuned locking)			
FSR	261.713	± 0.001	[MHz]
Cavity roundtrip length	1.145503	0.000005	[m]
FSR & Finesse (RFAM injection)			
FSR	261.715	± 0.001	[MHz]
Cavity roundtrip length	1.145491	± 0.000006	[m]
Finesse	400	± 2	
TMS			
TMS (Vertical)	57.703973	± 0.0001	[MHz]
	0.2204799	± 0.0000004	[FSR]
TMS (Horizontal)	57.839592	± 0.00008	[MHz]
	0.2209972	± 0.0000003	[FSR]
Total Optical Loss (2022/9/19)			
OMC unit throughput	0.975	± 0.007	
OMC optical loss	0.025	± 0.007	
PZT response			
PZT1:	14.8965	± 0.0001	[nm/V]
PZT2:	14.39	± 0.02	[nm/V]

Table 28: OMC(002R2): Summary of the cavity geometry tests

3.13.2 Cavity absolute length measurement with detuned locking

[Description]

The transfer function and the measurement results are shown in Figure 194.

3.13.3 Cavity length and finesse measurement with RFAM injection

[Description]

The transfer function and the measurement results are shown in Figure 195.

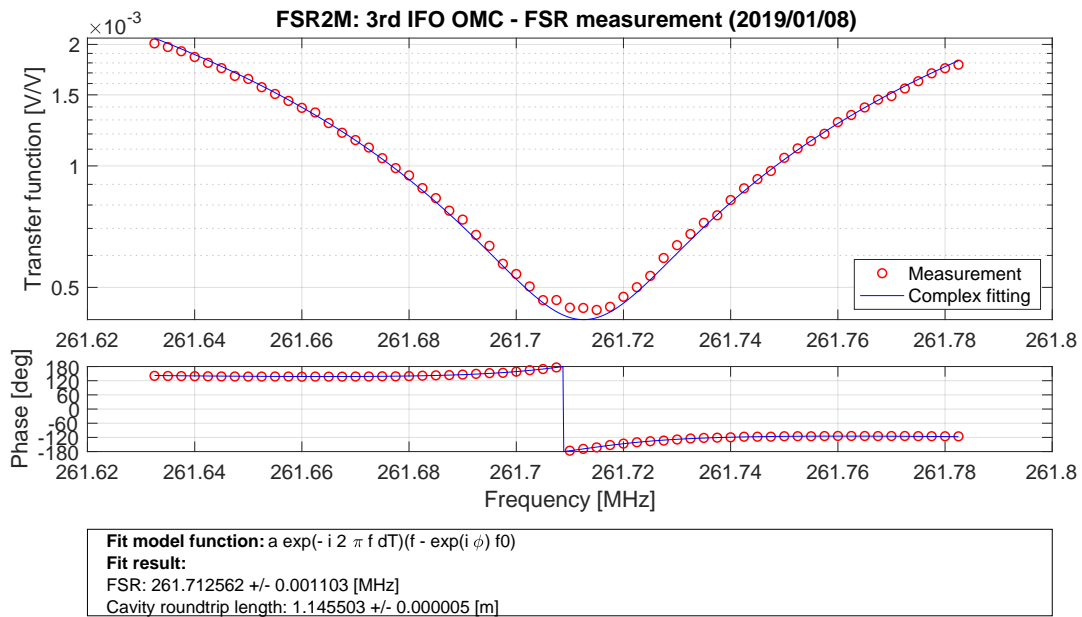


Figure 194: OMC(002R2): Cavity absolute length (FSR) measurement with detuned locking

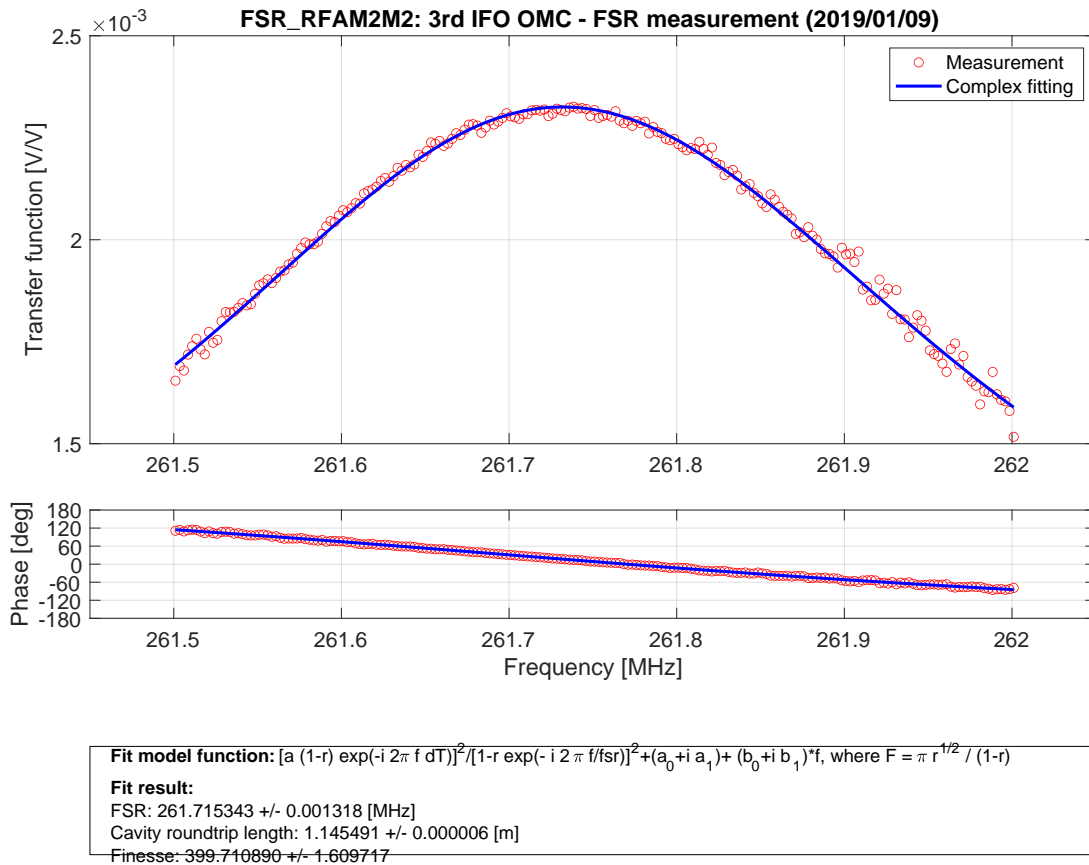


Figure 195: OMC(002R2): Cavity length (FSR) and finesse measurement with RFAM injection

3.13.4 Transverse-mode spacing measurement

[Description]

See Figures 196 and 197 for the transfer functions and the estimated TMSs.

Figure 198 shows that the 9th-order and 18th-order modes are close to the TEM00 resonance.

The dependence of TMSs on the PZT voltages is shown in Figure. 187). The dependence model is expressed as

$$\frac{\nu_{\text{TMS}}}{\nu_{\text{FSR}}} = P_0 + P_1 V_{\text{PZT1}} + P_2 V_{\text{PZT2}} , \quad (25)$$

the parameters for each TMS were estimated to be

Vertical TMS :

$$P_0 = 0.22047 \pm 2 \times 10^{-5}$$

$$P_1 = -9.4 \times 10^{-6} \pm 2 \times 10^{-7}$$

$$P_2 = -1.26 \times 10^{-5} \pm 2 \times 10^{-7}$$

Horizontal TMS :

$$P_0 = 0.22102 \pm 4 \times 10^{-5}$$

$$P_1 = -1.12 \times 10^{-6} \pm 5 \times 10^{-7}$$

$$P_2 = -1.44 \times 10^{-5} \pm 5 \times 10^{-7}$$

The prediction of the coincident resonance of the higher-order modes are shown in Figure 188). If the PZT voltage is suppressed low, only 18th and 19th modes are the possible coincident resonance.

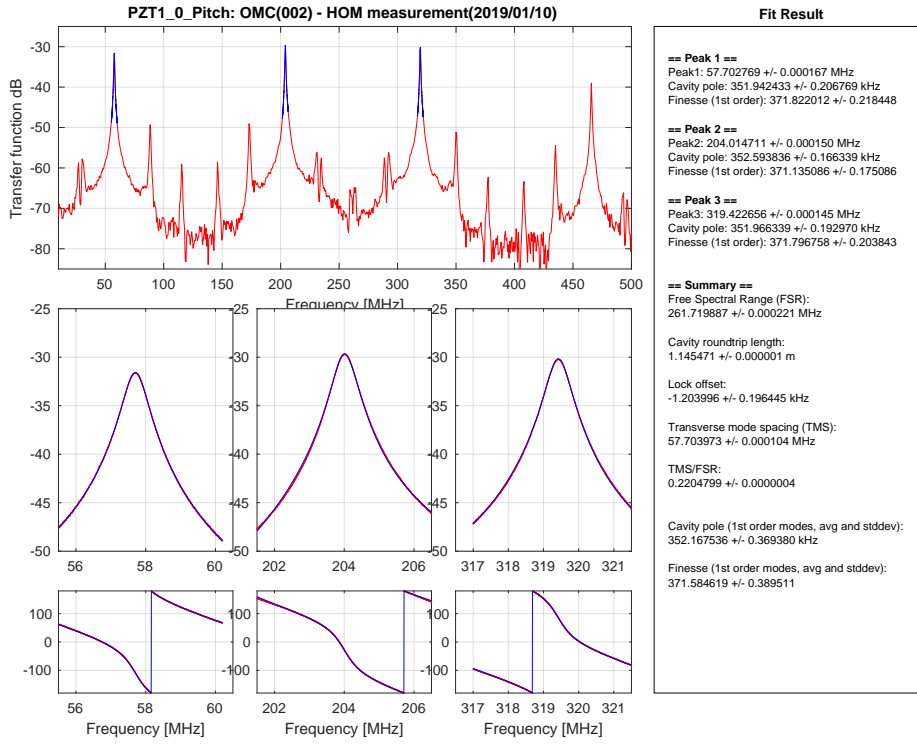


Figure 196: OMC(002R2): Vertical TMS measurement with no PZT voltages applied.

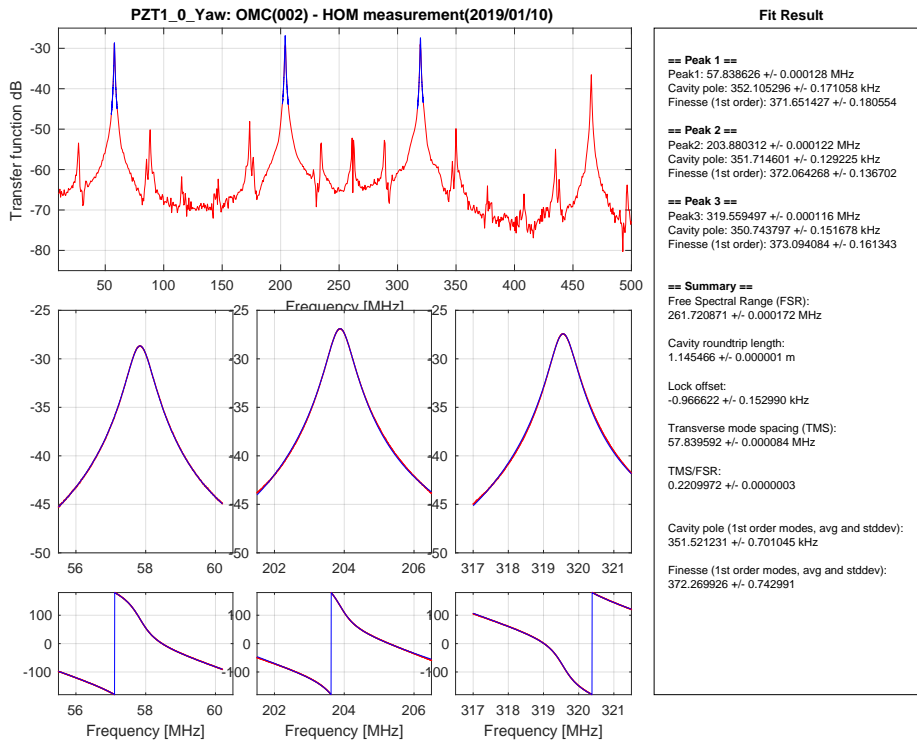


Figure 197: OMC(002R2): Horizontal TMS measurement with no PZT voltages applied.

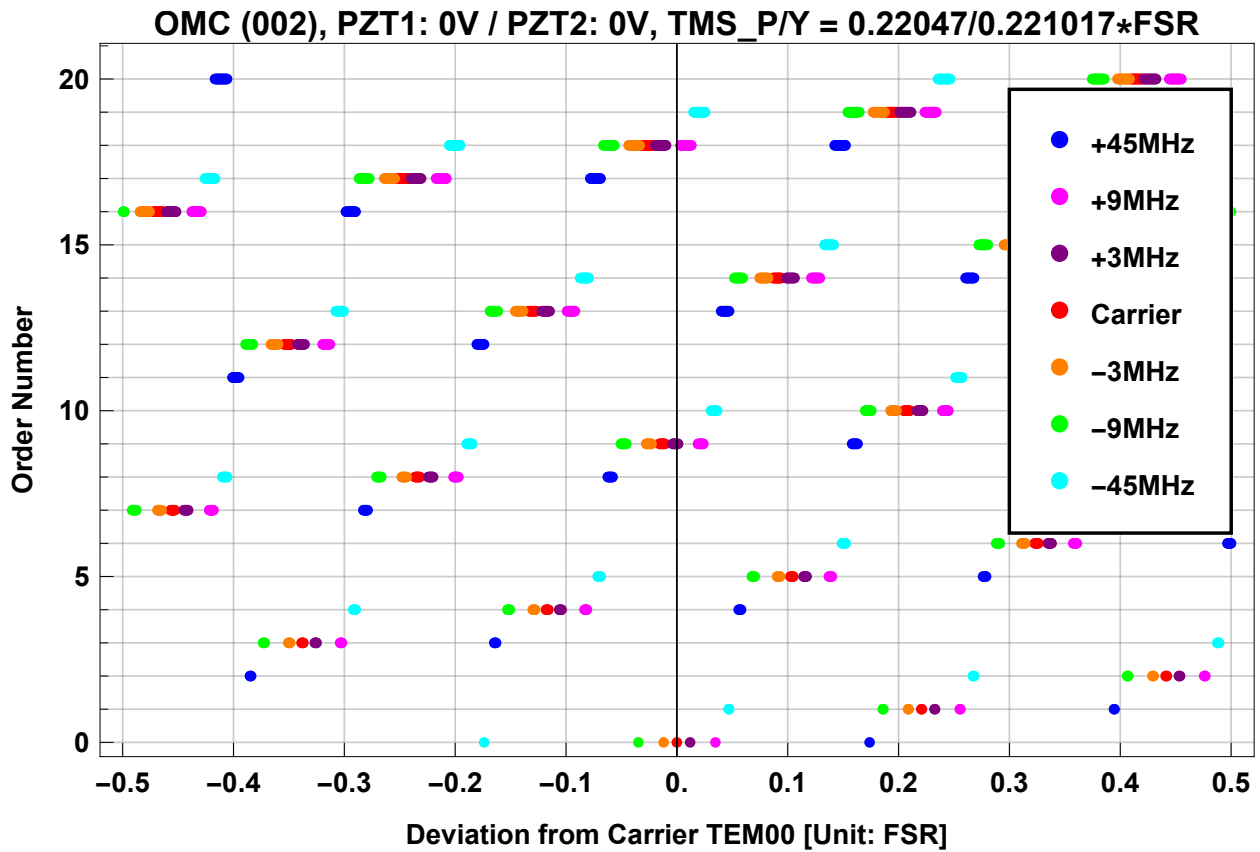


Figure 198: OMC(002R2): Higher-order modes distribution with no PZT voltages applied.

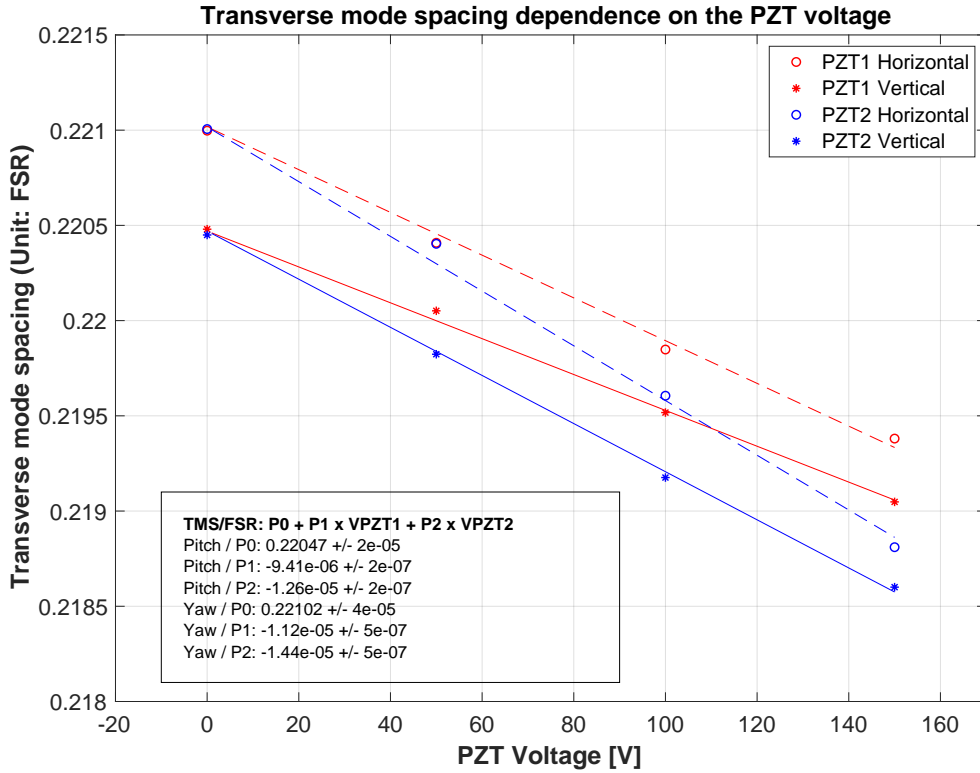


Figure 199: OMC(002R2): Dependence of the vertical and horizontal TMSs on the PZT voltages. The TMSs are expressed in the unit of FSR.

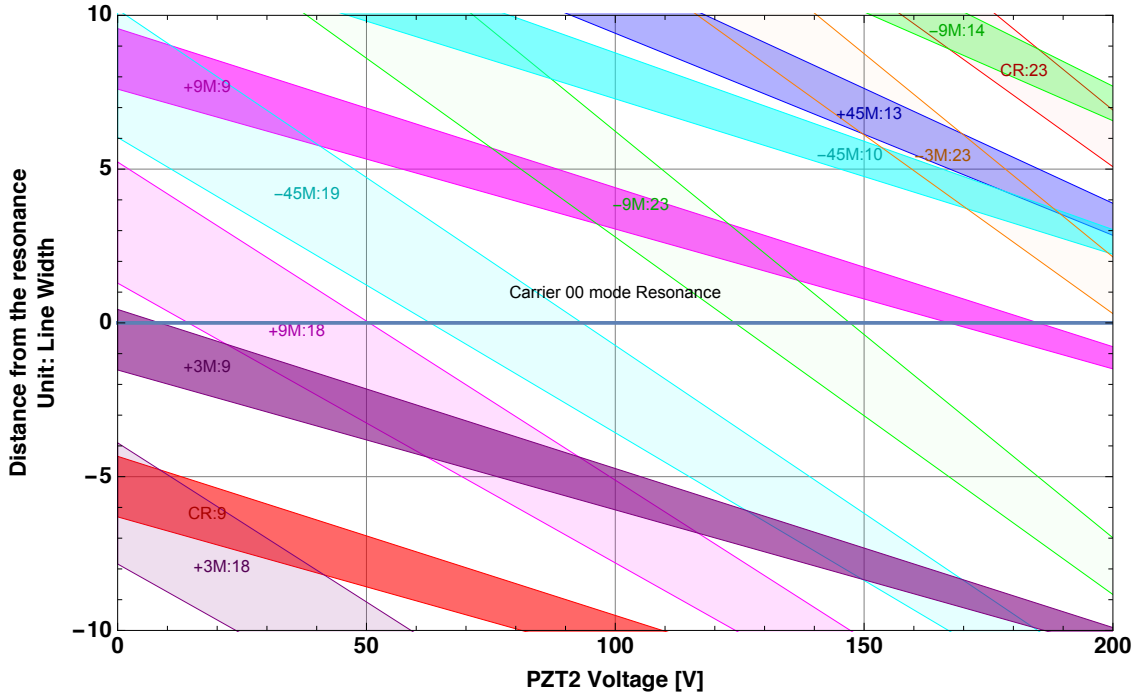


Figure 200: OMC(002R2): Modelled coincidental resonances of the higher-order modes as the PZT voltages scanned.

3.13.5 Power budget for OMC(002R2)

[Description]

The final optical test was performed at LLO optics lab. The equivalent test setup as the one at Caltech has been built there. Table 29 shows the each measurement set and the analysis result. The summary is shown in Figure 201. T. Cullen joined the characterization work at LLO.

Date	OMC Unit	#	2022/9/16	2022/9/16	2022/9/16	2022/9/19	2022/9/19	2022/9/19	2022/9/19	2022/9/19	2022/9/19						
Meas No	#	#	2	2	2	2	2	2	2	2	2						
			1	2	3	4	5	6	7	8	8						
			With Ref PD Take 1	With Ref PD Take 2	With Ref PD Take 3	With Ref PD Take 4	With Ref PD Take 5	With Ref PD Take 6	With Ref PD Take 7	With Ref PD Take 8	With Ref PD Take 8						
Notes																	
Measurements	Unit		Ref Voltage	Value	Error	Ref Voltage	Value	Error	Ref Voltage	Value	Error	Ref Voltage	Value	Error	Ref Voltage	Value	Error
DCPD T Power	mW		7.21	9.80	0.02	7.51	10.07	0.02	7.39	9.71	0.02	7.14	8.91	0.02	7.1	8.99	0.02
DCPD R Voltage	V		7.23	8.39	0.01	7.51	8.40	0.01	7.39	8.21	0.01	7.13	7.57	0.01	7.1	7.55	0.01
DCPD R Power	mW		7.20	9.31	0.02	7.49	9.69	0.02	7.37	9.42	0.02	7.16	8.61	0.02	7.12	8.69	0.02
DCPD R Voltage	V		7.20	7.87	0.01	7.49	8.07	0.01	7.40	7.91	0.01	7.14	7.23	0.01	7.11	7.27	0.01
CMI Transmission Power	mW		7.27	0.0934	0.01	7.61	0.0973	0.01	7.40	0.0938	0.01	7.2	0.0863	0.01	7.15	0.0852	0.01
CMZ Transmission Power	mW		7.26	0.0935	0.01	7.52	0.0963	0.01	7.40	0.0934	0.01	7.18	0.0869	0.01	7.13	0.0872	0.01
Reflection PD Voltage Locked	V		7.27	5.20E-03	2.00E-05	7.56	5.30E-03	2.00E-05	7.40	5.17E-03	2.00E-05	7.2	5.40E-03	2.00E-05	7.16	5.20E-03	2.00E-05
Reflection PD Voltage Unlocked	V		7.26	0.1600	1.00E-03	7.58	0.1650	1.00E-03	7.41	0.1610	1.00E-03	7.14	0.1480	1.00E-03	7.17	0.1490	1.00E-03
Incident Power to the OMC	mW		7.28	20.95	0.1	7.58	21.30	0.1	7.42	20.92	0.1	7.16	19.46	0.1	7.23	19.80	0.1
Ref Voltage Offset	V			0.004			0.004			0.009			0.009			0.009	
Voltage Meter Offset	V			-5.15E-04			-5.15E-04			-5.10E-04			-5.10E-04			-5.60E-04	
Finesse			400			400			400			400			400		
Input R5 Transmission	ppm		7400			7400			7400			7400			7400		
DCPD amp gain	V/A		999.7			999.7			999.7			999.7			999.7		
Derived Values	Unit																
Roundtrip Reflectivity			0.9922	0		0.9922	0		0.9922	0		0.9922	0		0.9922	0	
Pow OMC Incident	mW		20.95	0.10		21.30	0.10		20.92	0.10		19.46	0.10		19.80	0.10	
Pow Cavity Incident	mW		20.79	0.10		21.14	0.10		20.77	0.10		19.32	0.10		19.65	0.10	
Pow Leak at the cavity	mW		0.152	0.006		0.162	0.006		0.173	0.006		0.148	0.006		0.157	0.006	
Pow Coupled to the cavity	mW		20.06	0.10		20.40	0.10		20.04	0.10		18.57	0.10		18.82	0.10	
Mode Matching			0.9648	0.00027		0.9649	0.00025		0.9632	0.00027		0.9613	0.00034		0.9625	0.00032	
Cavity Reflectivity			0.00036	0.00010		0.00011	0.00005		0.0004	0.0001		0.00078	0.00015		0.00067	0.00014	
Cavity Transmission			0.962	0.0049		0.979	0.0049		0.960	0.0049		0.945	0.0052		0.977	0.0053	
OMC Unit Throughput			0.955	0.0049		0.972	0.0048		0.953	0.0049		0.938	0.0051		0.942	0.0051	
OMC Optical Loss			0.045	0.0049		0.028	0.0048		0.047	0.0049		0.062	0.0052		0.058	0.0051	
Loss per mirror	ppm		15.8	10.0		22.7	9.8		61.3	10.6		91.0	10.7		82.6	10.6	
FML/FM2 Transmission	ppm		7675	19.6		7740	19.2		7664	19.6		7605	21.1		7622	20.7	
CM1 Transmission	ppm		37.47	4.01		37.86	3.89		37.77	4.03		37.49	4.34		36.81	4.32	
CM2 Transmission	ppm		37.56	4.02		37.92	3.94		37.61	4.03		37.86	4.36		37.78	4.33	
DCPD T OE			0.974	0.0023		0.972	0.0023		0.986	0.0024		0.992	0.0026		0.979	0.0025	
DCPD R OE			0.985	0.0025		0.971	0.0023		0.975	0.0024		0.982	0.0027		0.979	0.0026	

Table 29: OMC(002R2): Summary of the power budget test

3.13.6 PZT response DC/AC

[External Link]

http://nodus.ligo.caltech.edu:8080/OMC_Lab/148

[Description]

Figures 202 and 203 show DC and AC responses of the PZTs. Estimated DC responses were

- **PZT1:** 13.2418 ± 0.003nm/V
- **PZT2:** 12.92 ± 0.01nm/V

Note that OMC(002R2) has one of the PZT not functioning any more. The link: <https://alog.ligo-la.caltech.edu/aLOG/index.php?callRep=8366>

3.13.7 DCPD/QPD shim height

[External Link] http://nodus.ligo.caltech.edu:8080/OMC_Lab/323

[Description]

Determined shim heights:

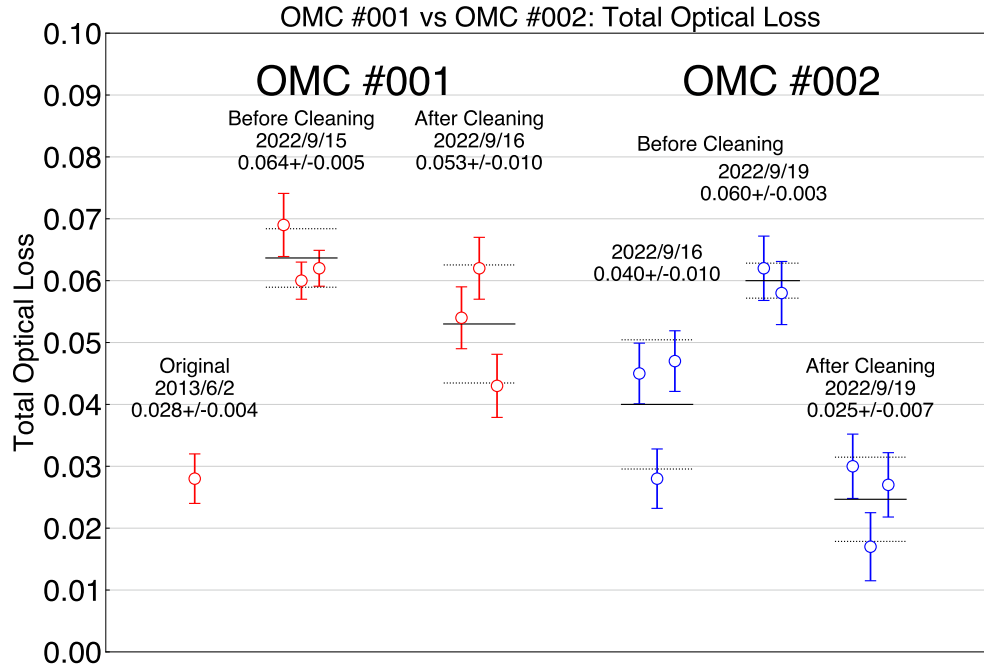


Figure 201: OMC(002R2): Summary of the power budget test (right half)

- DCPD1(TRANS):
D1201467-02 (SN 006) + D1201467-03 (SN 005)
(1.75mm + 2.0 mm = 3.75 mm)
- DCPD2(REFL):
D1201467-02 (SN 002) + D1201467-03 (SN 006)
(1.75mm + 2.0 mm = 3.75 mm)
- QPD1(SHORT):
D1201467-03 (SN 007) + D1201467-03 (SN 008)
(2.0 mm + 2.0 mm = 4 mm)
- QPD2(LONG):
D1201467-01 (SN 001) + D1201467-01 (SN 002)
(1.5 mm + 1.5 mm = 3 mm)

3.13.8 QPD alignment

[External Link]

http://nodus.ligo.caltech.edu:8080/OMC_Lab/324

[Description]

See Table 30 for the result.

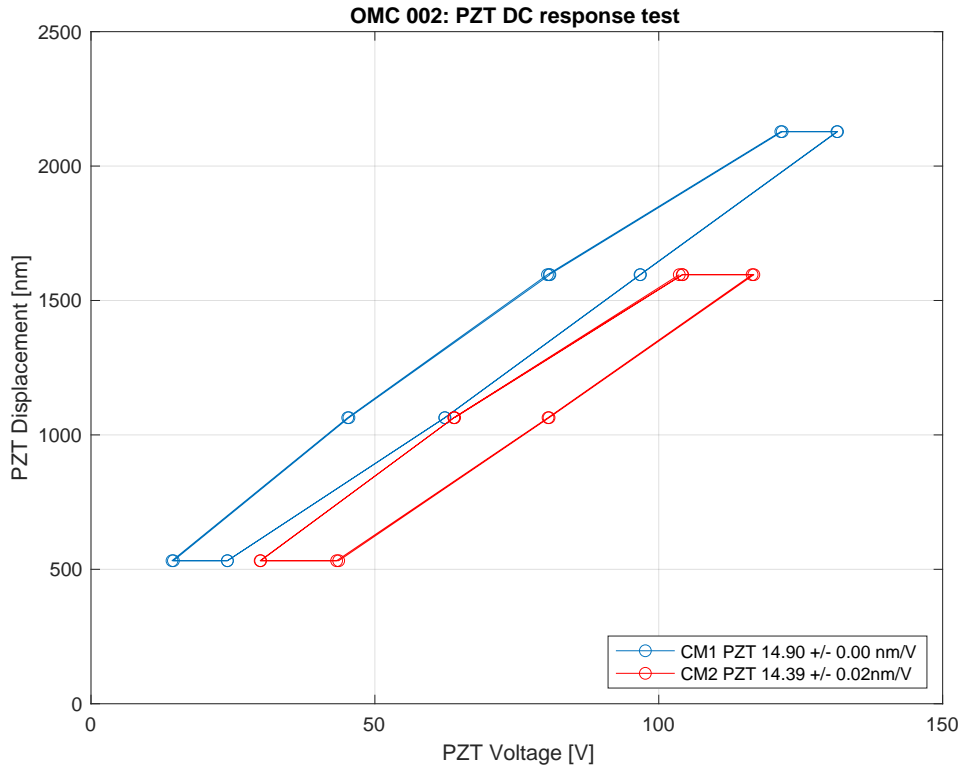


Figure 202: OMC(002R2): PZT sweep voltages and the OMC resonances.

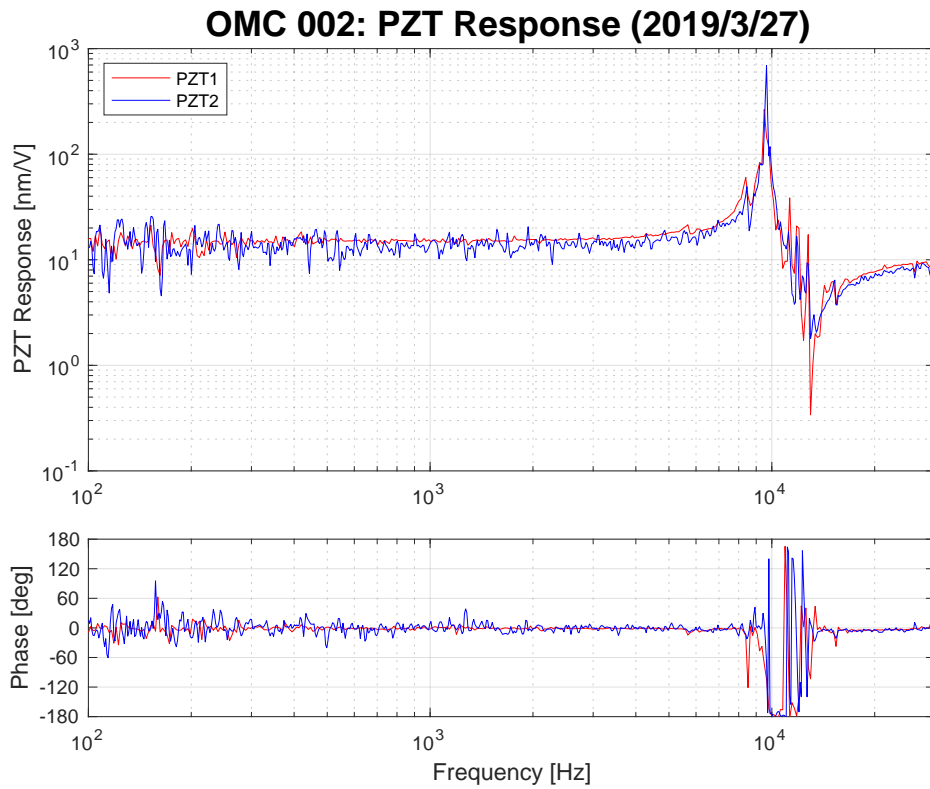


Figure 203: OMC(002R2): PZT AC responses. The DC gain was adjusted to match the DC scan result.

QPD#	QPD1		QPD2	
Diode#	#44		#46	
Incident power	252.3	[μ W]	266.0	[μ W]
Sum Out	174.2	[mV]	1176.0	[mV]
Vertical Out	+4.7	[mV]	+19.0	[mV]
Horizontal Out	-16.1	[mV]	-8.0	[mV]
SEG1	-52.4	[mV]	-53	[mV]
SEG2	-37.6	[mV]	-47	[mV]
SEG3	-41.8	[mV]	-34	[mV]
SEG4	-43.7	[mV]	-36	[mV]
Spot position X ^a	+39	[μ m]	+15	[μ m]
Spot position Y ^b	-8.1	[μ m]	-56	[μ m]
Responsivity	0.69	[A/W]	0.66	[A/W]
Q.E.	0.80		0.77	

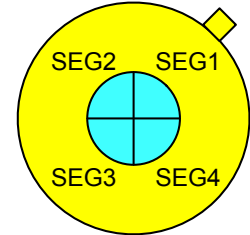


Figure 204:
OMC(002R2):
Arrangement
of the QPD
segments (beam
view)

Table 30: OMC(002R2): Measurement results for the QPDs and the derived spot positions

^apositive = more power on SEG1 and SEG4

^bpositive = more power on SEG3 and SEG4

3.13.9 Alignment / beam spot photos

[Description]

Collection of the spot photos for the DCPDs, DCPD reflections, QPDs (QPD2 photo missing), FMs, and CMs.

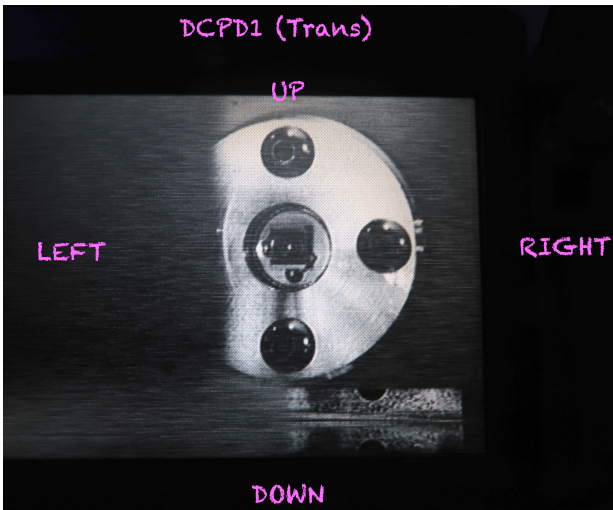


Figure 205: OMC(002R2): DCPD1 final spot position

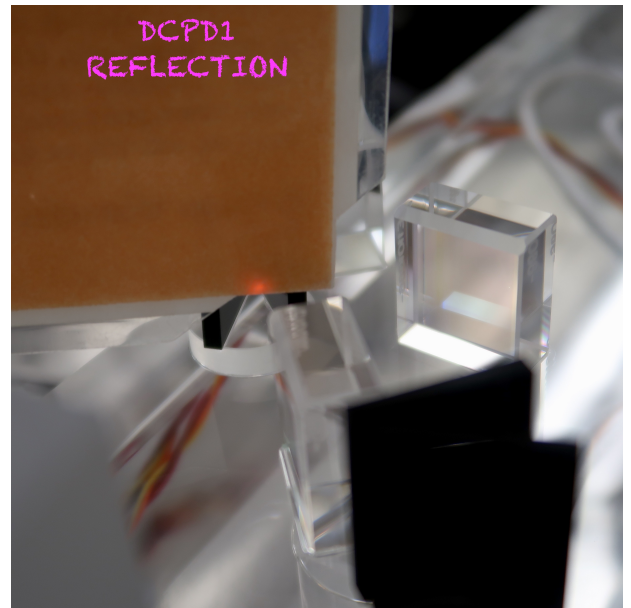


Figure 206: OMC(002R2): DCPD1 reflection on the beam dump

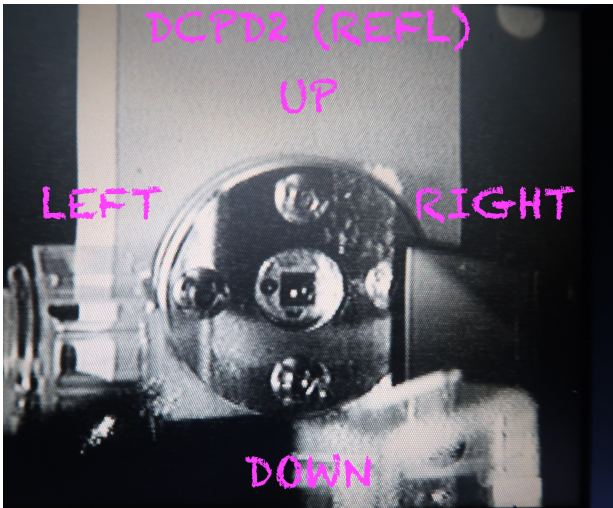


Figure 207: OMC(002R2): DCPD2 final spot position



Figure 208: OMC(002R2): DCPD2 reflection on the beam dump

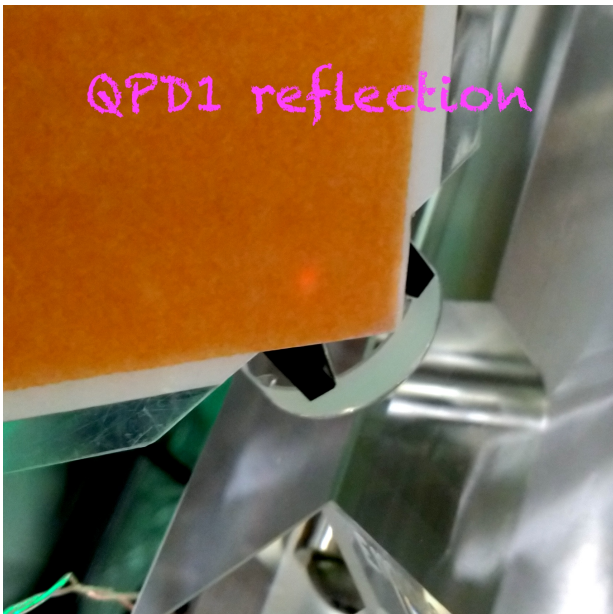


Figure 209: OMC(002R2): QPD1 reflection on the beam dump



Figure 210: OMC(002R2): QPD2 reflection on the beam dump

3.13.10 Balance Mass Distribution

Figure 211 (lower) shows the mass distribution when this OMC was installed to LLO in 2022 Oct. This OMC has the PEEK cable bracket that was expected to be ~ 40 g lighter than the metal version. The body mode damper was introduced to this OMC and it increased the mass by 10g, which compensated the weight difference of the cable bracket.

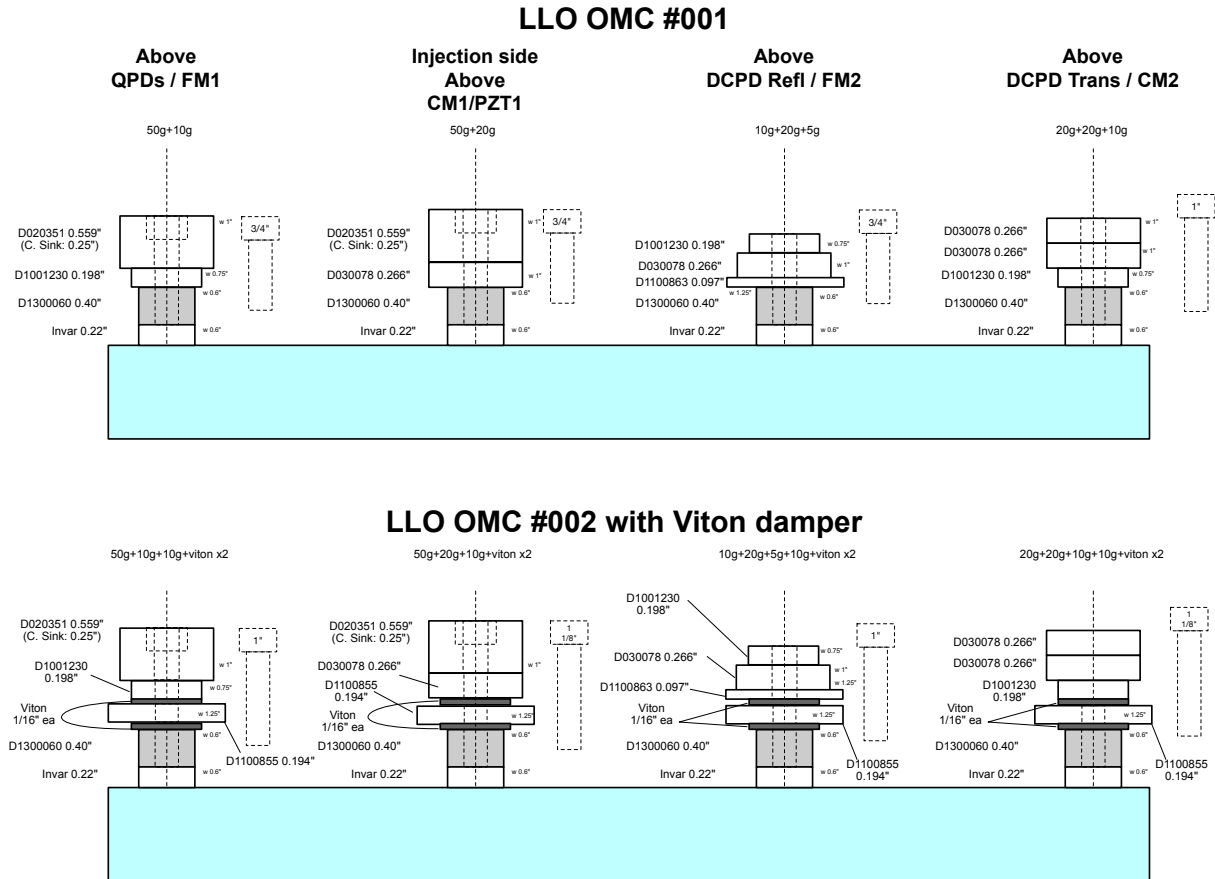


Figure 211: OMC(002): Balance mass distribution (lower)

3.14 Test results for OMC(004)

3.14.1 Summary of the OMC(004) tests

[Description]

The table shows the summary of the OMC(004) optical test results. The detailed results are shown in the following sections.

FSR (detuned locking)			
FSR	264.800254	± 0.000003	[MHz]
Cavity roundtrip length	1.1312146	± 0.000003	[m]
FSR & Finesse (RFAM injection)			
FSR	264.7939	± 0.0004	[MHz]
Cavity roundtrip length	1.132173	± 0.000002	[m]
Finesse	381.3	± 0.4	
TMS			
TMS (Vertical)	58.055520	± 0.0002	[MHz]
	0.2192556	± 0.0000007	[FSR]
TMS (Horizontal)	58.3661	± 0.0003	[MHz]
	0.220440	± 0.000001	[FSR]
Total Optical Loss (2013/6/2)			
OMC unit throughput	0.967	± 0.001	
OMC optical loss	0.033	± 0.001	
PZT response			
PZT1:	13.2418	± 0.0003	[nm/V]
PZT2:	12.92	± 0.01	[nm/V]

Table 31: OMC(004): Summary of the cavity geometry tests

3.14.2 Cavity absolute length measurement with detuned locking

[Description]

See Section 3.2.1 for the details of the measurement method.

The transfer function and the measurement results are shown in Figure 212.

3.14.3 Cavity length and finesse measurement with RFAM injection

[Description]

See Section 3.2.2 for the details of the measurement method.

The transfer function and the measurement results are shown in Figure 213.

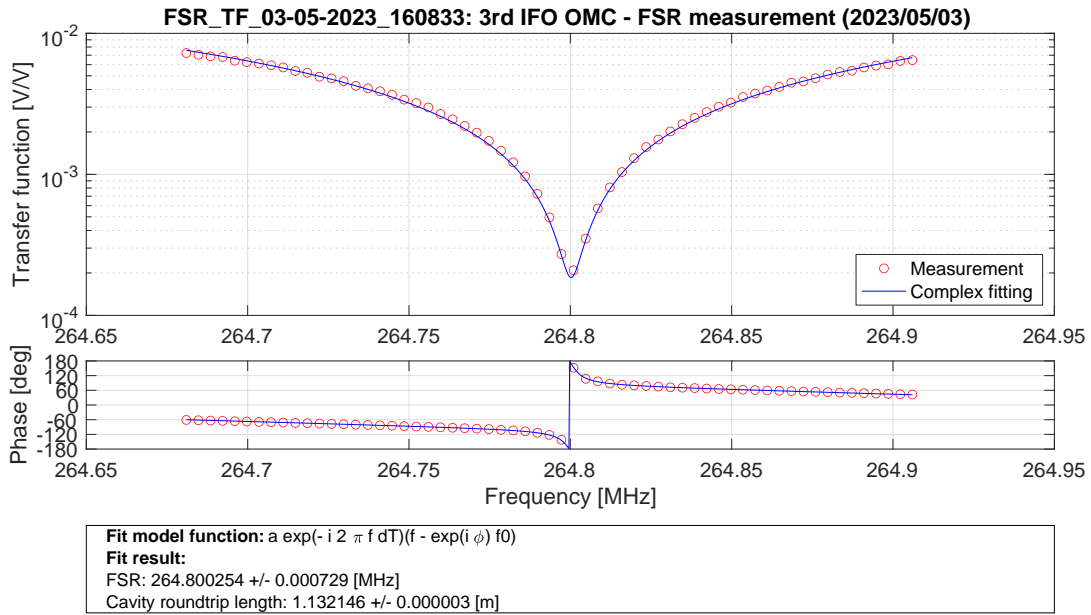


Figure 212: OMC(004): Cavity absolute length (FSR) measurement with detuned locking

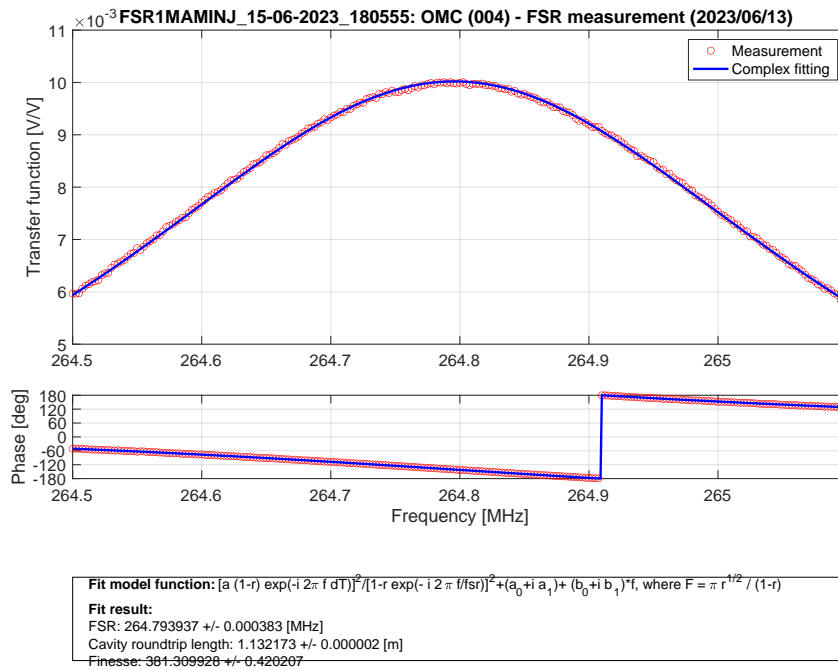


Figure 213: OMC(004): Cavity length (FSR) and finesse measurement with RFAM injection

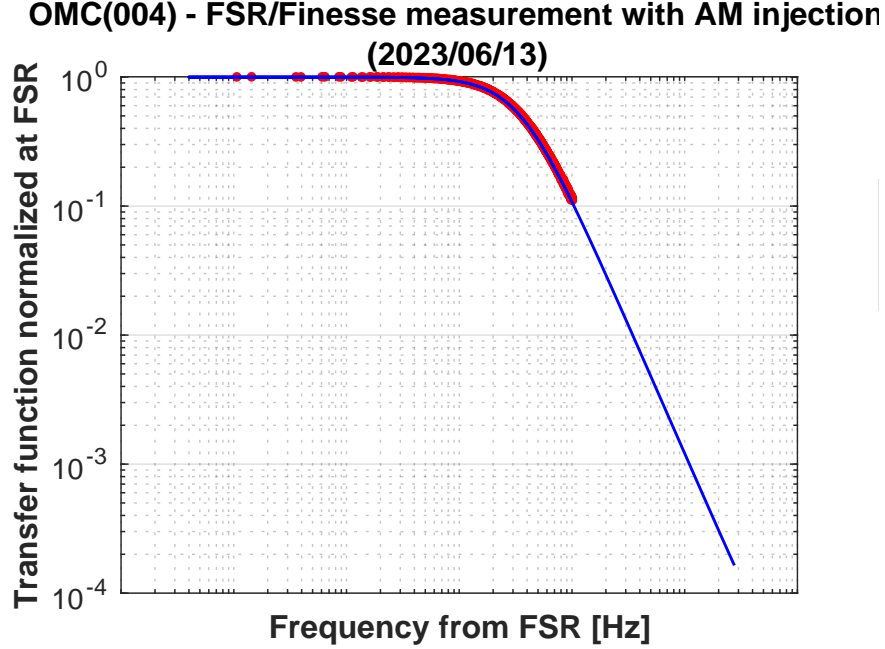


Figure 214: OMC(004): Cavity finesse measurement with RFAM injection

3.14.4 Transverse-mode spacing measurement

[Description]

See Figures 215 and 216 for the transfer functions and the estimated TMSs.

Figure 217 shows that the 9th-order and 18th-order modes potentially cause the problem of the coincident resonance.

The dependence of TMSs on the PZT voltages is shown in Figure. 218). The dependence model is expressed as

$$\frac{\nu_{\text{TMS}}}{\nu_{\text{FSR}}} = P_0 + P_1 V_{\text{PZT1}} + P_2 V_{\text{PZT2}} , \quad (26)$$

the parameters for each TMS were estimated to be

Vertical TMS :

$$\begin{aligned} P_0 &= 0.2193 \pm 1 \times 10^{-4} \\ P_1 &= -3 \times 10^{-6} \pm 1 \times 10^{-6} \\ P_2 &= -1.4 \times 10^{-5} \pm 1 \times 10^{-6} \end{aligned}$$

Horizontal TMS :

$$\begin{aligned} P_0 &= 0.2206 \pm 1 \times 10^{-4} \\ P_1 &= -4 \times 10^{-6} \pm 1 \times 10^{-6} \\ P_2 &= -1.4 \times 10^{-5} \pm 1 \times 10^{-6} \end{aligned}$$

Note that It is unusual not to have the TMS dependence with the PZT voltage. We also noticed that the cavity axis changes as a voltage is applied to PZT1. We suspected that the

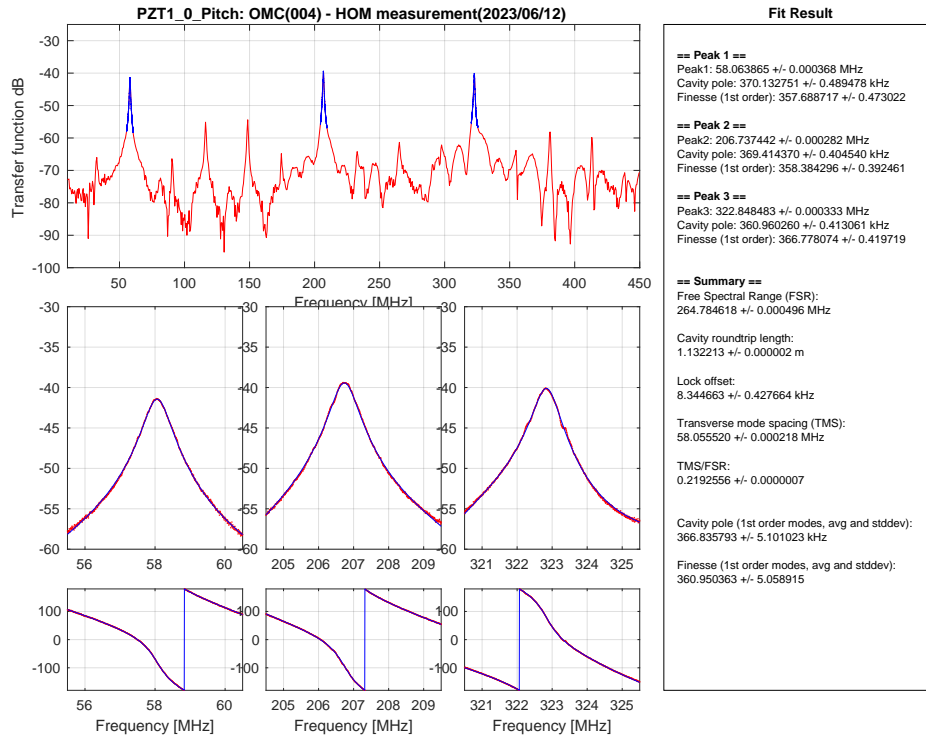


Figure 215: OMC(004): Vertical TMS measurement with no PZT voltages applied.

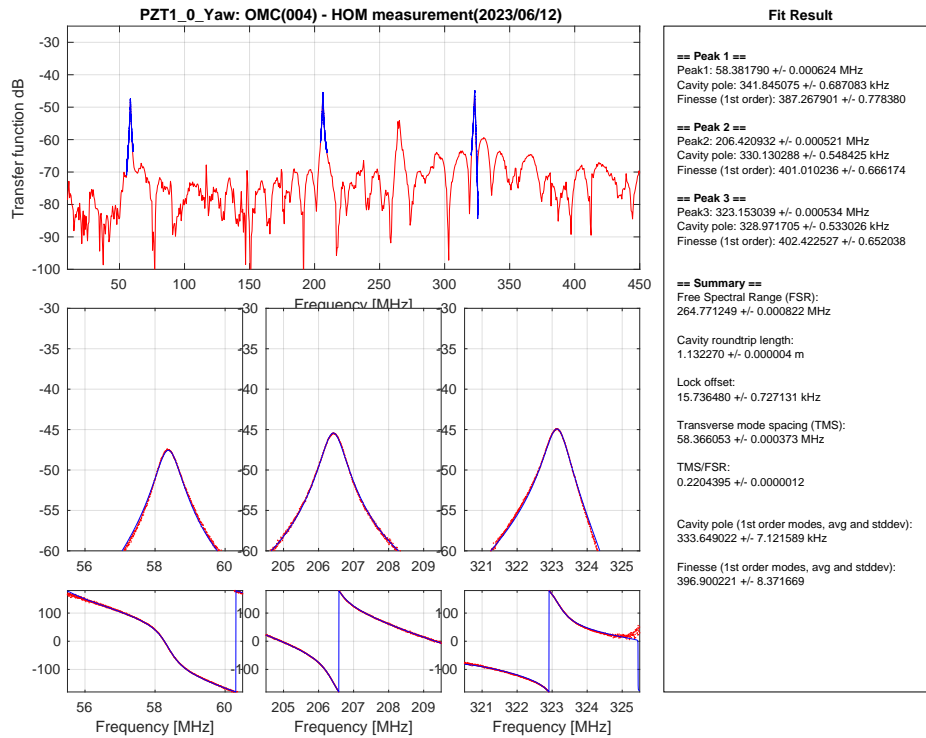


Figure 216: OMC(004): Horizontal TMS measurement with no PZT voltages applied.

PZT1 has a large length-to-angle coupling which causes the misalignment of the cavity as the voltage is applied. And this might be the cause of the (accidental) compensation on the RoC change for CM1. (Although this compensation story is just a speculation.)

We'll describe more peculiar behaviors of PZT1 in Section 3.14.6.

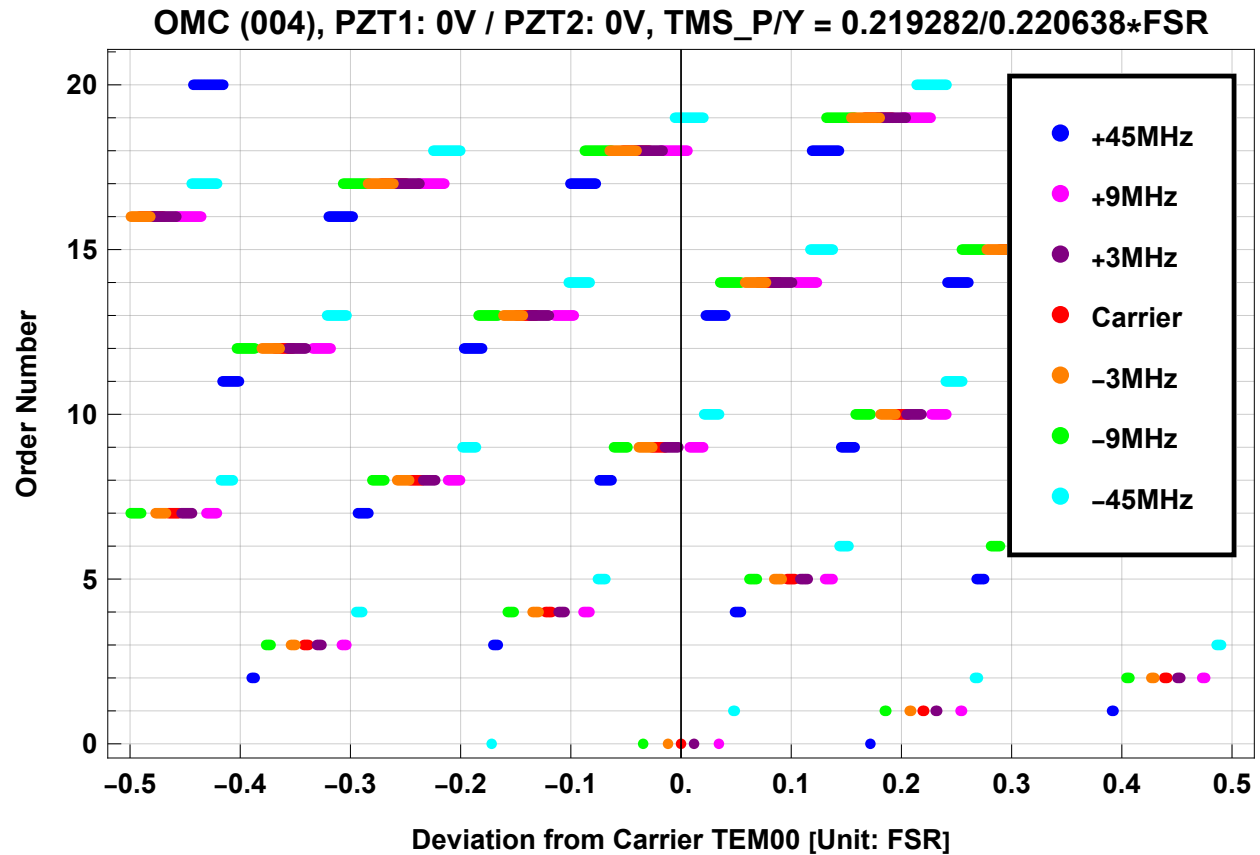


Figure 217: OMC(004): Higher-order modes distribution with no PZT voltages applied.

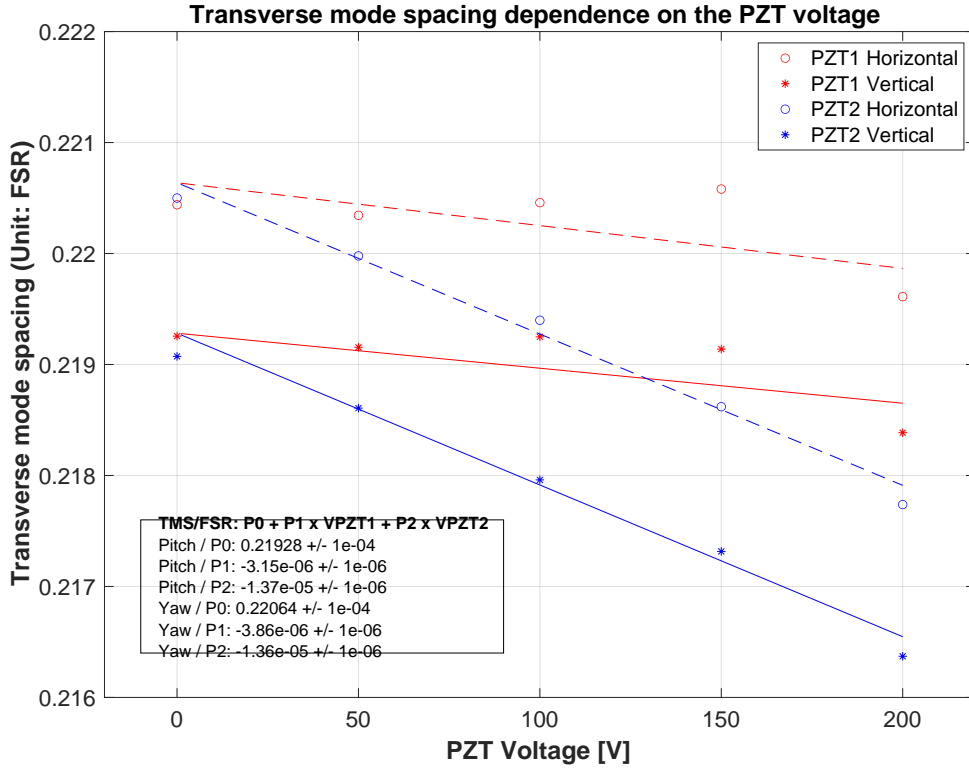


Figure 218: OMC(004): Dependence of the vertical and horizontal TMSs on the PZT voltages. The TMSs are expressed in the unit of FSR.

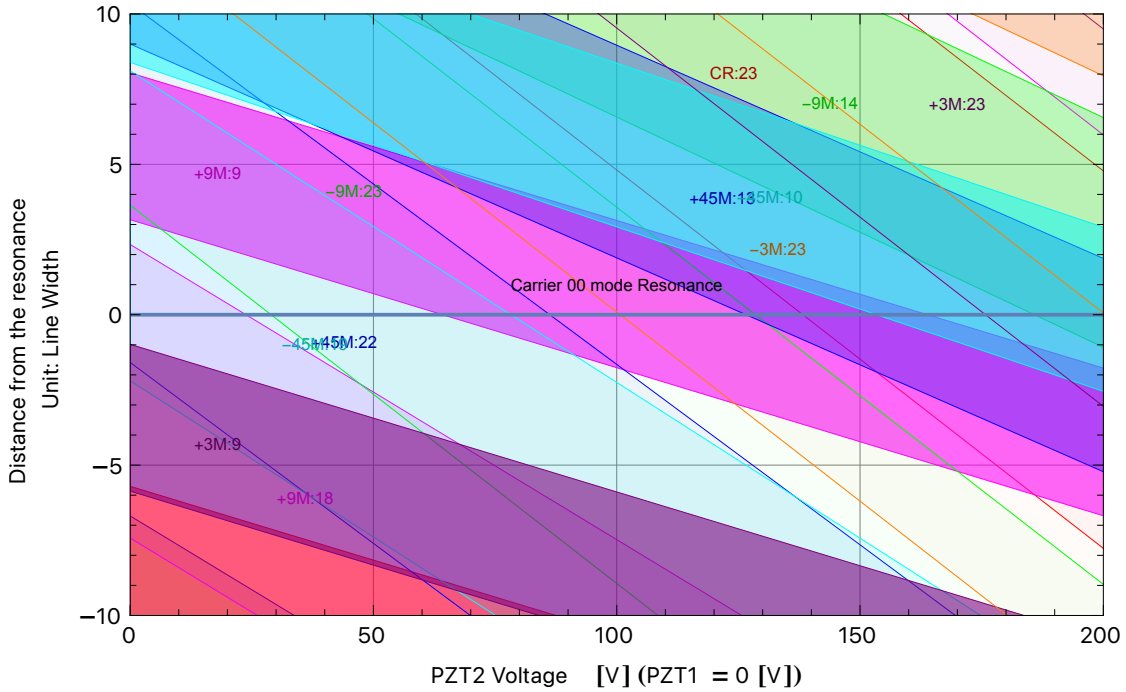


Figure 219: OMC(004): Modelled coincidental resonances of the higher-order modes as the PZT2 voltage scanned.

3.14.5 Power budget for OMC(004)

[External Link]

http://nodus.ligo.caltech.edu:8080/OMC_Lab/530

[Description]

Summary of the measurement on 2023/4/27 is shown in Table 32.

From the three measurements, the loss of 0.033 ± 0.001 (i.e., total unit throughput of 0.967 ± 0.001) was inferred.

Date		2023/4/27			2023/4/27			2023/4/27		
OMC Unit	#	4			4			4		
Meas No	#	1			2			3		
		After bonding/cleaning Take1			After bonding/cleaning Take2			After bonding/cleaning Take3		
Notes										
Measurements	Unit	Ref Voltage	Value	Error	Ref Voltage	Value	Error	Ref Voltage	Value	Error
DCPD T Power	mW	3.84	10.00	0.02	3.89	10.26	0.02	3.9	10.26	0.02
DCPD T Voltage	V	3.84	0	0	3.89	0	0	3.9	0	0
DCPD R Power	mW	3.85	10.53	0.03	3.88	10.67	0.02	3.92	10.70	0.01
DCPD R Voltage	V	3.85	0	0	3.88	0	0	3.92	0	0
		3.86	21.5	0.03	3.88	21.73	0.03	3.91	21.72	0.01
CM1 Transmission Power	mW	3.87	0.1050	3.00E-04	3.87	0.1031	1.00E-04	3.9	0.1004	4.00E-04
CM2 Transmission Power	mW	3.87	0.1000	3.00E-04	3.86	0.1005	2.00E-04	3.91	0.1001	2.00E-04
Reflection PD Voltage Locked	V	3.85	6.12E-02	5.00E-04	3.87	6.01E-02	1.00E-04	3.89	6.12E-02	4.00E-04
Reflection PD Voltage Unlocked	V	3.87	3.2310	2.00E-03	3.88	3.2300	2.00E-03	3.9	3.2410	5.00E-02
Incident Power to the OMC	mW	3.87	22.02	0.04	3.88	22.1	0.04	3.91	22.06	0.02
Ref Voltage Offset	V		4.69E-03	1.00E-06		4.67E-03	1.00E-06		4.67E-03	1.00E-06
Voltage Meter Offset	V		-5.90E-03	1.00E-06		-5.90E-03	1.00E-06		-5.89E-03	1.00E-06
Finesse			400			400			400	
Input BS Transmission	ppm		7400			7400			7400	
DCPD amp gain	V/A		999.7			999.7			999.7	
Derived Values	Unit									
Roundtrip Reflectivity			0.9922	0		0.9922	0		0.9922	0
Pow OMC Incident	mW		22.02	0.04		22.10	0.04		22.06	0.02
Pow Cavity Incident	mW		21.86	0.04		21.94	0.04		21.90	0.02
Pow Junk at the cavity	mW		0.449	0.004		0.444	0.001		0.451	0.008
Pow Coupled to the cavity	mW		21.41	0.04		21.49	0.04		21.45	0.02
Mode Matching			0.9795	0.00016		0.9797	0.00005		0.9794	0.00035
Cavity Reflectivity			0.00031	0.00004		0.00019	0.00003		0.0001	0.0000
Cavity Transmission			0.965	0.0025		0.973	0.0022		0.977	0.0014
OMC Unit Throughput			0.958	0.0025		0.965	0.0022		0.970	0.0014
OMC Optical Loss			0.042	0.0025		0.035	0.0022		0.030	0.0014
Loss per mirror	ppm		49.8	5.0		35.2	4.4		26.2	2.8
FM1/FM2 Transmission	ppm		7686	9.9		7715	8.8		7734	5.6
CM1 Transmission	ppm		39.36	0.12		38.45	0.06		37.43	0.15
CM2 Transmission	ppm		37.49	0.12		37.58	0.09		37.23	0.08
DCPD T QE			0.000	0.0000		0.000	0.0000		0.000	0.0000
DCPD R QE			0.000	0.0000		0.000	0.0000		0.000	0.0000

Table 32: OMC(004): Summary of the power budget test

3.14.6 PZT response DC/AC

[External Link]

http://nodus.ligo.caltech.edu:8080/OMC_Lab/557

[Description]

Figures 220 and 221 show DC and AC responses of the PZTs. Estimated DC responses were

- **PZT1:** $21.9 \pm 0.9\text{nm/V}$
- **PZT2:** $12.0 \pm 0.2\text{nm/V}$

PZT1 showed unusually large response to the applied voltage. As mentioned in Section 3.14.4, this PZT has large length-to-angle. It is better not to use this PZT for active (e.g. servo control) purpose.

It was puzzling that the AC response of PZTs measured at low voltage levels showed little difference. A further investigation revealed that PZT2 has a nonlinearity in that it moves as much as PZT1 at low voltages, but as it approaches 100V, the movement becomes smaller. Therefore, in actual use, the voltage applied to PZT2 should be limited to 100V or less (as before).

3.14.7 DCPD/QPD shim height adjustment

[Description]

The shims deviated from the nominal height about a mm thicker and thinner. i.e., DCPD1, DCPD2, and QPD1 were raised, while QPD2 was lowered. This indicates that the beam enters to the cavity high and gradually went down.

Determined shim heights:

- DCPD1: D1201467-04 (2.25mm)
- DCPD2: D1201467-03 (2.00mm)
- QPD1: D1201467-05 (2.50mm)
- QPD2: D1201467-08 (0.75mm)

3.14.8 QPD alignment

[External Link]

http://nodus.ligo.caltech.edu:8080/OMC_Lab/548

[Description]

See Table 33.

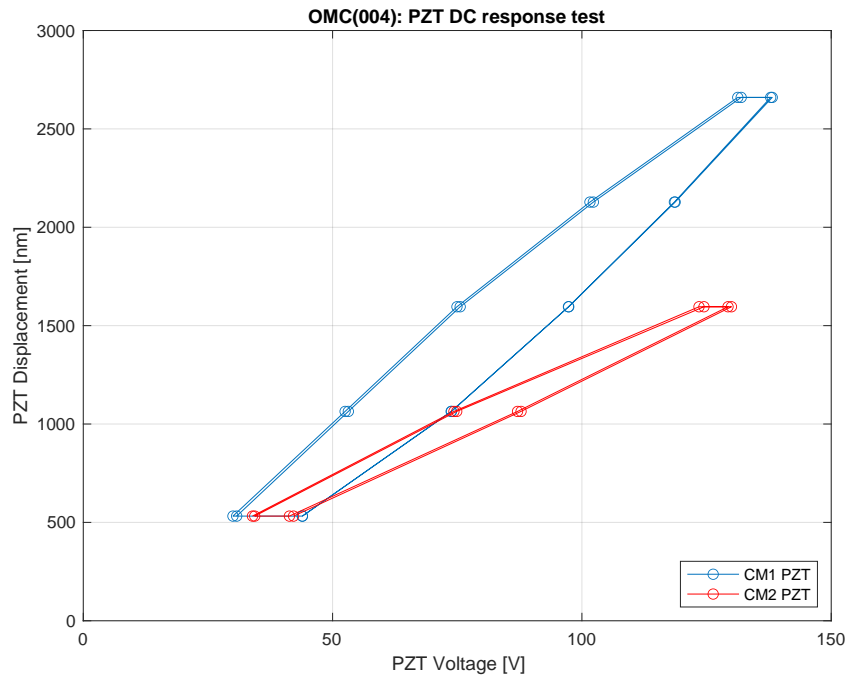


Figure 220: OMC(004): PZT sweep voltages and the OMC resonances.

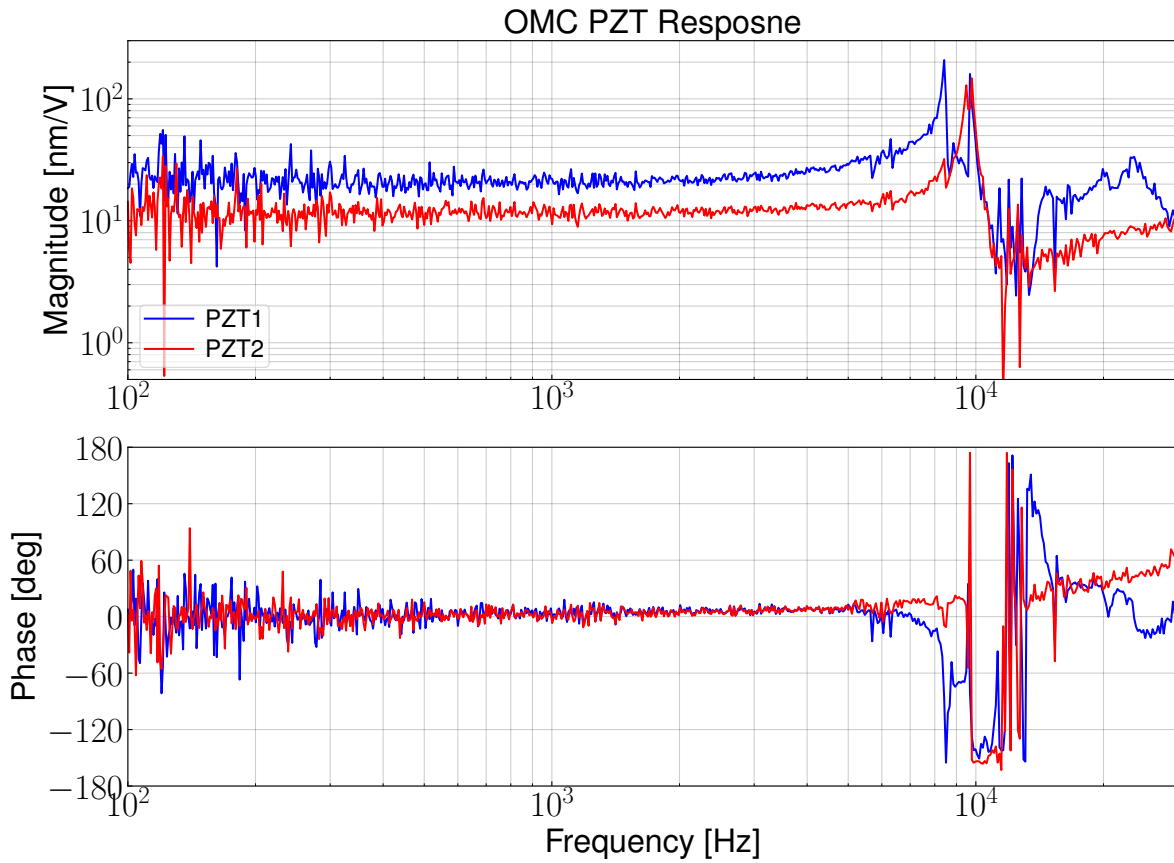


Figure 221: OMC(004): PZT AC responses. The DC gain was adjusted to match the DC scan result.

QPD#	QPD1		QPD2	
Housing#	#008		#009	
Diode#	#62		#70	
Shim	2.50mm (-05)		0.75mm (-08) see D1201467	
Incident power	76.5	[μ W]	71.5	[μ W]
Sum Out	49.0	[mV]	50.2	[mV]
Vertical Out	-16.0	[mV]	8.2	[mV]
Horizontal Out	-2.4	[mV]	-3.6	[mV]
SEG1	-8.2	[mV]	-16.2	[mV]
SEG2	-8.0	[mV]	-13.0	[mV]
SEG3	-15.1	[mV]	-9.5	[mV]
SEG4	-17.4	[mV]	-11.5	[mV]
Spot position X^a	+8	[μ m]	+33	[μ m]
Spot position Y^b	+81	[μ m]	-52	[μ m]
Responsivity	0.64	[A/W]	0.70	[A/W]
Q.E.	0.75		0.82	

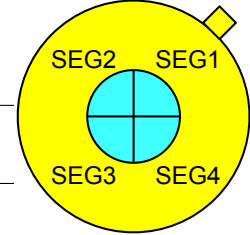


Table 33: OMC(004): Measurement results for the QPDs and the derived spot positions

Figure 222: OMC(004): Arrangement of the QPD segments (beam view)

^apositive = more power on SEG1 and SEG4

^bpositive = more power on SEG3 and SEG4

3.14.9 Alignment / beam spot photos

[Description]

Collection of the spot photos for the DCPDs, DCPD reflections, QPDs (QPD2 photo missing), FMs, and CMs.



Figure 223: OMC(004): DCPD1 final spot position

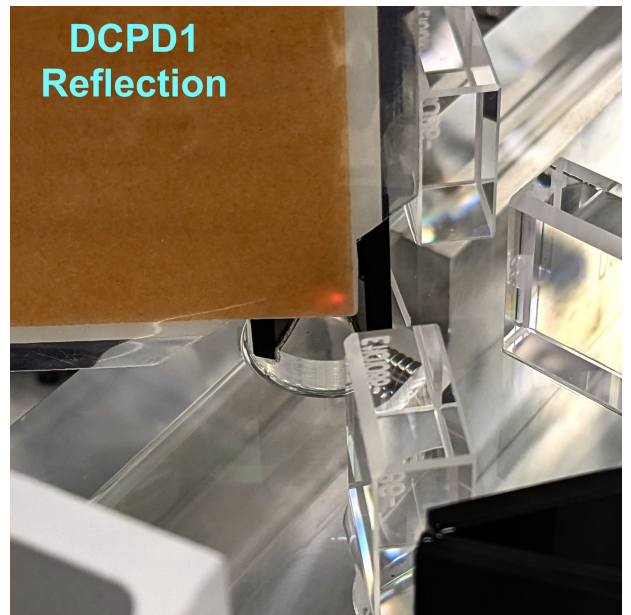


Figure 224: OMC(004): DCPD1 reflection on the beam dump

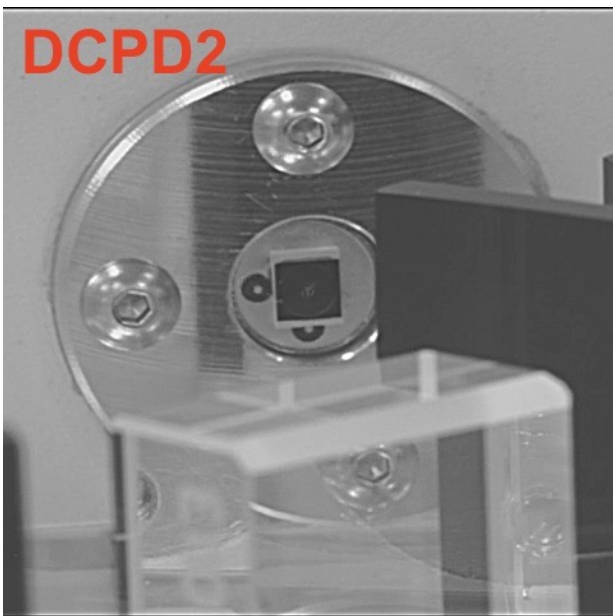


Figure 225: OMC(004): DCPD2 final spot position

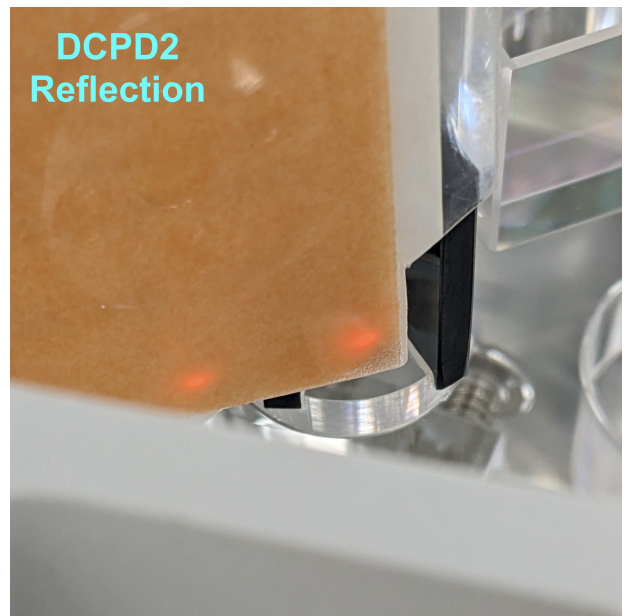


Figure 226: OMC(004): DCPD2 reflection on the beam dump

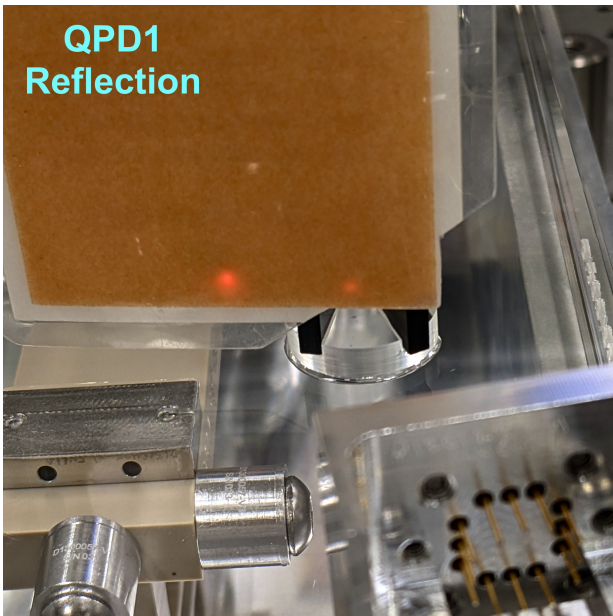


Figure 227: OMC(004): QPD1 reflection spot position

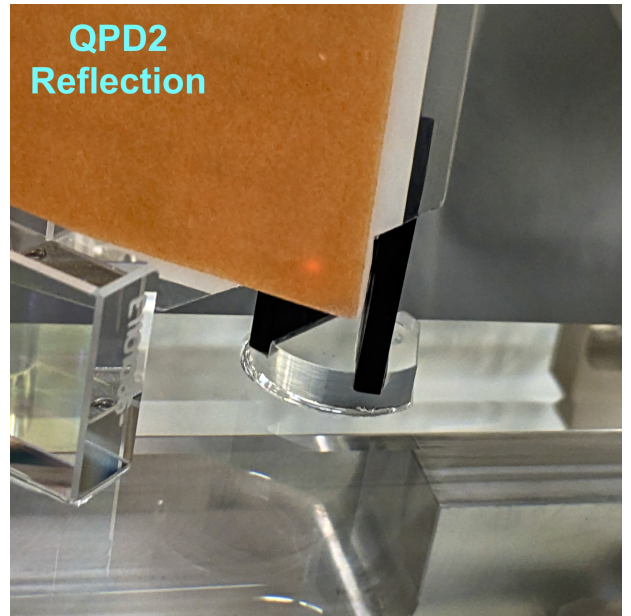


Figure 228: OMC(004): QPD2 reflection spot position

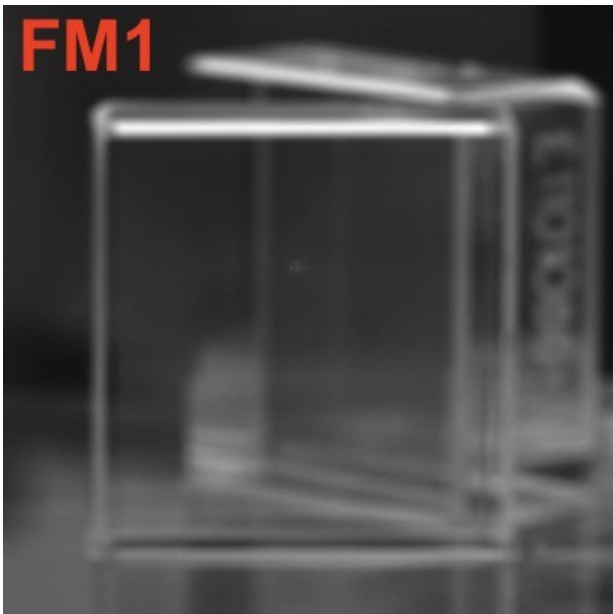


Figure 229: OMC(004): FM1 final spot position

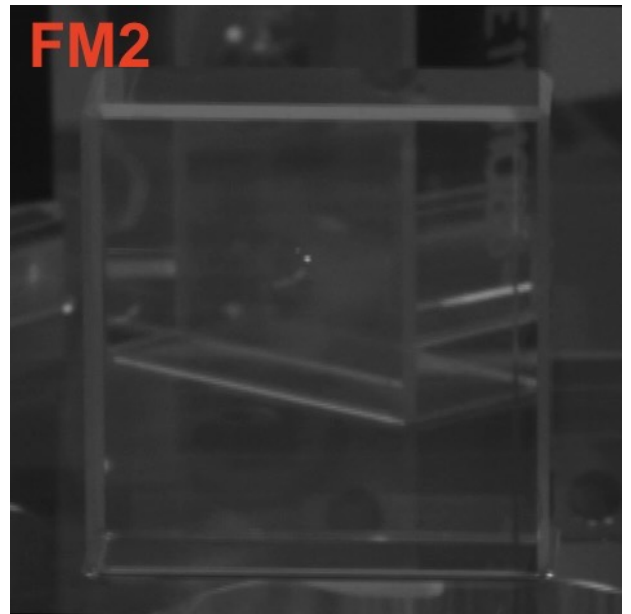


Figure 230: OMC(004): FM2 final spot position

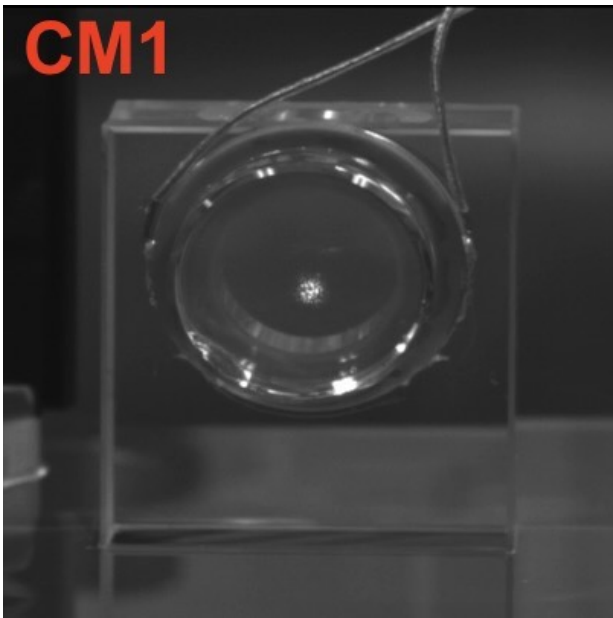


Figure 231: OMC(004): CM1 final spot position

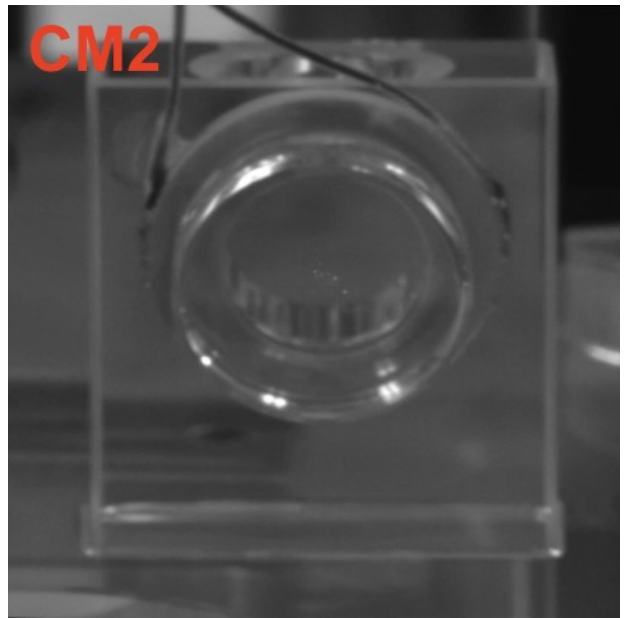


Figure 232: OMC(004): CM2 final spot position

Appendices

A Mirror List

[External Link]

http://nodus.ligo.caltech.edu:8080/OMC_Lab/152

Breadboard	
SN	Location
BB 1	OMC(001)
BB 2	OMC(002)
BB 3	-
BB 4	OMC(003)
BB 5	-
BB 6	OMC(004)

Mounting Prisms	
SN	Location
M 1	PZT ASSY #7 (destroyed)
M 2	
M 6	OMC(002) CM1 (PZT ASSY #6)
M 7	OMC(004) CM1 (PZT ASSY #8)
M 10	OMC(003) CM1 (PZT ASSY #5)
M 11	OMC(002) CM2 (PZT ASSY #4)
M 12	PZT ASSY #12
M 13	OMC(003) CM2 (PZT ASSY #3)
M 14	OMC(004) CM2 (PZT ASSY #11)
M 15	
M 16	OMC(001) CM1 (PZT ASSY #1)
M 17	PZT ASSY #9 (destroyed)
M 20	OMC(001) CM2 (PZT ASSY #2)
M 21	PZT ASSY #10
M 22	

Table 34: List and location for OMC breadboards and Mounting Prisms

Prism Mirror A	
SN	Location
A 1	OMC(004) FM1
A 2	@ Fullerton
A 3	OMC(004) FM2
A 4	
A 5	
A 6	OMC(003) FM2
A 7	OMC(001) FM2
A 8	OMC(001) FM1
A 9	OMC(002) FM1
A 10	
A 11	
A 12	OMC(003) FM1
A 13	OMC(002) FM2
A 14	

Prism Mirror B	
SN	Location
B 1	
B 2	
B 3	OMC(001) BS2 (QPD)
B 4	
B 5	OMC(003) BS2 (QPD)
B 6	OMC(004) BS3 (DCPD)
B 7	OMC(001) BS3 (DCPD)
B 8	OMC(004) BS2 (QPD)
B 9	OMC(002) BS2 (QPD)
B 10	OMC(002) BS3 (DCPD)
B 11	
B 12	OMC(003) BS3 (DCPD)

Table 35: List and location for Mirror A & B

Prism Mirror C	
SN	Location
C 1	OMC(003) CM1 (PZT ASSY #5)
C 2	@Fullerton
C 3	OMC(003) CM2 (PZT ASSY #3)
C 4	OMC(002) CM2 (PZT ASSY #4)
C 5	OMC(001) CM2 (PZT ASSY #2)
C 6	OMC(001) CM1 (PZT ASSY #1)
C 7	(faux OMC CM1)
C 8	(faux OMC CM2) → OMC(002) CM1 (with PZT ASSY #6)
C 9	OMC(002) CM1 (PZT ASSY #6) → BURNT
C 10	PZT Assy #9 → #12, Liyuan tested
C 11	OMC(004) CM1 (PZT ASSY #8), Liyuan tested
C 12	PZT Assy #10, Curvature untested
C 13	OMC(004) CM2 (PZT ASSY #7 → #11), curvature untested

PZT	
SN	Location
PZT 11	OMC(004) CM1 (PZT ASSY #8)
PZT 12	PZT Assy #9 → #12
PZT 13	OMC(004) CM2 (PZT ASSY #7 → #11)
PZT 14	OMC(003) CM1 (PZT ASSY #5)
PZT 15	OMC(003) CM2 (PZT ASSY #3)
PZT 21	OMC(002) CM1 (PZT ASSY #6)
PZT 22	PZT Assy #10
PZT 23	OMC(001) CM2 (PZT ASSY #2)
PZT 24	exclude (See Sec. 2.3.1)
PZT 25	OMC(002) CM2 (PZT ASSY #4)
PZT 26	OMC(001) CM1 (PZT ASSY #1)

Table 36: List and locations for Mirror C & PZTs

Prism Mirror E	
SN	Location
E 1	OMC(002) SM2
E 2	OMC(002) SM3
E 3	OMC(002) BS1
E 4	OMC(001) SM2
E 5	OMC(002) SM1
E 6	OMC(004) BS1
E 7	OMC(003) BS1
E 8	OMC(003) SM1
E 9	OMC(004) SM1
E 10	OMC(001) BS1
E 11	OMC(004) SM2
E 12	OMC(001) SM1
E 13	OMC(003) SM2
E 14	OMC(004) SM3
E 15	not perpendicular, reject
E 16	OMC(001) SM3
E 17	OMC(003) SM3
E 18	

Table 37: List and locations for Mirror E

B DCPD dimensions

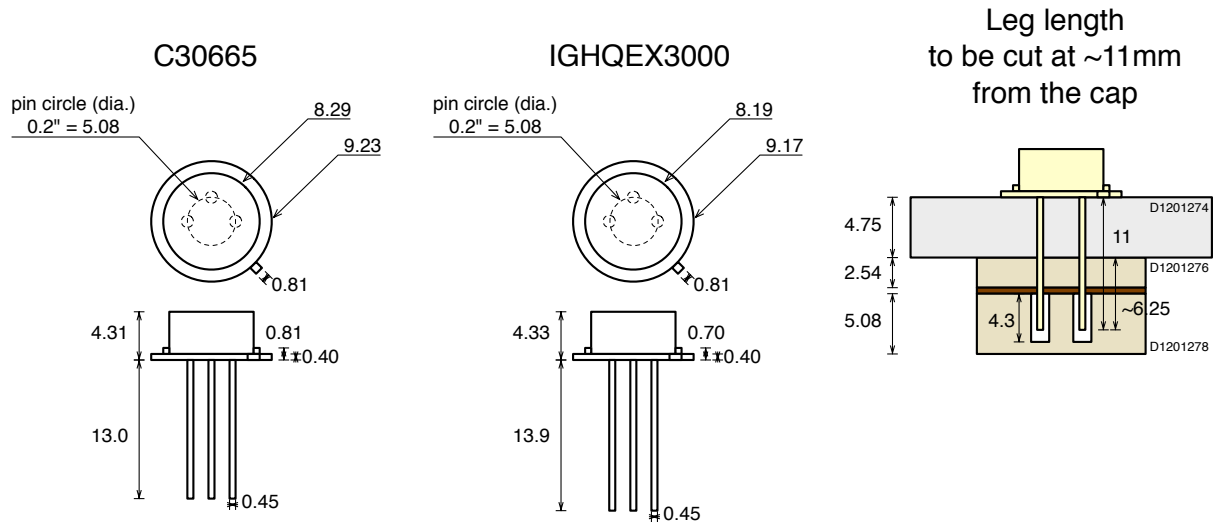


Figure 233: DCPD dimensions

C Cavity axis alignment

[External Link]

http://nodus.ligo.caltech.edu:8080/OMC_Lab/179

LIGO Document T0900647: Ray optics calculations of alignment matrices (by Sam Waldman).

[Description]

Relationship between mirror misalignment in yaw and the shift of the cavity mode was calculated.

[Experimental method]

The calculation technique is described in T0900647. The angles and displacement of the mirrors and beams are defined in Figure 234. Here only the misalignment in the horizontal plane is considered.

[Result]

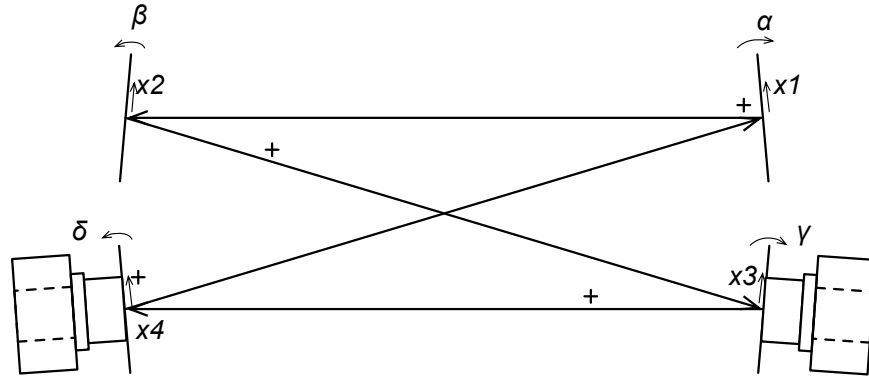


Figure 234: Definition of the parameters for the cavity axes and mirror alignment

$$\begin{pmatrix} x_1 \\ \theta_1 \\ x_2 \\ \theta_2 \\ x_3 \\ \theta_3 \\ x_4 \\ \theta_4 \end{pmatrix} = \begin{pmatrix} 0.893 & 1.107 & 1.323 & 1.246 \\ 0.759 & -0.759 & -0.271 & 0.271 \\ 1.107 & 0.893 & 1.246 & 1.323 \\ 0.759 & 1.241 & -0.271 & 0.271 \\ 1.323 & 1.246 & 1.169 & 1.400 \\ -0.271 & 0.271 & 0.819 & -0.819 \\ 1.246 & 1.323 & 1.400 & 1.169 \\ -1.241 & -0.759 & -0.271 & 0.271 \end{pmatrix} \begin{pmatrix} \alpha \\ \beta \\ \gamma \\ \delta \end{pmatrix}$$

Example:

Assuming the flat mirrors are fixed, if I want to move the x_3 spot up by 1mm without moving x_4 , the solution is

$$\begin{pmatrix} \alpha \\ \beta \\ \gamma \\ \delta \end{pmatrix} = \begin{pmatrix} 0 \\ 0 \\ -1.97 \text{ mrad} \\ +2.36 \text{ mrad} \end{pmatrix} \quad (27)$$

This yields:

$$\begin{pmatrix} x_1 \\ \theta_1 \\ x_2 \\ \theta_2 \\ x_3 \\ \theta_3 \\ x_4 \\ \theta_4 \end{pmatrix} = \begin{pmatrix} +0.33 \text{ mm} \\ +1.18 \text{ mrad} \\ +0.67 \text{ mm} \\ +1.18 \text{ mrad} \\ +1.00 \text{ mm} \\ -3.55 \text{ mrad} \\ +0.00 \text{ mm} \\ +1.18 \text{ mrad} \end{pmatrix}$$

D DCPD/QPD/PZT/Preamplifier arrangement

NOTE: Because the preamplifiers were replaced with a new design at the post O3 upgrade, this section is left here only for the historical reason.

[External Link]

H1 PD arrangement: http://nodus.ligo.caltech.edu:8080/OMC_Lab/176

L1 PD arrangement: http://nodus.ligo.caltech.edu:8080/OMC_Lab/144

L1 PD arrangement: <https://alog.ligo-la.caltech.edu/aLOG/index.php?callRep=26476>

L1 PZT failure: <https://alog.ligo-la.caltech.edu/aLOG/index.php?callRep=8366>

[Description]

LIGO-D060572 In-vacuum DCPD (preamplifier) for OMC

L1 OMC preamps are arranged as shown in Figure 235.

- DCPD response (LLO ALOG 26476):
 - Illuminate DCPD1 (T) \implies DCPD **B** responded in MEDM
 - Illuminate DCPD2 (R) \implies DCPD **A** responded in MEDM
- QPD response (LLO ALOG 26476):
 - Illuminate QPD1 \implies QPD A responded in MEDM
 - Illuminate QPD2 \implies QPD B responded in MEDM
- PZT arrangement:
 - One of the PZTs is broken. (LLO ALOG 8366)

H1 OMC preamps are arranged as shown in Figure 236.

- DCPD response:
 - Illuminate DCPD1 (T) \implies DCPD **B** responded in MEDM
 - Illuminate DCPD2 (R) \implies DCPD **A** responded in MEDM
- QPD response:
 - Illuminate QPD1 \implies QPD A responded in MEDM
 - Illuminate QPD2 \implies QPD B responded in MEDM
- PZT arrangement:
 - Mighty Mouse Pin1&2 \implies PZT2 (DCPD side)
 - Mighty Mouse Pin3&4 \implies PZT1 (QPD side)

Top View

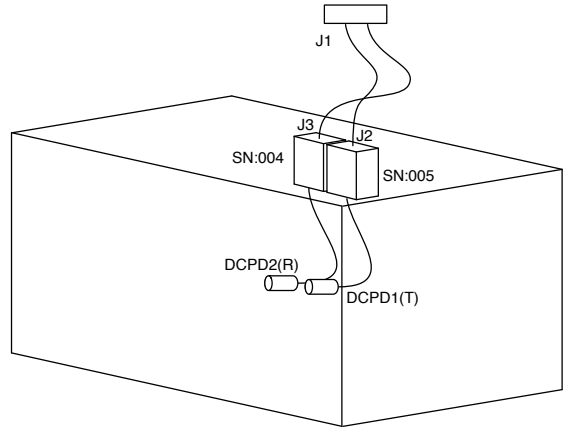
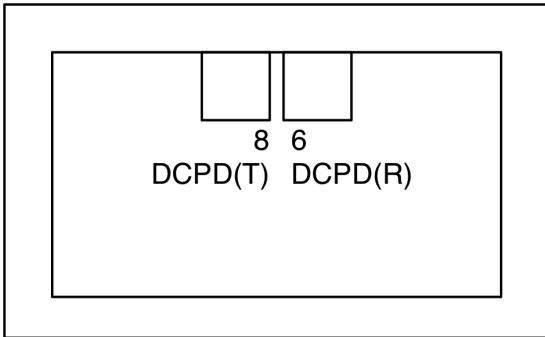


Figure 235: Preamp SNs and arrangement at LLO

Figure 236: Preamp SNs and arrangement at LHO

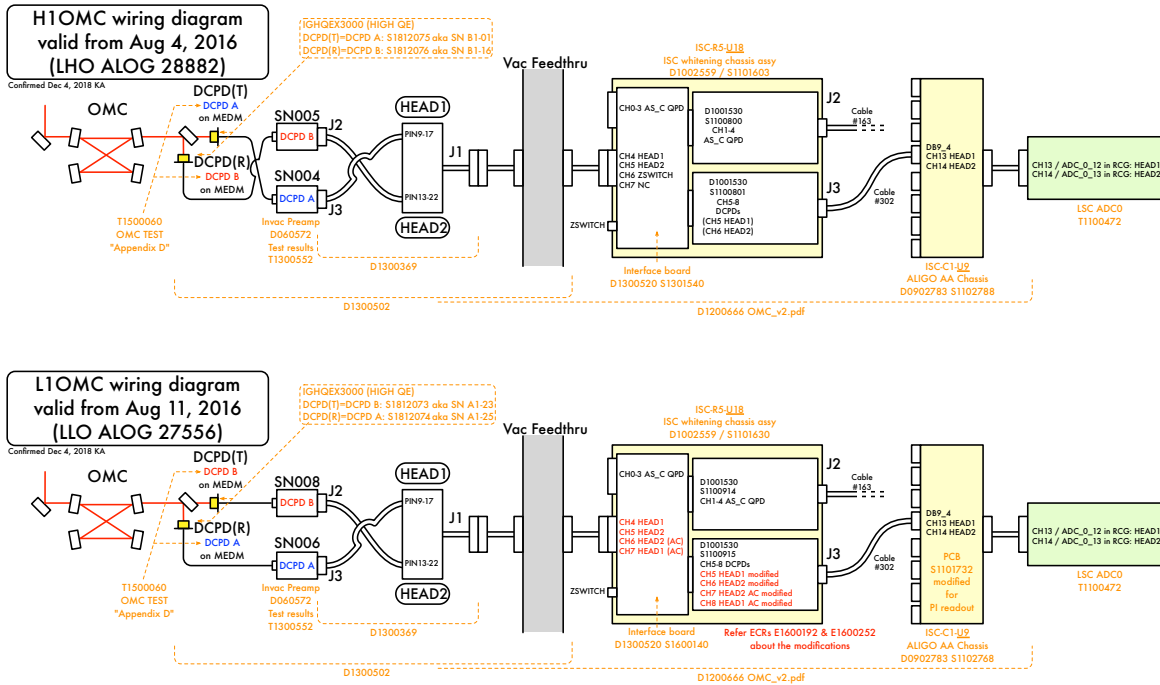


Figure 237: OMC Wiring - diagram as built

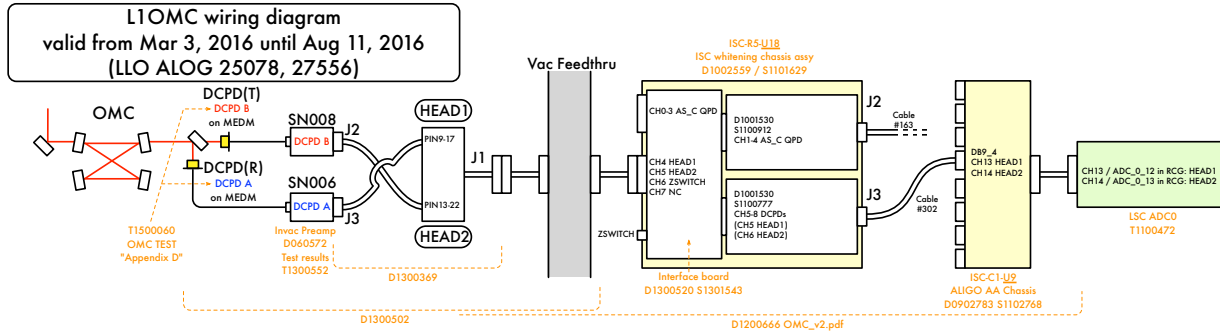


Figure 238: OMC Wiring - diagram as built (OLD)

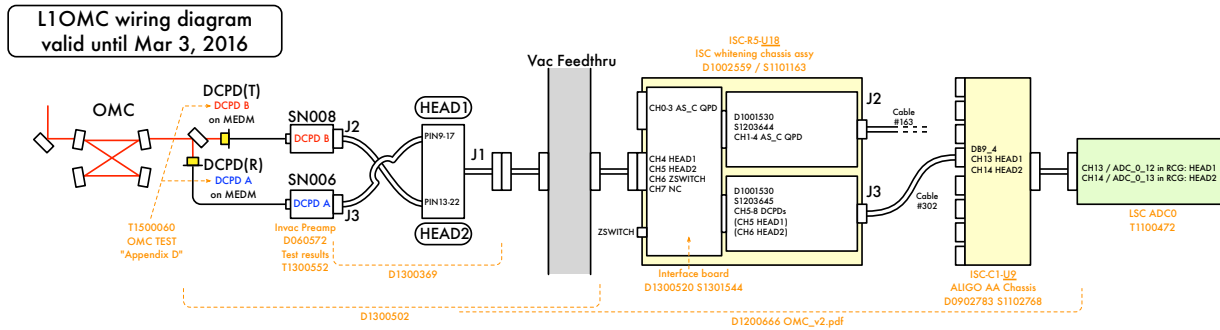
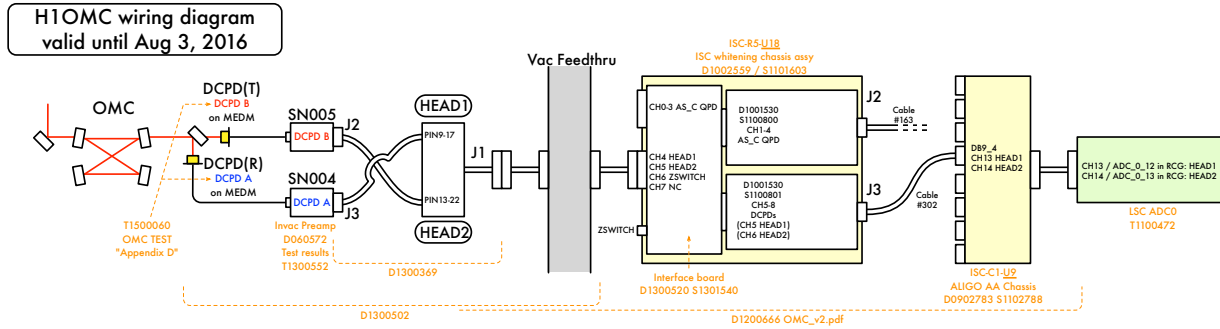


Figure 239: OMC Wiring - diagram as built (OLD)

List of installed photodiodes: as of March 14, 2015

- L1 OMC
 - DCPD1 (Trans): eLIGO diode, Vendor SN unknown, Preamp SN 008, Connected to J2
 - DCPD2 (Refl): eLIGO diode, Vendor SN unknown, Preamp SN 006, Connected to J3
 - QPD1: LIGO SN 43
 - QPD2: LIGO SN 38
- H1 OMC
 - DCPD1 (Trans): eLIGO diode, Diode Marked “A”, Vendor SN 0288, Preamp SN 005, Connected to J2
 - DCPD2 (Refl): eLIGO diode, Diode Marked “B”, Vendor SN 0721, Preamp SN 004, Connected to J3
 - QPD1: LIGO SN 44
 - QPD2: LIGO SN 46
- 3IFO OMC
 - DCPD1 (Trans): new diode with a glass window, LIGO SN 11, Vendor SN 1213
 - DCPD2 (Refl): new diode with a glass window, LIGO SN 12, Vendor SN 1208
 - QPD1: LIGO SN 50
 - QPD2: LIGO SN 51

List of installed photodiodes: as of June 10, 2016

- L1 OMC
 - DCPD1 (Trans): High QE diode IGHQEX3000, Vendor SN A1-23, Preamp SN 008, Connected to J2
 - DCPD2 (Refl): High QE diode IGHQEX3000, Vendor SN A1-25, Preamp SN 006, Connected to J3

References

- [1] N. Uehara and K. Ueda, *Accurate measurement of the radius of curvature of a concave mirror and the power dependence in a high-Finesse Fabry-Perot interferometer*, *Appl. Opt.*, **34** (1995) 5611-5619.
- [2] K. Arai, J. Lewis, P. Fritschel, *Output Mode Cleaner Assembly Procedure* [LIGO Document T1300201](#), (2015).

- [3] K. Arai, S. Barnum, P. Fritschel, J. Lewis, S. Waldman, *Output Mode Cleaner Design*, [LIGO Document T1000276](#), (2013).